Monitoring Concept to Detect Engine Oil Condition Degradations to Support a Reliable Drive Operation

Sascha Rigol

A thesis submitted in partial fulfilment of the
requirements of the University of East London
for the degree of Doctor of Philosophy

September 2011

Acknowledgement

First and foremost, I want to thank God for all the blessings in my life and for providing wisdom, strength and success to complete this research work.

Special thanks go to my advisor Professor Roy Perryman from the University of East London for the profound and qualified support during this research project. I was very grateful to have had an advisor who gave me the freedom to investigate my research topics and at the same time guidance to reach the research objectives. I appreciate and admire the patience he had shown in the diligent reading and corrections of all chapters and results of this work and to provide valuable comments and suggestions to improve the content and style of the work. I am also grateful to Dr. Wada Hosny from the University of East London for his interest in my work. I am honoured that he had agreed to act as a second supervisor for this PhD thesis.

I want to express special gratitude to the Daimler AG for the privilege they offered me to support my research work from the beginning and also to provide personal and career development opportunities. Thanks go to Michael Weber, Dr. Rainer Mäckel, Dr. Martin Haueis, Dr. Horst Haspeklo and Michael Pulvermüller from the 'Group Research & Advanced Engineering Department' for offering the possibility to launch this research project. I want to express my gratitude to Hubert Schnüpke, Michael Schenk, Dr. Christian Czermin, Petra Sorsche, Dr. Thorsten Gust and Dr. Detlef Scharr from the 'Operating Fluids Department' of the Mercedes-Benz Engine Development for all the valuable discussions around operating fluids related topics. I owe a debt of gratitude to my colleague Dr. Rene Linssen without his help the experimental part of this work especially with regard to the Matlab programming and modelling of the characteristic maps would not have been possible. I was very fortunate to have such an experienced and knowledgeable colleague to provide patiently scientific support in this study. Special thanks go to Dr. Stefan Keppeler for his efforts in supporting my personal development and career progress and the trustful delegation of responsible tasks.

Many thanks for the valuable and supporting discussions in the theoretical part of this study go to people from the oil and additive industry. Special thanks go to Dr. Helmut Leonhardt, Dr. Inken Klemens and Sven Hooijer from Shell Global Solutions. I want to thank Mark Peters from ExxonMobil Research & Development. Thanks go to Johann Ney and Dr. Stuart McTavish from Infineum.

And last but not least, I want to express my sincere gratitude to my parents Therese and Rainer Rigol. Their effort in my education, support and promotion has been of inestimable value through all my life. Thanks goes to all close friends who always provided support and encouragement during this research. Thank you all.

Abstract

The theoretical part of this research work summarised all the known potential lubricant degradation effects during engine operation and in particular with regard to the use of the current generation of biofuels. A qualitative risk assessment was conducted which outlined biodiesel as potentially the most critical fuel. A 'black box' model was used to outline the challenge of oil condition monitoring based on summative sensor measurement methods. The theoretical considerations were supported by a statistical analysis which investigated how the presence of multiple contaminants in the oil affects the most common sensor data of permittivity, conductivity and viscosity. 'Design of Experiments' (DoE) models were developed for the permittivity, conductivity and viscosity data and expressing mathematically the relationship between the contaminants having a significant influence on each of the sensor data. The findings of the multivariate analysis identified that the effects on permittivity and viscosity provided reliable information about oil condition changes. The concept of an oil condition algorithm in this research was aimed at addressing accuracy and efficiency in predicting the outcome. The core aspect of the algorithm was the use of characteristic maps based on bi-linear regression to predict the fuel, soot and oxidation levels in the oil using permittivity and viscosity as the input data. Based on the predictions using three contaminant components a method to assess the overall condition status is derived. The derived condition status provided the input for an oil drain forecast method which monitors the status within the predefined maximum mileage. Another achievement from this research was the vehicle simulation for different driving profiles and the corresponding simulation of oil degradations. The selected profiles were for a 'Taxi', 'Normal' driving and 'Long Distance' driving. The resulting simulation of fuel, soot and oxidation levels in the oil showed a high correlation compared with the use of real oil analysis based on engineering judgement. The quantitative assessment of the simulated contaminant levels compared with the predicted levels obtained from each characteristic map showed excellent prediction performance. The derived overall condition rating and mileage forecast prediction also showed very good results. The results from this research have shown that this new oil condition algorithm concept using bi-linear characteristic maps has enabled the compromise between predictive accuracy and an efficient and transparent algorithm structure. Validation of the results confirms that the algorithm has the potential to minimise and prevent oil condition related engine failures regardless of the actual fuel used.

List of Contents

List of Figures

List of Tables

List of Units and Abbreviations

Units

Index	Meaning	Unit
A	(IR-) Absorption	[A/cm]
A	Area	[m²]
α	Polarisability	[C·m²/V]
C	Capacitance	[As/V]
D	Damage parameter - fuel, soot, oxidation	[wt.-%], [A/cm]
D	Electric flux density	[As/m²]
D	Diffusion coefficient (constant)	[m²/s]
d	Distance	[m]
δ	Decay length	[m]
E	Electric field	[V/m]
E_{CM}	Gridfit error	[1]
$\dot{e}$	Shear rate	[1/s]
ε_r	Relative permittivity	[1]
ε_0	Free space permittivity (constant)	$8.8542 \cdot 10^{-12}$ [As/Vm]
F	Force	[N]
F_d	Faraday-Constant	96,485.3399 [C/Mol]
f	Frequency	[1/s], [Hz]
f_0, f_s	Resonant frequency	[1/s], [Hz]
G	Conductance	[S]
g	Gravity	9,81 [m/s²]
h	Height	[m]
Θ	Angle	[°]
i/I	Electric current	[A]
κ	Boltzmann-Constant	$1.381 \cdot 10^{-23}$ [J/K]
λ	Sommerfeld number	[1]
λ	Smoothing factor	[1]
L	Inductance	[H]
l	Length	[m]
μ	Friction coefficient	[1]
ν	Kinematic viscosity	[m²/s]
m	Mass	[g]
η	Dynamic viscosity	[mPa·s]
p/P	Polarisation	[As/m²]
p	Pressure	[Pa]
p	Significance	[1]
π	Pi	3,14159 [1]

Index	Meaning	Unit
Q	Electric charge	[As]
R	Electric resistance	[V/A], [Ω]
R	Gas constante	[J/(mol·K)]
R^2	Coefficient of determination	[1], %
r	Correlation coefficient	[1], %
r	Radius	[m]
S_e	Standard error of regression	[1]
ρ	Density	[kg/m³]
σ	Shear stress	[Pa]
σ	Specific conductivity	[S/m]
σ	Molar conductivity	[(S·cm²)/mol]
T	Absolute temperature	[K]
T	Temperature	[°C]
T_{IR}	IR-transmission	[1]
TAN	Total acid number	[mg KOH/g]
TBN	Total base number	[mg KOH/g]
tan δ	Dissipation/quality factor	[1]
t	Time	[s]
u/U	Voltage	[V]
υ	Velocity	[m/s]
$\dot{V}$	Volume stream gradient	[m³/s]
ω	Angular frequency	[1/s]
x	Distance, thickness	[m]
χ	Mass fraction	[g]
Y	Admittance	[S]
Z	Impedance	[V/A], [Ω]
Z_{CM}	Characteristic map matrix	[1]
z	Condition value	[1], %
$\hat{z}$	Predicted condition value	[1], %
z_p	Empiric oil contaminant value	[wt.-%], [A/cm]
$\hat{z}_p$	Predicted oil contaminant value	[wt.-%], [A/cm]

Abbreviations

Abbreviation	Meaning
ANOVA	Analysis of variance
ASTM	American society for testing and materials
BVD	Buttherworth van Dyke
Bx	Biodiesel fuel blend with x [wt.-%] biodiesel content
c	Concentration
CO_2	Carbon dioxide
DAI	Daimler
DI	Direct injection
DIN	Deutsches Institut für Normung (German institute for standardisation)
DoE	Design of experiments
DPF	Diesel particulate filter
ECU	Engine control unit
EIS	Electrochemical impedance spectroscopy
EU	European Union
Ex	Ethanol fuel blend with x [wt.-%] ethanol content
FAME	Fatty acid methyl ester
FIR	Far infrared
h	hour
HTHS	High temperature high stress
IR	Infrared
km	Kilometre
KOH	Potassium hydroxide
LWIR	Long-wavelength infrared
MB	Mercedes-Benz
mi	Mile
MRA	Multiple regression analysis
MWIR	Mid-wavelength infrared
NIR	Near infrared
NOx	Nitrogen oxide
OCA	Oil condition algorithm (Hella AG)
ODIS	Oil diagnosis system (Daimler AG)
QCM	Quartz crystal microbalance
QLT	Quality, level, temperature (Continental Temic)
RLC	Resistance-Inductivity-Conductivity
RME	Rapeseed methyl ester
RTFO	Renewable Transport Fuel Obligation
SAE	Society of Automotive Engineers
SME	Soybean methyl ester
SWIR	Short-wavelength infrared

Abbreviation	Meaning
TF	Tuning fork
TSM	Thickness shear mode
UK	United Kingdom
US(A)	United States of America
UV	Ultraviolet
V	Violet
VBN	Viscosity blend number
VGN	Viscosity gradient
VI	Viscosity improver
W	Window
wt	Weight

Chapter 1

1 Introduction

1.1 Motivation - Influence of Climate Protection Ambitions on the Engine Oil

The dramatic and rapid changes of global climate conditions within the last decades have motivated governments and legislation to compile and pass climate change commitments to protect and improve climate conditions. The eco-political declarations of intent have resulted in regional and national laws and regulations to implement the energy source improvements to achieve these goals. One of the most important global declarations of intent to adopt environmental protection into legislation was the Kyoto protocol. The purpose of the Kyoto climate change conference was to establish a legally binding international agreement, whereby all the participating nations commit themselves to tackling the issue of global warming and greenhouse gas emissions (UN, 1998). The resulting policy of the European Union to comply with the demands of the Kyoto protocol addressed, in particular, the new requirements for the transport section and outlined two key motivations (EU, 2003). First aspect was to reduce the dependence on fossil fuels and therefore the second aspect was the reduction of the CO_2 emissions. The EU directive 2003/30/EC therefore set indicative biofuel shares for the 25 EU member states with a gradually increasing rate up to 20 % in volume of fossil fuel replacement by 2020. Some of the EU member states in addition, defined national directives and laws to prescribe mandatory annual biofuel replacement rates to realise the achieved indicative biofuel targets of the EU. The UK Government introduced in April 2008 a 'Renewable Transport Fuel Obligation' (RTFO) requiring transport fuel suppliers to ensure that 2.5 % in 2008 rising to 5 % in 2010 of their total fuel supplies comes from renewable sources (http://www.dft.gov.uk).

The German 'Biokraftstoffquotengesetz' defines a mandatory annually increasing biofuel replacement rate even exceeding the EU goals (BioKraftQuG, 2006). The content of bioethanol in petrol fuels is currently 5 % in volume, also referred to as E5. The prescribed amount of biodiesel in diesel fuels was increased in 2009 to 7 % in volume, also referred to as B7. Other countries have identified even higher biofuel blend requirements. France has biodiesel blends up to B30 and ethanol blends up to E10 (ADM, 2007). Brazil and the USA are currently the dominant bioethanol markets for ethanol blends up to E25 (Giroldo et al., 2005). Flex-fuel applications with E85 are currently quite rare from a global prospective. ASTM International introduced a B20 biodiesel standard into effect at the end of 2008 which will result in an increasing share of B20 biodiesel blends in the US market (ASTM, 2008). The 'green technology' regardless if it is a new type of fuel or new engine concept is accompanied by significant challenges for the condition of engine oil. When biodiesel comes into contact with the oil it causes fuel accumulation and accelerated oil oxidation. The oxidation byproducts in the oil are the formation of acid and oil insoluble products which increase the viscosity significantly. Ethanol applications, especially E85, can cause problems at low engine temperature operation when the ethanol evaporates slowly from the oil. Acids from the ethanol and the formation of stable emulsion can occur due to the hygroscopic character of ethanol. If ethanol blends consist of a poor base fuel, the susceptibility for an accelerated oxidation process in the oil is similar to the unsaturated fatty acids of the biodiesel components. The presence of any of the current generation of biofuels in the sump bears a highly increased reliability risk for the engine. Recent measurements to achieve economical improvements have not only changed the fuel situation significantly but also the hardware design of modern engines to comply with the emission regulations to achieve the required CO_2 limits.

To achieve the rigorous emission regulations (e.g. EURO 6 from 2014 onwards) modern engines need to be equipped with complex exhaust after-treatment systems including 'Diesel Particulates Filter' (DPF). The current after-treatment systems contribute significantly to higher level of unburnt fuel reaching into the oil (Klemens, 2008). The implementation of CO_2 based tax regulations to replace former tax regulations based on engine size and emissions has forced the automotive industry to develop and improve new engine technologies to meet the CO_2 targets. The latest generation of petrol engines use direct fuel injection systems to increase the efficiency and reduce fuel consumption.

Direct injection can lead to increased fuel dilution especially due to wall spraying of unburnt fuel drops for low temperature driving cycles (Binder, 2007). Engines currently being developed are driven by the need for greater fuel economy; downsized (small turbo charged) engines, mostly 4 and 6 cylinder with significantly reduced engine displacement, are being developed to operate at performance levels of the 6 and 8 cylinder engines. These small and powerful engines thus operate in heavy cars up to the luxury range, and leads to significant fuel economy but the oil stress is a major concern especially due to the thermal stress and the small volume of oil in the sump. The reaction rate of chemical degradation in the oil, particularly in the presence of biofuels is much faster. Additionally there are many applications for the so called low ash engine oils which are required to prevent ash loading of the diesel particulate filters and the catalytic elements which are very cost sensitive due to the materials used. The ash forming substances in engine oil are from the additive components of the oil formulation. Metal additive components are essential for the oil to fulfil the wide range of duties besides the commonly known aspect of lubricating. One major task is to prevent and avoid the oxidation reaction chain initiated by combustion products and unburnt fuel, and to neutralise acids in the oil (McTavish and Ney, 2009). A small amount of oil gets burnt during normal engine operation. Ashes from the metal additive components unfortunately load and destroy the catalyst and prevent an effective exhaust after-treatment (Sappok and Wong, 2010). All modern diesel engines fulfilling the current and future European emission standards are equipped with DPF which requires the application of low ash engine oils. The reduced additive treatment makes these oils less robust against chemical degradation processes due to the reduced additive treatment.

The current situation outlines the ambition to contribute to the CO_2 reduction in the transport sector and results in a variety of technical innovations that pose a challenge for the reliability of engine oil. The engine oil condition can be regarded as the vital function of the engine operation and severe degradation results inevitably in a reliability risk. Reliability plays a dominant role in customer satisfaction which is annually ranked by independent organisations and plays an important role in the customer recognition of the automobile manufacturer. The subject of engine oil condition monitoring in this research work will become a more important topic to ensure a reliable automobile drive operation. The aim is therefore to prevent the loss of mobility due to degraded oil regardless of which fuels are used today or in the future.

1.2 Literature Review

1.2.1 Structure and Key Sources

An initial literature review in the thematic field of engine oil condition monitoring or oil quality monitoring was performed. The structure of the literature research to explore the related key subjects is illustrated in the concept map below, see Figure 1.1 (Novak and Musonda, 1991).

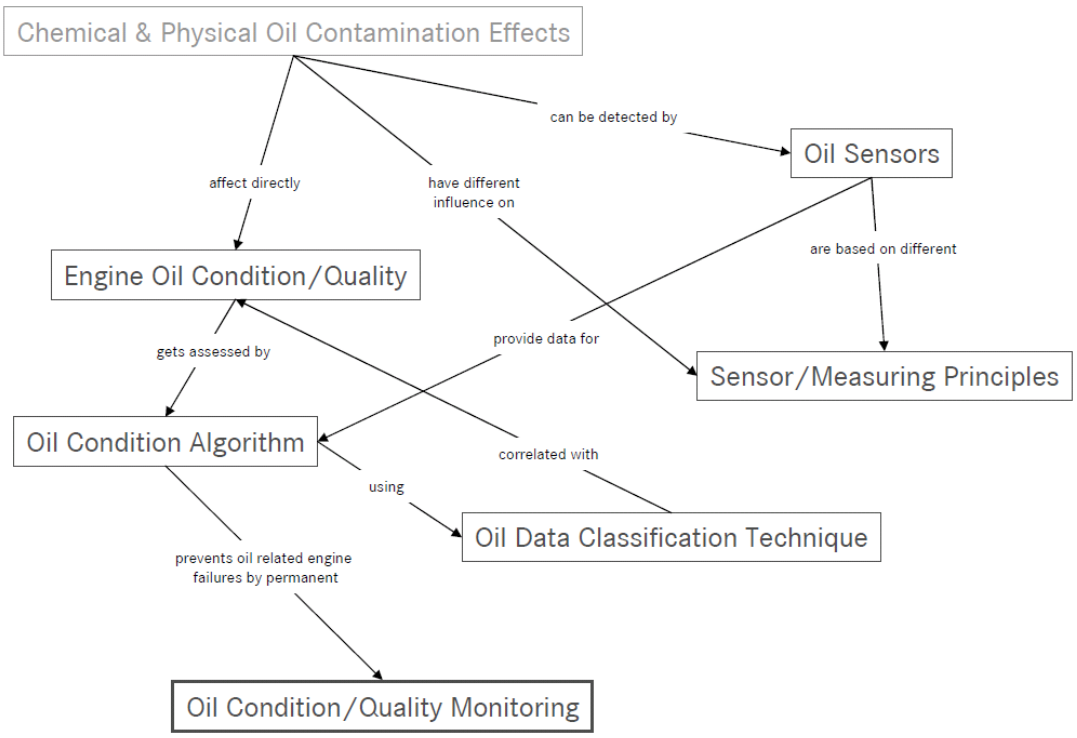

Figure 1.1: Concept map and thematic structure of the literature review
Each box represents the investigated key subject. The arrows with the explanations link the topics together to provide the thematic structure of the literature research.

The following major sources were identified as they provide key literature and the most recognised articles in this field of study:

- Automotive World - Synesis Media Ltd., UK.
- ATZ Online - Vieweg Verlag/GWV Fachverlage Ltd., GER
- Daimler 'Corporate Information & Research Management'
- DieselNet - Ecopoint Inc., CDN

- IEEE Xplore Digital Library – provided by Institute of Electrical and Electronics Engineers, USA
- Römpp Online – Thieme Chemistry, GER
- SAE Technical Papers - Society of Automotive Engineers Inc., USA
- Scopus – Database provided by Elsevier B. V., NL
- SpringerLink – Database provided by Springer Science+Business Media Ltd., GER
- SpringerMaterials – The Landolt-Börnstein Database, GER
- Studies and research work conducted by oil and additive companies provided to Daimler AG

It was noticeable that the overall number of researchers in this field is very limited. The main reason might be due to the fact that engine oil condition monitoring using a sensor is only rarely used in serial applications in the automotive but also in other industries. The following critique of key research articles will present the actual status of knowledge in this area.

1.2.2 Critique of Key Research Articles

Development and Testing of an Innovative Oil Condition Sensor (Basu et al., 2009)

The Ford Motor Company together with Hella GmbH conducted a study to evaluate the performance of the Hella PULS+C oil condition sensor. A short research plan was presented that consisted of empirical analyses using bench and vehicle tests. The aim of the bench tests was to determine the sensor performance, in particular the repeatability and hysteresis effects. The aim of the vehicle tests was to sense the oil data directly in the oil sump and to detect contaminants using the internal 'Oil Condition Algorithm' (OCA). The bench testing used fresh as well as degraded oil which was not further specified. The sensor with the oil samples was mounted in a test fixture and heated up in an oven from 30 – 100 [°C]. The viscosity over temperature results of the heat up and the cool down process were investigated. The analysis used scatterplot diagrams together with regression analysis results including the obtained R^2 value of the test. The results for all of the different viscosity plots were comparable. All curves were very close together and showed high R^2 results. Cool down curves were not plotted in the bench analysis results which makes it difficult to assess hysteresis effects. From the bench test it was concluded that the viscosity measurement with this sensor type provides reliable results for fresh and used oil. Vehicle tests were conducted for city and highway driving. The Hella PULS+C sensor was installed in a separate oil reservoir and the data were uploaded via telematics to a server for analysis. Oil samples were periodically collected and analysed to provide reference values. The results were presented and assessed using data plots. The data plot showed viscosity values of the sensor at 70 [°C] over a driving distance of 10,000 [mi]. The values were compared with calculated viscosity values which were not further specified. Statistical analysis was not presented. From a qualitative assessment it can be observed that the sensor viscosity values showed good correlation with the laboratory results. Sensor viscosity decreased with increasing temperature for the two vehicles. The analysis in the research report was primarily focussed to viscosity measurements over temperature with unknown oils for the bench test and viscosity over mileage plots for the vehicle tests. The oil condition algorithm was not presented.

Providing Embedded, In-situ Oil Quality Monitoring for Improved Maintenance and On-Board Diagnostics in Trucking and Automotive Applications (Mackos et al., 2008)

This research publication presented the development of an 'Electrochemical Impedance Spectroscopy' (EIS) to provide real-time on-board oil quality assessment. The report provided a detailed overview on the theoretical aspects of the EIS sensor development. The sensing architecture including underlying theoretical aspects, equivalent circuit and equations were discussed. Data fusion and classification approaches of the sensor device were presented in the paper. An exploratory research design approach was selected for experimental sensor evaluation. The research plan was briefly described and consisted of empirical analysis using a scaled lubrication test stand to replicate operation conditions of Navy diesel engines. The presented test plan of the study called for identifying and quantifying soot, fuel and water contamination in a lubricant based on military specifications. The study includes a brief summary of a test plan based on 'Design of Experiments' (DoE) methods providing a well structured test approach. The reference values were evaluated at different oil laboratories. The data were assessed using data plots and statistical analysis for the sensor and reference values for each type of contaminant. The report addressed primarily off highway or navy needs where the contaminants are basically water, soot and fuel. Other lubricant degradation effects such as oxidation or nitration which are important for automotive applications were not considered. From the report it can be concluded that water, soot and fuel can be sufficiently measured using EIS. The conclusion focused solely on the bivariate correlation between single contaminants and the resulting impedance values. The presence of multiple contaminants and the resulting influence on the data was not considered. A further consideration arose from the report which was to incorporate the viscosity value with the electrochemical measurement. The single impedance measurement seemed not to be able to reliably detect fuel and oxidation or nitration byproducts in the oil.

Lube Oil Condition Monitoring System - An Alternative Methodology (Murukesan 2008)

This research paper presented an oil condition monitoring system consisting of dielectric sensor, controller and display. The theoretical part of the article discussed some oil degradation mechanisms. An exploratory research design approach was selected for experimental system evaluation. The experimental part consists of empirical analysis using two different types of oils fresh and used after 5,000 [km] / 3,108 [mi] with one petrol engine vehicle and one diesel engine vehicle in city traffic. The sensor output voltage over temperature of fresh and used oil was measured in the range from 25 – 75 [°C]. The evaluation of the results was conducted using data plots where the sensor output voltage was plotted over temperature. A discussion about the cause of the output voltage changes in the experimental part would have been beneficial. Modern oil formulations are able to endure oil drain intervals of up to 30,000 [km] / 18,645 [mi] depending on the operation conditions. It should be considered if only slightly contaminated oil which was only used for 5,000 [km] / 3,108 [mi] will show sufficient sensor response to derive reliable findings. The findings presented with the data plots were not statistically supported to justify the results. The research outlined again the need to include related theoretical aspects of oil condition monitoring to understand the results. The proposed oil condition monitoring approach based on comparison of sensor data with predefined thresholds is similar to the research report by Irion et al. (1997). The presented paper identified the need for further research to better understand the primary drivers of dielectric oil sensors. It further outlined the lack of considering efficient and reliable oil condition rating techniques suitable for ECU applications to obtain a condition statement from the sensor data.

Combi-sensor for Oil Level and Oil Quality Management (Dobrinski et al., 2008)

The focus of the detailed research work published by Hella GmbH was to provide substantial background information on the Hella PULS+C sensor development. A similar article was already presented earlier with slightly different aspects and less details by Buhrdorf et al., (2005). The work presented the three main elements of the combined sensor namely ultra-sonic level detection, tuning fork mechanical resonator and the oil condition algorithm developed by Hella. The first section covered the theory of oil level detection using ultrasonic based device. All relevant basic equations and fundamentals were described together with schematic illustrations of the measuring principle. The experimental part consisted of empirical analysis of the ultra-sonic level detection and temperature measurement. The next section in the article covered the theory of the tuning fork mechanical resonator to measure viscosity, density and permittivity. The theory included all relevant explanations and mathematical equations supported by an equivalent electrical circuit. The empirical analysis of the tuning fork sensor measured viscosity, density, permittivity and impedance. Fresh oil was diluted stepwise with diesel, soot loaded oil and water. Viscosity decreased with increasing fuel dilution and density slightly increased with fuel dilution. The next measurement showed the response of permittivity over fuel dilution. The data points were not influenced by the stepwise increasing fuel dilution. The next experiment evaluated the influence of water on viscosity and density at constant temperature. Viscosity values showed a slight decrease with increasing amounts of water. The density value slightly increased. The next test covered the influence of water on the permittivity. The permittivity showed a noticeable increase with increasing water in the oil. The next test in the series assessed the change of viscosity and permittivity at constant temperature in the presence of soot in the oil which showed a noticeable increase of both values with increasing soot loading. All results were qualitative and did not include statistics. The final part of the research report presented briefly the integrated oil condition algorithm. The algorithm was based on a decision tree using predefined thresholds of the sensor parameters permittivity, viscosity, density and conductance. The value from this research publication was the insight into the tuning fork theory and the oil condition algorithm approach. Multiple contamination influences on the sensor parameter were not considered. The link between the defined static algorithm thresholds for the sensor values and the actual contaminant situation in the oil could be further investigated.

In-Situ Monitoring of Engine Oils through Electrical AC Impedance Measurements (Halalay and Schneider, 2007)

The research was conducted at the General Motors Research & Development Centre and studied the variation of electrical resistivity and permittivity under well controlled degradation conditions during engine dynamometer tests. Speed and load conditions were selected to approximate conditions of highway driving while pulling a trailer to accelerate oil degradation. An electrochemical impedance spectroscopy probe based on common laboratory standard was used to track changes in the electrical oil properties every 30 minutes providing a large number of data points. The test results were presented using data plots of permittivity and resistivity over engine runtime without incorporating any statistical methods. Visual evaluation of the plots highlighted comparable results for all tested oils. The electrical resistivity increased during the first test hours, dropped significantly in the middle of the test and finally increased steadily until end of test. The permittivity values increased continuously from the beginning of the test in a clear straight gradient. The gradient differed slightly between the used oil formulations. Unsurprisingly, the lowest gradient was measured with the synthetic oil, as synthetic oils are more robust against oxidation effects (Möller and Nasser, 2002: 74). The test results indicated high repeatability of the measurement results. Limiting factor in this study was the fairly brief discussion of measurement results without inclusion of relevant theoretical aspects to underpin the data. Justification for the initial decrease of resistivity value was not clearly provided or discussed. Reference oil analysis would have been advantageous to understand which effect had primarily driven the permittivity change over the test length. From the study it can be suggested that conductivity is a very questionable oil condition parameter and provides no additional benefit to permittivity. This conclusion is also supported by research work from Delphi (Basu et al., 2000) who investigated conductivity and permittivity sensor results. Both papers confirm in general better correlation results of key contaminants with permittivity than with conductivity.

Verfahren zur Bestimmung des Motorölzustands und Prognostizierung der Ölwechsel in Nutzfahrzeugen (Method to Determine the Engine Oil Condition and Prediction of the Oil Drain Interval for Truck Application) (Lorenz, 2007)

The research was conducted at the DaimlerChrysler Research & Development Centre and studied the oil condition assessment based on permittivity and indirect viscosity measurement. The work focused on the application of the ContiTemic QLT sensor. This sensor measures permittivity, level and temperature. The application was modified in this work to obtain a viscosity statement from this sensor by measuring the speed of oil level changing in dedicated driving situations where the oil movement is in the longitudinal direction. The oil condition model used viscosity, permittivity and the predicted soot and fuel content which were obtained from a linear regression model as input variables. The condition assessment was based on a comparison of each of the four input variables with three predefined classification thresholds 'good', 'medium' and 'high'. The oil drain forecast used a 2^{nd} order polynomial as a function of permittivity and viscosity. The aim was to calculate the trend of the two parameters in order to predict when they reach the predefined 'high' level for permittivity or viscosity. The polynomial coefficients were calculated using the last five measurements. Based on the intersection with the defined maximum level for permittivity and viscosity was the corresponding remaining mileage or hours of operation calculated. The model validation proved to provide sufficient condition and forecasting results.

New Solid State Oil Condition Sensor for Real Time Engine Oil Condition Monitoring (Bennett et al., 2006)

The research work was conducted by Symyx Technologies Inc. together with Thermo-King Corporation and targeted to increase oil drain intervals using oil condition sensor information. The empirical study included theoretical discussion of two different viscosity sensing principles based on crystalline quartz resonators. One was the tuning fork flexural resonator developed by Symyx and the other was a 'Thickness Shear Mode' (TSM) resonator also used in bioanalysis (Kaspar et al., 2000). The brief theoretical comparison suggested superior performance of tuning fork technology due to its ability to measure viscosity, density, permittivity and conductance with a single device (Dobrinski et al., 2008), (Buhrdorf et al., 2005). The research strategy of the quantitative experiments was based on engine test runs equipped with a tuning fork sensor and laboratory tests with the same sensor assembly to test artificially contaminated oil samples. Laboratory testing was based on a test series of oil samples with different soot and diesel concentrations. The presentation of lab results was based on scatterplots where viscosity and density values were plotted over soot and fuel content. Each plot includes the appropriate laboratory reference measurement. All of the results show good correlation of the tuning fork sensor data compared with the laboratory reference value. The study shows that viscosity and density measured by the sensor increased with increasing amount of soot in the oil. Viscosity and density dropped with increasing amount of diesel in the oil. Limiting aspect of the study was the poor oil analysis information of the engine test results to fully justify the sensor data. The low number of data points over test duration indicated a trend but they provided only limited reliability of the findings. Lubrizol conducted a similar study focusing only on the effect of soot on the permittivity and viscosity measurement using thickness shear mode resonator (Zhang et al., 2004). Soot loaded oil from real engine tests was used and indicated clear correlation between soot loading and increasing in viscosity and permittivity value. From the research work it could be concluded that additional density value to viscosity does not provide additional oil condition information. Reliable oil condition information about physical flow properties of oil are thus fully provided by a reliable viscosity value.

Einsatz eines Multisenors für ein Condition Monitoring von mobilen Arbeitsmaschinen (Application of a Multisensor for Condition Monitoring of Mobile Agricultural Machines) (Krallmann, 2005)

The research focus of the dissertation was the development and evaluation of a multi-sensor for condition monitoring of hydraulic liquids to be used in mobile agricultural machines. The work started with a detailed theoretical section where all relevant elements of the novel sensor were qualitatively investigated and discussed. Main elements of the novel sensor system were permittivity measurement electrodes, viscosity measurement using a thickness shear mode resonator, humidity measurement using permittivity measurement with polymer insulator and temperature measurement using a thermistor. Data classification methods were discussed and qualitatively evaluated to select the most suitable methods. The quantitative part of the research was based on an exploratory research starting with experimental pre-measurements of the developed sensor elements. The sensor was implemented into an assembled test stand with continuous flow of hydraulic liquid which was thermo-oxidised to simulate ageing effects of the medium. The test configuration was chosen to simulate real operating conditions of hydraulic oil in agricultural machines. Results were provided using data plot diagrams including statistical methods. The pre-measurement results showed good correlation of sensor parameter and ageing effects of hydraulic oil. The main testing in the quantitative research part was conducted in field trials where the sensor was used in a tractor. The review of raw data showed clearly the effects of oil loss, oil top-ups and the influence of ageing effects. The work identified permittivity and viscosity as reliable fluid condition data. The important research aspect was the quantitative assessment of data classification methods of the sensor data. Krallmann investigated neural networks, Dempster-Shafer method and Bayes theorem to assess the classification performance with the sensor data from the field trial. The outcome clearly identified that neural networks show superior classification performance for condition monitoring tasks compared to the other methods tested.

Viscosity Sensors for Engine Oil Condition Monitoring – Application and Interpretation of Results (Agoston et al., 2005)

The aim of the quantitative research was to investigate viscosity measurement performance of 'Thickness Shear Mode' (TSM) resonator compared to conventional laboratory viscosimeter. In the experiment were different mixtures of oil samples with pure base oil, oil with low additive content and full formulated heavy-duty oils used. The test matrix included beside artificially contaminated oil samples also a series of used low-ash oils. A Bosch TSM resonator was used for all tests, the reference measurements were obtained from an Ubbelohde viscosimeter. All viscosity values were measured at 40 [°C]. The quantitative results were assessed using data plots including regression analysis and regression coefficient calculation. Agoston et al. (2005) concluded from the results in general a good correlation of the viscosity values measured by the Bosch sensor in comparison with the Ubbelohde results. Differences occurred with the different types of base oils. Mineral base oils could be very reliable measured by the sensor. Synthetic base oils showed deviation from the reference results as the influence of the 'Viscosity Improver' (VI) is not detected by the sensor. The measured values were in this case over the entire temperature range slightly too low. However, the relative viscosity increase due to oxidation effects could be well measured. The research outlined the ability of a TSM resonator to monitor oil deterioration as the viscosity change correlated well with the laboratory results of the used oil samples.

Evaluation of Sensors for On-Board Diesel Oil Condition Monitoring of U.S. Army Ground Equipment (Schmittigal and Moyer, 2005)

The U.S. Army 'Tank-Automotive Research Development and Engineering Center' completed an experimental study to demonstrate the abilities of an on-board sensor system for monitoring the oil condition. Motivation of the quantitative research was to investigate the capability of commercially available sensors to reduce the Army's dependence on traditional analysis methods. The research design is based on empiric analysis using bench tests. Focus of the investigation was soot, oxidation, fuel and water in the oil. The test hardware consists of a 6.5L V8 diesel engine, dielectric sensors, conductivity sensor and an electromechanical viscosity sensor.

The test matrix consisted of tests where for each test run one of the interested contaminants is dominant in the oil. For soot detection the engine setup was changed to produce more soot and minimise other chemical lubricant changes. Detection of chemical compositional changes due to oxidation was tested by heating the oil up to 150 [°C] during operation. Fuel dilution situation was simulated by injecting fuel at constant rate into the test engine while running. Water detection test simulated a coolant leak where a mix of water and antifreeze was slowly added. Data results and discussion were based on quantitative exploration of measurement results using data plot diagrams. Data evaluation did not incorporate statistics such as correlation or regression analysis. Conclusions were drawn from visual comparison of each sensor value and the corresponding reference result. Schmitigal and Moyer concluded from the investigation of soot detection good correlation of soot increase with increasing output values for all three sensor systems. Investigation of oxidative byproducts detection with the dielectric and the viscosity sensor showed a continuously increasing positive correlation for the permittivity value with increasing oxidation. The viscosity value started to increase at a later stage of the test. The investigation of fuel dilution detection affected only the viscosity sensor value, which indicated a negative correlation with increasing amounts of fuel. Water dilution showed a positive correlation with permittivity and viscosity. The permittivity increase is reasonable due to high polarity of water. The viscosity increase with increasing amount of water is reasonable as the added antifreeze caused gelling of the oil. Based on the identified single sensor correlations Schmitigal and Moyer suggested that it is possible to monitor the soot content and oxidation, as well as fuel dilution and water contamination. This outcome is also supported by the study of Lubrizol testing these effects using acoustic wave and multi-frequency impedance measurement with different oil qualities (Goodlive et al., 2004). It should be considered that with a real engine operation all contaminants are simultaneous in different concentration in the sump. A research of the strength and significance of the multiple contaminants on dielectric or viscosity data would be beneficial to provide clarification of which contaminant effect influences the sensor data most.

Synthesis of the literature research and critique of key research articles

Table 1.1 provides a summary of the key findings from the conducted literature research based on qualitative assessment criteria.

Table 1.1: Synthesis of the literature research

Criteria	Findings
1. Consideration of oil degradation theories and effects (in particular with the use of biofuels)	▪ In general no theoretical facts about lubricant degradation mechanisms presented to justify findings. ▪ No contrast drawn between the different characteristic of fossil fuels and biofuels to explain sensor effects. ▪ Influence of biofuel blend rates and feedstock not presented to discuss the severity of contamination and resulting measurement impact.
2. Consideration of multiple oil degradation effects on sensor data	▪ Quantitative studies and experiments of degradation effects on sensor data only with single contaminants. ▪ Investigation of multiple effects and evaluation of strength and significance not found.
3. Presentation of results to explain derived relationships between the sensor data and contamination effects (e.g. mathematical models)	▪ Most research articles use qualitative assessment of results derived from scatterplots. ▪ Discussion of quantitative results very rare and typically only presented as bivariate, linear regression results including presentation of the coefficient of determination. ▪ Lack of discussion of the selected modelling approach. ▪ No justification of the findings with underlying theoretical facts. ▪ No consistent mathematical models of sensor effects found (e.g. DoE models).
4. Quality of statistical investigations and results	▪ Rare use of statistical methods. ▪ Typically only small data populations presented and assessed. ▪ No discussion of potential failures or interference in the raw data found.
5. Presentation and transparency of (oil condition, mileage forecast) algorithm models	▪ Published research work on oil condition algorithm models hardly found. ▪ Transparency for adaption to further application in general not provided.
6. Consideration of practical algorithm implementation aspects (e.g. suitability for cost sensitive segments such as automotive)	▪ Not found in the reviewed literature.

1.3 Identified Research Objective

The review of research work in the subject area of oil condition monitoring showed that most of the work conducted is strongly focused on testing of the measuring abilities of oil sensors from different manufacturers. The aim of all the presented research work is to derive bivariate correlations and to test how well the sensor performs to detect a single contaminant in the oil. Three important aspects could be identified from the review of the current status of knowledge in this area:

1. **Consideration of underlying theories and contexts of the oil degradations:** The study of key literature outlined lacks discussion of potential lubricant degradation mechanisms, how they affect the oil and how this then affects the sensor data. The proposed process would be (a) to collect information about the key lubricant degradation effects, and (b) evaluate which contamination effects have an influence on the existing sensor types. It would thereby be important to investigate the strength and significance of multiple contaminants on the sensor data.

2. **Data evaluation and conclusions:** The review revealed that research experiments were targeted to investigate single contamination effects on sensor data. Results were typically derived by single experiments with low data population. Many of the conclusions presented were based on bivariate data plots drawing correlations between individual oil contaminants and the few sensor parameters. Conclusions were drawn using this prior knowledge of the contaminant with regard to the sensor measurement. It is arguable if this is consistent with the multiple effects in the oil sump during real engine operations. The presence of an unknown number of concurrent degradation effects having potentially different effects on the sensor data is not discussed in any of the existing works. Knowledge of the strength of major influencing parameters on the main sensor values permittivity, conductivity and viscosity would be beneficial to derive an understanding of what are the main drivers of the sensor data. It would also help to understand what is possible to detect with the current on-board measurement techniques and what the limitations are.

3. **Development of an efficient and reliable oil condition monitoring concept:** Research work on engine oil condition algorithms or methods of how to interpret and process the sensor data to obtain a condition statement could only rarely be found. The most profound work to classify oil sensor data reviewed in the literature search was the research conducted by Krallmann (2005). He monitored hydraulic oil ageing in agricultural machines using artificial neural networks in comparison with other classification techniques. The experiments in that research were conducted by computer simulation outside any engine control unit. However, for automotive production applications with the applied techniques would not be appropriate as they consume valuable processor and memory capacity. Another aspect to consider is the overall efficiency of an oil condition algorithm. The major sensor data from current systems are permittivity, conductivity and viscosity. For this limited input data the use of neural networks for instance would be over-engineered. Therefore, a research challenge is to develop an efficient oil rating approach providing reliable lubricant condition statements.

The three key topics identified outline the intention for this research work to contribute knowledge to the field of oil condition monitoring and to introduce novel ideas and considerations. The resulting research objectives for this work are therefore summarised as:

- Exploratory summary of lubricant degradation effects and the resulting influence on oil condition sensor data. The impact of biofuels on the lubricant condition will be discussed in particular.

- Characterisation of the concurrent influences of the multiple contamination effects on selective oil condition sensor data. Their individual strength and significance will be statistically investigated. A ‘Design of Experiments’ (DoE) model representing the contaminant effects on the sensor data will be developed.

- Modelling and testing of an oil condition monitoring concept using a generalised linear model. This aim is to develop an innovative approach providing high efficiency and accuracy in the prediction of the lubricant condition and oil drain interval forecast.

1.4 Research Plan

The following research plan provides an overview of the key research activity of each chapter in this work. The purpose is to provide a summary of the line of thoughts and to outline how knowledge and arguments will be developed to achieve the research objectives.

The engine oil fundamentals are qualitatively explored in Chapter 2 to provide understanding of the main purposes of engine oil. The review will cover all relevant underlying physical and chemical fundamentals for each lubricant function. The main lubricating principles will be presented together with the most relevant technical issues for this research work. Oil formulating aspects such as the supportive work of additive components to fulfil the tasks will be briefly presented for the sake of completeness. The aims of this chapter will be to summarise the key functions, technical terms and definitions of engine oils and to outline the complexity and multi-functionality of modern lubricants.

Chapter 3 will provide a qualitative review of the different oil contamination effects, especially while using biofuel of the current generation. The research will use secondary data analysis to obtain the relevant information. Data will be extracted from acknowledged sources such as annual fuel reports and research papers from the industry. A brief overview of the current global biofuel situation and the globally varying feedstock will be discussed to introduce the different characteristics of biofuels compared with fossil fuels. A summary of the different ways of how unburnt fuel can travel into the sump to start degradation will be presented. A brief review of the major lubricant degradation processes will be presented. The aim is to identify and summarise the key parameters that potentially affect the lubricant condition, especially once fuel has reached the oil. The investigation of lubricant impact during engine operation will contrast how the contamination effects will influence the required oil performance to ensure a proper and efficient engine operation. The compilation of all these main effects will provide an overview of the multitude and complexity of oil degradation mechanisms.

An overview of the main electrical and and physical measurement principles of commercially available oil condition sensors for automotive applications will be presented in Chapter 4. The qualitative review will be focused on the chemical-related oil condition sensor parameters (permittivity and conductivity) and the physical oil condition sensor parameter (viscosity). The theoretical influence of previously identified lubricant contamination effects on the sensor parameters will be considered and qualitatively examined. The main challenges with oil condition monitoring based on the existing sensor data will be discussed.

The quantitative research in Chapter 5 will investigate the strength and significance of multiple contaminants on the existing sensor data. The data source will be existing oil analysis data from vehicle and test bench runs which will be statistically investigated. The analysis will cover the sensor data permittivity, conductivity and viscosity and the main lubricant contaminants. The aim of this component of the research is to characterise which of the key contamination effects in the lubricant has the most dominating effect on permittivity, conductivity and viscosity data. A novel aspect will be the investigation of multiple effects on the sensor data instead of focusing on a single contamination effect as to be seen in the reviewed literature. The strength of each degradation effect on the different sensor parameters can be ranked based on the outcome of the quantitative study. The knowledge derived from this chapter will be required for the next stage of the research which will be the development of a novel oil condition rating model.

The previously derived characterisation of the interaction of contaminants and selected sensor parameters will be the starting position for the research in Chapter 6. Based on the findings the most reliable sensor data will be used as input for the oil condition model. The aim of this qualitative research step is to find an efficient and reliable solution to predict the current oil condition and to forecast the remaining mileage. The basis for the concept of a suitable condition model will be presented as an initial step. The novel aspects of the lubricant condition monitoring algorithm will be outlined. The scheme of the condition rating algorithm will be drawn and the functional subgroups will be explained. The overall aim of this chapter will be to provide all considerations and theoretical background that are necessary to develop the innovative condition model in this research work.

Chapter 7 will present the quantitative validation of the individual elements of the oil condition monitoring algorithm. Starting with an analysis of the linear models in the format of modelled characteristic maps, the conditions for the modelling of these maps will be discussed together with a statement of the achieved predictive accuracy with experimental data from used oil analysis. The complete model validation including the mileage forecast requires sufficient data bases. The generation of this data will be presented in detail. The predictive fit of the algorithm model, including a quantitative mileage forecast, will be assessed.

The model validation outcome will provide a clear picture of the performance of the individual parts of the oil condition monitoring concept in this research. It will show how reliability could be improved by implementing the model to monitor the lubricant condition.

The conclusions and key findings of this research work will be presented in Chapter 8. The contribution to knowledge in the area of oil condition monitoring will be summarised by the discussion and critical reflection of the fulfilment of the research objectives in this work. A brief outlook of potential further research on the basis of the findings and novel pathways presented in this work will also be considered and proposed.

Chapter 2

2 Engine Oil – a Fundamental Constructional Element

2.1 Introduction

This chapter provides an introduction of the fundamentals of engine oil with respect to its main purposes in relation to the essential design and constructional features of any modern combustion engine. The focus will be particularly on the main responsibilities of engine oil which play a crucial role to ensure reliable engine operation. The oil viscosity can be regarded as an essential oil characteristic and is of critical importance. All degradation effects presented later in Chapter 3 affect at least this parameter. Insufficient oil viscosity due to degradation effects, regardless if this is too high or too low, can result in serious engine wear and a major risk of failure. All relevant physical and chemical lubricant fundamentals are presented here to provide understanding for later considerations and discussions. Alongside the description of the functions covered, this section also provides relevant technical terms and definitions. A brief summary of the involved additive components to enable or support each task shall outline the complexity of modern oil formulations and indicate how susceptible the oil is for contamination and what additive depletion means in terms of performance loss.

2.2 Main Functions of the Engine Oil

The functionality of engine oil is not limited to fulfil only a single task during the engine operation as for many other mechanical engine parts. Engine oil is an essential constructional element of modern engines and must contribute to the overall reliability requirements of the vehicle. Reliability is defined as 'the probability that an item can perform its intended function for a specified interval under stated conditions', (DoD, 1981). The definition of reliability addresses two important topics. First, reliability is unconditionally related to the 'intended functions' and second it is related to the 'stated conditions'. Engine oil is a multi-functional element and is responsible for a number of tasks and is intended to fulfil a range of complex duties. Figure 2.1 summarises the main responsibilities of modern lubricants. Engine oil provides lubrication in order to reduce friction and thus prevent wear, it provides cooling in order to support the thermal control of the engine, it must seal moving parts, it has to maintain engine cleanliness to ensure freedom of movement of the engine parts and protect against corrosion by neutralising acid components and prevent the formation of these components (SAE J 357, 2006). Each of these functionalities will be briefly discussed in order to provide a better understanding of the individual tasks. The 'stated conditions' for the oil to ensure the required reliability cannot be precisely defined. Since the lubricant is influenced and degraded by various effects during its operation in a combustion engine. It is therefore difficult to maintain the reliability which will be investigated in Chapter 3.

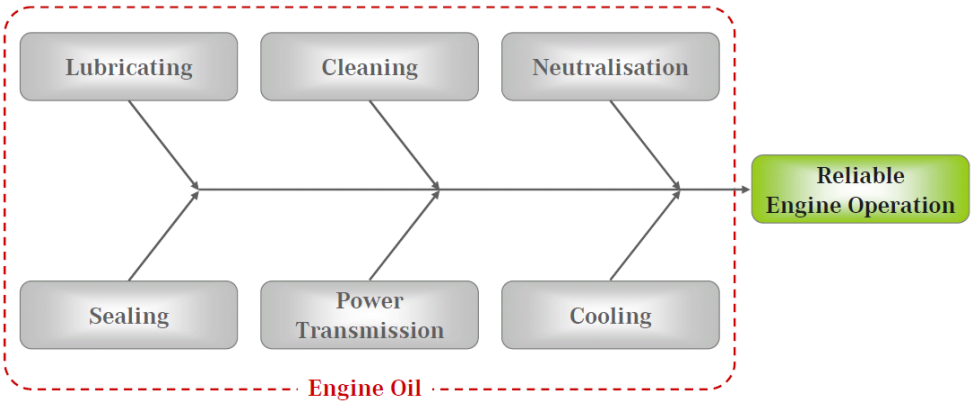

Figure 2.1: Range of responsibilities of modern engine oils
The grey boxes highlight the most important engine oil functions which need to be fulfilled by the oil to enable a reliable engine operation.

2.3 Lubricating

One of the major functions of the engine oil is to reduce friction and to protect the engine from wear in a combustion engine. As lubrication is the major responsibility of the oil some general aspects are summarised in more detail to ensure a comprehensive insight into its physical and chemical aspects.

2.3.1 Viscosity - Physical Characteristics and Definitions

The viscosity is a measure of the inner friction of a liquid and defines the required relative speed of two surfaces at which a stable hydrodynamic lubrication film is formed. The viscosity can be regarded as the essential parameter to prevent wear during the engine operation. Viscosity is a measure of a fluid's resistance to flow in the presence of an influencing force. As any substance opposes a force when it is deformed either by shear stress or longitudinal stress, the viscosity describes a fluid's internal resistance to flow and may be thought of as a measure of fluid friction. It can therefore be described as the internal friction of a moving fluid. A fluid with high viscosity resists motion because its molecular composition results in more internal friction in the presence of an applied force (Möller and Nasser, 2002: 160 - 163). High viscosity engine oil therefore requires more force and greater relative movement of the lubricating surfaces to form a hydrodynamic lubrication film but this results in a higher load carrying capacity. A fluid with low viscosity flows more easily because its molecular composition results in a lower level of friction when it is in motion. This requires less force and relative speed of the friction surfaces in forming a hydrodynamic lubricating film. However, the load carrying capacity of a lubrication film of low viscosity engine oil is lower compared to engine oil with high viscosity (Leonhardt et al., 2005: 37 - 40). Viscosity in a technical context in automotive applications can be expressed in two distinct forms, which are the ‘dynamic viscosity’ (sometimes known as absolute viscosity) and the ‘kinematic viscosity’ (Viswanath et al., 2007: 1 - 3). Dynamic viscosity η typically expressed in [mPa·s] is the tangential force per unit area required to slide the fluid between two flat plates which are parallel to one another. The shear stress σ [Pa] is the ratio of the tangential force F [N] needed to maintain the moving plate A [m²] at a constant velocity υ [m/s] to the plate layer ‘B’ as shown in Figure 2.2 when the two layers are maintained at a unit distance x [m] apart. As illustrated in Figure 2.2, the force F causes the liquid layers at surfaces ‘A’ and ‘B’ to slide at different velocities υ_1 and υ_2, respectively.

Velocity υ_2 is lower compared to velocity υ_1 in the presence of force. This causes a velocity gradient of the different liquid layers in the laminar flow of the medium within the two plates.

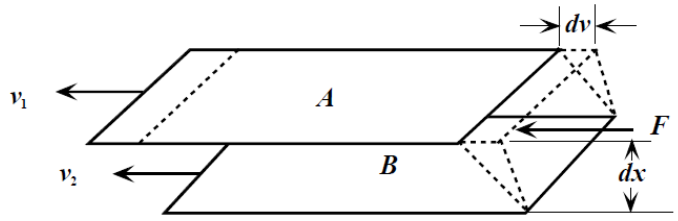

Figure 2.2: Shear of a liquid film to illustrated the dynamic viscosity (Viswanath et al., 2007)

Dynamic viscosity is the tangential force per unit area required to slide the fluid between two flat plates which are parallel to one another. The shear stress σ [Pa] is the ratio of the tangential force F [N] needed to maintain the moving plate 'A' [m²] at a constant velocity υ [m/s] to the plate layer 'B' when the two layers are maintained at a unit distance x [m] apart. The force F causes the liquid layers at surfaces 'A' and 'B' to slide at different velocities υ_1 and υ_2. This causes a velocity gradient $d\upsilon$ of the different liquid layers in the laminar flow of the medium within the two plates.

The velocity gradient or shear rate $\dot{e}$ [1/s], can be expressed by the fluid velocity$\upsilon = \frac{dx}{dt}$ and the distance of the gap x [m]; where

$$\dot{e} = \frac{1}{x}\frac{dx}{dt} = \frac{\upsilon}{x} \tag{2.1}$$

As the dynamic viscosity is defined as the ratio of shear stress and shear rate the final equation for the dynamic viscosity η [Pa·s] can be written as:

$$\eta = \sigma \frac{x}{v} \tag{2.2}$$

The dynamic viscosity, from a technical point of view, is the most significant viscosity form as it is related to the mechanical stress of the lubricant during the operation with respect to shear stress and shear rate. Measuring techniques do not determine the dynamic viscosity directly but provide its ratio to the oil density ρ [kg/m³].

The viscosity-density ratio is referred to as the 'kinematic viscosity' ν [mm²/s] and is currently the most widely used viscosity unit in nearly all practical applications as the measurements are more accurate and easier obtained (Klamann, 1982: 4). The kinematic viscosity is defined by equation 2.3:

$$\nu = \frac{\eta}{\rho} \tag{2.3}$$

Engine oil viscosity is in practice not constant as it is a function of temperature, pressure and shear rate and can therefore not be considered as a Newtonian liquid (Blume, 1987; Mang and Dresel, 2001: 21 – 28). The 'Viscosity Index' (VI) is an empirical number indicating the effect of temperature change on the viscosity of the oil. High VI means less change of viscosity with temperature (O'Donnell and Zakarian, 1984). High VI oils are required in practice to have low viscosity at low temperature in order to provide easy cold starting of the engine. On the other hand a sufficiently high viscosity is required to have a good lubrication and high load carrying capacity at full operating temperature. However, the natural viscosity-temperature characteristic of base oils is not sufficient to achieve these requirements. Modern oils have therefore VI-improver additives blended with the oil to meet both the high and low temperature requirements. VI-improvers are based on long-chained hydrocarbon polymers. These polymers can be visualised as small balls of polymers which are tightly folded at low temperatures and get unfolded as the temperature increases. The reduction in viscosity of the basic oil with increasing temperature becomes largely compensated by the volume increase of the VI-improver (Klamann, 1982: 84 - 86). Shearing of the oil occurs due to the relative movement of molecules or groups of molecules between each other in relation to the engine parts. If the viscosity decreases with increasing shear rate or shear stress the liquid is defined as pseudo-plastic or structure-viscous (Möller and Nasser, 2002: 163 – 166). Additive components such as VI-improvers, ashless detergents or dispersants, soaps, colloids and combustion products like soot, contribute to more shear dependence and thus structure-viscous behaviour of the engine oil (Klamann, 1982: 6). Temporary viscosity decrease usually occurs for engine parts with high mechanical stress and the 'High Temperature High Shear' (HTHS) viscosity is of importance for reliability considerations. The HTHS-viscosity is a dynamic viscosity and is measured at 150 [°C] and at a defined shear rate of 10^6 [1/s] (Möller and Nasser, 2002: 168). This viscosity value correlates with the real shear stress of the oil in high load engine operation at the camshaft, con rod bearing and between piston rings and cylinder wall.

High HTHS values provide in general, better wear performance as the hydrodynamic lubrication regime is reached quicker and the load carrying capacity is higher even under high shear rate. Low HTHS values, on the other hand, contribute significantly to better fuel economy.

2.3.2 Physical Principle of Lubrication - Stribeck Curve and Lubrication Regimes

The aim of all types of lubrication is to reduce friction between sliding surfaces in order to minimise wear (Möller and Nasser, 2002: 454 - 456). Friction is in general expressed and quantified by the dimensionless friction coefficient μ [1]. The friction coefficient is defined as the ratio of the applied force F [N] and the load F_N [N] (Liu et al., 1990).

$$\mu = \frac{F}{F_N} \tag{2.4}$$

All surfaces are characterised by an individual roughness, regardless of how plane they seem. A closer look with a microscope shows the roughness peaks on every surface. If two surface areas are in contact, the contact therefore only occurs at these roughness peaks which are in direct contact in the absence of a lubricant (Krause and Scholten, 1979). One of the main purposes of the engine oil is to separate these surfaces in order to prevent the roughness peaks touching each other and causing wear (Möller and Nasser, 2002: 15 – 19). This requires the engine oil to form a hydrodynamic lubrication film (Leonhardt, et al., 2005). The achievement of this hydrodynamic lubrication film reducing the friction coefficient μ depends on a sufficient angular frequency ω [1/s] of the friction surfaces, the dynamic viscosity η [Pa·s] of the engine oil and the specific pressure per area p [Pa] on the surfaces. These coefficients are summarised within the dimensionless 'Sommerfeld-Number' λ [1] (Vogelpohl, 1954; Bartz and Möller, 2000) in equation 2.5:

$$\lambda = \frac{\omega \cdot \eta}{p} \tag{2.5}$$

The four main lubrication regimes of 'boundary lubrication', 'mixed lubrication', 'elastohydrodynamic lubrication' and 'hydrodynamic lubrication' in an automotive engine are characterised in the field of Tribology by the 'Stribeck-Curve', see Figure 2.3. In 1902 Stribeck found that the friction coefficient depends on the relative speed or movement of the friction surfaces (Möller and Nasser, 2002: 14). On the vertical axis of the Stribeck-Curve, the friction coefficient μ is plotted and on the horizontal axis the Sommerfeld-Number λ.

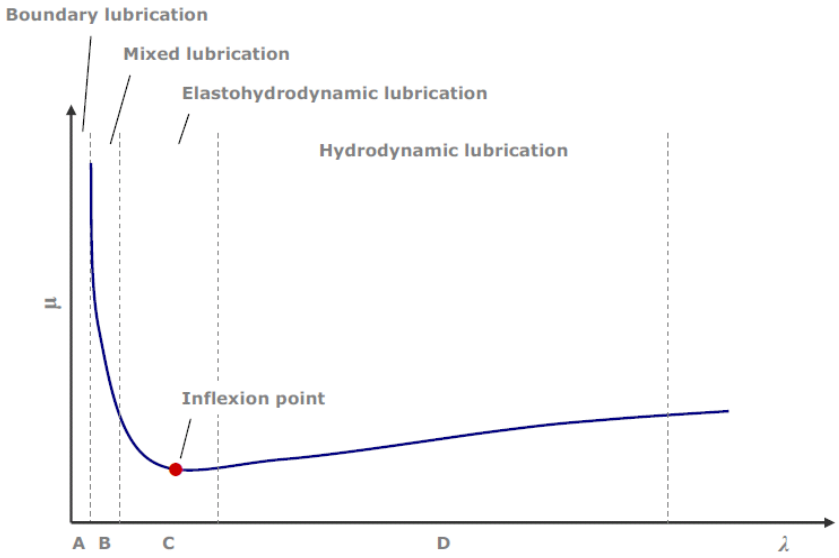

Figure 2.3: Stribeck-Curve with illustration of the main lubrication regimes
The individual regime depends on a sufficient angular frequency ω [1/s] of the friction surfaces, the dynamic viscosity η [Pa·s] of the engine oil and the specific pressure per area p [Pa] on the surfaces. These coefficients are summarised within the dimensionless 'Sommerfeld-Number' λ [1]. The change of the regime causes a change of the friction coefficient μ [1]. The preferable operating regime is the hydrodynamic regime after the inflexion point.

The lubrication regime in area 'A' in Figure 2.3 of the Stribeck-Curve is referred to as the 'boundary lubrication' and is present for low speeds of relative movement of the friction surfaces. This occurs during the engine operation, for instance, at the engine start or at the reversal point of the pistons. Boundary lubrication can also occur as a result of heavy loads, restricted contact areas or insufficient viscosity. Insufficient viscosity can result from shear loss and will be discussed later in this section, or from fuel dilution which will be presented in Chapter 4. In the operating state of boundary lubrication only the friction surfaces are covered by oil molecules and the load is carried by a very thin lubrication film. This results in a high friction level indicated by the high number of the friction coefficient in the Stribeck-Curve. Due to the contact of the surfaces, this causes the highest wear in practice with this lubrication regime and the wear performance of an engine oil formulation depends fully on the additive components (Leonhardt et al., 2005). To prevent metal-metal wear in this critical regime, anti-wear additive components are included in the oil formulation. Anti-wear additives made from organic compounds form a protection layer on the metallic surface to keep the friction areas separated in the absence of oil under critical operating conditions (Mang and Dresel, 2001: 103 – 110; Möller and Nasser, 2002: 28).

The ‘mixed lubrication’ in area ‘B’ of Figure 2.3 is characterised by a very steep negative slope of the friction coefficient μ. The thickness of the lubrication film is equal to the surface roughness and the load is not fully carried by the lubrication film. The roughness peaks of the surface are still in contact in this lubricating regime.

The ‘elastohydrodynamic lubrication’ in area ‘C’ of Figure 2.3 was included in the Stribeck-Curve to cover the elastic deformation of contact faces. This lubrication regime is only relevant for contact geometries particular for plain bearings like roller bearings and gear teeth (Mang and Dresel, 2001: 14). If the relative speed of the friction surfaces is further increased, the hydrodynamic pressure of the oil is continuously built up towards the inflexion point of the friction coefficient curve. At this point, indicated in area ‘D’ of Figure 2.3, the surfaces are completely separated by the lubrication film and friction is mainly determined by the oils internal resistance – the viscosity. This ‘hydrodynamic lubrication’ regime is the preferred operating condition for any moving engine part as the separation of the friction surfaces by the oil prevents any wear (Möller and Nasser, 2002: 14).

2.4 Cleaning

The cleaning function of the engine oil is based on two principles with two essential types of additives involved, the 'Dispersants' and the 'Detergents'. The engine cleaning properties of an oil formulation are also referred to as 'Detergent-Dispersant Characteristic' (DD-Characteristic) (Möller and Nasser, 2002: 459). Both types of additives are described as molecules containing a polar and non-polar section. They aggregate with orientation based on the polarity of the medium. The cleaning mechanism is the task of the dispersants which are metal-free, ashless additives (Leonhardt et al., 2005: 14). A dispersant consists of a long, non-polar oleophile (oil loving) tail and a polar head with less polarity compared to that of the detergents. The function of the dispersant is to wrap solid and liquid contaminations which have infiltrated into the oil during the engine operation and to keep them in suspension to prevent sedimentation and the formation of so called 'cold sludge'. Sludge can block the oil gallery, filter, piston grooves, rings and valves, and can cause severe engine failures or further rapid oil degradation. Two main mechanisms are present, the peptisation and the solubilisation (Möller and Nasser, 2002: 460). Peptisation is the wrapping and the keeping in suspension of solid oil contaminations, like dust, soot or solid oil ageing products, with a diameter of 50 – 150 [nm]. The non-polar tail of the molecules prevents agglomeration due to electrostatic repulsion. Solubilisation is known as the wrapping and suspension of liquid contaminations such as acids or condensate with a droplet size of < 20 [nm]. The purpose of the dispersants is to keep all the contaminations in suspension to get them out of the engine with the next oil drain. The second clean keeping mechanism is the task of the detergents. The structure of the detergent molecule is equal to the structure of the dispersant molecule explained earlier. The only difference in the molecule structure is their shorter tail and the higher strength of the polar head. Detergents are metal based additives typically in colloidal composition (Klamann, 1982: 91 - 93). Their function is to prevent or remove lacquer, carbon and varnish deposits on the hot engine parts by oriented adsorption of the detergent molecules at the metal surfaces. This is especially important on the engine's pistons in order to prevent ring sticking under severe high-temperature operating conditions. Detergents are multifunctional and their second important function is to neutralise acids either from blow-by gases from the combustion or acids from the oxidation or nitration process.

2.5 Neutralisation

During the engine operation the oil is in continuous contact with acid combustion products (Möller and Nassar, 2002: 460). There are two main mechanisms where the neutralisation effect of the oil is required to prevent the build-up of acids in the oil. The first is to neutralise aggressive acid products from the combustion gas that are in direct contact with the oil (Möller and Nassar, 2002: 462). The second is to neutralise acids that get formed in the oil as a by-product from the oxidation or nitration process, which will be explained later in Chapter 3. The acids formed in the oil cause corrosion and increase wear of the engine, especially of the bearings, and can also result in the formation of deposits in the engine, especially in the hotter parts. The engine oil thus needs to provide an alkaline reserve which is a characteristic value of engine oil and is defined by the 'Total Base Number' (TBN) in [mg KOH/g] (Möller and Nassar, 2002: 137). The TBN is mainly formed by the detergent additives mentioned earlier with the cleaning properties of the oil. Overbased detergents are typically used having additional calcium-carbonate or magnesium-carbonate in the compound that is surrounded by the detergent molecules in the form of micelles (Leonhardt et al., 2005: 12). This provides a high alkaline level of the oil and thus prevention of acid build up in the oil but it also causes the formation of ash if some oil is burned during the engine operation. Ash formation is problematic with DPF which is also the reason why engines equipped with DPF need to use low ash engine oils which also means lower TBN and thus less alkaline reserve (Sappok and Wong, 2010). During the operation of the additives in the engines, the detergents are conventionally depleted and provide no more protection against the formation of acid build up in the oil once they are at a low level. Increasing acidity is thus a strong indicator for a necessary oil drain as the functionality of the oil is strongly affected. The acidity of engine oil is defined by the 'Total Acid Number' (TAN) in [mg KOH/g] (Möller and Nasser, 2002: 136 – 137).

2.6 Sealing

Engine oil needs to provide an important sealing function at two separate friction points in an engine (Möller and Nasser, 2002: 463). First, sealing between the piston rings and the cylinder wall is required to prevent large amounts of blow-by gas passing through, see Chapter 3, section 3.3. Insufficient sealing at this point would cause power loss, thermal stress for the piston and would accelerate the oil degradation process significantly due to higher contamination with nitrogen oxide from the combustion gas as well as with more unburnt fuel passing by. The second important sealing function of engine oil is between the valve stems and the valve stem guides. Insufficient sealing at this point would result in pressure fluctuations at the intake and exhaust gas system and would affect the combustion and may result in unburnt fuel reaching into the engine oil. The appropriate viscosity of the engine oil plays an important role to ensure the sealing functions. If the engine oil viscosity is too thin due to shear losses or fuel dilution the sealing lubrication film can tear off and the amount of blow-by gases will increase resulting in fast depletion of the additive components responsible for the neutralisation of the acid components. Once these additives are depleted, the oxidation or nitration reaction chain can accelerate generating even more acids and oil insoluble products which can result in engine failure. The oil degradation processes are explained in more detail in the next chapter.

2.7 Power Transmission

The engine oil acts as a hydraulic medium in current engine concepts. It is used to control the tappet clearance adjustment, the timing chain tensioner and the camshaft adjustment unit (Leonhardt et al., 2005: 35). Sufficient viscosity is of importance to fulfil the function as a hydraulic medium. Low viscosity due to degraded oil can result in leakage of the oil from the pressure reservoirs for the hydraulic applications. This can be detected by noise from a clacking hydraulic valve lifter or oscillating timing chain. It can further result in functional deficiency such as power loss due to incorrect working camshaft adjustment. A similar effect occurs in the case of high gas content in the oil. This effect can result from foam formation of the oil due to the permanent movement of the circulating oil and the splashing of the oil in the sump. Foam makes the oil compressible and causes fail functions in the hydraulic systems and can lead to severe engine problems (Magorian, 1980). Foam also affects the lubrication as the lubrication film may tear off and can cause increased wear especially of the bearings.

To prevent stable oil foam build up and to improve the air removal ability the additive composition of engine oils contains foam inhibitors in a concentration of 0.0001 - 0.001 % (Klamann, 1982: 98). Effective foam inhibitors are based on silicon oils and need to fulfil three basic requirements (Awe, 1963). They need to be insoluble in oil, have a low surface tension and need to be dispersible. The foam destructing effect of the small silicon oil droplets is based on their oil insolubility and their low surface tension. The surface-active (oil-air) agent adsorbs the foam bubbles and starts to expand due to the lower surface tension of the additive. The oil foam surface layer gets ripped due to this expansion and the air bubble bursts (Möller and Nassar, 2002: 210).

2.8 Cooling

The cooling and heat dissipation function of the oil is especially important for the engine parts that are not in direct contact with the engine coolant. These parts are mainly the pistons and the crankshaft. Due to the high circulation rate of the oil, the intensive movement is a sufficient cooling function of these parts, although the cooling effect of oil is lower compared to the cooling effect of the engine coolant liquid (Leonhardt et al., 2005: 36). Heat occurs at all lubricating points due to friction. The main heat transport mechanism of the oil in the lubricating points is based on heat convection and conduction (Möller and Nassar, 2002: 19 – 23).

2.9 Summary

This chapter illustrates the main functions of engine oil which is an important versatile component performing numerous tasks to maintain reliable and efficient engine operation. The key performance areas include an explanation of lubricant functions including all related technical and physical terms, definitions and units. This provides a common understanding for the subsequent chapters of this thesis. It should be recognised that of all the tasks performed, oil viscosity control can be regarded as the most crucial parameter of oil performance. Viscosity is directly related to engine wear and has thus a direct influence on the reliability. Chapter 3 will present the major oil contamination effects leading to oil degradation especially with regard to the influence of biofuels. This is one of the major current challenges for engine oils and the resulting overall engine reliability. It will become transparent how sensitive the lubricant and in particular the viscosity is regarding contamination. The summary of the current status of knowledge on lubricant degradation effects, especially when using biofuels, will outline why oil condition monitoring contributes to maintaining engine reliability.

Chapter 3

3 Impact of Biofuels on Crankcase Lubricants Performance

3.1 Introduction

This chapter presents the influence of the current generation of biofuels on lubricant performance. The research is based on an exploratory summary of theoretical facts and experience reported by different industries. It starts with an overview of the global biofuel landscape and gives an understanding of the actual global market share and the typical biodiesel and bioethanol markets. The next step in this chapter is to provide a brief summary of the manufacturing process, the chemical compositions and general properties of biodiesel and bioethanol to illustrate the reasons for the initiation of the degradation processes. A summary of the possible ways that the fuels can affect the engine oil, which forms the starting point for all further negative effects, is also presented. The resulting interaction and the resulting oil degradation mechanisms and the impact on the previously outlined important lubricant functionalities will be explained in detail to illustrate the serious risk for the engine. Most of the contamination effects discussed in this chapter also occur with regular fossil fuels. The overall degradation risk of the lubricant is thus present with any fuel. Nevertheless the effects which are described are much more severe and in most cases much more serious with biofuels compared to fossil fuels.

3.2 Global Biofuel Scenario

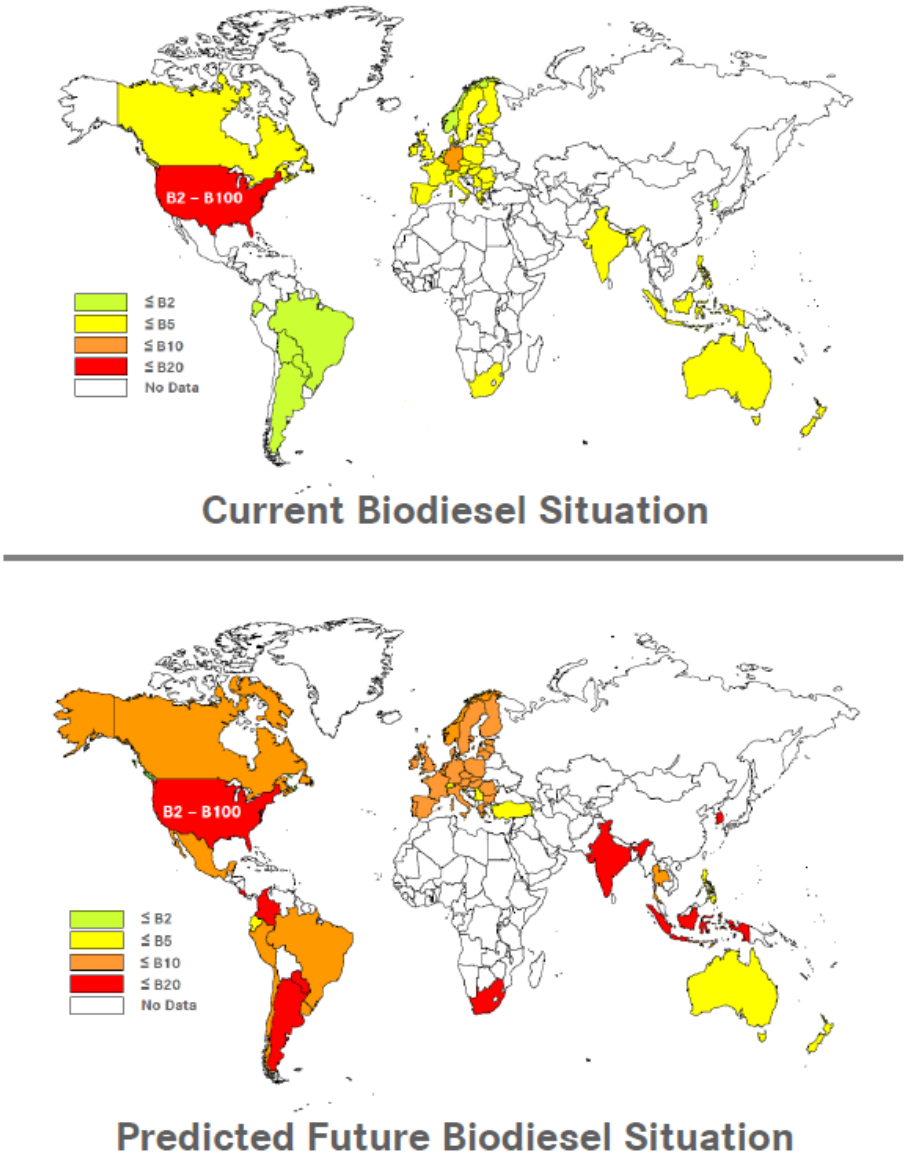

Figure 3.1: Summary of the global biodiesel situation
The key market for biodiesel today is Europe with blend rates up to B7. In the US market B20 fuels are available and B100 can occasionally be found for dedicated fleets. It is expected that the global blend rates for all global main markets will go up to B10 and B20.

The key market for biodiesel is currently Europe. Based on current EU biofuel directive most member states, including the UK, today use B5 biodiesel blends (EU, 2003; Department for Transport, 2010). Since 2009 the Germany national diesel standard has allowed blends up to B7 (DIN EN 590, 2010). Other key markets such as Canada, Australia, India, South Africa and the Pacific Region follow the European standardisation and use biodiesel blends up to B5.

The effective US diesel fuel standards cover blends between B6 and B20 (ASTM D7467, 2008). There is also a B100 ASTM standard in effect (ASTM D6751, 2001). The expected future biodiesel blends will be significantly higher as legislation promotes the increase of biofuel to comply with climate protection declarations. It is expected that the biodiesel blend in Europe will increase to B10 within the next few years as indicated in Figure 3.1. Other markets such as Brazil, Canada, Peru, Chile and China will also probably allow blends up to B10. Argentina, Colombia, South Africa, Mexico, India and the Pacific Region are expected to allow up to B20.

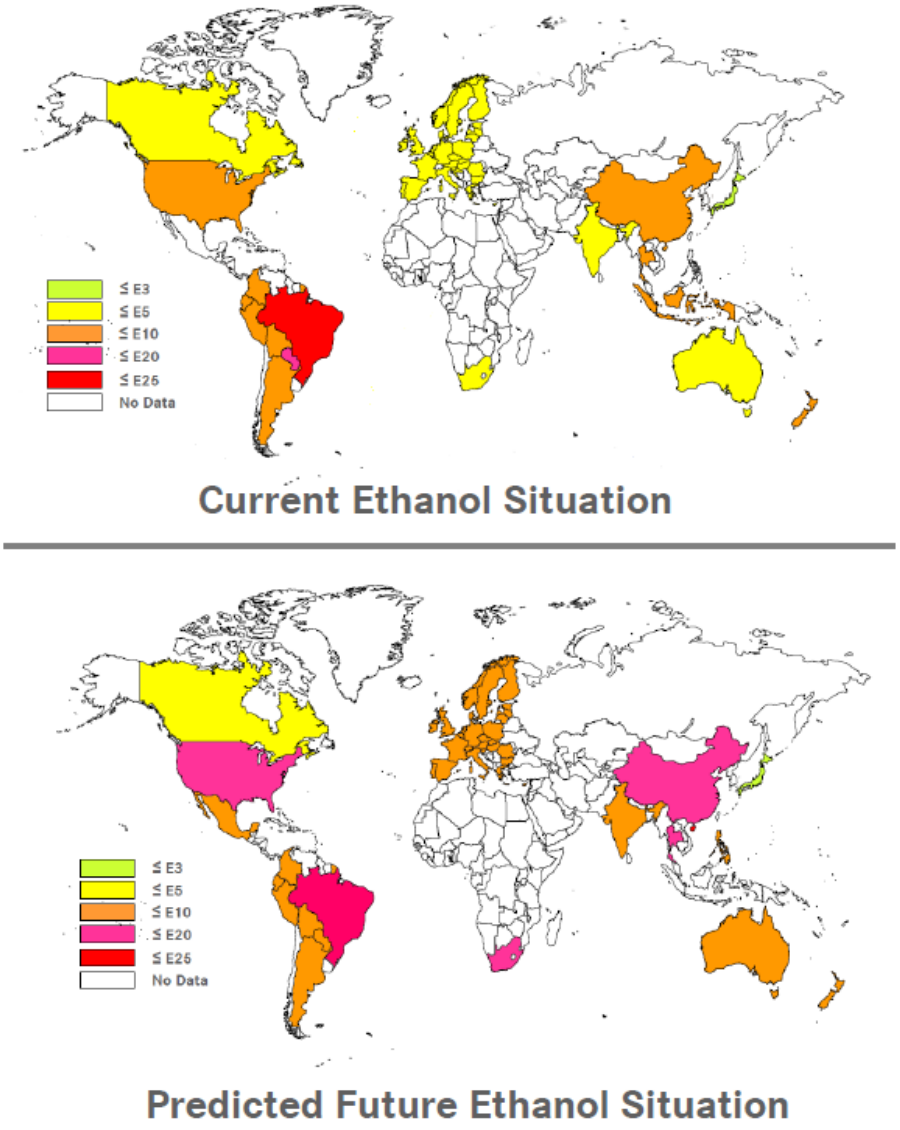

Figure 3.2: Summary of the global ethanol situation
The key markets for ethanol are today the US and Brazil. In most European countries the blend rates are up to E5 (Germany with up to E10). It is expected that the US, China and South Africa will use blends up to E20. Mexico, Europe, India and Australia will probably increase their legislated bioethanol contents to E10.

Key markets for ethanol are today the US and Brazil where Brazil has a flex-fuel market allowing ethanol blends from E25 to E100 (Kremer and Fontes, 2004). Local regions with E85 such as Sweden for specially adapted flex-fuel vehicles were not considered in the ethanol map in Figure 3.2 (Kapus et al., 2007). In the US market as well as in most of the South American countries, China and the Pacific region ethanol blends up to E10 are found in the market today. In most European countries, India, South Africa and Australia, typically blends up to E5 are found in the market based on the gasoline fuels regulations in effect.

Since 2011 E10 'Super 95' fuel replaces the former E5 'Super 95' fuel in Germany (DIN 51626-1, 2009). Upcoming biofuel replacement rates, to improve use of renewable fuels in order to reduce the dependency on fossil fuels and to reduce greenhouse gases, will also affect the ethanol situation in the next 5 - 10 years. It is expected that the US, China and South Africa will use blends up to E20. Mexico, Europe, India and Australia will probably increase their legislated bioethanol contents to E10.

3.2.1 Biodiesel Production

Vegetable oils offer good ignition characteristics and have occasionally been used in the past in diesel engines that were adapted to run on pure vegetable oil (Ollus and Juoperi, 2007). However, the application of neat vegetable oil in modern diesel engines is very complicate due to the high viscosity and the low oxidation stability of pure vegetable oil and is therefore today only rarely used. With pure vegetable oil, and with B100 biodiesel the existing severe exhaust gas limits cannot be met due to the higher formation of NOx emissions (Graboski et al., 2003; Büngert et al., 2007). As the use of pure oils made of fatty acid triglycerides is problematic, conversion to methyl esters before use as diesel fuel is necessary. The designation of biodiesel thus refers to 'Fatty Acid Methyl Esters' (FAME). FAME can be produced from vegetable and animal fats and oils by transesterification where the most commonly used process due to its superior economy is the base-catalysed transesterification mechanism (Schwab et al., 1987; van Gerpen et al., 2004). In this process, biodiesel is produced through a transesterification reaction of a natural oil triglyceride either vegetable oil or animal fat with a short chain alcohol, typically methanol, in the presence of a catalyst like sodium or potassium hydroxide (Taupp 2001; Boocock, 2003). The resulting products are glycerin and three monoalkyl esters, the biodiesel or FAME, with carbon chains of typically 12 - 22 atoms (Waynick, 1997; Berry, 1999). Transesterification lowers the molecular weight to about one third and the viscosity to approximately one eighth and increases at the same time the fuel volatility. The resulting parameters are now in a range that is suitable for use as diesel fuel (Kinast, 2003). The feedstock depends mainly on the climate conditions and occurrence in the different countries. In moderate climates, rapeseed, soybean and sunflower FAME is common. For climates in hot and tropical regions, olive, coconut palm oil and jatropha are prevalent. Non-vegetable feedstocks are typically fish oil and tallow.

Figure 3.3 illustrates the FAME feedstock in different regions and climate conditions of the world (van den Bulk, 2008).

Figure 3.3: Summary of the globally used biodiesel feedstock (van den Bulk, 2008)
The feedstock depends mainly on the climate conditions and occurrence in the different countries. In moderate climates, rapeseed, soybean and sunflower FAME is common. For climates in hot and tropical regions, olive, coconut palm oil and jatropha are prevalent. Non-vegetable feedstocks are typically fish oil and tallow.

3.2.2 (Bio-)ethanol Production

Ethanol can be made from biomass based on locally available vegetable feedstock that contains high amounts of starch or sugar to ferment it to alcohol (Kaltschmitt and Hartmann 2001). From a global prospective the most common feedstock is corn (as it is used in the US) followed by sugar cane in Brazil. The US have recently overtaken Brazil as the largest producer of ethanol. About 20 % of the US corn crop goes into ethanol fuel production. The basic product for the European ethanol production is wheat, barley, rye or sugar beet (McTavish and Ney, 2009). Technology now also exists to use wastes and residues to produce ethanol from lignocellulosic material (Murphy and McCarthy, 2004: 149). The first step of the ethanol production process is milling of the feedstock and mixing with water to form mash. Enzymes are added to the mash to convert the starch to simple sugar like dextrose or glucose. This process is known as saccharification. The next process step is fermentation where yeast is added to ferment the sugar to alcohol, i.e. (ethanol). After fermentation, the resulting ethanol is transferred to distillation columns where the ethanol is separated from the remaining water. After the removal of undesired by-products the final step is the concentration and dehydration to remove the final moisture from the alcohol in order to achieve 99 % pure ethanol.

3.3 Pathways of Oil Contamination by Fuel

There are three main ways for the fuel to contaminate the engine oil. One option is transportation of unburnt fuel with the blow-by gases. Blow-by is combustion gas from the combustion chamber that passes along the pistons and reaches the crankcase (van Basshuysen and Schäfer, 2002). Blow-by gas always contains a certain amount of unburnt fuel as complete fuel combustion is not possible in practice (Pruckner, 2007). The function of the piston rings is to provide a sealing of the combustion chamber to the crankcase. However, complete and reliable sealing cannot be guaranteed based on current technology. The typical ways for the blow-by gas to pass the pistons are between the piston ring and the cylinder wall, between the piston ring groove and the ring and through the piston ring space as summarised in Figure 3.4.

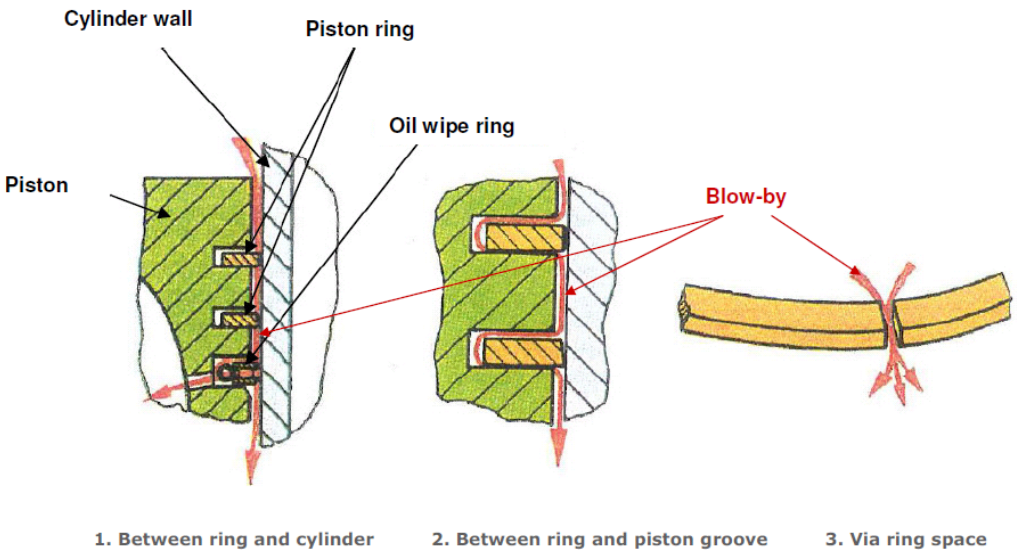

Figure 3.4: Illustration of blow-by pathways (Kunz cited by Herrmann, 2009)
The typical ways for the blow-by gas to pass the pistons are (1) between the piston ring and the cylinder wall, (2) between the piston ring groove and the ring and (3) through the piston ring space.

A key factor for the amount of blow-by gas and thus the amount of unburnt fuel contaminating the engine oil is the temperature. With low temperatures, the thermal expansion of the rings is low and the gap between the piston rings and the cylinder wall is wider. The oil viscosity is higher at low engine temperatures which results in thicker oil film on the cylinder wall. As discussed earlier sealing is one of the oil functionalities but if the oil film is too thick between the cylinder wall and the piston it cannot seal properly against the high pressure peaks from the combustion process.

When the engine operates under cold conditions the unburnt fuel typically condenses at the cold cylinder wall. With the next piston movement the fuel is wiped downwards to the oil sump by the oil wipe ring. Another serious blow-by problem occurs when the engine temperature is very high due to high load operation. Thermal expansion of the piston rings widens the rings and reduces the gap between the piston ring and the cylinder wall. Due to the narrow gap and the decreased viscosity caused by the higher temperature, there is only a very thin oil film on the cylinder wall and on the pistons. If the temperature at the piston, especially at the top groove, exceeds a critical temperature the heat capacity of the thin oil film is not sufficient. The oil therefore becomes thermally destroyed at this hot spot which results in the oil cooking at these hot engine parts (Möller and Nassar, 2002: 130 – 131). This effect is worse when biodiesel is present in the oil; glycerines in the biodiesel (that may remain from the synthesis process) are even more temperature sensitive than oil and the cooking effect of hot engine parts can thus be worse when FAME is present (Sem, 2004). The cooking leads to stuck piston rings that cannot properly fulfil their sealing functionality. This results in a high amount of blow-by and thus much more fuel dilution during the subsequent engine operation regardless of the engine load (Marsh and Corradi, 2007). There is the further risk of much faster oil oxidation and nitration caused by the blow-by gases (which will be discussed later).

Another mechanism contributing to fuel dilution comes with the application of the Diesel Particulate Filter, DPF (Krüger and Breuer, 2007: 506 – 507). Soot and solid combustion residues accumulate on the DPF during engine operation. To avoid blocking of the filter element it needs to be regenerated at certain intervals to remove the particulate loading. Regeneration is achieved by the burning of the soot particles and requires elevated temperatures in the range of 600 – 650 [°C] (Mollenhauer and Tschöke, 2007). The exhaust gas temperature in normal operation reaches up to 500 [°C]. If the engine control unit detects loading of the DPF it initiates the regeneration process by late post injection in order to achieve a higher internal temperature to burn the soot from the filter (van Basshuysen and Schäfer, 2002; Mollenhauer and Tschöke, 2007). Post late injection promotes fuel dilution especially in two operating modes: (a) if the engine temperature is very cold due to low load or start-stop operation or especially during wintertime, then more unburnt fuel from the post injection will condense at the cylinder wall and travels down to the sump; (b) the other fuel dilution effect with post injection occurs if the active regeneration cycle gets aborted due to the engine stopping and completely unburnt fuel spray reaches into the oil.

3.4 Biodiesel – Potential Areas of Concern for the Lubricant and the Engine

Biodiesel has a significantly different distillation curve compared to fossil diesel fuel as illustrated in Figure 3.5. Luther (2008) demonstrated with this measurement the different evaporation characteristics of fossil and biodiesel fuel. The red line in Figure 3.5 represents a fossil reference diesel without biodiesel components. The evaporation curve is very steep between 240 [°C] and 300 [°C] where almost 60 % of the fuel gets evaporated. The blue line represents a typical diesel fuel from the petrol station according to DIN 51628 specification containing up to 7 % biodiesel. The evaporation curve is noticeably flatter and between 240 [°C] and 300 [°C] and only about 35 % fuel evaporated. The green line shows the evaporation curve of a B100 RME biodiesel. The evaporation starts at 328 [°C] which outlines the essential problem with biodiesel in the engine oil. Biodiesel that enters the sump remains there and accumulates if the oil temperature does not reach the Biodiesel evaporation temperature during engine operation.

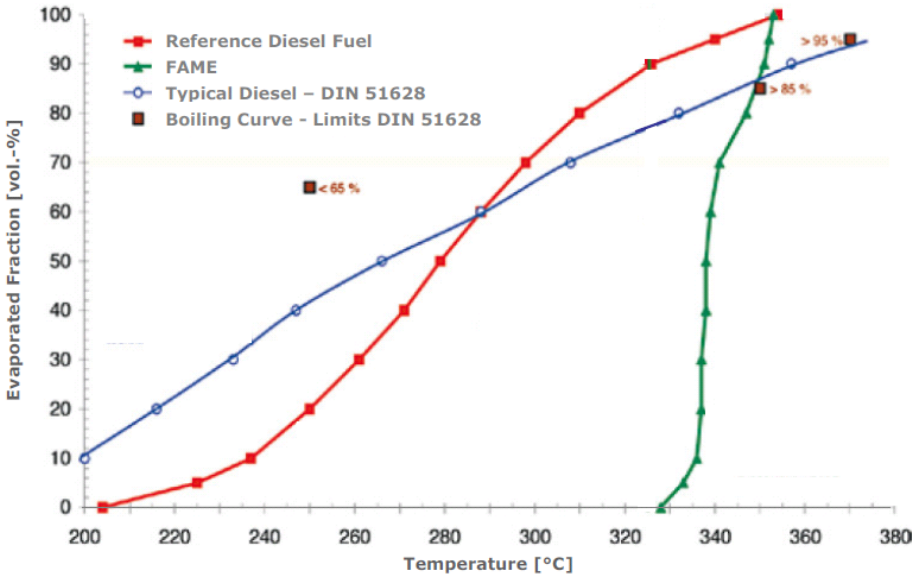

Figure 3.5: Evaporation characteristic of diesel and FAME (Luther, 2008)

The evaporation curve (red line) is very steep between 240 [°C] and 300 [°C] where almost 60 % of the fuel gets evaporated. The blue line represents a typical diesel fuel from the petrol station according to DIN 51628 specification containing up to 7 % biodiesel. This evaporation curve is noticeably flatter and between 240 [°C] and 300 [°C] and only about 35 % fuel evaporated. The green line shows the evaporation curve of a B100 RME biodiesel. The evaporation starts at 328 [°C] which outlines the essential problem with biodiesel in the engine oil.

3.4.1 Fuel Dilution

In 2008, Shell Global Solutions conducted a vehicle field trial with B5 and B15 fuels. The aim of the study was to investigate the fuel dilution and fuel evaporation characteristic with different load profiles (Klemens, 2008). The applied load profiles were defined as snail cycle, nursery operation and motorway operation. In the snail cycle the speed was always below 60 [km/h] / 37.29 [mph] with engine stops at every red traffic light. After every cold start the car was driven for a maximum of 15 minutes or 10 [km] / 6.22 [mi]. The engine cooling was accelerated by opening the bonnet for at least 15 minutes with each stop. The nursery cycle is not specified in detail. The cycle consists only of city driving with driving distances between 1 [km] / 0.622 [mi] and 6 [km] / 3.73 [mi] per trip. The motorway profile simulated a high load operation to promote evaporation of the fuel from the oil. Figure 3.6 shows detail of the typical fuel dilution progress over the different cycles with different biodiesel blends. The blue bars represent the amount of fossil diesel in [wt.-%]. The red bars the amount of FAME in [wt.-%].

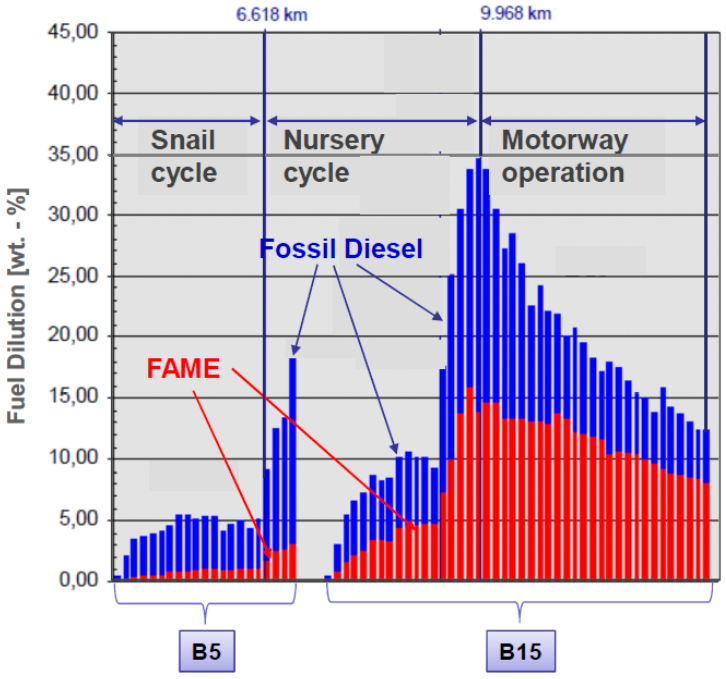

Figure 3.6: Field trial data of fuel accumulation (adapted from Klemens, 2008)
The bar diagram illustrates the fuel accumulation in the oil with low load operation (snail and nursery cycle). The blue bars represent fossil diesel and the red bars biodiesel. The dilution effect is higher with higher amount of biodiesel in the fuel (B5 vs. B15). With hot engine operation (motorway) the fossil fuel starts to evaporate while the biodiesel level remains high due to the different evaporation characteristic.

It was observed that the nursery cycle in particular facilitated fuel dilution. It was also observed that the amount of dilution correlated with the amount of biodiesel in the fuel. The fuel dilution with B15 fuel was significantly higher and reached levels of up to 35 [wt.-%]. The subsequent motorway operation caused slow fuel evaporation. The analysis showed that mainly the fossil fuel was evaporated, whereas the FAME content remained at high levels due to its evaporation characteristics. The data presented further showed that the fuel evaporation is a very slow process even with a continuous hot operation mode. In the meantime, the thinned fuel may cause increased wear and is likely to accelerate the oxidation process. The study underlines the potential reliability risk with the fuel dilution risk due to the biodiesel contamination.

Another process contributing to higher fuel dilution with biodiesel can result from the poor oxidation stability of the fuel itself (Bondioli et al., 1995; Fang and McCormick, 2006). The oxidation stability of biodiesel depends mainly on the fatty acid configuration of the feedstock (McTavish and Ney, 2009-1). When the biodiesel oxidises it forms polymers that increase the fuel viscosity (DGMK, 2005). Thus oxidised biodiesel will result in higher fuel viscosity which can have a noticeable influence on the fuel spray characteristic of the injected fuel (Vaughn et al., 2006). The droplet size is larger and impedes the spray decomposition to evaporate the fuel before ignition (Binder, 2007: 68 - 84). As a result less fuel is completely burned, leaving more unburnt fuel in the combustion chamber that can travel down to the sump. Alternatively, the larger fuel droplets that spray directly onto the cylinder wall can result in fuel travelling down into the oil. Both effects are simultaneous and are summarised in Figure 3.7 (a) vs. (b) (Spicher and Lüft, 2007).

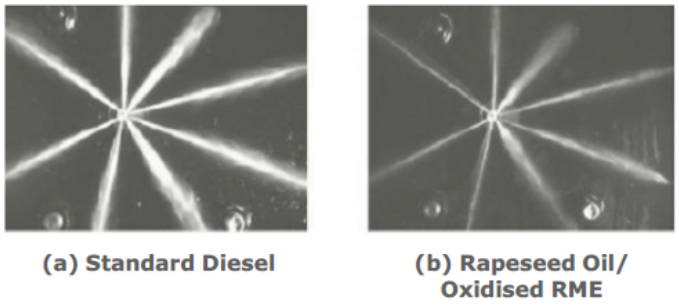

Figure 3.7: Fuel spray characteristic – standard diesel vs. rapeseed oil/oxidised RME (Spicher and Lüft, 2007)
(a) shows a proper gaseous spray which is indicated by the white area in the picture showing the high amount of fine droplets. (b) shows a rapeseed oil fuel with a viscosity in the range of an oxidised RME biodiesel, and injection spray with higher viscosity resulting in a lean spray without proper fuel evaporation.

Figure 3.7 (a) shows the evaporation characteristic of a standardised diesel fuel with a fine evaporation of the fuel and having nearly completely turned into a gaseous stage before ignition. The gaseous spray is indicated by the white area in the picture showing the high amount of fine droplets. Figure 3.7 (b) shows a rapeseed oil fuel with a viscosity in the range of an oxidised RME biodiesel, and injection spray with higher viscosity resulting in a lean spray without proper fuel evaporation. The absence of white areas in the picture indicates that some of the fuel spray directly reaches the cylinder wall, as no evaporation occurs.

As presented earlier with the 'Stribeck-Curve' the formation of a hydrodynamic lubrication film is a function of the relative speed gradient, the dynamic viscosity and the specific pressure. When the oil viscosity becomes thinned by the fuel a higher relative speed of the friction partners is required to form a hydrodynamic lubrication film. This results in a shift of the inflexion point to the right. The hydrodynamic lubrication regime and the separation of the friction components occur later as illustrated in Figure 3.8.

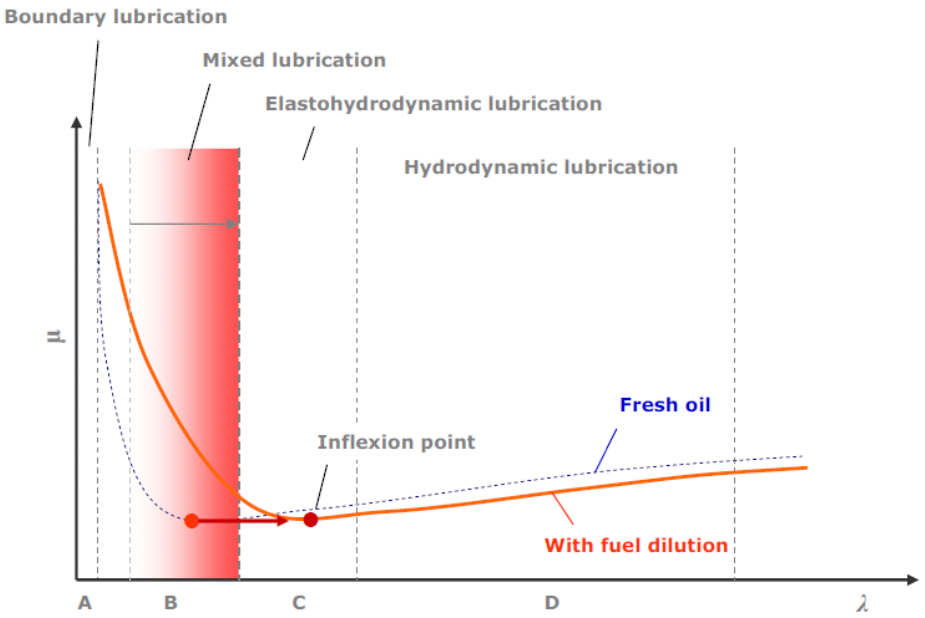

Figure 3.8: Impact of fuel dilution on the hydrodynamic lubrication regime
If the oil viscosity becomes thinned by fuel dilution a higher relative speed of the friction partners is required to form a hydrodynamic lubrication film. This results in a shift of the inflexion point to the right. The mixed lubrication regime is wider. The hydrodynamic lubrication regime and the separation of the friction components occur later.

The noticeably wider 'mixed lubrication' regime results which will likely result in increased engine wear as critical parts sensitive to lubrication (such as the main and con rod bearings) will have to function for significantly longer under non-hydrodynamic conditions. The result is more friction causing increased wear in a mid to long term process. The situation could become more critical with new start-stop systems and turbo-charged engines used in modern downsizing concepts to achieve CO_2 reduction as the main bearings will be subject to more mixed lubrication with more starts. The additive components discussed in Chapter 2 cannot compensate for such dilution impacts and the oil safety margin in terms of load carrying capacity is badly affected.

3.4.2 Oxidation

The fuel dilution effect with biodiesel and the resulting viscosity loss is only one concerning factor with the presence of FAME in the oil sump. The second area of concern is related to the oxidation susceptibility of the different fatty acids that have a significant impact on the oil oxidation process. The susceptibility to oxidation depends on the level of poly-unsaturated fatty acids as indicated in Figure 3.9 summarised by McTavish and Ney (2009-1).

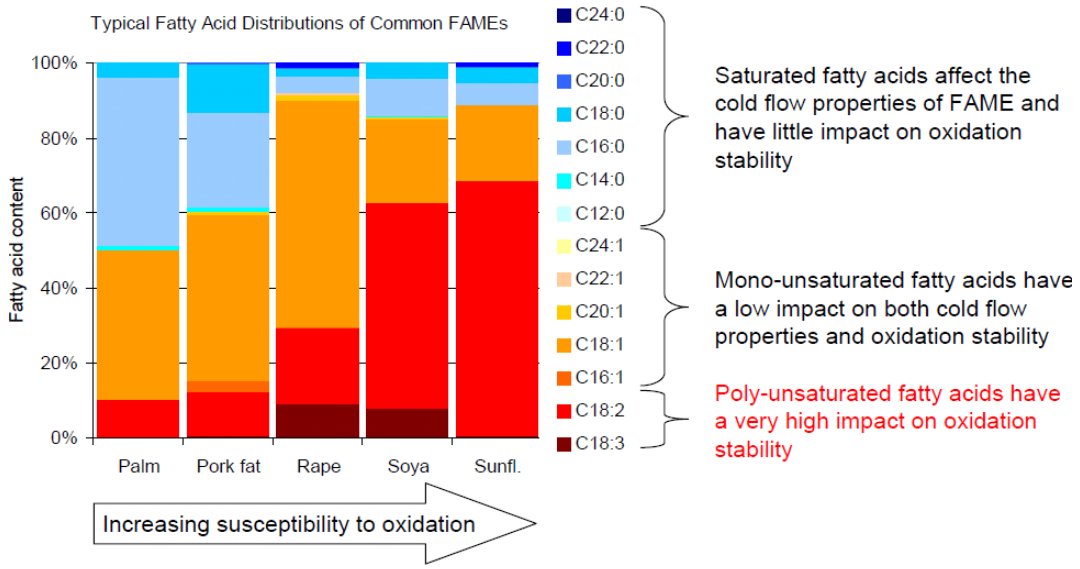

Figure 3.9: Oxidation susceptibility of common FAMEs (McTavish and Ney, 2009-1)
The description of fatty acids often uses an abbreviating nomenclature of the form Cn:m in which n represents the number of carbon atoms and m the number of double bonds in the molecule. The fatty acid molecule determines the reaction rate for degradation processes in the oil due to oxidation.

The oil oxidation process is facilitated by the presence of FAME in the oil compared to conventional fuels as a result of the auto-oxidation of the FAME itself in the oil (Gunstone, 1967; Canakci et al., 1999). Over 95 % of all fatty acids have a chain length of 16 – 18 carbon atoms (DGMK, 2005: 7). The description of fatty acids often uses an abbreviating nomenclature of the form Cn:m in which n represents the number of carbon atoms and m the number of double bonds in the molecule. The main representatives are stearic acid C18:0, oleic acid C18:1, linoleic acid C18:2 and linolenic acid C18:3.

The fatty acid configuration of biodiesel is of high importance for the oil condition as the fatty acid molecule determines the reaction rate for degradation processes in the oil due to oxidation. Fatty acid methyl esters with a high content of saturated fatty acids C14:0, C16:0, C18:0 have a high cloud point, pour point and cetane number and have good oxidation stability (DGMK, 2005: 8). FAME molecules with a high number of unsaturated fatty acids indicated by the number of double bonds C18:2, C18:3 act in the opposite direction (Ullmann, 2007). The relative speed of the oxidation reaction is for a C18:3 molecule up to 98 times higher than for a C18:0 molecule (DGMK, 2005). As outlined in paragraph 3.2 the types of FAME mostly used from a global perspective are RME and SME. They are both composed of 80 – 85 [wt.-%] total unsaturated fatty acids and have a relatively high degree of polyunsaturation. The number of polyunsaturated fatty acids is higher with SME resulting in even worse oxidation stability than RME. In contrast palm oil methyl or coconut oil methyl esters used in the Far East contains 50 – 90 [wt.-%] saturated fatty acids giving high oxidation stability but insufficient cold flow properties (Clarke et al., 2003). The oil oxidation reaction end products have a noticeable impact on the oil condition which is the formation of acids and oil insoluble products (Möller and Nassar, 2002: 212 – 214). Oxidation of the engine oil gets initiated by incomplete combustion of fuels, i.e. hydrocarbons reaching into the oil and getting attacked by oxygen. The level of oxygen attack is determined by the strength of the hydrocarbon bond (Paddon, 2008). The oil impact now results from formed aldehydes during the oxidation process. In the first mode the aldehydes oxidise easily to aggressive carbon acids resulting in acidification of the oil (Tojo and Fernández, 2007). In the second mode at higher temperatures the oil viscosity increases significantly as a result of polymerisation and polycondensation (Atkins, 1988: 735 – 737). FAME oxidation rate increases with the increasing availability of oxygen and with increasing temperature. Lubricant oxidation can in general be influenced by the oil formulation using oxidation inhibitors (McTavish and Ney, 2009-1). If the oil oxidation is significantly increased due to the influence of auto-oxidation of biodiesel, the antioxidant additives are depleted rapidly and cannot prevent further acid formation and increased oil viscosity. Oxidation is thus a major concern for the engine and bears the risk of high engine wear and accelerated breakdown. The oxidation reaction rate is further influenced by current engine design to meet CO_2 regulations. Engine downsizing results in small, very powerful and mostly turbocharged engines driving large and heavy vehicles up to the luxury sector. Smaller engines have less oil volume resulting in less additive reserve but also higher oil temperature due to the lower heat capacity. Turbochargers further heat the oil more and the sum of all these effects results in high oxidation risk of the oil in modern engines.

3.4.3 Nitration

Oil nitration is another area of concern with the application of biodiesel due to the different emission characteristics of biodiesel and biodiesel blends compared to fossil diesel. Nitration is initiated by nitrogen oxides NOx from the combustion process (van Basshuysen and Schäfer, 2002). NOx emissions formed in an engine are highly dependent on combustion temperature, along with the concentration of oxygen in the combustion process (Binder, 2007: 77 – 78). Most publications and studies on the NOx formation using biodiesel report higher NOx emissions compared to standard diesel (Schumacher and Borgelt, 1996; Wang et al., 2000; Kawano, et al., 2007). Higher NOx emissions are mainly due to the fact that biodiesel blends have a shorter ignition delay time. The shorter ignition delay results from the higher cetane number of biodiesel and increases peak pressure and temperature (Wang et al., 2000). NOx enters the crankcase as a mixture with the blow-by gases. It can react to form acids and promote sludge formation of the oil. Many different reaction pathways for NOx exist (McTavish and Ney, 2009-1). NOx can react to form nitrous and nitric acids, which can result in acidification comparable to the formation of carbon acids from the oxidation reaction. Sludge formation occurs directly in the oil where NOx reacts with olefins from the fuel in the oil and generates nitrated hydrocarbons that can further react with each other to form sludge. Sludge causes an increase in viscosity and bears a high risk of blocking the oil filter or oil gallery (van Basshuysen and Schäfer, 2002). Deposits can become formed causing potential piston ring sticking resulting in even more blow-by, fuel dilution and oxidation or nitration.

3.4.4 Soot

The build-up of soot in oils (‘soot loading’) when biodiesel is used should not exist for a proper and complete combustion of biodiesel. Many studies have shown that the particulate matter is reduced with biodiesel as the FAME molecule contains more oxygen and has a higher cetane number (Wang et al., 2000; Babu and Devaradjane, 2003). The concerns summarised here are focused on the side-effects of the biodiesel application that can lead to high soot formation. Soot becomes formed during combustion if the air/fuel ratio approaches zero and if the fuel is not fully homogenised before ignition (Binder, 2007: 69 – 74). The injected fuel needs to be evaporated and mixed with air within milliseconds. It is therefore important that the fuel spray decays very quickly forming small droplets with a large surface. Two potential problems arise with biodiesel that can impede this fuel evaporation process. These effects could not only result in more fuel dilution, but also in the formation of soot. As presented earlier this causes the oxidation of FAME fuel to a higher fuel viscosity.

This leads to poor and incomplete combustion due to insufficient fuel evaporation and can result in more soot formation (Sem, 2004; FAL, 2005). Biodiesel of poor quality can further affect the injectors as observed in studies and field experiences where injector cooking with biodiesel was reported (Choi et al., 1997; Marsh and Corradi, 2007). The negative impact on the fuel spray will lead to incomplete combustion and the formation of soot. Soot loading of the oil with the application of biodiesel or biodiesel blend is therefore also an indicator for incomplete combustion due to problems with the fuel system likely caused by the biodiesel. Soot loaded oil can result in deposits causing further engine problems (Möller and Nassar, 2002: 470). Soot particles can be abrasive and increase engine wear (Sato et al., 1999). Dispersant additives can control a certain amount of soot in the oil but they cannot prevent viscosity increase with excessive soot loading.

3.5 Bioethanol - Potential Areas of Concern for the Lubricant and the Engine

Studies and publicised research work on ethanol as an automotive fuel were in the past mainly focused on materials compatibility and the different fuel characteristics as the most concerning aspect (Kapus et al., 2007). Alcohols are more reactive than hydrocarbons and have solvency characteristics affecting sealings, tubes and some metals (McTavish and Ney, 2009-2). Therefore special precautionary measures are required especially for cars suitable for flex fuel application. Positive aspects regarding the use of ethanol-containing fuels include octane enhancement and a more complete and cleaner combustion (van Basshuysen and Schäfer, 2002). The evaporation characteristic of Bioethanol is also a positive aspect as its boiling end temperature is at 78.4 [°C] and potential side-effects of ethanol are minimised due to quick evaporation (Atkins, 2001: 59). Nevertheless, ethanol can build up in the oil under extreme cold driving and low load operation. One of the main problems with ethanol in the sump is due to its hygroscopic characteristics; ethanol absorbs water from the combustion and the atmosphere, resulting in increased water levels in the oil. Both ethanol and water will evaporate under normal driving conditions over a short period of time, and the lubricating oil can “self-heal”. However, the presence of ethanol and water in the sump is a concern from a lubricant point of view as it promotes the formation of acids.

3.5.1 Acid Formation

Field trials operating in cold driving conditions to promote ethanol build up in the lubricant showed high ethanol levels > 15 % and due to the hygroscopic character even higher levels of water > 20 % with E85 ethanol fuel (McTavish and Ney, 2009-2). The main concern with the presence of ethanol and water is the formation of acid that can be formed in the oil at very low activation energy levels and does not require high temperatures as with the acid byproducts from the oxidation or nitration process. Unburnt ethanol reacts with oxygen and oxidises further and forms acetic acid. The presence of acetic acid and water in the oil bears a high risk of engine corrosion. Especially critical is the corrosion of soft metals like aluminium as used as bearings (McTavish and Ney, 2009-2). Aluminium corrosion with ethanol is primarily due to corrosive wear and occurs when the aluminium oxide layer gets removed and the surface is in contact with acetic acid. As discussed earlier the TBN reserve of the oil suppresses an acidification of the oil as long as a sufficient alkaline reserve exists and the additive components are not depleted.

3.5.2 Sludge Formation

Unburnt fuel from ethanol blends can cause the formation of sludge in the sump. Sludge formation was occasionally reported in the past mainly with the use of ethanol blends up to E25 with low or varying fuel qualities in markets such as Brazil, China or Malaysia (Herrmann, 2009). The addition of ethanol to fossil petrol increases the octane number and low quality fuels topped with ethanol can meet national specifications. Low quality petrol fuel is typically characterised by a high amount of olefins in the oil. Olefins are unsaturated hydrocarbon molecules that react in a similar fashion to unsaturated fatty acids in biodiesel. Acetic acid at low temperatures accelerates the polymerisation of olefins and can result in the formation of resinous products in the oil (Herrmann, 2009). These resinous products, when initially formed, can be held in suspension by the dispersants. However, if they agglomerate the compounds formed are too heavy for the dispersant additives to keep in suspension. The resinous products will thus fall out of the oil and can accumulate in the sump and form sludge or lacquer causing an increase in viscosity and resulting in a higher risk of further engine damage due to blocking of oil circulation components. Another type of sludge that can be formed with the application of ethanol is known as ‘white-sludge’. This effect was reported with the use of E85 fuel under worst case conditions causing high fuel dilution in the oil (McTavish and Ney, 2009-1).

Cold conditions resulted in high levels of ethanol dilution (> 15 %) and due to the hygroscopic effect also resulted in high levels of water (> 20 %) in the oil forming a stable emulsion – appearing as 'white sludge'. Ethanol mixes with water but is not miscible with lubricants. The water level with the combustion of ethanol is inevitably higher compared to the water level in the oil with fossil fuel. Above a certain amount of ethanol in the sump this results in phase separation where the ethanol-water mixture is the lower phase. The ethanol-water emulsion in the oil can be stable for over 18 hours and results in phase separation that can last for a period of weeks (McTavish and Ney, 2009). This effect bears a high risk of oil filter and oil gallery blocking especially in wintertime when the emulsion can possibly freeze and the engine will receive no lubrication immediately after ignition. The engine will therefore become damaged within minutes as no hydrodynamic lubrication film gets formed in the bearings and the resulting friction rapidly destroys the bearings. Dispersant additives can in principle solubilise water droplets and keep them in suspension unless they get evaporated when the oil temperature is high enough. In certain conditions the amount of water present can be too high for the dispersants to handle.

3.5.3 Wear

In comparison with the biodiesel dilution effect described earlier, ethanol/water dilution is only critical in applications at low engine temperatures and is not critical under normal driving profiles due to rapid evaporation. Ethanol is also more viscous than fossil petrol improving the viscosity drop with higher blends of ethanol (McTavish and Ney, 2009-1). Thus although the viscosity decrease is less significant in comparison to biodiesel, other aspects can result in worse wear under ethanol dilution. As mentioned earlier, ethanol is not completely miscible with lubricants. This increases the risk of increased engine wear, especially for those engine parts requiring high HTHS viscosity. Due to its solvency characteristics ethanol can also potentially remove oil molecules from metal surface and thus reduce the remaining oil film between metal surfaces. Complete separation of roughness peaks from the surfaces cannot be ensured and wear increases. Increased amounts of iron and aluminium wear have been observed in studies, but only with E85 in combination with low temperature operation (McTavish and Ney, 2009-2). Another concern is present with the application of modern 'Direct Injection' (DI) engines. As the fuel spray is directly injected in the combustion chamber high ethanol concentrations can reach the cold cylinder liner unburnt and can remove partially the thin oil film (Kappus et al., 2007). This will cause abrasive wear of the liners and the piston rings.

3.6 Summary

This chapter has explored and summarised the major areas of concern regarding lubrication with the application of the current generation of biofuels. The risk of massive fuel accumulation along with the significantly increased oxidation tendency is a serious challenge for engine reliability. Based on the concerns summarised with biodiesel and bioethanol, the following risk evaluation outlines which of the biofuels is potentially more critical on the basis of the reviewed studies. The criteria that are qualitatively assessed are summarised in Table 3.1.

Table 3.1: Biofuel risk assessment criteria

Criteria	Biodiesel	Bioethanol
Risk of reaching into oil	+++	+
Risk of fuel accumulation	+++	+
Immediate influence on viscosity	+++	+
Susceptibility to acid formation	+++	++
Susceptibility to form oil insoluble products	+++	+
Risk of resulting viscosity increase	+++	+
Engine wear risk	++	++
Engine cleanliness risk	+++	+
Resulting risk with higher blends	+++	○
Overall risk assessment	**+++**	**+**

Risk Rating:
○ - neutral
\+ - weak
++ - medium
+++ - high

The biodiesel risk rating is higher than the bioethanol rating due to the fact that the fuel accumulates in the oil regardless of the load profile. The potential of bioethanol accumulation is much lower and occurs only rarely under very specific conditions. The resulting potential impact on the lubricant is therefore more critical with biodiesel on the basis of the detailed investigation of existing research work. The further research presented in this work will therefore focus on diesel applications.

While increasing biofuel blends seems, at least from a legislative perspective, a convenient and quickly realisable instrument to 'reduce' global CO_2 emissions and to comply with environmental protection protocols and conventions, it is questionable if the entire 'CO_2 footprint' of agriculture, transport and the process of vegetable feedstock to biofuel is in sum CO_2 neutral as is often claimed. Available studies and research reports discussing this topic have typically taken the stance of the lobby funding the individual research work. It is therefore almost impossible to derive a reliable statement about the actual CO_2 benefits and ethical discussions like the 'fuel vs. food' debate have been mentioned but not fully explored. Nevertheless, it seems likely that biofuel blending limits will be increased in future, with ethanol blends up to E25 and biodiesel blends up to B20 highly realistic. The intensity of the biofuels discussion and the actual timeline for the adoption of fuel standards permitting higher blends will be driven by the progress of the crude oil debate.

Chapter 4

4 Oil Condition Measurement Techniques and the Influence of Oil Contaminants

4.1 Introduction

The first application of oil sensors in passenger cars was in the 1990s and was mainly driven by comfort aspects. The first types of sensors measured typically the oil level and temperature. The motivation for the use of these novel devices was first of all to monitor the actual oil level in the sump and therefore to replace manual measuring using an oil dipstick. As many vehicle users neglect a regular oil level check, the more convenient level monitoring with the sensor ensures a sufficient amount of lubricant to prevent increased engine wear or even engine failure. Another aspect was to have an additional onboard diagnostic functionality to inform the driver when the oil level drops below a critical, predefined oil level. The most common procedures for oil level sensing use a dielectric or an ultrasonic sensor device (Stöckl and Winterling, 1973; Zabler, 2001). The first generation of these sensors had besides the level sensing elements also an integrated temperature sensor (Fleming, 2001). The measurement of the oil temperature provides a second data point in addition to the coolant water temperature to monitor the engine operation temperature. The functionality of the oil level measuring method was soon extended to provide the permittivity value to detect oil condition changes. The purpose of this was to extend the oil drain intervals in order to reduce the servicing costs for the customer based on their driving profile. Some load level indicators where evaluated from the vehicle parameters and together with the measured oil permittivity, the oil drain interval could be forecasted (Irion et al., 1997). One of these applications was launched on the market in the 2000s in the Mercedes-Benz E-Class as part of the ‘ASSYST’ system (Warnecke et al., 1998).

Due to higher oil stress caused by modern engine hardware and the globally varying fuel quality this has led to the motivation to further monitor the quality within the existing drain intervals. The ambition for oil condition monitoring today would be to use an oil sensor to detect oil degradation before it affects the engine.

A summary of current oil condition sensors technology and their general measuring principles is provided in this chapter. Impedance, permittivity and conductivity are covered within the 'dielectric measurement'. These dielectric parameters measure changes from the fresh oil values caused by contaminants during operation. The main theories about polarisation and ion conductivity will be discussed. Infrared spectroscopy is only used by a single sensor model and will be briefly introduced in this chapter. Viscosity and density are discussed within the physical oil condition parameters. From the indirect parameters only the indirect viscosity measurement is explained. Due to a lack of insight of the sensor integrated algorithms all parameters obtained indirectly by the sensor will not be discussed here. However, the theoretical findings of the reviewed work will be discussed in order to identify the main challenges with oil condition monitoring. The discussion will also outline why the conclusion of being able to detect individual contaminants from discrete correlations in reviewed key literature was questioned. One of the research objectives of this work will be accomplished from the findings at the end of this chapter.

4.2 Chemical Related Oil Condition Parameter

4.2.1 Dielectric Measurement

Permittivity is typically used in dielectric spectroscopy applications to evaluate and characterise systems having low conductivity and where the measurement is dominated by polarisation effects which is also the case with lubricants over their lifetime. The polarisation effect will be discussed separately. Admittance $\underline{Y}$ [S] or impedance $\underline{Z}$ [Ω] are in general only used in dielectric spectroscopy with mediums having a conductor or semi-conductor characteristic (Halalay and Schneider, 2007). The following formula have been derived from (Atkins, 2001; Kastner, 2001; Fichtner, 2002).

The parameter electric flux density $\vec{D}$ [As/m²] and the electric field $\vec{E}$ [V/m] are typically used to describe dielectric processes and are related to the presence of polarisable substance by the permittivity ε_r as defined in equation 4.1. The permittivity of free space is defined as $\varepsilon_0 = 8.8542 \cdot 10^{-12}$ [As/Vm].

$$\vec{D} = \varepsilon_0 \cdot \varepsilon_r \cdot \vec{E} \tag{4.1}$$

Equation 4.1 can also be rewritten introducing the polarisation $\vec{P}$ [As/m²] which is proportional to the increase of the flux density caused by the presence of the dielectric medium.

$$\vec{D} = \varepsilon_0 \cdot \vec{E} + \vec{P} \tag{4.2}$$

In most cases $\vec{P}$ is proportional to $\vec{E}$ and the relative permittivity can be defined as:

$$\varepsilon_r = 1 + \frac{1}{\varepsilon_0} \cdot \frac{P}{E} \tag{4.3}$$

Evaluation of the dielectric characteristic is usually measured with a capacitive device that can be defined by the general capacitor equation 4.4 with the capacitance C [As/V]. The cross sectional area of the capacitor plates is A [m²] and the distance between the plates is d [m].

$$C = \varepsilon_0 \cdot \varepsilon_r \cdot \frac{A}{d} \tag{4.4}$$

Applying an alternating voltage $\underline{u} = u \cdot \sin(\omega \cdot t)$ [V] to a capacitor results in losses due to the frequency dependent influence of the conductance G [S] as the specific resistivity of the dielectric material is not infinite as illustrated in the equivalent circuit of a real capacitor in Figure 4.1.

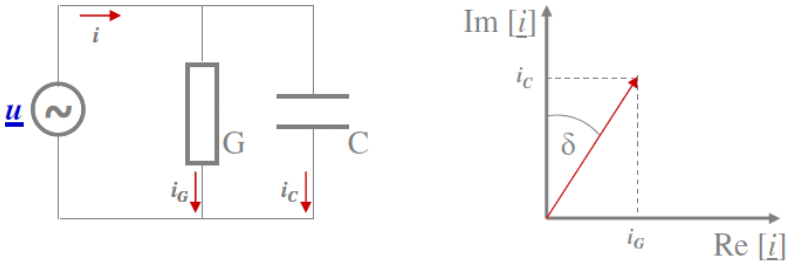

Figure 4.1: AC capacitor configuration and loss tangent vector diagram

The applied alternating voltage u to the capacitor causes the current $\underline{i}$ to split into a current i_G which is in phase with $\underline{i}$ and a phase shifted current i_C related to the imaginary part of C. The loss tangent $\tan\delta$ defines the ratio of the imaginary part to the real part and is also referred to as the dissipation factor.

The applied alternating voltage u to the capacitor causes the current $\underline{i}$ [A] to split into a current i_G which is in phase with $\underline{i}$ and a phase shifted current i_C related to the imaginary part of C.

$$\underline{i} = i_G + j i_C = \underline{u} \cdot (G + j\omega \cdot C) \tag{4.5}$$

The dielectric properties of the dielectric medium are expressed by the complex permittivity $\underline{\varepsilon}_r$ where the real part $\varepsilon_r^{'}$ is equal to ε_r from equation 4.4.

$$\underline{\varepsilon}_r = \varepsilon_r^{'} - j\varepsilon_r^{''} \tag{4.6}$$

The loss tangent $\tan\delta$ defines the ratio of the imaginary part of $\underline{\varepsilon}_r$ to the real part and is also referred to as dissipation factor or quality factor.

$$\tan\delta = \frac{\varepsilon_r''}{\varepsilon_r'} \tag{4.7}$$

The admittance Y [S] of the capacitor configuration in Figure 4.1 can now be derived using equation 4.4, 4.5 and 4.6 as

$$\begin{aligned} \underline{Y} &= \frac{\underline{i}}{\underline{u}} = j\omega \cdot \varepsilon_0 \cdot \underline{\varepsilon}_r \cdot \frac{A}{d} = j\omega \cdot \varepsilon_0 \cdot \left(\varepsilon_r' - j\varepsilon_r''\right) \cdot \frac{A}{d} = \\ &= \underbrace{\omega \cdot \varepsilon_0 \cdot \varepsilon_r'' \cdot \frac{A}{d}}_{G} + j\omega \cdot \underbrace{\varepsilon_0 \cdot \varepsilon_r' \cdot \frac{A}{d}}_{C} \end{aligned} \tag{4.8}$$

The imaginary part of permittivity ε_r'' in equation 4.8 expresses the losses of the capacitor and is a measure of how dissipative the insulating material, i.e. the oil is. The real part of permittivity ε_r' is a measure of how much energy from an external field is stored in the material due to the polarisation effects of the contaminants. The measured loss of the material ε_r'' in equation 4.8 can be expressed as a function of both dielectric loss ε_{rd}'' and specific conductivity σ [S/m] as provided in equation 4.9.

$$\varepsilon_r'' = \varepsilon_{rd}'' + \frac{\sigma}{\omega \cdot \varepsilon_0} \tag{4.9}$$

Fresh oil permittivity ε_r for mineral based lubricants is typically in the range of 2.1 – 2.2 [1] and increases due to the influence of polar or polarisable contaminants in the oil as discussed earlier. The polarisation mechanisms will be discussed in a separated step to understand the effect of permittivity increase during oil ageing. It should be mentioned that for all considerations in this work it is assumed that the sensor is temperature compensated as the volumetric expansion of oil can potentially lower the density of polar or polarisable molecules for the effective sensing area of the capacitor configuration and can falsify the measurement.

4.2.2 Multi-Frequency Impedance Spectroscopy

Electrical ac impedance measurements performed on engine oils requires calibration of the measurement cell, i.e. the plates of a capacitance cell filled with oil connected to a frequency response analyzer or an RLC bridge (Smiechowski, 2005). The impedance of the cell is then measured as a function of frequency based on the general equations introduced in the previous section. This technique is called electrical ac impedance spectroscopy (abbreviated as 'EIS') because it involves a frequency scan with a range of different orders of magnitude in frequency. The typical range for engine oil measurements is from 10^{-1} [Hz] $\leq f \leq 10^{6}$ [Hz] over which ac impedance bridges can be used (Halalay and Schneider, 2007). The electrical ac impedance represents the response of the circuit to a time varying excitation (voltage or current) and is defined through Ohm's law as:

$$\underline{Z} = \frac{\underline{u}(t)}{\underline{i}(t)} \tag{4.10}$$

where all quantities are complex numbers, reflecting the fact that the current and voltage are not necessarily varying in a synchronized fashion (Orazem and Tribollet, 2008). The ac impedance therefore consists of a real part $R = Z \cdot \cos\varphi$ and an imaginary part $Y = Z \cdot \sin\varphi$ where φ is the phase angle of the impedance.

$$\underline{Z} = R + jY \tag{4.11}$$

Oil condition sensor using multi-frequency impedance measurements typically use three defined frequencies, high, medium and low. At each of these frequencies only one parameter is usually measured (Smiechowski, 2005). At high frequencies f < 10^{5} [Hz] the permittivity measured correlates with the polarisability of the lubricant affected by the contaminants. The medium frequency 10^{3} [Hz] < f < 10^{4} [Hz] measures the real part of the impedance and correlates with conductivity losses occurring from ion conductivity. At low frequencies 10^{-1} [Hz] < f < 10^{3} [Hz] the imaginary impedance measured determines the content of surface active additive components.

4.2.3 Polarisation Mechanisms

If the sensor electrodes are separated by a liquid medium the electric charge transport of a free electric charge Q [As] is due only to the force $\vec{F}$ [N] caused by the electric field $\vec{E}$ in the medium.

$$\vec{F} = Q \cdot \vec{E} \tag{4.12}$$

The number of free electric charges contributing to the electric conductivity in lubricants is very low. The dominating electric charge transportation mechanism in low conductivity liquids such as lubricants is caused due to polarisation $\vec{P}$. The following equations and formulas have been derived from (Atkins, 2001; Fichtner, 2002; Ivers-Tiffée and von Münch, 2007).

The three main polarisation mechanisms are the electron polarisation, the ion polarisation and the orientation polarisation. Each polarisation mechanism contributes to the overall permittivity of the oil. The measured permittivity is due to the total polarisation measured by the sensor and is the sum of all induced or permanent dipoles in the lubricant and will be discussed later in this chapter but forms of polarization will be reviewed first.

Electron Polarisation

All atoms consist of a positive charged nucleus and negative charged electron shells. The application of an external electric field causes a deformation or shift of the electron shell as indicated in Figure 4.2.

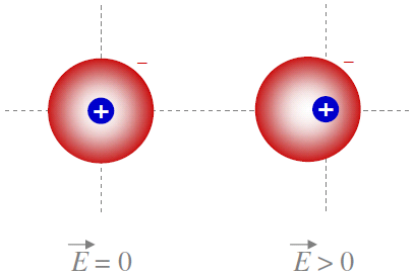

Figure 4.2: Electron polarisation

The application of an external electric field $\vec{E}$ causes a deformation or shift of the electron shell.

The nucleus does not move and an electric charge transport or movement occurs due to the applied field. Electron polarisation occurs with every substance (gaseous, liquid or solid) and is the only polarisation mechanism of atoms with covalent bond. The polarisability α_{el} of a single atom depends only on the atom radius R and is defined as:

$$\alpha_{el} = 4 \cdot \pi \cdot \varepsilon_0 \cdot R^3 \tag{4.13}$$

Ion Polarisation

An external electric field applied to ions in polar substances causes an elastic deformation of the ion configuration resulting in a shifted electric charge and thus increasing the electric susceptibility. Figure 4.3 illustrates the ion polarisation in the presence of an electric field.

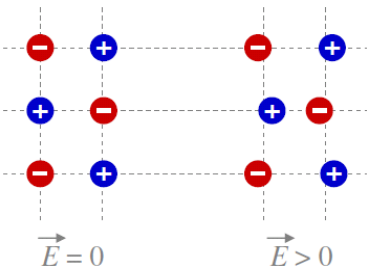

Figure 4.3: Ion polarisation

The application of an external electric field $\vec{E}$ to ions in polar substances causes an elastic deformation of the ion configuration resulting in a shifted electric charge and thus increasing the electric susceptibility.

Ions in the engine oil result mainly from acid components and salts resulting from the oxidation and nitration processes. Ion polarisability depends on the electric charge and on the characteristic repulsion force defined by the 'Boltzmann-constant k' with $k = 1.381 \cdot 10^{-23}$ [J/K]. The polarisability α_{ion} of a single atom depends only on k is defined as:

$$\alpha_{ion} = \frac{Q^2}{k} \tag{4.14}$$

Orientation Polarisation

Polar molecules have a permanent dipole arising from partial charges on its atoms. Permanent dipoles are distributed in the lubricant without the presence of an electric field. The application of an external electric field causes the dipoles to become orientated in the direction of the applied field as illustrated in Figure 4.4.

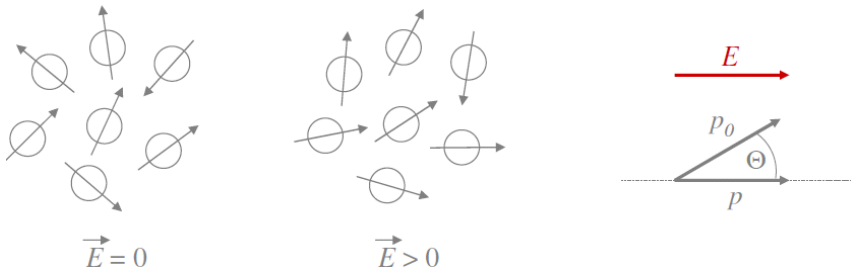

Figure 4.4: Orientation polarisation
Permanent dipoles are distributed in the lubricant without the presence of an electric field $\vec{E}$. The application of an external electric field $\vec{E}$ causes dipoles to become orientated in the direction of the applied field. The thermal movement of the dipoles are opposing a repelling moment in the opposite direction of the applied field. The orientation, i.e. contributing polarisation p, in the direction of the applied field of a permanent dipole p_0, depends on the angle Θ; $p = p_0 \cdot \cos\Theta$.

The thermal movement of the dipoles are opposing a repelling moment in the opposite direction of the applied electric field in order to achieve an equal distribution of the dipoles. The orientation, i.e. contributing polarisation p, in the direction of the applied field of a permanent dipole p_0, depends on the angle Θ and is defined as:

$$p = p_0 \cdot \cos\Theta \tag{4.15}$$

The polarisability of a single dipole is defined as:

$$\alpha_{or} = \frac{p_0^2}{3 \cdot k \cdot T} \tag{4.16}$$

4.2.4 Frequency Response of Polarisation Mechanisms and Ion Conductivity

The frequency response of ε_r' contributing to the energy stored and of ε_r'' indicating the energy loss with regard to the polarisation mechanisms is shown in Figure 4.5. The two spectrums are also referred to as dispersion spectrum and loss spectrum (Ivers-Tiffée and von Münch, 2007: 137 - 138). The abscissa shows the individual frequency regions [Hz] and indicates in which region each of the polarisation mechanisms contribute most to the complex permittivity values. The typical dielectric measurement frequency of oil condition sensors is $f < 10^6$ [Hz]. The dominant polarisation mechanism measured is the orientation polarisation followed by the ion polarisation and then the electron polarisation. However, the overall frequency response of molecules forming the permittivity number typically results from a combination of polarisation effects. Most molecules are susceptible to more than one polarisation effect.

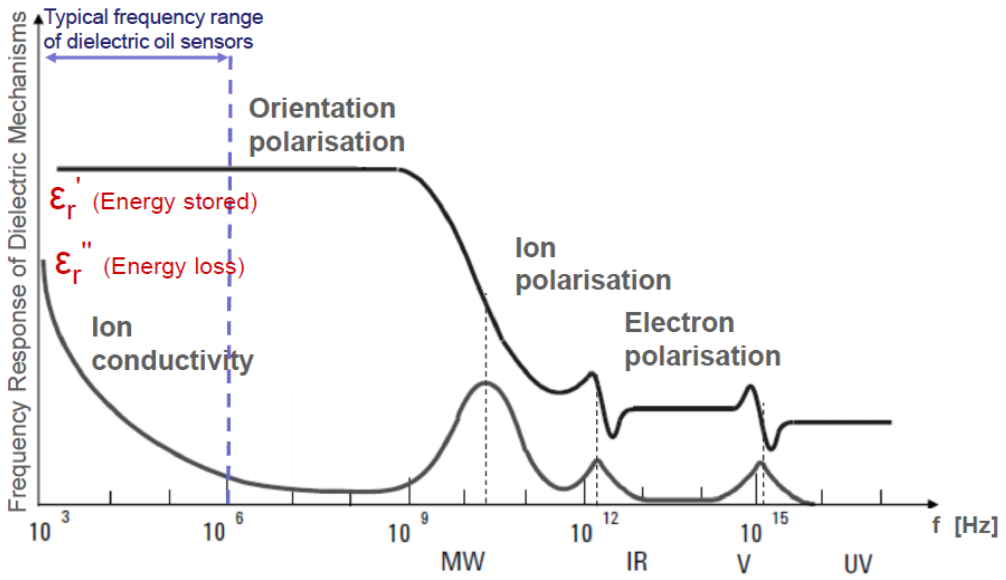

Figure 4.5: Frequency response of polarisation mechanisms relative to frequency
The typical dielectric measurement frequency of oil condition sensors is $f < 10^6$ [Hz]. The frequency response of ε_r' contributing to the energy stored and of ε_r'' indicating the energy loss with regard to the polarisation mechanisms. The dominant polarisation mechanism measured is the orientation polarisation followed by the ion polarisation and then the electron polarisation.

Strong dipoles that reach into the oil during operation are water, esters from the biodiesel and ethanol. Acids formed in the oxidation and nitration process are typically susceptible to orientation and ion polarisation. Soot consists of > 99 % of carbon and is susceptible to electron polarisation (Ivers-Tiffée and von Münch, 2007: 124). The main losses in this frequency region occur from ion conductivity. Changes in the lubricant conductivity are mainly caused by the presence of electrolytes in the oil increasing the ionic concentration and thus the ionic conductivity (Atkins, 2001: 188 – 189). Typical electrolytes are acids, bases and salts.

The presence of contamination products such as carbonic acid from the oxidation or nitrous acid from the oil nitration would generally increase the conductivity due to the higher number of ions. The ionic conductivity is the part of electrical conductivity which is caused by cation and anion. With ionic conductive substances the charge transport is due to mass transfer, i.e. the diffusion of the charged ions. The conductivity is provided as an equivalent molar conductivity with the symbol σ in [(S·cm²)/mol] based on the conductivity κ and the concentration c. Typical ionic conductors or electrolytes are in the liquid state of aggregation. Acids, bases, saline solutions or molten salts apply to this category. The contamination mechanisms in the oil occur with all the oxidation and nitration by-products or acid combustion products reaching into the oil. If more than one ionic substance is present in a medium all individual conductivity values sum up to the overall ionic conductivity based on equation 4.17.

$$\sigma_i = z_i^2 \cdot c_i \cdot Fd^2 \cdot \frac{D_i}{R \cdot T} \tag{4.17}$$

where the charge number of the ions is z_i, the ionic concentration is c_i, Faraday's constant is Fd [C/mol], the diffusion coefficient is D_i [m²/s], the gas constant is $R = 8.314472$ [J/(mol·K)] and temperature is T [K].

4.2.5 IR – Spectroscopy

The electromagnetic wave spectrum can be divided into several different wavelength areas. The infrared area is subdivided into near-infrared (NIR, IR-A) with wavelength of (0.75 – 1.4 µm), short-wavelength infrared (SWIR, IR-B) with (1.4 – 3 µm), mid-wavelength infrared (MWIR, IR-C) with (3 – 8 µm), long-wavelength infrared (LWIR, IR-C) with (8 – 15 µm) and far infrared (FIR) with (15 – 1,000 µm) wavelength (Byrnes, 2009: 21 – 22). The IR analysis is based on interaction of photons and molecules. Energy transfer occurs in the way of molecule rotation, molecule oscillation and electron excitation (Boeker and Grondelle, 1999: 329 – 332). The infrared spectrum for analysis purposes is typically a graphical representation of the IR-transmission over the wavelength. The measured parameters with IR-spectroscopy are usually based on either the transmission or the absorption which is then plotted on the axis of the ordinate in IR-graphs (Bell, 1972). The transmission illustrates the IR-transmittance through the medium as a function of wavelength. The transmission T_{IR} represents the intensity if the IR-beam passing through the medium I, divided by the intensity of the initial IR-beam I_0, see equation 4.18. If no energy is absorbed $(T_{IR} = 1)$ 100% is passed through (Kauppinen and Hollberg, 1997).

$$T_{IR} = \frac{I}{I_0} \tag{4.18}$$

For oil condition analysis purposes the IR-absorption A per measuring distance [A/cm] is a widely used laboratory analysis method. The absorption is defined as the logarithm to the base of 10 of the inverse transmission (Mitra and Kebbekus, 1998).

$$A = Log_{10}\left(\frac{1}{T_{IR}}\right) \tag{4.19}$$

The interpretation of spectra becomes simplified as specific absorption bands, (also referred to as group frequencies,) can be assigned to specific molecular parts (Meislish et al., 1977). Tables are available to look up the absorption bands for the molecules or molecular parts of interest in order to be able to interpret the IR-analysis results. IR-spectroscopy is widely used in laboratory oil analysis. The IR-oil condition sensors could in general be used to detect certain substances like soot or polymers in the oil.

It can also be programmed to measure other bands such as for oxidation by-products. Due to reliability concerns and cost issues, an automotive application is very unlikely. This measurement principle is therefore only presented in this work to provide a more complete technological overview.

4.3 Physical Related Oil Condition Parameters

4.3.1 Quartz Resonator Viscosity/Density Measurement

Influence of Liquid Properties on Quartz Resonator

The influence of mass absorption on quartz resonators was theoretically defined by Sauerbrey (1959). The resulting frequency shift Δf_m [Hz] is given in the 'Sauerbrey Equation' as:

$$\Delta f_m \approx -\frac{2 \cdot f_0^2}{A\sqrt{\mu_Q \cdot \rho_Q}} \cdot \Delta m = -c \cdot \Delta m \tag{4.20}$$

with an electrode area A [m²], mass loading Δm [kg] and a fundamental resonance frequency $f_0 = \left(\sqrt{\mu_Q / \rho_Q}\right)/(2 \cdot d)$ [Hz] depending on the piezoelectric stiffened elastic constant μ_Q [Pa], the density ρ_Q [kg/m³] for quartz and the thickness d [m]. Equation 4.20 shows that for a defined resonant configuration the frequency shift is linear with mass loading. Based on Sauerbrey's work Kanzawa and Gorden (1985) presented an empirical model to determine the resonant frequency shift due to loading with a liquid having the viscosity η_L and the density ρ_L.

$$\Delta f = f_0^{3/2} \cdot \sqrt{\frac{\eta_L \cdot \rho_L}{\pi \cdot \mu_Q \cdot \rho_Q}} \tag{4.21}$$

The complex oscillation characteristic of quartz in a liquid media cannot be simulated. Models are used to describe the electrical behaviour of the quartz and to obtain feedback of physical media properties in terms of viscosity and density. The most common equivalent circuit model is the 'Butterworth-van-Dyke Model' (BVD-Model) (Liebau, 1998). Figure 4.8 shows the simple BVD-Model to introduce the parameters.

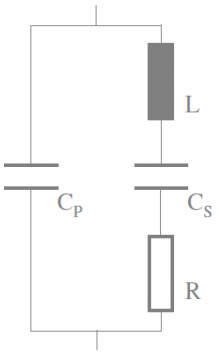

Figure 4.6: Simple Butterworth-van-Dyke model
The oscillating quartz mass is expressed by the inductance L, the mechanical elasticity by the capacitor C_S and dissipative energy losses caused by radiation and friction defined by R. The only 'real' existing physical value is the parallel capacitance C_P from the plate capacitor defined by the electrode/quartz substrate.

The oscillating quartz mass is expressed by the inductance L [H], the mechanical elasticity by the capacitor C_S and dissipative energy losses caused by radiation and friction defined by R. The only 'real' existing physical value is the parallel capacitance C_P from the plate capacitor defined by the electrode/quartz substrate with ε_{rQ} as the quartz permittivity, A_{El} the electrodes area and d_Q the quartz thickness.

$$C_P = \varepsilon_0 \cdot \varepsilon_{rQ} \cdot \frac{A_{El}}{d_Q} \tag{4.22}$$

The other entire model parameters are related to C_P as summarised below (Liebau, 1998).

$$C_S = \frac{8 \cdot K_0^2 \cdot C_P}{(h \cdot \pi)^2} \tag{4.23}$$

with the piezoelectric coupling coefficient K_0 and the number of harmonics h.

$$L = \frac{1}{\omega_S^2 \cdot C_S} \tag{4.24}$$

where ω_S [1/s] is the series resonant frequency.

$$R = \frac{\eta_Q}{c_{66} \cdot C_S} \cdot \left(\frac{\omega}{\omega_S} \right)^2 \tag{4.25}$$

R includes the quartz viscosity η_Q [Pa·s] and c_{66} is a quartz constant. The interaction between the physical oil properties of viscosity and density and the influence on the electrical properties of the resonator are now derived. These equations are the theoretical fundamentals for all quartz resonator applications or modes. The individual application of the most common viscosity measuring application in liquid media is the 'BVD-Model' and according to Figure 4.6 this is expanded to include the fluid properties of viscosity and density of the quartz resonator configuration. The following brief descriptions of the 'Thickness Shear Mode' and the 'Tuning Fork' flexural resonator will only be focused to highlight the specific aspects of each device.

Thickness Shear Mode (TSM) Resonator

Crystalline quartz based 'Thickness Shear Mode' (TSM) resonators, also referred to as 'Quartz Crystal Microbalance' (QCM), are widely used as mass-sensitive devices to measure the properties of liquid or gaseous media (Martin et al., 1994; Kaspar et al., 2000). TSM sensors consist of an AT-cut quartz disc with electrodes patterned on both sides of the disc (Hauptmann, 1990: 158 – 160). An electrode in direct contact with the measuring media is not favourable as the media could affect the electrode, i.e. acid oil contaminants could corrode the electrode. Vectron therefore developed the 'Thickness Shear Mode – Monolithic Piezoelectric Sensor' (TSM-MPS) geometry where both electrodes are placed on the bottom side of the quartz disc within the housing and are therefore not in contact with the oil. Only the quartz surface is exposed to the medium (Schweyer et al., 1997). TSM sensors typically operate in a frequency range of 5 – 30 [MHz] (Kaspar et al., 2000). When excited at resonance the crystal vibrates and causes in-plane displacement of the quartz. Surface oscillation radiates a damped shear wave into the contacting fluid with a decay length typically in [µm] depending on the fluid viscosity and density where f_s [Hz] is the series resonance frequency of the undamped device (Kanazawa and Gordon, 1985). The decay length δ is given by the equation 4.26.

$$\delta = \sqrt{\frac{\eta}{\pi \cdot f_s \cdot \rho}} \tag{4.26}$$

Tuning Fork (TF) Flexural Resonator

'Tuning Fork' (TF) resonators are made of mono crystalline quartz typically cut in the x-y plane and are known for stable resonant frequency (Dobrinski et al., 2007). Electrodes of opposite polarities are positioned on adjacent sides of the prongs. A sinusoidal electrical voltage is then applied to the prongs and induces a mechanical stress which leads to a periodic, elastic bending of the resonator material. This vibration produces a corresponding electrical current through the electrodes. The time between stimulating a sinusoidal voltage and the resulting sinusoidal current depends on the electrical impedance of the system. This impedance is a function of the excitation frequency, the elastic properties of the material, the hydrodynamic properties of the sensor surface, and the physical properties of the surrounding medium. The geometry of the prongs also defines the resonant frequency which for the oil condition sensor application is $f_0 = 32{,}768\,[\text{Hz}]$ (Matsiev, 1999). The TF technology for oil condition monitoring was developed by Symyx and is currently used by Hella/Symyx and Measurement Specialties (Bennett et al., 2006; Dobrinski et al., 2007). Matsiev (2000) found that the acoustic waves from the elastic bending process radiate into the contacting fluid with a decay length δ as defined by equation 4.26 for the TSM. In contrast to TSM resonators, there is no theory or equation available to connect the Tuning Fork flexural resonator response, i.e. frequency shift Δf to the properties of the surrounding liquid. Flexural resonators produce a far more complicated three-dimensional hydrodynamic flow in a liquid than the simple one-dimensional decaying viscous wave produced by TSM resonators (Matsiev, 1999). A controller measures the electrical current produced by the stimulation of the 'Tuning Fork' with a sinusoidal alternating voltage of $f_0 = 32{,}768$ [Hz] via the sensor electrodes. The impedance is then calculated and provides together with the excitation frequency and the measured oil temperature, a digital signal at the sensor data interface. An external microcontroller calculates the dynamic viscosity, density, permittivity, and the conductance by application of a mathematical 'fit algorithm' developed by Hella and based on the electromechanical equivalent model according to the 'BVD-Model' for the TF application (Dobrinski et al., 2007). The mechanical and hydrodynamic influence of the surrounding medium is described in the 'BVD-Model' by a term Z(ω), which is given for the Tuning Fork according to the following equation (Buhrdorf et al., 2005: 292).

$$Z(\omega) = A \cdot j\omega \cdot \rho + B \cdot \sqrt{\omega \cdot \rho \cdot \eta} \cdot (1 + j) \tag{4.27}$$

In equation 4.27 the surrounding medium is described by the dynamic viscosity and the specific density and ω is based on the TF resonant frequency. The values A and B are geometrical factors that in normal measurement conditions only depend on the resonator geometry and mode of oscillation. In practical applications the first step is to determine the vacuum parameters from one frequency sweep of the unloaded TF sensor. In the next step the sensor is submerged into a reference fluid with known density and viscosity, and another frequency sweep of the sensor impedance (now in the fluid) is performed. The parameters A and B are now determined. The sensor is now fully calibrated and ready for measurements. Finally, during the measurements, frequency sweeps are continuously performed, and the unknown values of fluid density, viscosity and dielectric permittivity are evaluated by the 'fit algorithm' within the sensor microcontroller.

4.3.2 Indirect Viscosity Measurement

Oil level measurements with a capacity device within a tube-like sensor configuration offer the possibility of an indirect viscosity measurement using the capillary viscosity measurement principle (Möller and Nasser, 2002: 177). The fundamental principle is based on the 'Hagen-Poiseuille' equation (Spurk, 1996: 160 – 164):

$$\eta = \frac{\pi \cdot r^4 \cdot \Delta p \cdot t}{8 \cdot \dot{V} \cdot l} \tag{4.28}$$

where r [m] is the inner radius of the tube, Δp [Pa] is the pressure loss over the tube length, t [s] is the flow time of the medium, $\dot{V}$ [m³/s] is the volume stream per second and l [m] the tube length. Substituting the pressure loss over the tube length by the product of density, gravity $g = 9.81$ [m/s²] and the hydrostatic pressure height h [m]

$$\Delta p = \rho \cdot g \cdot h \tag{4.29}$$

and the kinematic viscosity ν can then be obtained, which gives:

$$\nu = \frac{\pi \cdot r^4 \cdot g \cdot h \cdot t}{8 \cdot \dot{V} \cdot l} \tag{4.30}$$

Daimler evaluated in a former research project viscosity measurement with the Temic QLT 75G sensor based on oil movement, i.e. the change of the measured oil level with this sensor to derive the viscosity based on equation 4.30 (Lorenz, 2007). The effect of low viscosity results in fast level change over time and high oil viscosity has the opposite effect. The system uses the oil movement in the sump when the vehicle brakes and no lateral acceleration is measured, which is schematically illustrated in Figure 4.7.

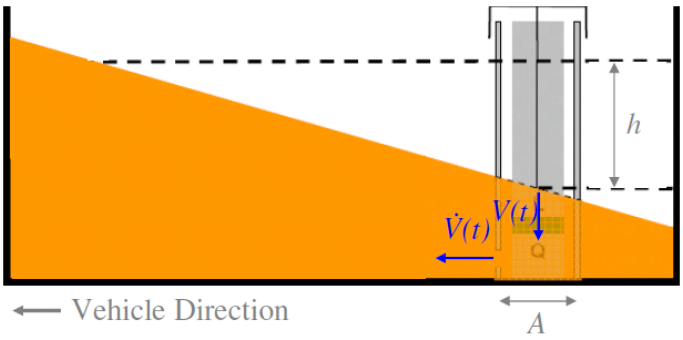

Figure 4.7: Oil movement during braking (Lorenz, 2007)
Braking causes an oil level change h .With the stream diameter of the sensor A the level change defines an oil volume stream $\dot{V}$ which goes into the 'Hagen-Poiseuille' equation to derive the kinematic viscosity ν .

Figure 4.8 shows the measurement of the oil level during braking of the vehicle indicated by the two straight slopes that are calculated by measuring the fluid level at a time t and after a defined time of xxx [ms] again. The measurement is triggered by a signal on the vehicle bus which indicates that the vehicle brakes and no lateral acceleration occur at the same time. The parameters in Figure 4.8 are 'Viscosity Gradient down' (VGN_d) when the oil flows out (down) of the capacitor due to the negative acceleration from the braking and 'Viscosity Gradient up' (VGN_u) when the oil flows back upwards after the braking sequence. The measurement frequency is selected to be fast enough to measure level changes even with inclined gradients.

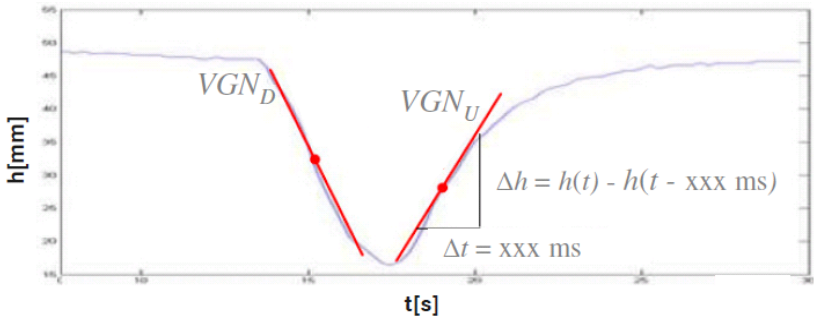

Figure 4.8: Viscosity gradient number during braking (Lorenz, 2007)

The oil level measurement h during braking of the vehicle is indicated by the two straight slopes that are calculated by measuring the fluid level at a time *t* and after a defined time of xxx [ms] again. The parameters are 'Viscosity Gradient down' (VGN_d) when the oil flows out (down) of the capacitor due to the negative acceleration from the braking and 'Viscosity Gradient up' (VGN_u) when the oil flows back upwards after the braking sequence.

$$VGN_d = VGN_u = \frac{h(t) - h(t - xxx\ ms)}{\Delta t} \tag{4.31}$$

$$VGN = \frac{VGN_d + VGN_u}{2} = \dot{h}(t) \tag{4.32}$$

The viscosity measurement is now based on the following equations and with regard to Figure 4.7 where A [m²] represents the stream diameter of the sensor.

$$V(t) = h(t) \cdot A \tag{4.33}$$

$$\dot{h}(t) = \frac{\dot{V}(t)}{A} = VGN \tag{4.34}$$

With equation 4.30 this provides the final equation to derive the viscosity value from the relative oil movement and is given by:

$$\nu = \frac{\pi \cdot r^4 \cdot g \cdot h \cdot t}{8 \cdot VGN \cdot A \cdot l} \tag{4.35}$$

This algorithm was developed by the Daimler R&D Department to use an established and reliable oil level sensor to generate the permittivity value and also a viscosity measurement. The benefit of this approach is to use a well-known and reliable device with the Temic QLT sensor. The viscosity values are not as accurate as data from quartz resonator sensors, however the sensor has proven to work reliably and the indirect viscosity measurement is a very cost efficient solution. The viscosity measurement needs a precise longitudinal oil movement to obtain more accurate results.

4.4 Main Challenge with Oil Condition Monitoring

With regard to the initial research objective the following theoretical discussion introduces a novel view about what is identified by the sensor during engine operation. Figure 4.9 provides a graphically representation of the approach to condition monitoring and outlines the key challenge which will be developed as a theoretical basis to the discussion.

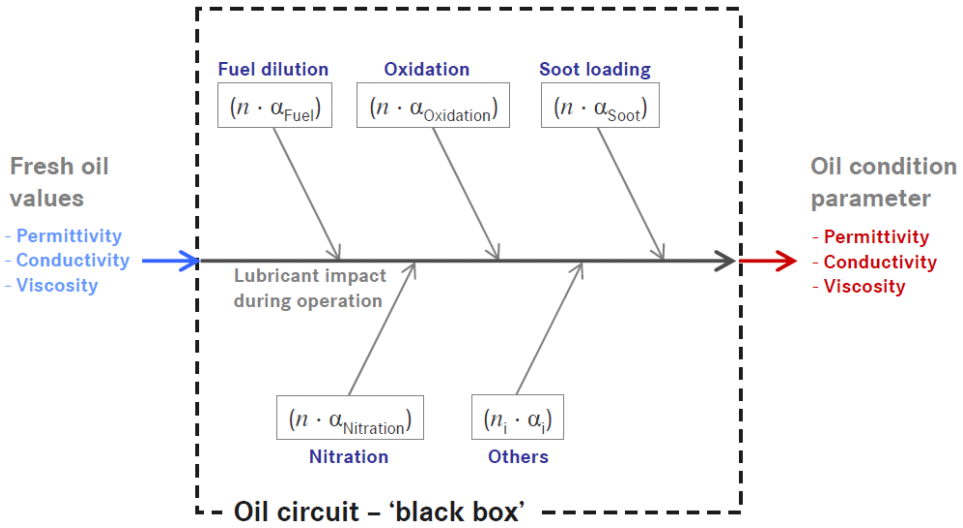

Figure 4.9: 'Black-box' model of the oil circuit

The model parameters that we have certain knowledge of are the initial fresh oil value of permittivity, the conductivity and viscosity. Multiple oil contamination occurs during engine operation which affects the oil to an unknown intensity illustrated by each box where n indicates the number of molecules α . The aim of the condition monitoring and the oil condition parameters measured by the sensor (permittivity, conductivity and viscosity) is to obtain a correlation to the oil condition without having any prior knowledge about the actual oil consistency resulting in any polarisability, conductivity or viscosity. The oil circuit is assumed to be a 'black-box' approach as it is not possible to know the actual condition of the oil without a complete oil analysis. All that is 'seen' by the sensor element is the resulting value of an unknown quantity of influencing parameters which will affect the initial value.

For this model the parameters that we have certain knowledge of are the initial fresh oil value of permittivity, the conductivity and viscosity. As outlined in Chapter 3 multiple oil contamination occurs during engine operation which affects the oil to an unknown intensity. The aim of the condition monitoring and the parameters measured by the sensor is to obtain a correlation to the oil condition without having any prior knowledge about the actual oil consistency resulting in any polarisability, conductivity or viscosity. These effects are illustrated by each box where n indicates the number of molecules α affecting the oil.

The oil circuit is assumed to be a ‘black-box’ approach as it is not possible to know the actual condition of the oil without a complete oil analysis. All that is ‘seen’ by the sensor element is the resulting value of an unknown quantity of influencing parameters which will affect the initial value. In adopting this critical standpoint, the following theoretical considerations support the position of this initial hypothesis. All of the present measurement techniques are ‘sum parameters’ and a subsequent separation of individual effects with only one value, e.g. permittivity, conductivity or viscosity is not possible.

4.4.1 Theoretical Influence of Multiple Contaminants on the Permittivity Value

Table 4.1 outlines typical permittivity values of the key contamination substances and provide an indication in what direction and with what intensity these effects can potentially influence the overall permittivity value.

Table 4.1: Permittivity values and influencing direction of key contaminants

Contaminant	Permittivity value[ ] (@ 298 K)	Influence on lubricant permittivity	Direction
Fresh Oil Value	2.10 – 2.25		
Base oil	1.88 – 1.96		
Fuel Dilution			
Fossil diesel fuel	2.05 – 2.27	o	–
Biodiesel	2.95 – 3.10	+	↑
Oxidation			
Carbon acid	6.18 – 56.20	+++	↑
Polymerisation	-	o	–
Nitration			
Nitric acid	19.00 – 33.60	++	↑
Sludge/Polymerisation	-	o	–
Soot			
Carbon	18.80	++	↑

o - neutral
\+ - weak
++ - medium
+++ - strong

Most of the substances are, with different intensity, susceptible to one or more of the previously discussed polarisation mechanisms. To quantify the overall polarisability contributed by the presented mechanisms, see equations 4.13, 4.14 and 4.16, the 'Clausius-Mossotti-Equation' is usually applied (Atkins, 1988: 594; Ivers-Tiffée and von Münch, 2007: 131):

$$\frac{n \cdot \alpha}{3 \cdot \varepsilon_0} = \frac{\varepsilon_r - 1}{\varepsilon_r + 2} \tag{4.36}$$

From equation 4.36 it can be derived that the resulting permittivity of any medium depends only on the polarisability contributed by each molecule within the volume exposed to the alternating electric field of the sensor element. Based on the possible contamination effects it must be hypothesised that during engine operation the initial fresh oil polarisation distribution defined by the sum of lubricant and contaminant molecules is continuously changing. Following this consideration the product $n \cdot \alpha$ in equation 4.36 can be replaced by $(n \cdot \alpha)_{sum}$ summarising all the effects identified in Figure 4.9.

$$(n \cdot \alpha)_{sum} = \sum_i n_i \cdot \alpha_i \tag{4.37}$$

From the illustrated dispersion and loss spectrum in Figure 4.5 it can be seen that even with a multi-frequency approach the traceability of individual contaminants using dielectric measurement is questionable as the spectrum does not change for $f < 10^9$ [Hz]. All sensors for automotive applications use frequencies $f < 10^6$ [Hz] due to cost and electromagnetic compatibility reasons. There is currently no proven evidence about the actual benefits from using multiple-frequency measurements to obtain more detailed results. The difficult aspect here is to interpret the results correctly if differences can be measured. Table 4.1 outlines the intensity and direction of the permittivity of key contaminants. As the contamination effects in the lubricant are very complex and occur simultaneously it is not possible to draw conclusions from the different measurement results at various frequencies. The conclusion for the permittivity value with regard to the summarised theoretical facts is that all contaminants, except fossil fuel, increase the polarisability and therefore the permittivity of the lubricant. This summative parameter is measured by the sensor and a subsequent differentiation into the individual degradation effects requires additional information such as from an additional sensor. The strategy of processing the input signals within an oil condition algorithm will play a crucial role in predicting the current contaminant situation.

4.4.2 Theoretical Influence of Multiple Contaminants on the Conductivity Value

Table 4.2 outlines the typical conductivity values of the key contamination substances and gives an indication in what direction and with what intensity these effects will drive the overall value. The conductivity values vary significantly with temperature and concentration. The values provided therefore only provide an indication of the expected intensity and direction of influence (Römpp, 2009).

Table 4.2: Conductivity values and influencing direction of key contaminants

Contaminant	Conductivity value (@ 298 K)	Influence on lubricant conductivity	Direction
Fresh Oil Value	2.99 – 3.19 [nS/cm]		
Fuel Dilution			
Fossil diesel fuel	< 0.5 [pS/cm]	o	-
Biodiesel	> 1.5 [pS/cm]	o	-
Oxidation			
Carbon acid	318 – 5.500 [µS/cm]	+++	↑
Polymerisation	-	o	-
Nitration			
Nitric acid	312.000 [µS/cm]	+++	↑
Sludge/Polymerisation	-	o	-
Soot			
Carbon	0.005 – $30*10^{10}$ [pS/cm]	+++	↑

o - neutral
\+ - weak
++ - medium
+++ - strong

The 'Nernst-Einstein-Equation' defines that the resulting conductivity of electrolytes is mainly based on the number of charged ions and the ionic concentration, see equation 4.17. Table 4.2 indicates that especially the acid degradation products increase the ion conductivity significantly. Fuel, regardless if fossil diesel or biodiesel (B100) does not affect the lubricant conductivity noticeably. It must be considered that this value can vary due to the use of additives in the fuel which increase the conductivity to prevent electrostatic charging. However, as with permittivity, the conductivity is a summative parameter and individual components cannot be precisely identified solely on the conductivity value.

4.4.3 Theoretical Influence of Multiple Contaminants on the Viscosity Value

Table 4.3 provides the absolute viscosity value for fresh oil and the relative viscosity change with each of the listed contaminants. The reason for this approach is based on the fact that contaminants like soot or polymerisation products are not liquid or gaseous and therefore by definition have no viscosity. With the presence of these substances in the oil, the kinematic viscosity changes in accordance with the concentration of each contaminant as shown in Table 4.3.

Table 4.3: Viscosity values and influencing direction of key contaminants

Contaminant	Viscosity change [mm²/s / unit] (relative change to fresh oil value @ 100 °C)	Influence on lubricant viscosity	Direction
Fresh Oil Value xW-30 (@ 100°C – SAE J300)	9.3 – 12.5 mm²/s (abs.)		
Fuel Dilution			
Fossil diesel fuel	0.4 – 0.6 / [wt-%]	+++	↓
Biodiesel	0.6 – 0.8 / [wt-%]	+++	↓
Oxidation			
Carbon acid	-	o	-
Polymerisation	0.06 – 0.11 / [A/cm]	++	↑
Nitration			
Nitric acid	-	o	-
Sludge/Polymerisation	0.06 – 0.09 / [A/cm]	++	↑
Soot			
Carbon	0.6 – 0.8 / [wt-%]	+++	↑

o - neutral
\+ - weak
++ - medium
+++ - strong

All results obtained are from observations of used oil analysis showing the individual contamination effects. Fuel and soot is relative to weight-% [wt-%] and oxidation and nitration is related to IR-absorption per centimetre [A/cm]. Three different chemical mixture processes are present as the contaminants mix with the oil. They are divided into homogenisation (mixing of soluble liquids), emulsification (mixing of limited soluble products) and suspension (mixing of solids in liquids). Homogenisation occurs with fuels mixing with the oil or acids formed in the oil. However, the amount of acids in the oil is too low to affect the viscosity value and has therefore not been listed in the table.

Emulsification is present with oxidation or nitration by-products resulting in jelly-like long chained polymerisation products. Suspension occurs with soot loading of the oil or solid abrasion elements in the oil. Modern oil formulations can keep a certain amount (~ 3 – 4 %) of solid substances in suspension to maintain the viscosity but this effect is not considered here. As the viscosity is also temperature dependent the kinematic viscosity at 100 [°C] is the reference value for all data. The values presented therefore only provide an indication of the expected intensity and direction of influence.

During operation the lubricant can therefore be considered as a blend of different viscosity mixtures. Each blend component included in the engine oil is considered as an individual dilution and can be characterised by the individual kinematic viscosity υ [mm²/s]. (Evaporation, volatilisation losses and temperature effects are not considered here). The 'Viscosity Blend Number' (VBN) for any substance is given as (Maples, 2000):

$$VBN = 14.534 \cdot \ln\left[\ln\left(\upsilon + 0.8\right)\right] + 10.975 \tag{4.38}$$

The VBN of the final blend can be derived by the definition from Kendall and Monroe (Stepina and Vesely, 1992):

$$VBN_{Blend} = \left[\chi_A \cdot VBN_A\right] + \left[\chi_B \cdot VBN_B\right] + \ldots + \left[\chi_{n\cdot} \cdot VBN_n\right] \tag{4.39}$$

where χ_A to χ_n are the mass fraction of each blend component, i.e. oil with the different contaminants. The overall kinematic viscosity is derived by solving equation 4.38 for υ:

$$\upsilon = e^{e^{\frac{VBN_{Blend} - 10.975}{14.534}}} - 0.8 \tag{4.40}$$

Equation 4.40 shows the resulting viscosity value that is measured by the viscosity sensor. This shows that the sum of blend components determine the viscosity. A subsequent separation of the individual effects based on the measured viscosity value is therefore not possible.

4.5 Summary

This chapter presented the theoretical sensing principles of current oil condition sensors. It also illustrates how the lubricant contaminants can affect each of the sensor parameters. The intention was to summarise all underlying theoretical aspects in order to build a pathway to the key challenge – the presence of multiple contaminants in the oil and the resulting effect on the sensor data. The aim was to move by this theoretical investigation one step forward based on the status of research in this area outlined in Chapter 1. The theoretical research outlined that the major oil sensor parameters of permittivity, conductivity and viscosity are all summative parameters. Also without knowledge of the oil constitution is it not possible to derive information which individual effect has led to a sensor data change, as illustrated in Figure 4.10.

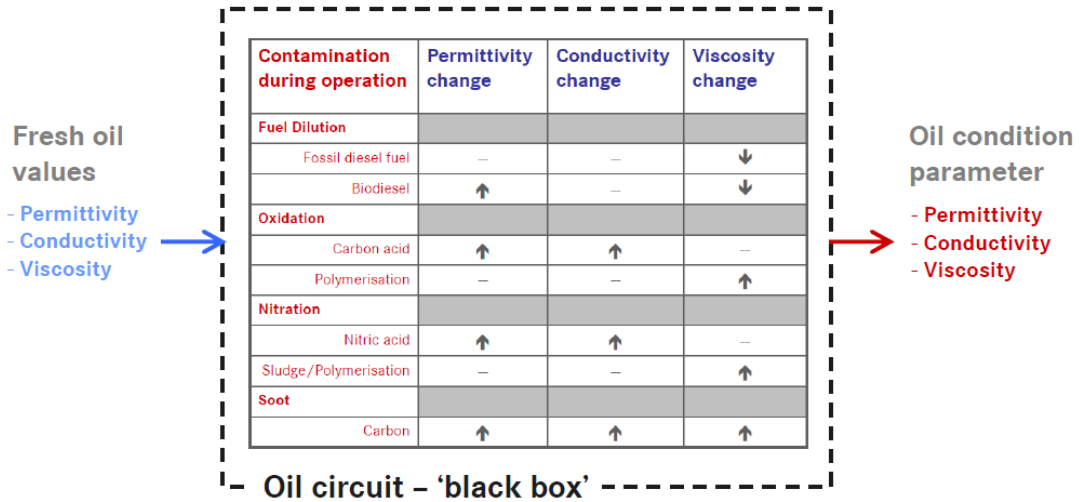

Figure 4.10: Viscosity values and influencing direction of key contaminants
All major oil sensor parameters of permittivity, conductivity and viscosity are summative parameters. Without knowledge of the oil constitution is it not possible to derive information of which the individual effect has led to a change of the individual sensor data.

The next quantitative research step is to investigate the strength and significance of each of the main contaminants on the permittivity, conductivity and viscosity value based on used oil analysis data. The aim is to determine which of the concurrent effects has a dominating influence on the sensor data. A summary of the underlying effects in this chapter will be beneficial to justify or explain the quantitative findings of the results in the next chapter.

Chapter 5

5 Characterisation of Lubricant Contaminants Influence on Sensor Data

5.1 Introduction

This chapter will investigate and characterise the interactions of the identified key lubricant contaminants fuel, soot, oxidation and nitration on the sensor parameters of permittivity, conductivity and viscosity. As the research will use empirical oil analysis data, a brief illustration will present how the data for this research was generated and retrieved. The definition and requirements of the selected data will be provided and will establish an understanding of the data generation. A discussion of the potential errors in the raw data and how these can be detected, corrected or eliminated will show how carefully the data was screened before the first statistical pre-analysis was undertaken. The first step in the characterisation of the data uses correlation analysis, both visual and calculated, to identify if a linear model of the sensor data is sufficient to characterise the interactions of the oil contaminants. The characterisation of strength and significance of the lubricant contaminants and functions of the contaminants uses multiple regression analysis. The outcome of this chapter will provide information about the oil condition assessment and monitoring to understand the most dominant effects in the oil, that cause changes in the sensor data.

5.2 Empirical Data Source – Oil Diagnosis System

Oil analysis data was retrieved from an oil analysis database called 'Oil Diagnosis System' (ODIS). The purpose of this database is to store all engine oil analysis data from vehicle trials and engine bench test runs. Oil samples are taken in fixed intervals during all vehicle or engine tests. These oil samples are internally analysed in the chemical laboratory at Daimler. The purpose of this regular oil analysis during engine development is to monitor all oil analysis values in order to detect irregular values during testing before an engine failure occurs. Another reason for this analysis is to be able to trace differences in the oil data that might have occurred with different test profiles or modified engine setups. Figure 5.1 illustrates the process from taking the oil sample from the engine to the final output of the data analysis.

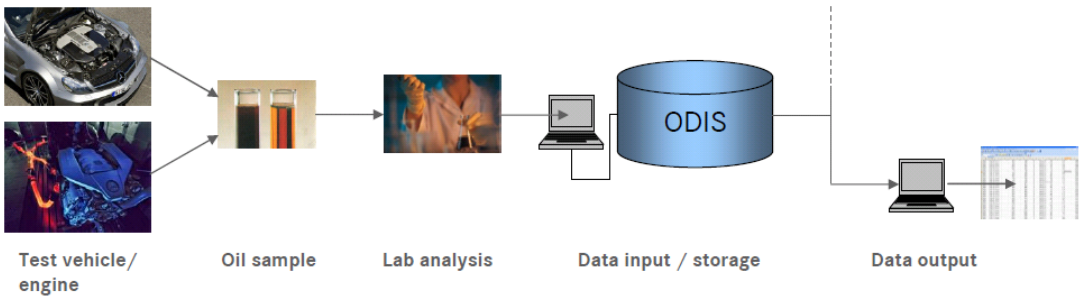

Figure 5.1: ODIS oil analysis and storage steps

According to this sequence, the oil samples are taken from the vehicle or engine and are analysed by the Daimler oil laboratory. The analysis is based on standardised test procedures and specifications as well as internal test methods defined by Daimler. Table 5.1 outlines which analysis methods were applied with regard to the key lubricant contaminants and the oil sensor values. Most analyses are based on DIN standards or, if no standard exists, on Daimler internal standards. Table 5.1 also provides an indication of the typical accuracy of each method if this is not defined in accordance with the standard or method. The permittivity and conductivity measurement is related to the dielectric measurement of the oil condition sensors presented in the previous chapter.

Table 5.1: Sensor and oil parameters in the ODIS lab analysis content

Analysis / Measurement	Unit	Standard	Accuracy
Permittivity	[1]	DAI	n.a.
Conductivity	[pS/cm]	DAI	n.a.
kinematic Viscosity – 100 [°C]	[m²/s]	DIN 515 2 (1999)	± 0,7% (max)
Diesel fuel – 350 [°C]	[wt. - %]	DIN 51380 (1990)	± 0.8% (max)
FAME	[wt. - %]	DIN 51380-2 (n.a.)	± 0.4% (max)
Soot	[wt. - %]	DIN 51452 (1994)	± 10% (max)
Oxidation	[A/cm]	DIN 51453 (2004)	± 5% (max)
Nitration	[A/cm]	DIN 51453 (2004)	± 5% (max)

The sum of the fossil and FAME diesel fuel, outlined in Table 5.1, will be used as the 'fuel' value for all further studies in this work. This definition is consistent with the real situation in the oil sump where both fuel components are present at the same time and are mixed to give an overall fuel value which affects the sensor measurement.

5.3 Empirical Data - Definitions and Requirements

The empirical data population for modelling and statistical analysis in this research was selected by the criteria explained below. The following requirements were drawn for each data set in order to provide a representative analysis outcome:

- Contaminants - The oil analysis data needs to contain complete measurements of the key contaminants fuel, soot, oxidation and nitration. The fuel data value for the further analysis will be the sum of the measured fossil fuel and the measured biofuel content. The two types of fuel will not be investigated separately. The fuel which is considered herein is only diesel and biodiesel respectively as Chapter 3 outlined the potential higher reliability risk.

- Sensor data - The previous investigation and discussion of commercially available oil condition sensors identified permittivity, conductivity and viscosity as the most established lubricant condition monitored parameters for automotive applications. The oil analysis investigated will therefore only consider analyses that contain this data. All the sensor data was measured off-line in the laboratory as illustrated in Figure 5.1. Permittivity and conductivity was measured at $f = 100$ [kHz] and provides comparable results as with the actual on-board sensors. As viscosity is strongly temperature dependent all measurements are taken at 100 [°C] to have a fixed and comparable point.

- Engine – The most critical lubricant degradation effects potentially occur in practice with the use of biodiesel. Therefore only diesel engine oil data will be considered in this investigation. Analysis results were only selected where the 'comment' row for the analysis did not indicate potential failures or irregular observations of the engine during the test run. This could result in higher levels of particular contaminants that cause a distortion in the measurement of other contaminants.

- Load profile – The derived data samples cover the full bandwidth of load profiles from engine test bench to vehicle test runs. This provides a general picture for all potential engine applications. Typical engine test bench and vehicle trial programmes include high load with DPF regeneration, low load with idling, cold / hot climate testing, transient load cycles, urban test cycle and accelerated conditions such as trailer operation or high speed tests. The oil analysis data from the vehicle tests were generated with different car models, all with the same engine type. The empirical data therefore aims to have the highest possible consistency for oil degradation occurring for an extensive range of operational profiles.

- Fuels – The data samples contain oil analysis data from test runs which were conducted with complete fossil diesel fuel (B0) and various biodiesel blends according to current European fuel standard (B5/B7) and test fuel up to B10 RME. This provides good correlation with applications where the actual biodiesel level in standardised fuel can vary with every filling. B10 test fuel is the only fuel which has a constant level of 10 [wt.-%] FAME with every batch.

- Engine oils - The oils in the sample data used for analysis are approved service-fill oils from different lubricant manufacturers according to Mercedes-Benz specification ‘MB 229.31’ and ‘MB 229.51’ and the current diesel factory-fill oil. No particular oil was chosen as a basis for the study. This definition is consistent with application behaviour as during an engine lifetime different engine oils are used either for the oil drain or as a top up during the drain interval. Oil analysis results were completely removed if the type of engine oil was not correctly labelled or could not correctly be determined. If the infrared spectroscopy measurement could not correctly identify the type of used oil, a note in the ‘comment’ row of the analysis documentation indicates a potential oil mixture or unidentifiable oil.

5.4 Potential Source of Errors in the Empirical Data

The Ishikawa diagram in Figure 5.2 presents the potential sources of error in oil analysis raw data (Ishikawa, 1990). The aim is therefore to consider the potential effect on the data, for each cause of error. The Ishikawa Diagram does not indicate scale of error, but assumes that any error can have the same scale of impact and thus to identify the number of errors is important. Another issue to consider is if the error might be identifiable in the raw data set and which method could be applied to detect the faulty data. The measure of how a detected error may be eliminated or corrected is also provided. A qualitative estimation of the potential impact on the data accuracy and the probability of such an error is summarised based on the experience of best practice. The discussion of potential errors in the data outlines the principle of removing faulty values of raw data from the empirical oil analysis data set. This will improve the accuracy of the subsequent modelling and statistical analysis and prevent the occurrence of having outliers or noise in the data which will distort the results. The details of this failure consideration are provided in Appendix A.

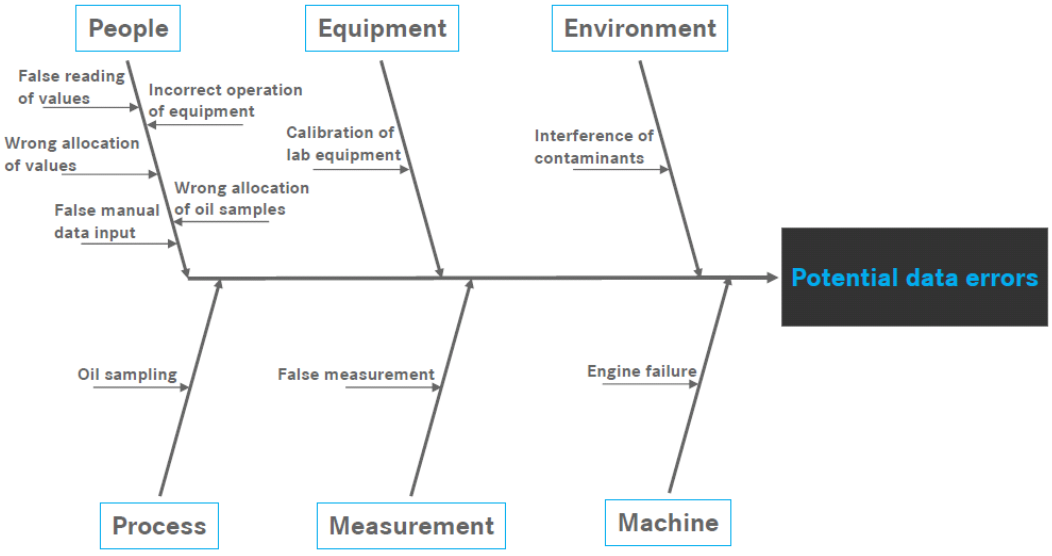

Figure 5.2: Ishikawa-diagram: Potential error sources in oil analysis data
Qualitative summary of main error reasons in the oil data – the effects are not weighted. Errors caused by people form the largest group of potential error sources in the raw oil analysis data.

It is noticeable that errors caused by people form the largest group of potential error sources in the raw oil analysis data. The only instruments to identify resulting outliers in the sensor parameters are visual methods such as bivariate correlation plots and box-plot diagrams (Fox, 2008: 37 - 49).

The raw data inspection of conductivity has turned out to be very difficult as the data is noisy and no clear bivariate correlations could be observed to identify outliers. The focus of the data cleaning was therefore necessary for the permittivity and viscosity values.

If the visual inspection indicated potential outliers for a sensor parameter, the plausibility was checked based on the data plots and the theoretical influences identified in Chapter 4. The particular analysis of potential outliers was cross-checked if the measured level of one or more lubricant contaminants provided potentially outlying sensor parameters. If this plausibility check proved to be valid, the analysis data was left in the complete data set. If no logical reasons from the oil analysis data could be derived then this particular oil analysis was discarded from the data set. It is important to establish that deleting implausible single analysis results is the only way to achieve accurate data for the statistical analysis.

5.5 Empirical Data Analysis

The purpose of examining the empirical data is to characterise which contaminant or combination of contaminants influences the oil condition sensor data. Over 180 oil analysis data sets were used for this investigation. Initially, over 220 raw data sets were first checked for errors or potential outliers as described. The first step of the investigation used a bivariate correlation plot matrix which allowed a first qualitative assessment of the visual correlations. The subsequent correlation analysis according to Pearson verified if a linear relationship exists between the dependent sensor data and the independent engine oil contaminants (Mohr, 2003). The derived correlation factors together with the shape of the scatterplots were used as an indicator to determine the most suitable approach for the multiple regression models. One of the key research objectives of this work was to investigate and assess the concurrent influences of the contaminants on the sensor data. A multiple regression model will therefore be used to investigate the strength and significance of the influencing parameters and to derive a knowledge base for this field of research (Fox, 2008). The sensor data forms the dependent variables and the contaminants are the independent or explanatory variables of the mathematical model. The statistical tools to conduct the following data analysis were Minitab 15 and Matlab R2009a.

5.5.1 Matrix Plot – Lubricant Contaminants vs. Sensor Data

Figure 5.3 shows the scatterplot matrices of the over 180 selected measurement data points for each parameter. The dependent sensor variables permittivity, conductivity and kinematic viscosity are plotted on the ordinate. The predictor or independent variables are the major lubricant contaminants of fuel dilution, soot, oxidation and nitration and are plotted on the abscissa.

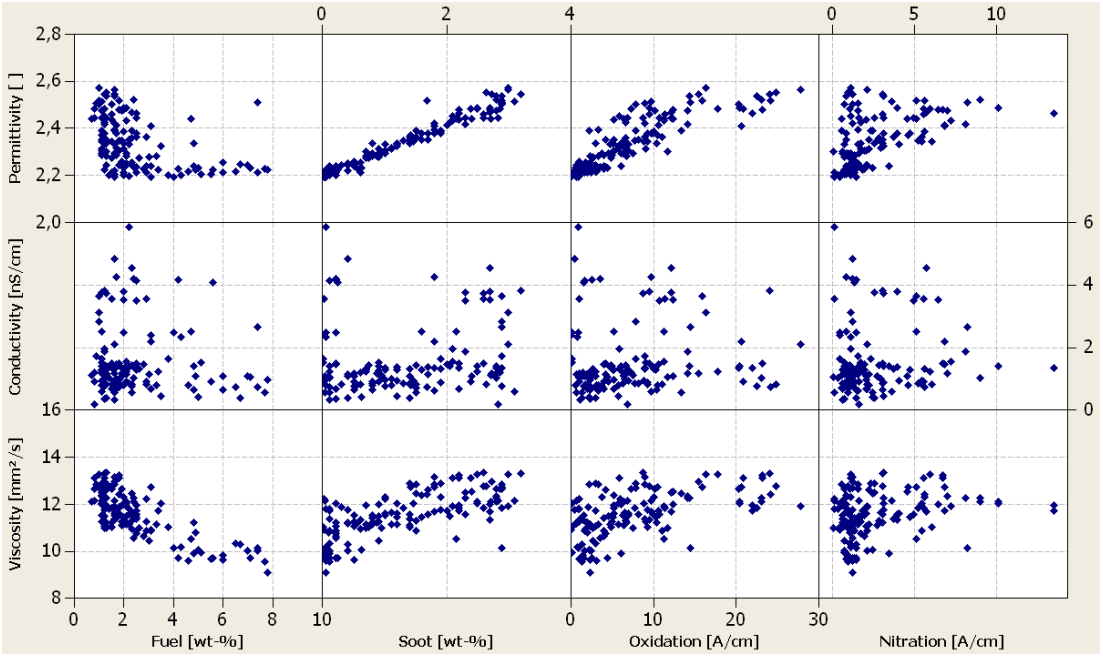

Figure 5.3: Matrix plot – oil and sensor data correlation

The blue dots represent empirical used diesel engine oil data. The correlation between the contaminants fuel, soot, oxidation and nitration and the sensor data permittivity, conductivity and viscosity is assessed. Permittivity shows good correlation with soot and oxidation. No clear correlation between any of the contaminants and conductivity. Viscosity correlates with fuel, soot and oxidation.

Based on a visual inspection of the data from the matrix plot the following correlation trends can be observed:

- The predictor variables soot and oxidation generally increase in a linear fashion with permittivity.
- Nitration shows very moderate correlation with permittivity, and a lot of scatter between 0 and 5 [A/cm].
- The fuel plot shows also only a low correlation with permittivity.
- There is no clear correlation observable between any of the contaminants and the conductivity value.
- Fuel, soot and oxidation are linearly correlated with kinematic viscosity. A significant negative slope of the viscosity can be observed with increasing fuel.

- Increasing soot and oxidation values show a positive correlation with viscosity. Nitration shows no correlation with viscosity.

From a visual inspection of the interactions of the main contaminants of the sensor data with regard to the theoretical findings in Chapter 4 the following correlations are clearly identifiable. For permittivity and viscosity the interactions and observed trends are clearly identified as expected from a theoretical standpoint. It was expected that nitration would have had a stronger impact on all of the parameters. However, the overall nitration of the used oil analysis samples is low and the resulting acidification is probably too low. The correlation results for conductivity are surprising as it was expected that the contaminants which cause the formation of acids such as oxidation and nitration and also soot as a partially conducting substance, and would have had a clear influence on conductivity. However it might require higher concentrations in the oil to measure a significant response.

5.5.2 Correlation Analysis

The aim of the correlation analysis was to assess if a quantitative linear relationship exists between the dependent sensor data and the independent engine oil contaminants. The null hypothesis that was tested defined H_0: $r(X_i, Y_i) \leq |0,5|$ indicating that no linear correlation between the dependent and independent variable exists. The alternative hypothesis was defined as H_a: $|0,5| < r(X_i, Y_i) \leq |1|$ indicating the assumption of a linear relationship between the two rows of data. The threshold of $r < 0.5$ was sufficient for this analysis as some scatter remained even after the initial data inspection. The values used for the statistical analysis have proved to be reasonable from the initial data screening. The remaining scatter indicates the complexity in the analysis due to the contrary influences on the sensor data. Table 5.2 shows the results of the correlation analysis. The correlation analysis provides for each value the corresponding p-value from the significance test based on F-statistics (Mohr, 2003). The significance level to test the hypothesis is defined as $p < 0.05$.

Table 5.2: Correlation analysis matrix - oil contaminants vs. sensor data

	Fuel	**Soot**	**Oxidation**	**Nitration**
Permittivity	$r = -0.104$ $p = 0.123$	$r = 0.932$ $p < 0.001$	$r = 0.758$ $p < 0.001$	$r = 0.463$ $p < 0.001$
Conductivity	$r = 0.098$ $p = 0.143$	$r = 0.189$ $p = 0.004$	$r = 0.161$ $p = 0.016$	$r = 0.211$ $p = 0.002$
Kin. Viscosity	$r = -0.741$ $p < 0.001$	$r = 0.582$ $p < 0.001$	$r = 0.439$ $p < 0.001$	$r = 0.198$ $p = 0.003$

On the vertical axis of the correlation matrix in Table 5.2 are the dependent sensor variables. On the horizontal axis are the influencing variables fuel, soot, oxidation and nitration.

- Fuel shows no correlation with permittivity confirming the null hypothesis and the result is not significant.

- Soot and oxidation have a very strong positive correlation with permittivity so the null hypothesis can be rejected and the result is significant.

- Nitration shows no correlation with permittivity confirming the null hypothesis, the result is significant.

- Fuel, soot, oxidation and nitration show no correlation with conductivity and the null hypothesis of no linear relationship of the variables on conductivity is confirmed. Except for fuel the results are significant.

- Fuel has the strongest correlation with viscosity which is negative and the result is significant and the null hypothesis can be rejected.

- Soot correlates with viscosity and the result is statistically significant, the null hypothesis can be rejected.

- Oxidation and nitration show no correlation confirming the null hypothesis and the results are statistically significant.

The correlation analysis has shown that not all lubricant contaminants correlate in a linear way with the sensor parameter. Conductivity particularly has shown no clear linear trend in the analysis. The analysis verified that the linear multiple regression model to investigate the multiple influences on the sensor data is not sufficient.

5.5.3 DoE Modelling of Sensor Data to Characterise Oil Contaminants Influence

The previous correlation analysis in section 5.5.2 provided a first indication of the existence of linear relationships of oil contaminants and sensor data. However, the correlation analysis was a discrete and linear analysis where the bivariate correlations were examined individually. Multiple regression analysis was used to obtain a 'Design of Experiments' (DoE) model which expressed the relationship between the dependent sensor variables permittivity, conductivity and kinematic viscosity and the concurrent independent contaminants fuel, soot, oxidation and nitration. The model enabled an examination of the strength of the explanatory variables on the sensor data. This research step provides knowledge about the dominating effects within the 'black-box' oil sump that have an impact on the measured sensor data. A closer look to the curvature of the bivariate scatterplots in Figure 5.3 indicates, that the curvature for recognisable correlations is either linear or changes in an exponential fashion without changing directions. The selected DoE model enables an investigation and assessment of the concurrent influences and the individual strength of the sensor data based on used oil analysis data using a 2^{nd} order polynomial regression model. The 'Multiple Regression Analysis' (MRA) and the 'Analysis of Variance' (ANOVA) were applied to examine the strength and significance of the identified main contaminants for each sensor parameter (Fox, 2008). The following analysis presents the results derived from the nonlinear multiple regression model for each of the dependent variables, i.e. permittivity, conductivity and kinematic viscosity at 100 [°C]. The explanatory variables are scaled before the regression analysis to provide better comparability of the regressor effects. This was necessary as from Figure 5.3 it is recognised that the contaminants have a different absolute range of values. The presentation of the regression data is summarised in the tables 5.3, 5.4, 5.6, 5.7, 5.9, 5.10 and will be used to examine the model parameters in more detail. The first column shows the individual coefficient value. The second column shows the standard deviation of each coefficient which provides an estimate of the reliability of the coefficients estimate which is influenced by measurement noise and assumed model structure.

The third column of the table contains the t-value from the distribution test (Fox, 2008). The t-statistics tests whether each estimated coefficient β_i has a significant influence on the dependent variable. The initial null hypothesis for testing each single coefficient is defined as H_0: $\beta_i = 0$ versus H_a: $\beta_i \neq 0$, i.e. the coefficient has an influence on the dependent variable. The significance level for the t-test value is $p < 0.05$. The p-value is given in the fourth column indicating the significance level in order to assess the probability and whether the coefficient contributes to the model.

If the p-value indicates for a certain coefficient that the null hypothesis is valid, i.e. $p > 0.05$, the particular explanatory variable or function of more than one explanatory variable will be removed from the regression model and the analysis will be repeated. If the significance test identifies non-significant explanatory variables or terms that can be ruled out due to logical grounds then the principle of marginality is applied (Fox, 2008: 135) This specifies that a model including a high-order term should also include the lower-order 'relatives' of that term, i.e. the main effects that compose the interaction. The iteration of the regression analysis therefore starts with the individual removal of the highest order terms $\beta_m \cdot X_n^2$, then the product terms of functions of more than one explanatory variable $\beta_m \cdot X_n \cdot X_o$ and then the lowest order terms with one explanatory variable $\beta_m \cdot X_n$. The derived regression equation together with the adjusted R^2 value defines the percentage of the dependent variable in the nonlinear regression equation. Based on the final regression model is the overall quality of the model tested using the ANOVA data. The main part that is used is the F-statistics testing the significance of the coefficient of determination R^2 to assess the overall quality of the model (Fox, 2008). The null hypothesis is defined as H_0: $\beta_i = \beta_{i+1} = \ldots = \beta_{i+n} = 0$ expressing that none of the coefficients contribute to the overall quality of the model. The null hypothesis can be rejected if the alternative hypothesis defined as H_a: at least one $\beta_j \neq 0$ is confirmed and the corresponding p-value of the F-statistics indicates the result is significant.

Permittivity Model

The initial full nonlinear regression model of the permittivity value is provided by equation 5.3.

$$\begin{aligned} &Permittivity\left(Fuel, Soot, Oxidation, Nitration\right) = 2.46 + 0.03 \cdot Fuel + 0.13 \cdot Soot \\ &+ 0.03 \cdot Oxidation + 0.05 \cdot Nitration - 0.01 \cdot Fuel^2 - 0.01 \cdot Fuel \cdot Soot \\ &+ 0.08 \cdot Fuel \cdot Oxidation - 0.07 \cdot Fuel \cdot Nitration - 0.01 \cdot Soot^2 \\ &+ 0.08 \cdot Soot \cdot Oxidation - 0.09 \cdot Soot \cdot Nitration - 0.1052 \cdot Oxidation^2 \\ &- 0.1 \cdot Oxidation \cdot Nitration + 0.18 \cdot Nitration^2 \end{aligned} \tag{5.3}$$

The full coefficient list together with the t-values and the corresponding p-values are summarised in Table 5.3 indicating which explanatory variables or functions of explanatory variables are not statistically significant to model the permittivity value.

Table 5.3: Initial regression model – predicted variable: Permittivity

Multiple Regression Analysis				
Predictor	**Coefficient**	**Standard Deviation**	**t**	**p**
Constant	2.4594	0.0108	228.4735	< 0.05
Fu l	0.0267	0.0222	1.2030	0.2307
Soot	0.1306	0.0205	6.3787	< 0.05
Oxidation	0.0256	0.0619	0.4135	0.6798
Nitration	0.0493	0.0574	0.8584	0.3919
Fuel²	-0.0061	0.0107	-0.5732	0.5673
Fuel*Soot	-0.0055	0.0134	-0.4097	0.6826
Fuel*Oxidation	0.0816	0.0269	3.0326	< 0.05
Fuel*Nitration	-0.0714	0.0398	-1.7933	0.0747
Soot²	-0.0133	0.0112	-1.1795	0.2399
Soot*Oxidation	0.0798	0.0348	2.2942	< 0.05
Soot*Nitration	-0.0895	0.0384	-2.3333	< 0.05
Oxidation²	-0.1052	0.0439	-2.3964	< 0.05
Oxidation*Nitration	-0.0989	0.0954	-1.0368	0.3013
Nitration²	0.1776	0.0754	2.3553	< 0.05
Standard Error of the Estimate	**R²**	**Adjusted R²**		
0.0245	94.96 %	94.54 %		

Analysis of the coefficients of the permittivity model shows clearly that not all explanatory variables or functions of explanatory variables contribute to the model with statistical significance, i.e. $p < 0.05$. Based on the defined iteration rule the non-significant explanatory variables are removed from the model starting with the highest order term, i.e. soot², then the permittivity is re-modelled without this term. Terms which can be ruled out based on grounds of logic are also removed from the model. This procedure is repeated until all explanatory variables are statistically significant. The final result is a polynomial regression model for permittivity after several iterations containing only empirical significant and theoretical defensible variables and is provided in equation 5.4.

$$Permittivity\left(Fuel, Soot, Oxidation\right) = 2.47 + 0.02 \cdot Fuel + 0.16 \cdot Soot + 0.1 \cdot Oxidation \tag{5.4}$$

The full coefficient list of the final permittivity model together with the t-values and the corresponding p-values is summarised in Table 5.4. This also includes the R^2 values, indicating the percentage of the permittivity variable which can be explained by reference to the combined influence of the remaining explanatory variables.

Table 5.4: Final regression model – predicted variable: Permittivity

Multiple Regression Analysis				
Predictor	**Coefficient**	**Standard Deviation**	**t**	**p**
Constant	2.4718	0.0063	389.7502	< 0.05
Fuel	0.0241	0.0046	5.2484	< 0.05
Soot	0.1628	0.0053	30.8417	< 0.05
Oxidation	0.0999	0.0098	10.2332	< 0.05
Standard Error of the Estimate	**R^2**	**Adjusted R^2**		
0.0285	93.04 %	92.93 %		

The strength of the coefficients contributing to the final permittivity regression model is visualised using a bar chart, see Figure 5.4. All of the coefficients with the related error bars are statistically significant and outline which explanatory variable, i.e. lubricant contaminant has the most dominant impact on the permittivity value. The bar chart of the corresponding t-test values outlines the significance of each of the coefficients to the derived permittivity model, see Figure 5.5. The critical t-test value to assess the significance of each explanatory variable is (t_{95} = 1.6525) (Mohr, 2003), see Figure 5.5.

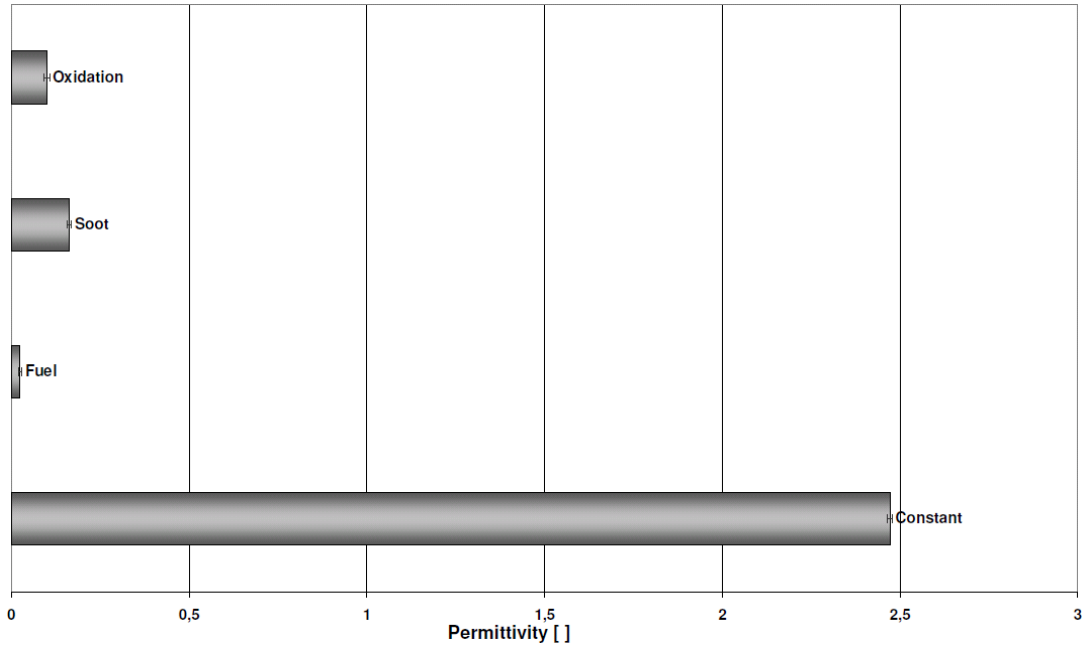

Figure 5.4: Final permittivity model - strength of coefficients

Each bar indicates the strength of the coefficient to contribute to the permittivity model. Soot plays a major role in predicting permittivity followed by oxidation. The influence of fuel is comparatively small.

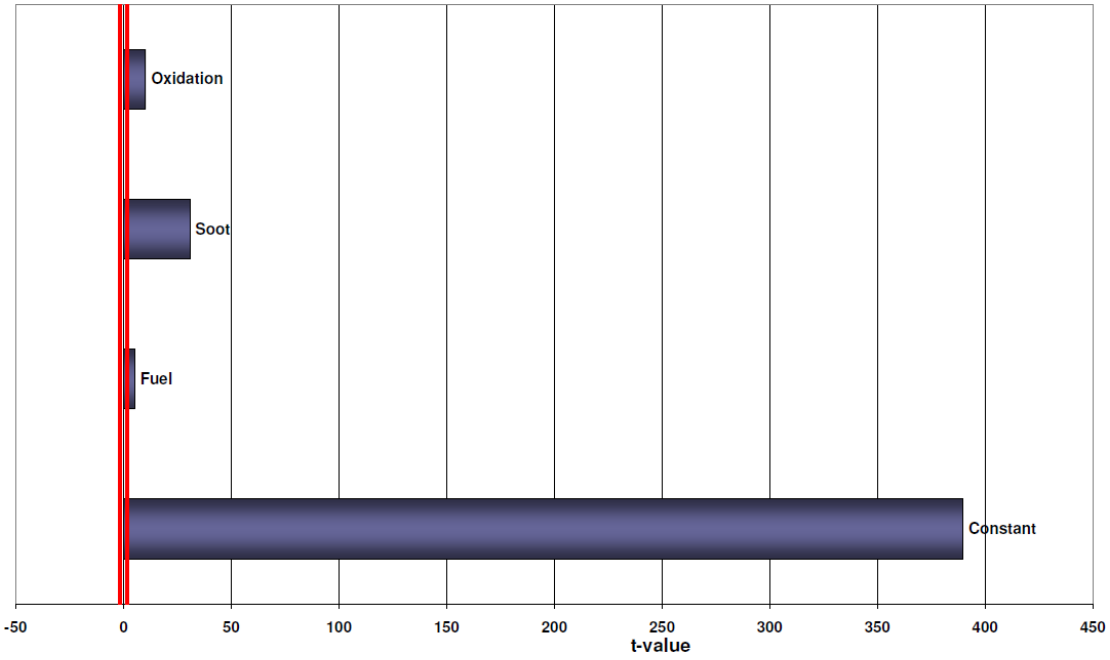

Figure 5.5: Final permittivity model - significance of coefficients
Each bar represents the significance of the particular coefficient to contribute to the permittivity model. The red lines represent the critical t-test value (+/- 1.6525). All coefficients to the permittivity model are statistically significant.

From the regression model results in Table 5.4 and the charts in Figure 5.4 and 5.5 it is clear that soot plays a major role in predicting permittivity. Oxidation also has a considerable influence on permittivity. The influence of fuel on the permittivity is comparatively small.

All of the coefficients are positive confirming the theoretical discussion in the previous chapter that all chemical changes in the oil result in increasing polarisable components causing an increase in permittivity.

- The results for soot and oxidation fully align with the expectations from the theoretical considerations.

- The statistically significant influence of fuel can be explained by the amount of biodiesel in most of the fuel that has contaminated the oil having a higher permittivity than fossil fuel.

- An interesting result is that nitration does not play a role in predicting the model as the resulting acids from the nitration process normally increase the polarity of the oil from theoretical aspect. The reason for these findings is that it is most likely due to the low overall nitration value compared to the significantly higher oxidation content in the used engine oils derived from the empirical data.

- Another interesting observation is that interactions of the explanatory variables do not have an effect on the permittivity data and it is only the main effects of the contaminants soot, oxidation and fuel that cause permittivity increase.

- The adjusted R^2 value in Table 5.4 indicates that 92.93 % of the variability in permittivity can be explained by reference to the combined influence of fuel, soot and oxidation, which is a very significant result.

- The ANOVA summary for permittivity as a function of fuel, soot and oxidation in Table 5.5 contains the F-test value and the p-value of the complete model $F = 798.2$, $p < 0.05$. From the F-table the required critical value of ($F95 = 1.26$) can be derived (Moore, 1999). Since F(calculated) >> F(table) the null hypothesis can clearly be rejected. This result proves that the derived model as a whole reflects a real and significant association between the dependent variable permittivity and the independent explanatory variables as a group.

Table 5.5: ANOVA – predicted variable: Permittivity

ANOVA					
	df	**Sum of Squares**	**Mean of Squares**	**F**	**p**
Regression	3	2.1161	0.7054	798.1988	< 0.05
Residual	179	0.1582	0.0009		
Total	182	2.2743			

Conductivity Model

The initial full nonlinear regression model of the permittivity value is provided in equation 5.5.

$$\begin{aligned} &Conductivity\left(Fuel, Soot, Oxidation, Nitration\right) = 2.12 + 0.46 \cdot Fuel \\ &+ 1.14 \cdot Soot + 0.67 \cdot Oxidation - 0.55 \cdot Nitration - 0.35 \cdot Fuel^2 \\ &+ 1.4 \cdot Fuel \cdot Soot - 0.1 \cdot Fuel \cdot Oxidation - 0.52 \cdot Fuel \cdot Nitration + 1.02 \cdot Soot^2 \\ &+ 1.11 \cdot Soot \cdot Oxidation - 1.46 \cdot Soot \cdot Nitration - 1.44 \cdot Oxidation^2 \\ &+ 2.6 \cdot Oxidation \cdot Nitration - 0.97 \cdot Nitration^2 \end{aligned} \quad (5.5)$$

The full coefficient list together with the t-values and the corresponding p-values indicates which explanatory variables or functions are not statistically significant.

Table 5.6: Initial regression model – predicted variable: Conductivity

Multiple Regression Analysis				
Predictor	**Coefficient**	**Standard Deviation**	**t**	**p**
Constant	2.1209	0.4505	4.7077	< 0.05
Fuel	0.4605	0.9275	0.4965	0.6202
Soot	1.1424	0.8566	1.3336	0.1841
Oxidation	0.6662	2.5916	0.2571	0.7975
Nitration	-0.5493	2.4018	-0.2287	0.8194
Fuel²	-0.3492	0.4488	-0.7781	0.4376
Fuel*Soot	1.3950	0.5614	2.4849	< 0.05
Fuel*Oxidation	-0.0916	1.1263	-0.0813	0.9353
Fuel*Nitration	-0.5220	1.6672	-0.3131	0.7546
Soot²	1.0162	0.4706	2.1596	< 0.05
Soot*Oxidation	1.1047	1.4550	0.7592	0.4488
Soot*Nitration	-1.4564	1.6060	-0.9068	0.3658
Oxidation²	-1.4445	1.8372	-0.7862	0.4328
Oxidation*Nitration	2.6037	3.9931	0.6520	0.5153
Nitration²	-0.9743	3.1562	-0.3087	0.7579
Standard Error of the Estimate	**R²**	**Adjusted R²**		
0.3924	13.88 %	6.7 %		

Analysis of the coefficients of the conductivity model shows that almost none of the explanatory variables or functions of explanatory variables contribute to the model with statistical significance, i.e. $p < 0.05$. The final result of a polynomial regression model for conductivity after the defined re-modelling iterations contains only empirical significant and theoretical defensible variables and is provided in equation 5.6.

$$Conductivity\left(Fuel, Soot\right) = 1.87 + 0.76 \cdot Fuel + 1.34 \cdot Soot + 1.07 \cdot Fuel \cdot Soot + 1.1 \cdot Soot^2 \tag{5.6}$$

The full coefficient list of the final conductivity model together with the t-values and the corresponding p-values is summarised in Table 5.7. This also includes the R^2 values, indicating the percentage of the conductivity variable can be explained by reference to the combined influence of the remaining explanatory variables.

Table 5.7: Final regression model – predicted variable: Conductivity

Multiple Regression Analysis				
Predictor	**Coefficient**	**Standard Deviation**	**t**	**p**
Constant	1.8652	0.1923	9.7015	< 0.05
Fuel	0.7626	0.2234	3.4130	< 0.05
Soot	1.3397	0.2772	4.8331	< 0.05
Fuel*Soot	1.0676	0.3276	3.2594	< 0.05
Soot²	1.0998	0.3326	3.3070	< 0.05
Standard Error of the Estimate	**R²**	**Adjusted R²**		
0.3751	12.48 %	10.51 %		

The strength of each of the coefficients contributing to the final conductivity regression model is visualised using a bar chart, see Figure 5.6.

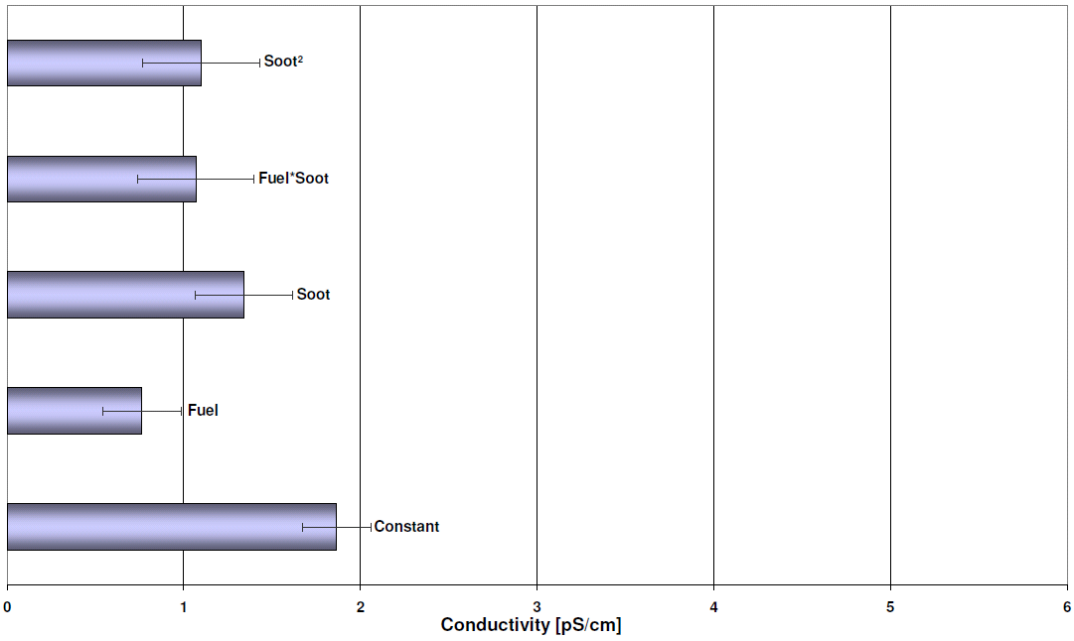

Figure 5.6: Final conductivity model - strength of coefficients

Each bar indicates the strength of the coefficient to contribute to the conductivity model. Soot plays a strong role in predicting conductivity followed by the influence of fuel. Oxidation and nitration do not contribute to the model. The error bars are relatively large compared to the permittivity model.

The bar chart of the corresponding t-test values for each predictor outlines the significance of each coefficient against the critical t-test value, see Figure 5.7.

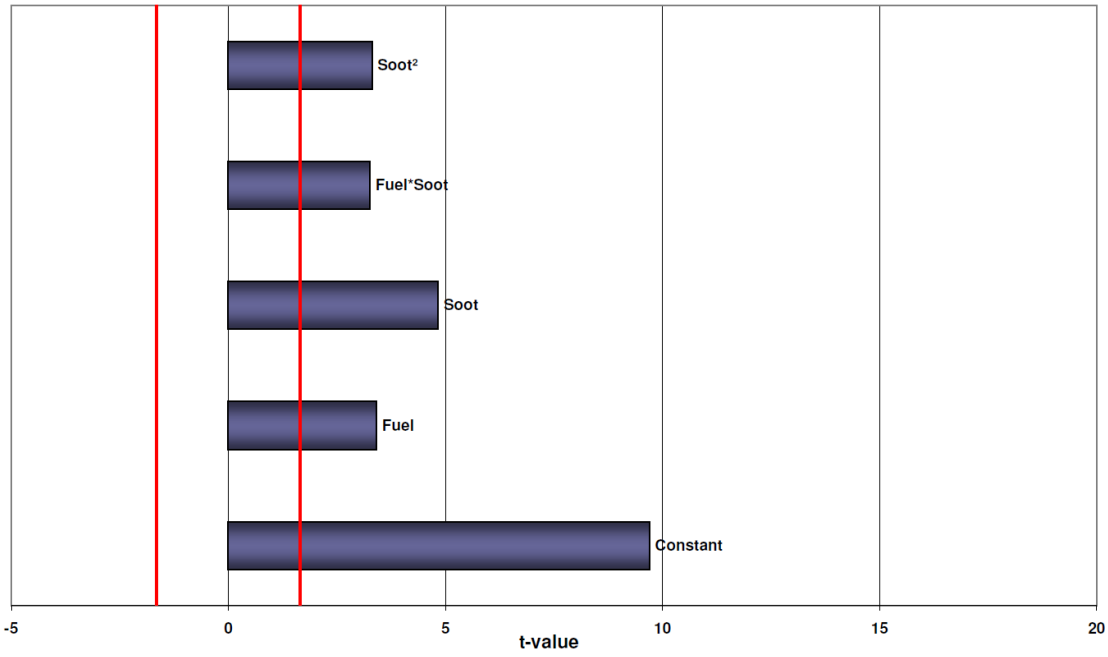

Figure 5.7: Final conductivity model - significance of coefficients

Each bar represents the significance of the particular coefficient to contribute to the conductivity model. The red lines represent the critical t-test value (+/- 1.6525). All coefficients to the conductivity model are statistically significant. The significance is much smaller compared to the permittivity model.

All of the coefficients are positive confirming the theoretical discussion in Chapter 4.

- The regression model results in Figure 5.6 and 5.7 show that soot plays a strong role in predicting conductivity. The result for soot is as expected from the theoretical considerations.

- Fuel has also a considerable influence on conductivity. The strong and statistically significant influence of fuel provides an interesting observation and can be explained by the amount of conducting additives in modern fuels which prevent electrostatic charging.

- An unexpected finding is that the acids formed in the oxidation and nitration process do not play a role in predicting the model since the resulting acids where expected to increase the ion conductivity from a theoretical basis. The potential reason for these findings could be that ionic conductivity caused by the formed acids from oxidation and nitration require higher acid concentrations in the oil to be clearly measurable. The used oils still had enough alkaline reserve to prevent a stronger acidification of the oil leading to more ion conductivity.

- The adjusted R^2 value in Table 5.7 indicates that 10.51 % of the variability in conductivity can be explained by reference to the combined influence of soot and fuel which shows a very poor result with regard to the result for permittivity.

- The ANOVA summary for permittivity as a function of soot and fuel in Table 5.8 contains the F-test value and the p-value of the complete model $F = 6.34$, $p < 0.05$. Since F(calculated) > F(table) the null hypothesis can be rejected. This result proves that the derived model as a whole reflects a real and significant association between the dependent variable conductivity and the independent explanatory variables as a group. However, the model has a very low overall quality compared to the findings for permittivity.

Table 5.8: ANOVA – predicted variable: Conductivity

ANOVA					
	df	**Sum of Squares**	**Mean of Squares**	**F**	**p**
Regression	4	29.0983	7.2746	6.3460	< 0.05
Residual	178	204.0471	1.1463		
Total	182	233.1454			

Kinematic Viscosity @ 100 [°C] Model

The initial full nonlinear regression model of the kinematic viscosity with all possible explanatory variables and functions of it is provided in equation 5.7.

$$\begin{aligned} kin.Viscosity\left(Fuel, Soot, Oxidation, Nitration\right) &= 11.35 - 3.03 \cdot Fuel \\ &+ 0.49 \cdot Soot + 8.26 \cdot Oxidation - 4.09 \cdot Nitration + 0.82 \cdot Fuel^2 \\ &- 0.29 \cdot Fuel \cdot Soot - 1.53 \cdot Fuel \cdot Oxidation + 0.51 \cdot Fuel \cdot Nitration \\ &+ 0.29 \cdot Soot^2 - 0.58 \cdot Soot \cdot Oxidation + 0.56 \cdot Soot \cdot Nitration \\ &+ 1.45 \cdot Oxidation^2 + 6.9 \cdot Oxidation \cdot Nitration - 5.73 \cdot Nitration^2 \end{aligned} \tag{5.7}$$

Table 5.9 presents the complete coefficient calculation together with the significance test results for each variable.

Table 5.9: Initial regression model – predicted variable: Viscosity

Multiple Regression Analysis				
Predictor	**Coefficient**	**Standard Deviation**	**t**	**p**
Constant	11.3477	0.2549	44.5066	< 0.05
Fuel	-3.0338	0.5249	-5.7794	< 0.05
Soot	0.4867	0.4848	1.0039	0.3169
Oxidation	8.2646	1.4667	5.6348	< 0.05
Nitration	-4.0864	1.3593	-3.0063	< 0.05
Fuel²	0.8209	0.2539	3.2325	< 0.05
Fuel*Soot	-0.2919	0.3177	-0.9191	0.3594
Fuel*Oxidation	-1.5307	0.6374	-2.4015	< 0.05
Fuel*Nitration	0.5077	0.9435	0.5381	0.5912
Soot²	0.2921	0.2663	1.0968	0.2743
Soot*Oxidation	-0.5818	0.8234	-0.7066	0.4808
Soot*Nitration	0.5636	0.9089	0.62	0.5361
Oxidation²	1.4541	1.0398	1.3984	0.1638
Oxidation*Nitration	6.8959	2.2599	3.0514	< 0.05
Nitration²	-5.7348	1.7862	-3.2106	< 0.05
Standard Error of the Estimate	**R²**	**Adjusted R²**		
0.5603	88.35 %	87.38 %		

The p-values of the predictor variables of the viscosity model indicate that not all explanatory variables or functions of explanatory variables contribute to the model with statistical significance, i.e. $p < 0.05$. Based on the defined iteration rule the non-significant explanatory variables are removed from the model starting with the highest order term, i.e. soot², and then the viscosity is re-modelled without this term. From theoretical considerations negative coefficients for the 'Nitration' values are not logical. The re-modelling of viscosity according to the defined procedure was repeated until the remaining explanatory variables are all statistically significant and theoretically defensible. The final result is a polynomial regression model for viscosity containing only statistical significant variables and is provided in equation 5.8.

$$kin.Viscosity\left(Fuel, Soot, Oxidation\right) = 11.66 - 3.19 \cdot Fuel + 0.51 \cdot Soot + 3.29 \cdot Oxidation + 0.96 \cdot Fuel^2 - 1.7 \cdot Fuel \cdot Oxidation + 1.84 \cdot Oxidation^2 \quad (5.8)$$

The complete table of the remaining predictors of the final kinematic viscosity model includes the R^2 values which indicate the percentage of the kinematic viscosity variable which can be explained by reference to the combined influence of the remaining explanatory variables and is provided in Table 5.10.

Table 5.10: Final regression model – predicted variable: Kinematic viscosity @ 100 [°C]

Multiple Regression Analysis				
Predictor	**Coefficient**	**Standard Deviation**	**t**	**p**
Constant	11.1573	0.1977	56.4334	< 0.05
Fuel	-3.4735	0.2514	-13.8139	< 0.05
Soot	0.4309	0.1286	3.3519	< 0.05
Oxidation	3.49201	0.3459	10.0928	< 0.05
Fuel²	0.9564	0.2368	4.0395	< 0.05
Fuel*Oxidation	-1.8080	0.3453	-5.2359	< 0.05
Oxidation²	2.2150	0.4652	4.7619	< 0.05
Standard Error of the Estimate	**R²**	**Adjusted R²**		
0.4068	87.03 %	86.59 %		

Figure 5.8 shows the contribution of each explanatory variable and interaction of regressor to the final viscosity regression model and indicates which lubricant contaminant has the most dominant impact on the viscosity.

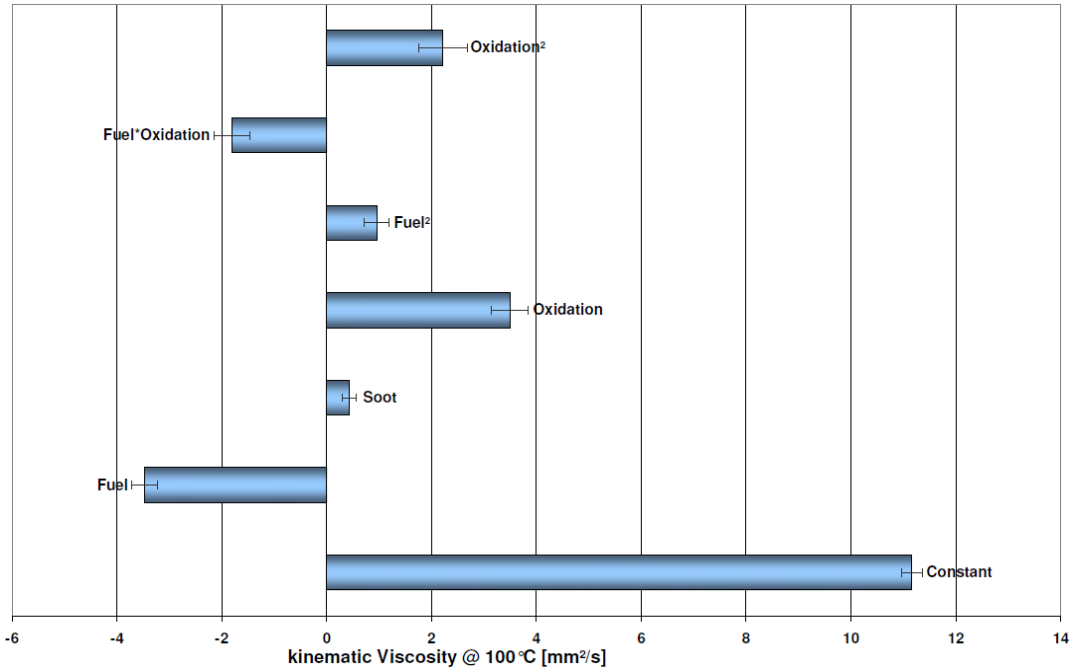

Figure 5.8: Final viscosity model - strength of coefficients

Each bar indicates the strength of the coefficient to contribute to the viscosity model. Fuel and oxidation are the main effects influencing the viscosity sensor value. The influence of soot on the viscosity value is relatively small. In the mixed term of fuel and oxidation it is fuel that dominates the direction towards lower viscosity. This effect might change with higher oxidation values.

The bar chart of the corresponding t-test values for each predictor outlines the significance of each coefficient against the critical t-test value.

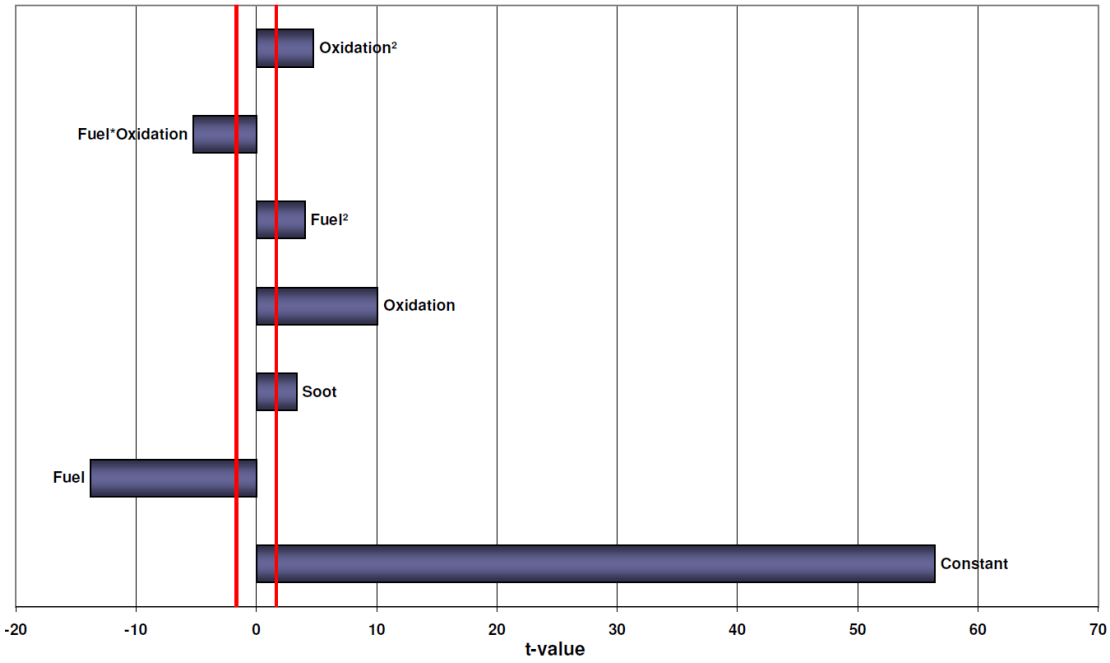

Figure 5.9: Final viscosity model - significance of coefficients
Each bar represents the significance of the particular coefficient to contribute to the viscosity model. The red lines represent the critical t-test value (+/- 1.6525). All coefficients to the viscosity model are statistically significant. The significance is high confirming the quality of the viscosity model.

From the regression model results in Table 5.10 and the charts in Figure 5.8 and 5.9 the following observations can be drawn.

- All of the derived results for the strength and significance of the contaminants on viscosity fully align with the expectations from the theoretical considerations defined in Chapter 4.

- Fuel and oxidation can clearly be identified as main effects influencing the viscosity sensor value.

- The influence of soot is also considerable but was expected to be higher.

- Fuel seems to be the most dominating effect in the interaction with oxidation due to the negative sign of this product. This is probably due to the fact that the polymerisation process of the used oils is not in an advanced stage. It can be expected that oxidation will dominate the product of fuel and oxidation at a certain point in time.

- Again nitration does not play a role in predicting the model due to the low overall nitration values and due to the fact that no oil insoluble reaction products have been formed in the oil which would have caused an increase in viscosity.

- The adjusted R^2 value in Table 5.10 indicates that 86.59 % of the variability in viscosity can be explained by reference to the combined influence of fuel, soot and oxidation which is a significant result.

- The ANOVA summary Table 5.11 for the kinematic viscosity model as a function of fuel, soot and oxidation contains the F-test value and the p-value of the complete model $F = 196.84$, $p < 0.05$. This result proves that the derived model as a whole reflects a real and significant association between kinematic viscosity at 100 [°C] and the identified independent explanatory variables and functions of these variables as a group.

Table 5.11: ANOVA – predicted variable: Kinematic viscosity @ 100 [°C]

ANOVA					
	df	**Sum of Squares**	**Mean of Squares**	**F**	**p**
Regression	6	480.41	80.07	196.84	< 0.05
Residual	176	71.59	0.41		
Total	182	551.99			

5.6 Summary

The research in this chapter uses empirical data of used diesel engine light duty oils to study the influence of the main lubricant contaminants on permittivity, conductivity and viscosity. The initial identification of the most suitable regression model outlined that a linear model is not sufficient to study the effects. The characterisation of lubricant influences on the sensor parameters provides information about which contaminant in the 'black-box' oil sump has the strongest impact on each of the sensor values. Changes of permittivity are mainly caused by soot and oxidation. However, fuel also has an important influence. Conductivity increases could only be verified with increasing soot and higher fuel content. Acid components in the oil from the oxidation and nitration process had no provable influence on conductivity. Viscosity increase was primarily caused by oxidation and by the effects of soot. Viscosity decrease is caused by fuel dilution which is also dominating in the interaction of fuel and oxidation based on the analysis which was undertaken. However, strongly oxidised oils in real applications cause the viscosity to increase even with fuel dilution, as the polymerisation will dominate the direction of viscosity change from a certain level on. This is typically not the case for oxidation levels within regular oil drain intervals and such effects were therefore not observed in this work. The impact of nitration on the permittivity and viscosity models would probably have been higher with higher nitration values in the used oils. As nitration of oils is nowadays a rare problem with diesel and gasoline engines the findings are justifiable (van Basshuysen and Schäfer, 2002). The quality of the three DoE models with regard to the R^2 values and the F-test values proves that the derived permittivity and viscosity model reflect a reliable and significant association between the contaminants and the sensor values. The R^2 and F-test value for conductivity proved no connection between the contaminants and the sensor values. The research identified that permittivity and viscosity are able to provide reliable information about changes of the oil condition. The modelling of an oil condition algorithm will therefore be based on these two values.

Chapter 6

6 Oil Condition Model

6.1 Introduction

The previously derived characterisation of the interaction of contaminants and selected sensor parameters provide the starting position for the considerations in this chapter. The research in this chapter will go one step further in defining a new way to monitor the lubricant condition using permittivity and viscosity data. The aim is therefore to find an efficient and reliable solution to predict the current oil condition and to forecast the remaining oil drain mileage. The premise for a suitable condition model will be presented in an initial step. The intended contrast to the few existing lubricant condition monitoring approaches which were presented in Chapter 1 will be reviewed. This will provide an overview of how the monitoring concept in this research will follow an individual and novel pathway to assess the oil condition and the remaining oil drain mileage. The scheme of the condition rating algorithm is presented by subdividing the complete model into functional subgroups. All parts of the developed concept are discussed in detail and the relevant theoretical background to solve the research objective for each step is presented. The aim of this chapter is to provide all considerations and theoretical background necessary to develop the innovative condition model for a reliable and efficient monitoring approach.

6.2 Oil Condition Model Approach

This section will provide the rationale for the selection of the intended oil condition rating model approach. Based on the initial literature review and the few reported oil condition algorithms the following aspects can be identified for the different models. The comparison between the classification performance of neural networks, Dempster-Shafer method and Bayes theorem conducted by Krallmann (2005) outlines that neural networks show better classification results compared to the other methods. Neural networks proved to work well and to provide reliable condition statements. Krallmann fed the raw sensor data into the neural network to obtain directly a condition status. The main drawback with each of these investigated methods was a lack of transparency of how the method derived the outcome of the condition status. Due to the lack of clarity in the results is it difficult to improve the outcome or to adapt the algorithm for dedicated applications. Neural network applications are not efficient in terms of ECU capacity and the actual effort-benefit ratio of such a sophisticated method for the few input and output data needs to be considered. The linear regression model developed by Lorenz (2007) provides a more suitable condition status outcome. It is also efficient in terms of storage and computing capacity. The analysis uses viscosity and permittivity sensor data to predict the fuel and soot content using a regression analysis. The simple threshold model as studied by Murukesan (2008) or the extended application of a decision tree algorithm by Dobrinski et al. (2008) use experimentally derived sensor values to develop thresholds to classify the raw sensor data. The benefit of these systems is their robustness and the computation efficiency. The accuracy of the results depend significantly on the defined resolution of the measurement steps. With this algorithm design, typically the actual underlying degradation effect is of minor interest as only the absolute sensor value change is assessed.

To address the identified points of optimisation in the existing condition models and to focus on an innovative approach the following initial requirements of the oil condition model development have been formulated:

- The lubricant rating model should provide a reliable and accurate lubricant statement with sufficient resolution to quickly react to sudden oil condition changes in order to achieve the best monitoring and remaining mileage prediction performance.

- The transparency of the model should be easy to understand to follow the current condition prediction without expert knowledge. This will also enable easy adaption and transfer of the model to other engine types in future.

- The mathematical and programmable resources should be efficient to obtain a fast algorithm. It must be suitable for on-board purposes complying with storage and processor capacity constraints of the engine control unit.

The model will first predict the contaminants from the sensor data input and in a sequential step will provide a condition statement based on this prediction. It is proposed that this will yield the most accurate output as individual effects can be assessed individually to avoid interference. Chapter 4 outlined the inadequacy of using single, bivariate sensor information to derive the contaminant situation from theoretical grounds. The research in Chapter 5 identified permittivity and viscosity as the most reliable sensor input data. The investigation yield further the results that fuel, soot and oxidation are the key contaminants having the most dominant effect on the sensor measurements. Based on these findings, the defined requirements and the model targets the decision is to use a model approach based on bi-directional linear characteristic maps (Fox, 2008). The new idea that will be investigated for the application in this research work with the characteristic maps will be to assess the three-dimensional shape and gradient change of permittivity and viscosity to predict the fuel, soot and oxidation level in the oil. For each contaminant an individual map will be modelled based on a set of experimental data. Characteristic maps are widely used in the combustion engine applications and have proved to reliably model combustion or exhaust parameters that cannot be measured directly (Wenzel, 2006). The use of a characteristic map for oil condition monitoring is a completely novel approach and this investigation will verify the suitability for the application.

6.3 Scheme of the Oil Condition Rating Model

Figure 6.1 shows the main components of the oil condition rating model. The input parameters of permittivity and viscosity have proved to provide the most reliable information of oil condition changes.

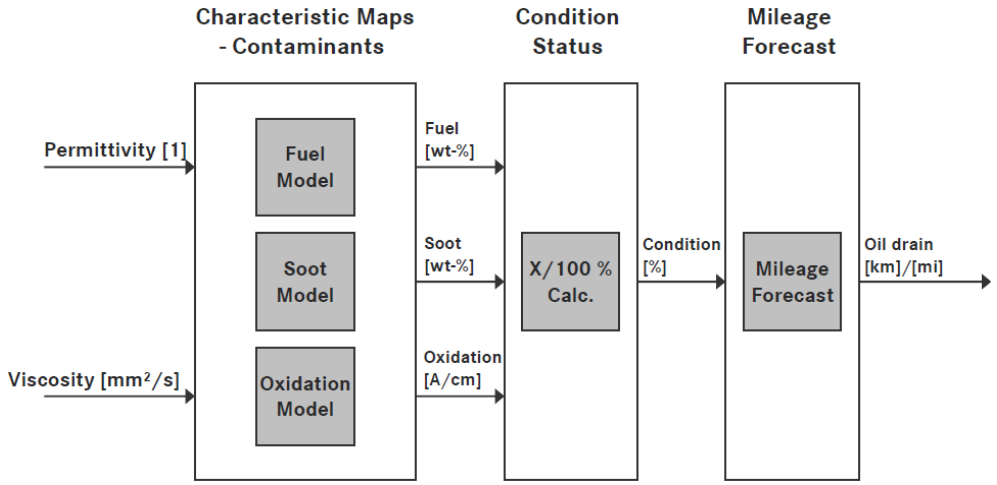

Figure 6.1: Oil condition rating model

The oil condition model consists of three core elements. The initial block 'Characteristic Maps – Contaminants' is to model an individual characteristic map for fuel, soot and oxidation based on viscosity and permittivity. The individually predicted contaminant values are used as input for the next section of the algorithm the 'Condition Status' block to calculate a rating of the overall oil condition status as a percentage value starting from 0 to 100 % with 100 % indicating fresh oil. The 'Mileage Forecast' block will then convert the derived condition status to forecast the remaining mileage until the next drain interval.

The purpose of the initial block 'Characteristic Maps – Contaminants' is to model an individual characteristic map for fuel, soot and oxidation. These contaminants have proved to have a significant influence on viscosity and permittivity and are therefore used to derive the oil condition status. Each of the characteristic maps shall predict the respective contaminant based on the viscosity and permittivity input data. The individually predicted contaminant values are then used in the next section of the algorithm as the input of the 'Condition Status' block for the calculation of the overall oil condition status. The lubricant status is then estimated as a percentage value starting from 0 to 100 % with 100 % indicating fresh oil. The 'Mileage Forecast' block will then convert the derived condition status in percentage terms to a forecast of the remaining mileage to the next drain interval. The premise and considerations of each of these elements will be investigated in detail in the following section.

6.3.1 Characteristic Map Modelling

The following explanation will develop the principal of the modelling of the characteristic lubricant contaminant maps (Linssen, 2010). This modelling uses the two input variables permittivity and viscosity and the empirical oil condition analysis data from the previous chapter. Figure 6.2 illustrates the principle of the applied piecewise bi-linear mapping procedure where x and y represent the input data and the blue dots represent the empirical target data where z_p is one data point to explain the mapping procedure as an example.

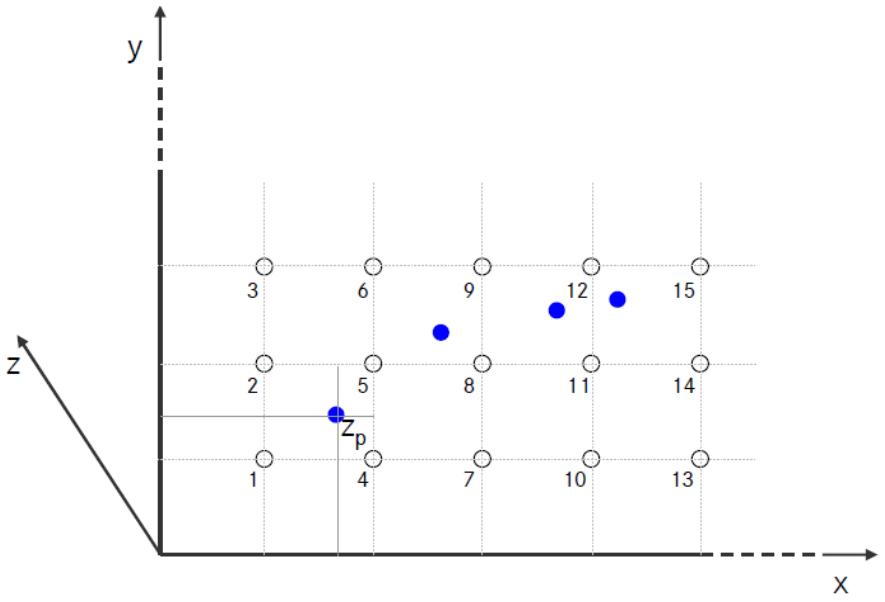

Figure 6.2: Oil condition rating model
General scheme of the bi-linear mapping procedure where x and y represent the input data and the blue dots represent the empirical data where z_p is one data point. The piecewise bi-linear mapping procedure uses the four surrounding map values z_1, z_2, z_4, z_5 to predict $\hat{z}_p$ using a linear regression.

All of the plotted characteristic map values $z_1 - z_{15}$ are unknown. As illustrated in Figure 6.2 the measured data point z_p is surrounded by four map values. The area of these four map values z_1, z_2, z_4, z_5 now need to be modelled around the particular data point z_p to then provide a similar predicted value $\hat{z}_p$ when the same input values x_p and y_p are applied to the characteristic map (Press et al., 2007: 132 – 133).

$$z_p = f_0 \cdot z_1 + f_1 \cdot z_2 + f_2 \cdot z_4 + f_3 \cdot z_5 = \begin{bmatrix} f_0 & f_1 & 0 & f_2 & f_3 & 0 \ldots 0 \end{bmatrix} \cdot \begin{bmatrix} z_1 \\ z_2 \\ z_3 \\ \vdots \\ z_{15} \end{bmatrix} \quad (6.1)$$

This procedure is repeated for all existing data points and equation 6.1 can now be rewritten for z_p in matrix format where the interpolation functions f_n form a $[n \times p]$ matrix F and the characteristic map values z_n form the unknown $[p \times 1]$ matrix Z_{CM}.

$$z_p = F \cdot Z_{CM} \quad (6.2)$$

As the matrix F and the unknown characteristic map matrix Z_{CM} are modelled with the empiric data z_p then the map needs to be able to predict the values $\hat{z}_p$ later on with the input data equation 6.2 can be written as:

$$\hat{z}_p = F \cdot Z_{CM} \quad (6.3)$$

The position of each cell point of the map in the z-direction is modelled using the least square method (Fox, 2008: 79 ff.). The least square method aims to match the data points of the unknown characteristic map Z_{CM} as close as possible to the empiric data z_p to achieve an accurate prediction of $\hat{z}_p$. This method therefore aims to minimise the sum of the squared individual residuals e_i.

$$S_E = \sum_i e_i^2 = \left(\hat{z}_p - z_p\right)^T \cdot \left(\hat{z}_p - z_p\right) \quad (6.4)$$

Using equation 6.3 in equation 6.4 results in

$$S_E = \sum_i e_i^2 = \left(F \cdot Z_{CM} - z_p\right)^T \cdot \left(F \cdot Z_{CM} - z_p\right) \quad (6.5)$$

Expanding equation 6.5 leads to equation 6.6 where the characteristic map Z_{CM} forms the unknown matrix at the beginning of the modelling process.

$$S_E = (F \cdot Z_{CM})^T \cdot F \cdot Z_{CM} - (F \cdot Z_{CM})^T \cdot z_p - z_p^T \cdot F \cdot Z_{CM} + z_p^T \cdot z_p = \\ = Z_{CM}^T \cdot F^T \cdot F \cdot Z_{CM} - 2 \cdot Z_{CM}^T \cdot F^T \cdot z_p + z_p^T \cdot z_p \quad (6.6)$$

A minimal grid fit error E_{CM} in the modelling requires:

$$min_{Z_{CM}} E_{CM} \Rightarrow \frac{\partial S_E}{\partial Z_{CM}} = 0 \quad (6.7)$$

Using the premise of the minimal error defined in equation 6.7 and the result of equation 6.6 will lead to equation 6.8.

$$\frac{\partial S_E}{\partial Z_{CM}} = 0 = 2 \cdot F^T \cdot F \cdot Z_{CM} - 2 \cdot F^T \cdot z_p \quad (6.8)$$

Rewriting equation 6.8 leads to the final equation for the unknown characteristic map matrix Z_{CM}.

$$Z_{CM} = (F^T \cdot F)^{-1} \cdot F^T \cdot z_p \quad (6.9)$$

Equation 6.9 is now the general form of the linear least-square design matrix (Fox, 2007: 195).

The general procedure of modelling a characteristic map to predict an unknown value based on a set of known input variables has now been derived in detail. If the cell of the characteristic map grid does not contain any data point during the modelling this characteristic map cell value is normally set to 0. As the existing modelling data typically does not fill every individual cell, this would result in a very irregular map. In other words, equation 6.9 will provide an undetermined set of equations, i.e. there are more variables in Z_{CM} than linearly independent equations. Some type of regularisation must therefore be introduced.

To avoid this and to interpolate between adjacent quadrants containing data points greater than 0 requires the gridfit error E_{CM} based on the standard error of the regression S_E now to be expanded by the product of a smoothing factor λ and a matrix H containing the so called 'penalty terms'.

There are two possibilities to adjust the map to increase the predictive performance. One is to set the smoothing factor λ to a fixed value and to adjust the resolution of the map. The other is to define a fixed matrix size of the Z_{CM} matrix and then adjust the smoothing factor λ. The trade-off with the first version is the increasing size of the Z_{CM} matrix. The coded terms of the H matrix form gradients and curvatures to bridge and link empty cells of the grid with adjacent cells containing data points greater than 0. Adjusting the map towards a finer resolution therefore causes an increase in the H matrix size. For automotive applications a characteristic map matrix of the size of about $[20 \times 20]$ is favourable as a larger matrix requires more storage capacity. A fixed value of λ and a varying map resolution can also lead to localised smoothing instead of global smoothing which is preferable to achieve a more universal map.

The most common approach is to define the size of the Z_{CM} matrix first and then adjust the smoothing factor λ during the modelling process. The aim is to achieve an optimum method between accuracy and universality of the model in terms of predicting the unknown data. A small smoothing factor improves the prediction of the data values and contributes to the accuracy expressed in the R^2 value of the map. Attention must also be given to ensure that the universality is not lost if it can be expected that the actual data during operation can vary from the data used for modelling. The goal is therefore to design an optimum approach between accuracy and efficiency to achieve a smooth map that will allow the forecast of unknown data points during operation. The probability that the location of data points in the grid cells during the operation of the algorithm is equal to the data points used to design the map is very low. Designing the characteristic map therefore requires the modelling areas of the map which are not defined with data points during the modelling phase as some grid cells are empty. The goal is to forecast all unknown data points with a high accuracy in the entire mapping range. C in equation 6.10 is referred to as the overall cost of the modelling process to interpolate between the non-empty quadrants in order to achieve a smooth curvature map and to forecast data points which were not covered during the design process.

$$C = S_E + \lambda \cdot Z_{CM}^T \cdot H \cdot Z_{CM} \tag{6.10}$$

Using equation 6.5 the overall costs can now be written as:

$$\begin{aligned} C &= \left(F \cdot Z_{CM} - z_p\right)^T \cdot \left(F \cdot Z_{CM} - z_p\right) + \lambda \cdot Z_{CM}^T \cdot H \cdot Z_{CM} = \\ &= \left(F \cdot Z_{CM} - z_p\right)^T \cdot \left(F \cdot Z_{CM} - z_p\right) + \lambda \cdot Z_{CM}^T \cdot H \cdot Z_{CM} \end{aligned} \tag{6.11}$$

To achieve a minimal gridfit error, refer to equation 6.7, then equation 6.12 needs to be equated to 0.

$$\begin{aligned} \frac{\partial C}{\partial Z_{CM}} &= 0 = 2 \cdot F^T \cdot F \cdot Z_{CM} - 2 \cdot z_p^T \cdot F + \lambda \cdot H \cdot Z_{CM} = \\ &= \underbrace{\left(2 \cdot F^T \cdot F + \lambda \cdot H\right)}_{B} \cdot Z_{CM} - 2 \cdot z_p^T \cdot F = \\ &= B \cdot Z_{CM} - 2 \cdot z_p^T \cdot F = 0 \end{aligned} \tag{6.12}$$

Solving equation 6.12 leads again to an expression for the characteristic map matrix Z_{CM}, which is similar to equation 6.9, but this time including the smoothing factor λ and the H matrix to forecast all values within the data range of the Z_{CM} matrix. The modelling of the characteristic maps in this research work was conducted using an expanded gridfit function (D'Errico, 2005). This is a part of the MathWorks online catalogue for Matlab code which is based on the presented theoretical steps explained in this section. The gridfit function enables the modelling of a characteristic map from a combination of experimental data and manual calibration. The most important aspect in the modelling is the definition of data points, the characteristic map size resolution and the smoothing adjustment using a graphic user interface (Linssen, 2010). The output of the map modelling consists of the Z_{CM} matrix provided as absolute values and a three-dimensional plot of the map. The data is used to plot the correlation of the experimental data versus the predicted data and to calculate the coefficient of determination R^2 to assess the quality of the modelled map. The flow-chart in Figure 6.3 illustrates the steps involved to model each of the characteristic maps.

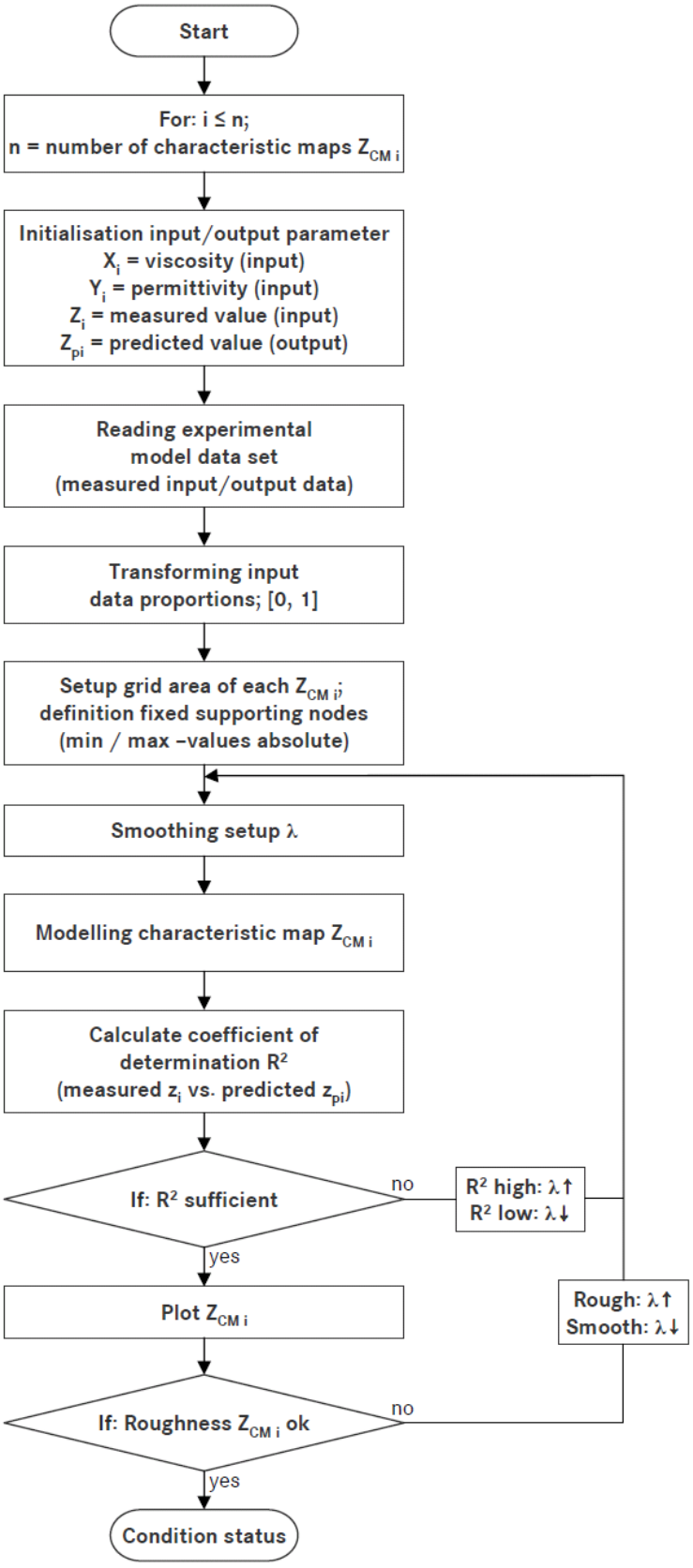

Figure 6.3: Flow-chart – characteristic map modelling

The first step is to initialise the input data X_i, Y_i, viscosity and permittivity. The experimental data set contains measured or manually adapted input and output data, i.e. the individual contaminant Z_i. The predicted value Z_{pi} is also initialised. The next step is to transform the data in order to achieve equal proportions which enable more accurate modelling (Fox, 2007: 66 - 68). The setup of the grid area and the definition of the supporting nodes require knowledge of the intended application. The typical size of maps to be used in automotive applications is approximately $[20 \times 20]$. The experimental data used to model the grid needs to be reviewed to define reasonable supporting nodes, i.e. minimum and maximum values for each map. Tuning the smooth curvature setup when modelling the characteristic map $Z_{CM\,i}$ is the fundamental task in the modelling process. This step has a significant influence on the modelling outcome as it defines the accuracy and the robustness of the model. Every characteristic map is typically modelled on the basis of experimental data containing the input and respective output values. The map is modelled to fit around this particular data and enables to predict similar output values compared to the experimental data with the input values applied during operation. A low level of smooth curvature of the map will provide high accuracy to model and forecast the particular experimental data set. These maps are typically characterised by a very rough surface shape. Such a map will be highly accurate if it can be assumed that all data during the operation is nearly identical to the experimental data used to model this map. The trade-off of such a map is the lack of accuracy if the data during operation is different from the experimental data used to model the map. This is the general case during operation due to different input values or noisy data. Also since repeated measurements of the same data sample to model the map are not generally available, potential noise on the data needs to be taken into account during the modelling. For practical applications a smoother, less rough map is preferred as this provides higher robustness and provides better compensation of noise on the data. The accuracy of the iterative manual modelling process can be assessed by two aspects. One is the calculation of the R^2 value between the measured and the predicted value for each map. This provides a measure of the achieved accuracy of the map. The roughness of the map which provides information of the robustness of the model needs to be assessed on a visual basis. Awareness of the underlying theories and interactions must be taken into account in order to obtain a characteristic map that will reliably predict the contaminants value of interest. In most cases an iterative improvement process is required to model the optimal map solving the forecasting problem, i.e. the lubricant contaminants based on permittivity and viscosity. The next step after modelling the three characteristic maps to predict fuel, soot and oxidation is to obtain the resulting lubricant condition status.

6.3.2 Lubricant Condition Rating

All the equipment of a system is subject to stress during operation. This stress causes damage and reduces the deterioration reserve of the particular part. If the condition of a part falls below a specific damage limit the functionality is no longer ensured and damage to the component part can occur. The damage of component parts can be subdivided into two main categories (DIN 40041, 1990):

- Immediate or spontaneous damage
- Continuous or drift damage

The focus of the consideration with engine oil is on continuous damage of the lubricant during the engine operation. The damage of the oil occurs in the form of the degradation effects during engine operation. Immediate damage of the oil is very rare and occurs only in the case of mechanical engine failure such as a broken head gasket leading to immediate glycol dilution of the oil with a spontaneous gelling and viscosity increase. The characteristic of continuous damage is that the damage reserve of the operating part is continuously consumed and the lifetime of the part is therefore reduced and therefore limited. Drift damages allow a continuous monitoring and knowledge of the limit of damage enables the prediction of imminent breakdown. The status definition of the operating part requires condition monitoring and knowledge of the actual damage limit of the part. The following consideration is therefore focused on the definition of the condition status of the lubricant. The general operation and damaging process of an operating part is illustrated in Figure 6.4 (Sturm cited by Engelhardt, 2007: 18). The input variable vector $\underline{U}$ defines the usage of the operating part which causes corresponding stress of the part. In the case of the engine oil this is the contact with exhaust gases, shearing in the bearings, contact with friction surfaces in the combustion chamber etc. The influencing variables $\underline{N}$ are the resulting unknown disturbances, e.g. poor (bio-)fuel quality, soot loading or thermal stress affecting the oil condition which accelerate the degradation. The output variable vector $\underline{Y}$ is the remaining ability of the lubricant to fulfil its defined functions in the engine. The stress caused by the operation responds in the damaging processes which will over time influence the operating process. The impact due to damage or wear influences the operation and damage parameter and leads to different output characteristics of the operating part, i.e. oil condition.

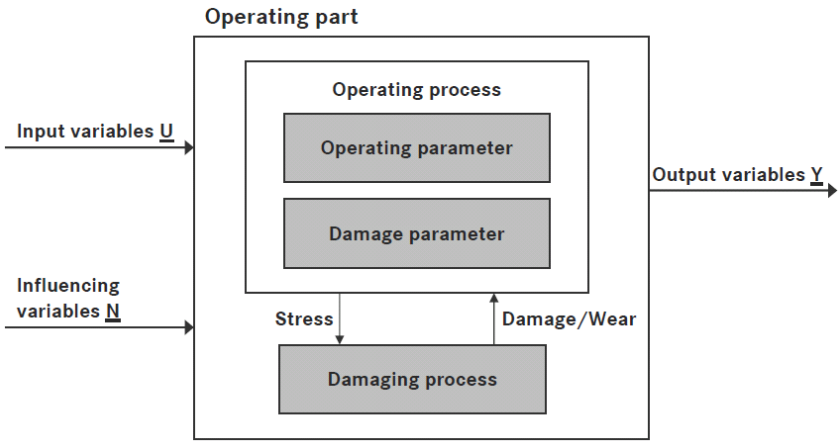

Figure 6.4: Operation and damaging process of an operating part (Sturm cited by Engelhardt, 2007: 18)

The input variable vector U defines the usage of the operating part which causes corresponding stress of the part. The influencing variables N are the resulting unknown disturbances, e.g. poor (bio-)fuel quality, soot loading or thermal stress affecting the oil condition which accelerate the degradation. The output variable vector Y is the remaining ability of the lubricant to fulfil its defined functions in the engine. The stress caused by the operation responds in the damaging processes which will over time influence the operating process. The impact due to damage or wear influences the operation and damage parameter and leads to different output characteristics of the operating part,

The output characteristic of the lubricant is defined by the permittivity value which indicates the lubricant damage caused by polar contaminants. The viscosity value indicates the damage caused by effects having an impact on the flow properties.

There are numerous methods to define the condition status which can be divided into five main categories (Engelhardt, 2007):

- Direct methods
- Indirect methods
- Parameter based methods
- Load/Stress based methods
- Reliability based methods

The basis for all methods to describe the condition status is the processing of the input, influencing and output variables. In some cases it is impossible to quantify all the input and influencing variables. The lubricant condition monitoring is therefore only based on the assessment of the output variables to derive the actual condition status. A universal approach to describe the state condition of parts therefore does not exist. It requires an engineering solution to define the condition status for each operating part or application which meets the requested accuracy, reliability and efficiency.

The condition status according to Reichard (cited by Engelhardt, 2007: 19 - 20) can be illustrated using two mathematical functions. In the step f_1 the observation dimension O is the input, influencing and output variable transformed into a characteristic dimension C. This is expressed by equation 6.13:

$$f_1: \; O \in |R^m \Rightarrow C \in |R^n \tag{6.13}$$

In step f_2 is the characteristic dimension C transformed into a scalar value z representing the condition status of the operating part. The scalar value z is typically provided in a normalised fashion from 0 to 1 (Fox, 2007: 79).

$$f_2: \; C \in |R^n \Rightarrow z \in [0, 1] \tag{6.14}$$

Figure 6.5 illustrates the general process to describe the condition of operating parts.

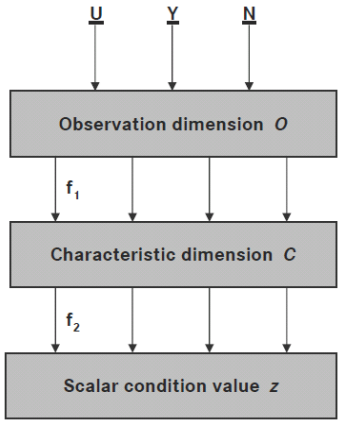

Figure 6.5: Process to describe the operation condition (Engelhardt, 2007)
The condition status can be illustrated using two mathematical functions. In the step f1 the observation dimension O is the input, influencing and output variable transformed into a characteristic dimension C. In step f2 is the characteristic dimension C transformed into a scalar value z representing the condition status of the operating part. The scalar value z is typically provided in a normalised fashion from 0 to 1.

From the five main categories to derive the condition status of component parts the proposed condition rating model can be categorised to the direct methods. The direct method is characterised by having a sensor that measures directly or via known correlations, the condition of the part, i.e. the lubricant. The elements of the observation dimension *O* therefore consist only of the data of the output variables Y, i.e. the sensor data. This approach is in general the most accurate way to determine the condition status of parts (Engelhardt, 2007: 21). To obtain the actual condition status as a scalar value a damage threshold or limit needs to be defined.

The predicted oil contamination from each modelled characteristic maps is compared with the individual damage limit. The distance from each damage limit is used to derive the overall oil condition rating. The definition of the damage limits for the condition algorithm will be considered in the following step using the stress or load based method (Engelhardt, 2007: 26). The stress based method evaluates the stress that affects the condition of the operating part. The correlation between the applied stress, i.e. the contaminant, and the change in the oil condition uses empirical oil analysis data. The principle of this method is to ascribe the applied stress, i.e. the contaminant, to the resulting damage or loss of initial condition of the oil.

All of the contaminants with significant statistical influence on the sensor data affect the viscosity. An assessment of the damaging influence of the contaminants on the viscosity data will therefore be used to define the damage limits. For the oxidation limit the loss of alkaline reserve expressed by the TBN value will also be taken into account. Permittivity proved to be the most sensitive sensor parameter to predict the contaminant level in the oil but it cannot be used to define damage levels of the oil caused by contaminants as it has no characteristic engine oil performance parameter. The selected data from the engine oil database consists of over 400 diesel engine oil analysis samples. The assessment of the damage level of the particular contaminant uses bivariate scatterplots.

Fuel Rating

Figure 6.6 shows the viscosity value as a function of fuel dilution.

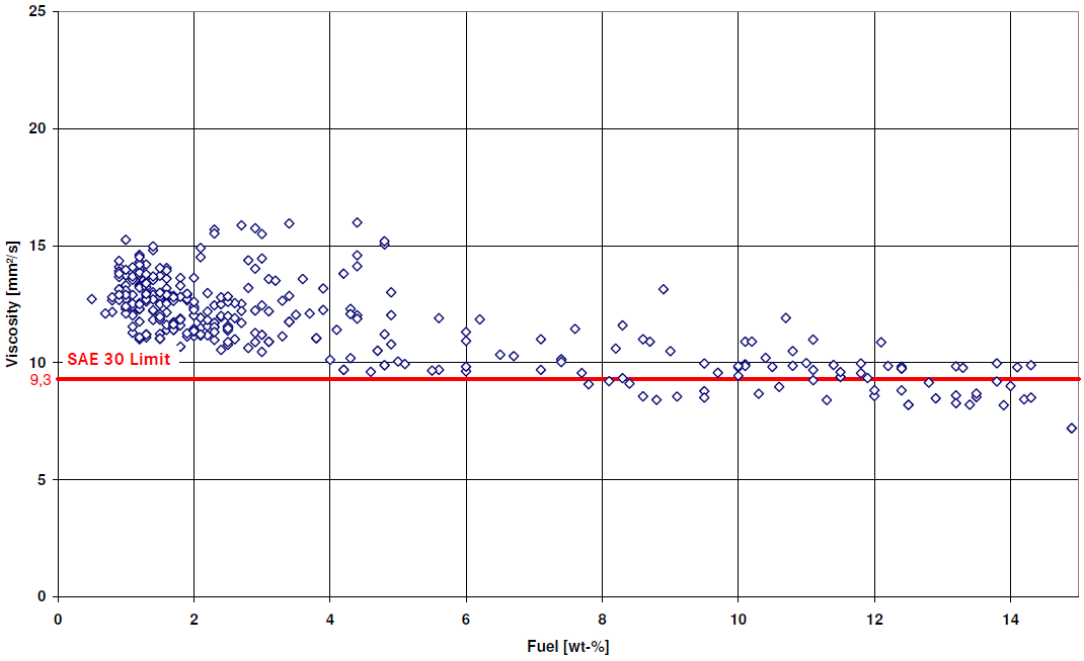

Figure 6.6: Damage limit fuel - viscosity over fuel dilution

The blue dots represent the used diesel engine oil data. The red line indicates the lower viscosity limit of 9.3 [mm²/s] for SAE 30 grade oils defined by the SAE J 300 (SAE J300, 2009). This lower limit is defined as the damage limit for the damage parameter. From the data plot it can be observed that the operating parameter of viscosity starts to fall below the damage limit with fuel concentrations of 7.8 – 8.0 [wt-%]. The fuel damage limit is therefore defined as 8.0 [wt-%].

The characteristic dimension C is defined by the operating parameter, the kinematic viscosity at 100 [°C] and the damage parameter fuel D_{Fuel} on the lubricant performance.

$$D_{Fuel} = [0-15][wt-\%] \tag{6.15}$$

The red line indicates the lower viscosity limit of 9.3 [mm²/s] for SAE 30 grade oils defined by the SAE J 300 (SAE J300, 2009). This lower limit is defined as the damage limit for the damage parameter as low viscosity is critical regarding higher potential wear. Alternatively the accumulated fuel is prone to oxidation processes and a more conservative damage limit is therefore favoured. From the data plot in Figure 6.6 it is observed that the operating parameter of viscosity starts to fall below the damage limit with fuel concentrations of about 7.8 – 8.0 [wt-%].

The maximum fuel damage limit $D_{MaxFuel}$ is therefore defined as:

$$D_{MaxFuel} = 8\,[wt-\%] \tag{6.16}$$

The scalar predicted condition value $\hat{z}_{Fuel}(i)$ is defined by the i-th predicted fuel value obtained from the characteristic map for fuel $\hat{z}_{p\,Fuel}(i)$ at a certain sampling point.

$$\hat{z}_{Fuel}(i) = 1 - \frac{\hat{z}_{p\,Fuel}(i)}{D_{MaxFuel}} \tag{6.17}$$

Soot Rating

Figure 6.7 shows the viscosity value as a function of soot loading of the oil.

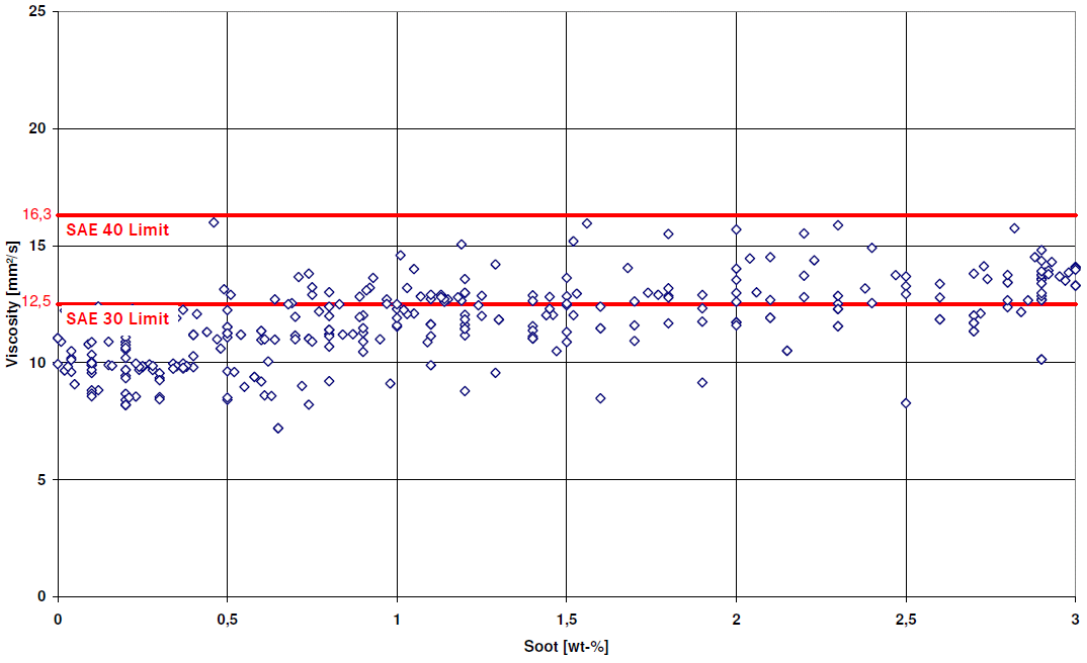

Figure 6.7: Damage limit soot - viscosity over soot concentration

The blue dots represent the used diesel engine oil data. The two red lines indicate the upper viscosity limits of 12.5 [mm²/s] for SAE 30 grade oils and 16.3 [mm²/s] for SAE 40 grade oils (SAE J300, 2009). From the data plot it is observed that the majority of data points up to 3 [wt-%] are below the upper limit for SAE 40. The soot damage limit is therefore defined as 3 [wt-%].

The characteristic dimension C is defined by the operating parameters kinematic viscosity at 100 [°C] and the damage parameter soot D_{Soot} on the lubricant performance.

$$D_{Soot} = [0-3][wt-\%] \tag{6.18}$$

The two red lines indicate the upper viscosity limits of 12.5 [mm²/s] for SAE 30 grade oils and 16.3 [mm²/s] for SAE 40 grade oils (SAE J300, 2009). From the data plot in Figure 6.7 it is observed that the majority of data points up to 3 [wt-%] soot are below the upper limit for SAE 40. The maximum soot damage limit $D_{MaxSoot}$ is therefore defined as:

$$D_{MaxSoot} = 3\,[wt-\%] \tag{6.19}$$

The i-th predicted condition value $\hat{z}_{Soot}(i)$ is defined by the soot value obtained from the characteristic map for the predicted soot level $\hat{z}_{pSoot}(i)$.

$$\hat{z}_{Soot}(i) = 1 - \frac{\hat{z}_{pSoot}(i)}{D_{MaxSoot}} \tag{6.20}$$

Oxidation Rating

Figure 6.8 shows the kinematic viscosity as a function of oxidation.

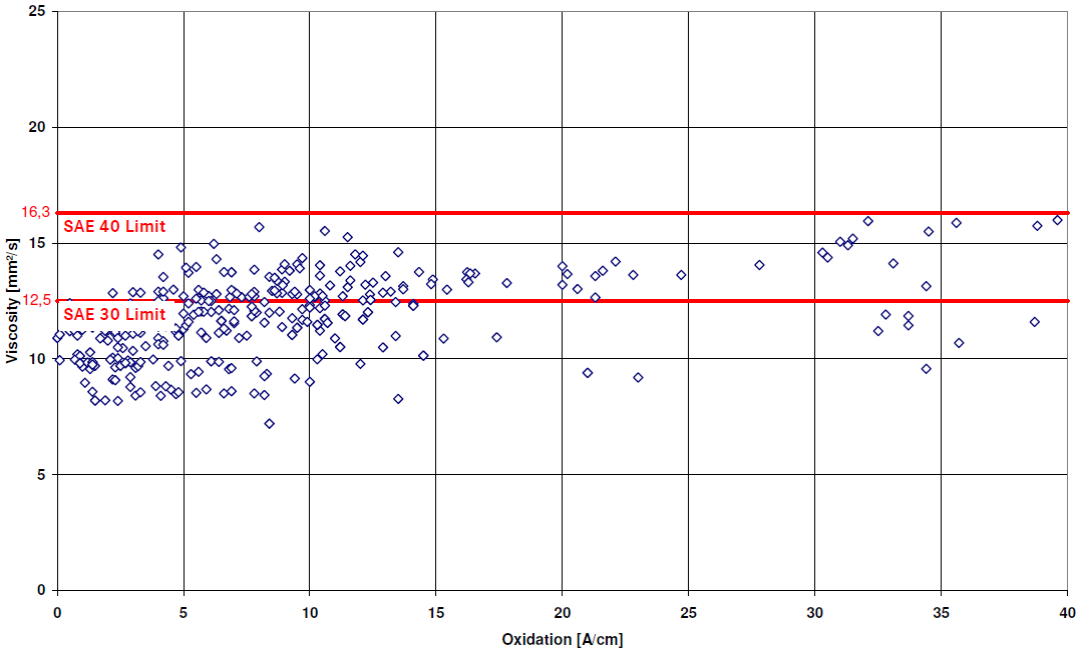

Figure 6.8: Damage limit oxidation - viscosity over oxidation level
The blue dots represent the used diesel engine oil data. The two red lines indicate the upper viscosity limits of 12.5 [mm²/s] for SAE 30 grade oils and 16.3 [mm²/s] for SAE 40 grade oils (SAE J300, 2009). The data plot shows that the critical viscosity values exceeding the SAE 40 limit occur with oxidation level > 30 [A/cm]. The oxidation damage limit is therefore defined as 30 [A/cm].

The characteristic dimension C is defined by the operating parameters kinematic viscosity at 100 [°C] and the damage parameter oxidation D_{Oxi}.

$$D_{Oxi} = [0 - 40][A/cm] \tag{6.21}$$

The two red lines indicate the upper viscosity limits of 12.5 [mm²/s] for SAE 30 grade oils and 16.3 [mm²/s] for SAE 40 grade oils (SAE J300, 2009). The data plot in Figure 6.8 shows that the critical viscosity values exceeding the SAE 40 limit occur with oxidation level > 30 [A/cm]. Lower viscosity levels in this region of oxidation are most likely due to the dominating thinning effects of the fuel in the oil. It must be considered that it is only a matter of time until the oxidation at this level dominates the viscosity change towards a higher viscosity level due to polymerisation.

The TBN against oxidation plot in Figure 6.9 is used to confirm the assessment based on the evaluation of the oxidation impact on the lubricant operating parameter TBN.

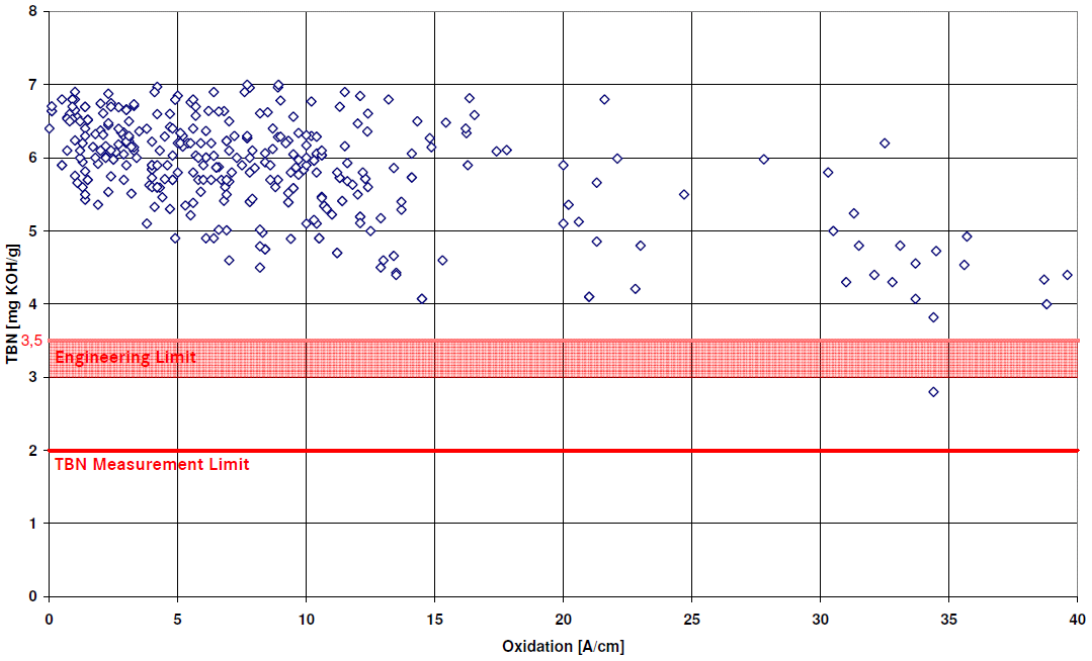

Figure 6.9: Damage limit oxidation - TBN over oxidation level

The blue dots represent the used diesel engine oil data. The generally accepted engineering limit in the industry to consider an oil drain is when the TBN value has dropped below 50 % of its fresh oil value. This is indicated by the red shaded area. The lowest possible TBN value that can be measured relatively accurately is 2 [mg KOH/g]. The data plot shows that the TBN value decreases considerably towards the oxidation value of 30 [A/cm]. The noticeable impact of oxidation on the lubricant performance for oxidation levels > 30 [A/cm] is consistent with the observations of the oxidation influence on viscosity and confirms the damage limit for oxidation with 30 [A/cm].

All of the used engine oils are modern low ash diesel engine oils. The low ash formulation was developed to prevent DPF blocking (Sappok and Wong, 2010). The ash reduction based on other additive components and additive treatment rates result in lower initial TBN values compared to conventional oil. Most fresh oil TBN values are in a region of 6 – 7 [mg KOH/g]. There is no hard threshold to judge when the TBN value has reached its limit as the TBN depletion is not a linear function over time. The generally accepted engineering limit in the industry to consider an oil drain is when the TBN value has dropped below 50 % of its fresh oil value. This is indicated in Figure 6.9 by the red shaded area. Another issue is that the TBN value can even with today's methods only be determined with an accuracy of about ± 10 %. Also the lowest possible TBN value that can be measured relatively accurately is 2 [mg KOH/g]. The data plot in Figure 6.9 shows that the TBN value decreases considerably towards the oxidation value of 30 [A/cm].

There is only one critical TBN value that falls below the indicated engineering limit. However, it is apparent from the data plot that the TBN level is significantly reduced between 30-40 [A/cm]. The noticeable impact of oxidation on the lubricant performance for oxidation levels > 30 [A/cm] is consistent with the observations of the oxidation influence on viscosity shown earlier. A reliability focused oxidation damage limit D_{MaxOxi} is therefore defined as:

$$D_{MaxOxi} = 30\,[wt-\%] \tag{6.22}$$

The scalar predicted condition value $\hat{z}_{Oxi}(i)$ is defined by the i-th predicted oxidation value $\hat{z}_{pOxi}(i)$ obtained from the characteristic map for oxidation.

$$\hat{z}_{Oxi}(i) = 1 - \frac{\hat{z}_{pOxi}(i)}{D_{MaxOxi}} \tag{6.23}$$

Lubricant Condition Rating

All of the assessed characteristics show a linear decreasing condition i.e. progressive damage. Most applications of the stress based condition evaluation method define the overall damage of a part or system by adding all identified individual damage values (Engelhardt, 2007: 27). This proposal will not be applied here as this research work has shown that all contaminants have an equally high potential in damaging the lubricant condition and subsequently the engine. To achieve maximum engine protection it is defined that the lowest independent rating of each of the three predicted condition values $\hat{z}_{Fuel\,/\,Soot\,/\,Oxidation}(i)$ defines the overall i-th oil condition prediction $\hat{z}_{Oil}(i)$, refer to equation 6.24.

$$\hat{z}_{Oil}(i) = \left| \hat{z}_{Fuel}(i), \hat{z}_{Soot}(i), \hat{z}_{Oxi}(i) \right|_{\min} \tag{6.24}$$

The algorithm steps to derive the oil condition are schematically summarised in the flowchart in Figure 6.10. For each interval *i* the respective fuel, soot and oxidation prediction from each characteristic map is compared with the defined damage thresholds for each contaminant. The individual condition values $\hat{z}_{Fuel\,/\,Soot\,/\,Oxidation}(i)$ are predicted according to equations 6.17, 6.20 and 6.23. The predicted overall oil condition rating of the i-th interval is calculated according to equation 6.24. There is no rule for the length of the interval steps *i*. As the oil condition changes are in general relatively slow a sampling interval of 10 [km] / 6.22 [mi] for the prediction absolutely sufficient.

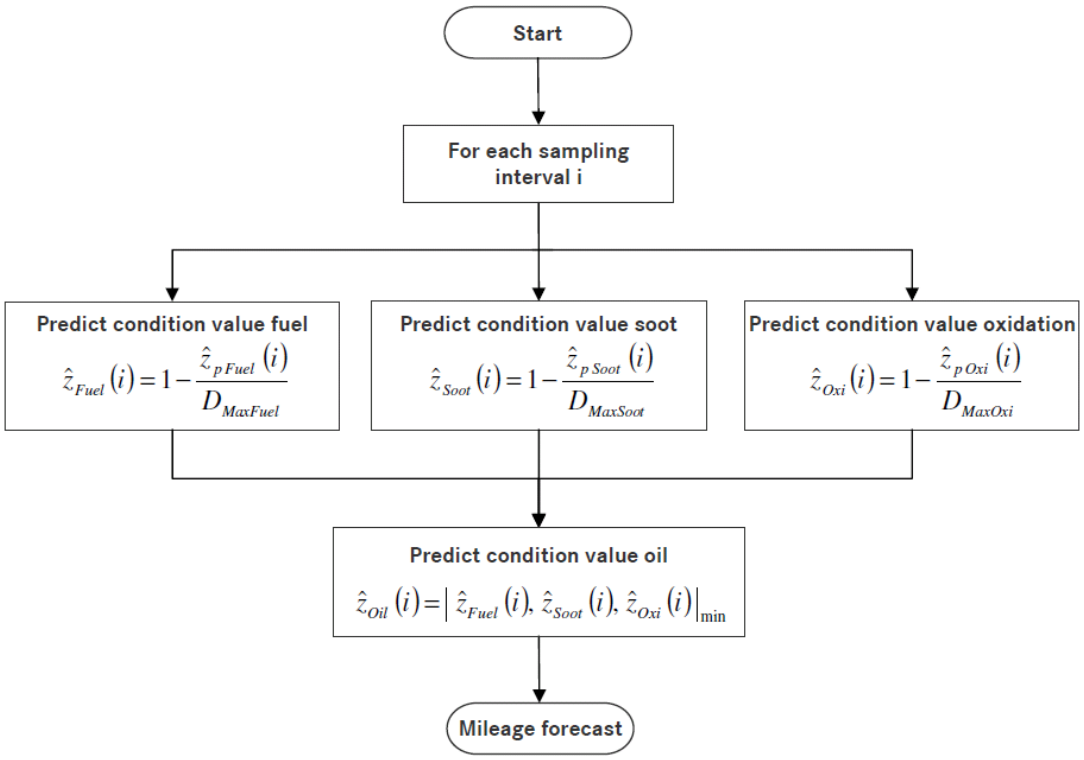

Figure 6.10: Flow-chart – oil condition rating process

6.3.3 Mileage Forecast

The remaining mileage forecast algorithm presented in this section is guided by a set of conditions which are explained in a first step.

Monitoring and forecasting area

Most of the current Mercedes-Benz passenger cars have a fixed maintenance interval of 25,000 [km] / 15,534 [mi]. The aim of the mileage algorithm concept is to forecast whether this regular interval can be maintained without any risk to the reliability for the engine due to degraded oil. As the algorithm design is conservative to maximise reliability, it is assumed that with the regular oil drain interval at 25,000 [km] / 15,534 [mi] at least one of the damage limits $D_{Max\,n}$ of fuel, soot and oxidation is reached, see equations 6.17, 6.20 and 6.23.

The monitoring and mileage forecast area where the algorithm operates is illustrated with the grey shaded area in Figure 6.11. This assumes that the fresh oil quality starts at 100 % and is continuously consumed until the condition becomes 0 % at the maximum mileage.

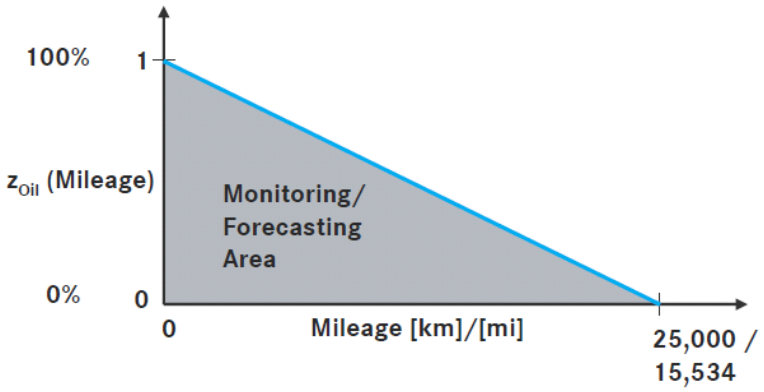

Figure 6.11: Remaining mileage forecasting area
The monitoring and mileage forecast area where the algorithm operates is illustrated with the grey shaded area. This assumes that the fresh oil quality starts at 100 % and is continuously consumed until the condition becomes 0 % at the maximum mileage.

Condition progress

The general condition of the operating parts is monitored at discrete points $i = 1, 2, 3, \ldots n$ and is assigned the following characteristic:

$$\begin{aligned} &z_i \in [0, 1] \\ &z_i \geq z_{i+1} \quad i = 1, 2, \ldots, n-1 \end{aligned} \tag{6.25}$$

It is assumed that for all operating parts the condition status over the lifetime or the operating time will remain at the previous condition status or will be lower than when the condition status was sampled at discrete intervals, see equation 6.25. The general assumption is that the status of a part cannot improve during its operation without maintenance. The dynamic of the condition loss can be described as progressive, linear or degressive, see Figure 6.12.

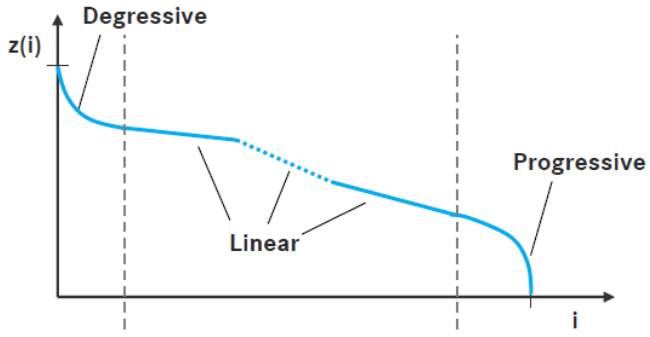

Figure 6.12: Characteristic condition progress

The general assumption is that the status of a part $z(i)$ cannot improve during its operation without maintenance. The dynamic of the condition loss can be described as progressive, linear or degressive.

One distinctive aspect which conflicts with the general condition equation 6.25 which needs to be taken into consideration regarding the engine oil condition is the process of oil top-ups. Although oil drain is regarded as the main maintenance activity where the oil is replaced, oil top-ups between the drain intervals where partial maintenance occurs must also be considered. Since the fresh oil additives can improve the condition status $\hat{z}_{Oil}(i)$ of the oxidation process or can result in a thinning of the soot particles per volume then equation 6.26 must also be considered with equation 6.25 where I_0 is the point in time of the oil top-up.

For oil top up:

$$z_i \in [0,1] \qquad z_i \leq z_{i+1} \quad i = I_0, \ldots, I_{0+n} \tag{6.26}$$

The effect of a sign reversal in the condition progress will only be temporary as the degradation will continue after a certain delay when the amount of fresh additives becomes depleted. This is illustrated schematically in Figure 6.13. By definition, the resulting mileage forecast cannot exceed the overall drain interval of 25,000 [km] / 15,534 [mi] even in the case of an improvement in the oil condition due to the addition of fresh oil.

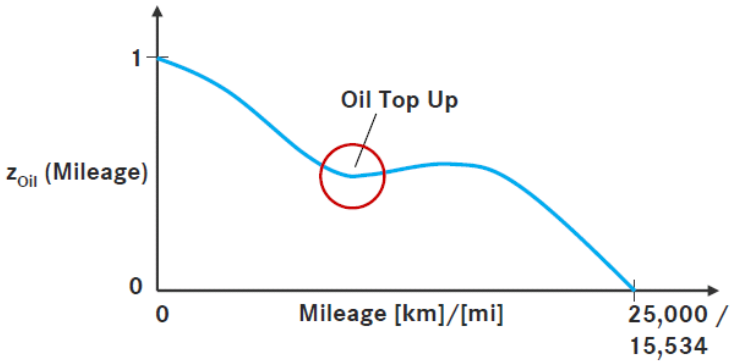

Figure 6.13: Characteristic oil condition progress – sign reversal with top up
Oil drain is regarded as the main maintenance activity where the oil is replaced. Oil top-ups between the drain intervals where partial maintenance occurs must also be considered since the fresh oil additives can improve the condition status and can cause a temporary sign reversal.

Mileage forecasting principle

Models used to predict the remaining lifespan of the oil assess the condition loss gradient in order to identify structural interruptions in the gradient which can cause faster or slower condition loss. The general assessment to predict the future end of use of the operating part uses linear regression analysis which enables approximating the progress of the regression interval, see the scalar format in equation 6.27 and in matrix form in equation 6.28 (Fox, 2008: 79).

$$y_i = \beta_0 + \beta_1 \cdot x_i + \varepsilon_i \quad i = 1,\ldots,n \tag{6.27}$$

$$Y = X \cdot \beta + \varepsilon \tag{6.28}$$

The response variables y_i or respectively the $[n \times 1]$ response vector Y contains the predicted condition value $\hat{z}_i$ from the previous condition rating. The regressor x_i is a defined mileage sampling point where a new condition status $\hat{z}_{Oil}(i)$ is calculated. This is in the matrix form defined by the $[n \times 2]$ design matrix X. The important aspect of linear regression analysis is the estimation of the unknown regression coefficients β_0 and β_1 which is in the matrix form defined by the $[2 \times 1]$ parameter vector. The error terms ε_i are in the matrix form defined by the $[n \times 1]$ vector ε.

Typical end of useful life prediction methods assess a retrospective interval $\hat{W} = [n, \tau]$ with $\tau < n$ and there are three methods of defining the forecasting window $\hat{W}$.

The regression using an expanding window considers all data from the current point in time n back to the beginning of the analysis. This results in a continuous increase in data. The resulting observation vector and the regressor matrix are:

$$Y_{n,1} = z_{n,1} = \left(z_n \; z_{n-1} \; z_{n-2} \; \ldots \; z_1\right)^T \tag{6.29}$$

$$X_{n,1} = \left(x_n \; x_{n-1} \; x_{n-2} \; \ldots \; x_1\right) \tag{6.30}$$

Changes in the gradient have a relatively low impact on forecasting the results as all the data, including the data before the gradient change, are used to derive the parameter matrix. The convergence characteristic is therefore poor.

With the regression using a fixed window size $\hat{W} = c$, which is referred to as rolling window, the amount of data used to predict the end of life can be defined individually. The resulting response vector and the regression matrix are:

$$Y_{n,n-c+1} = z_{n,n-c+1} = \left(z_n \; z_{n-1} \; z_{n-2} \; \ldots \; z_{n-c+1}\right)^T \tag{6.31}$$

$$X_{n,n-c+1} = \left(x_n \; x_{n-1} \; x_{n-2} \; \ldots \; x_{n-c+1}\right) \tag{6.32}$$

The beneficial aspect with this approach is the dimension of the window which limits the amount of data to adjust the precision of the prediction. If the window is too large the forecast will be slow and inaccurate. A small window size increases the accuracy but may lead to rapid changes in the forecast. However, there is no specific rule to choose the appropriate size of the window. By applying this method requires sufficient knowledge about the component to be monitored and how quickly structural interruptions are expected.

Another approach is the weighted window method where the observed condition value z_i is weighted by a factor α_i. The weighting factor in this case is defined according to equation 6.33 (Engelhardt, 2007).

$$\alpha_i = \alpha_{n-i}, \text{ with } i = 1, 2, 3, \ldots n, \ \alpha \in]0, 1] \tag{6.33}$$

This method results in an exponential weighting of the values z_i where the latter values have more influence on the regression than the previous values. The resulting observation vector and the regressor matrix are defined as:

$$Y_{n,1}(\alpha) = z_{n,1}(\alpha) = (\alpha_0 \cdot z_n \ \alpha_1 \cdot z_{n-1} \ldots \alpha_n \cdot z_1)^T \tag{6.34}$$

$$X_{n,1}(\alpha) = (\alpha_0 \cdot x_n \ \alpha_1 \cdot x_{n-1} \ldots \alpha_n \cdot x_1)^T \tag{6.35}$$

The settings of α has a significant influence on the forecast characteristic. A smaller value of α cause previous values to have less influence and the prediction might be unstable. Larger values of α have a stronger influence on all z_i values and might result in an inert forecast performance. There are no rules to determine α, and it must be adapted for the intended application based upon engineering judgement and experience (Engelhardt, 2007).

The intended design of the mileage forecast algorithm is to achieve an efficient and lean solution. A low number of data points and an effective calculation approach are therefore being favoured to save processor and storage capacity resources. From the forecasting models presented the rolling window approach has been selected with a window size of c = 100 [km] / 62.15 [mi] and a rolling forward step size of x_i = 10 [km] / 6.215 [mi]. This means that the regression steps are 10 [km] / 6.215 [mi] where the window is shifted forward and the calculated condition value $\hat{z}_{Oil}(i)$ plus the 9 previously examined oil condition form the response variables:

$$Y_{i,i-9} = (\hat{z}_{Oil\,i} \ \hat{z}_{Oil\,i-1} \ \hat{z}_{Oil\,i-2} \ \ldots \hat{z}_{Oil\,i-9})^T \tag{6.36}$$

$$X_{i,i-9} = (x_i \ x_{i-1} \ x_{i-2} \ \ldots x_{i-9}) \tag{6.37}$$

One condition of the algorithm is the slope which is defined in the linear regression as β_1, see equation 6.27. The slope is referred to as the nominal condition loss gradient and is defined by the fixed maximum oil interval:

$$\beta_1 = \frac{100\%}{25{,}000km} = \frac{100\%}{15{,}534mi} \tag{6.38}$$

The only unknown value which is calculated using linear regression with the 10 values in the window is the offset β_0 of the calculated regression slope at the end of the window. The remaining mileage x_0 is calculated by extrapolating from this offset with the nominal condition loss gradient until $\hat{z}_{Oil} = 0\ \%$.

$$\hat{z}_{Oil} = 0 = \beta_0 + \beta_1 \cdot x_0 \tag{6.39}$$

Figure 6.14 illustrates the mileage forecast scheme using the rolling window approach and the shifting of the nominal condition loss gradient based on the calculated offset. The orange dots represent the individual condition results in percentage within the defined rolling window derived from the previous condition rating.

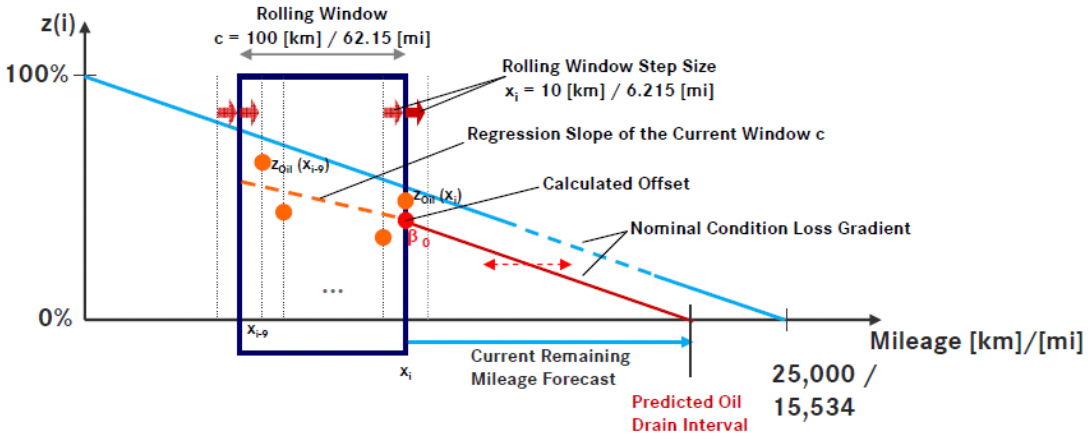

Figure 6.14: Rolling window remaining mileage forecasting principle

A rolling window approach has been selected with a window size of c = 100 [km] / 62.15 [mi] and a rolling forward step size of x_i = 10 [km] / 6.215 [mi]. The regression steps are 10 [km] / 6.215 [mi] where the window is shifted forward and the calculated condition value plus the 9 previously examined oil condition values are used to calculate the current offset. The nominal condition loss gradient is then shifted, based on the offset and extrapolates to predict the next oil drain interval.

The implementation of a driver information concept based on the outcome of this algorithm will not be discussed in this research work.

Figure 6.15 illustrates the algorithm using a flow chart to summarise the main steps of the mileage forecast calculation process.

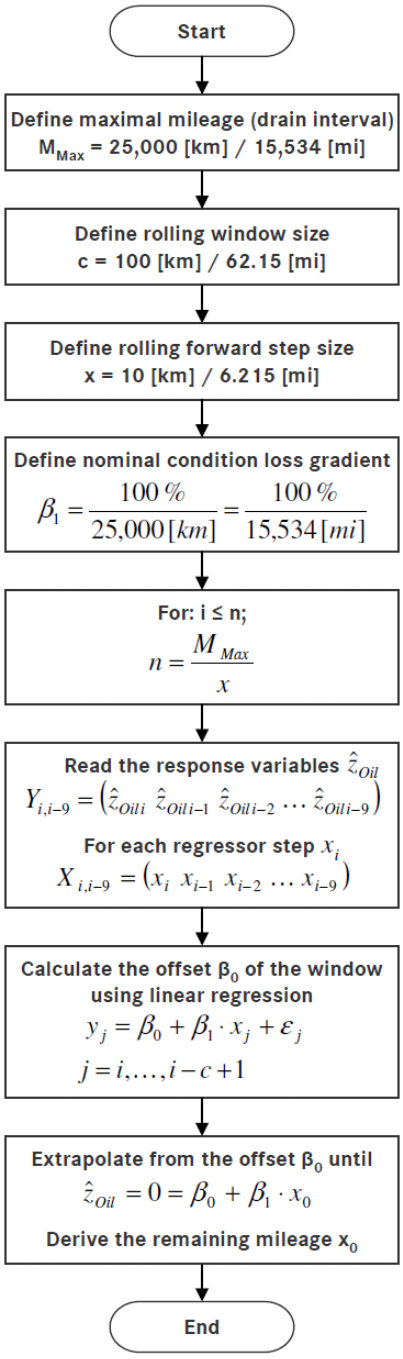

Figure 6.15: Flow chart mileage forecast

One aspect that will need to be adapted for practical vehicle use is that the window is not only rolled mileage-wise but also time-wise. This is particularly important for vehicles that idle a lot such as taxis or chauffeur driven cars.

The time between 10 [km] / 6.215 [mi] steps may be too long to ensure an appropriate mileage forecast. The rolling forward mechanism therefore needs to be adapted to count the mileage and also the engine operation time. A reasonable sampling time must be evaluated and the event, i.e. sampling mileage limit or sampling time limit, that occurs earlier triggers the forward rolling of the window.

6.4 Summary

This chapter has presented the initial conditions and innovative aspects of the oil condition algorithm to support a reliable and efficient lubricant monitoring system. The model has shown three main functional blocks of the algorithm. The map modelling characteristic, the calculation of the condition status and the mileage forecast. The approach of using modelled characteristic maps to predict the current contaminant status can be regarded as one of the novel research outcomes of this work. The theory of the applied piecewise bi-linear map modelling characteristic is presented in detail to contribute knowledge to this research area. The oil condition rating uses the outcome of the predicted contaminants of fuel, soot and oxidation from the characteristic maps and is driven by conservative design considerations to maximise reliability. The discussion of the rating method includes the quantitative definition of the individual lubricant damage threshold for each contaminant based on used oil analysis data. The derived overall lubricant condition status is the key input component for the mileage forecast. This part of the algorithm monitors the condition status of the oil to identify the regular drain interval. Different forecasting models are presented and the rolling window was chosen as it is the most efficient approach in combination with the linear regression model. Flow-chart diagrams illustrate the algorithms of all three functional steps of the monitoring concept. The knowledge derived can therefore easily be transferred for all other engine types. The presentation of the lubricant condition monitoring concept is driven by the engineering target to minimising risk and maximise reliability, whilst also taking practical considerations into account such as computational and hardware efficiency. The next chapter will assess the performance of this monitoring concept.

Chapter 7

7 Model Validation

7.1 Introduction

This chapter presents the results of the individual elements of the oil condition modelling concept. This starts with an analysis of the modelled characteristic maps for fuel, soot and oxidation. The condition for the modelling of these maps will be discussed together with an assessment of the prediction accuracy of the experimental data. The complete model validation consists of four consecutive steps. The first step was to generate an adequate data base. However, due to lack of consistent data about the oil, cost and efficiency it was decided to develop a vehicle simulation to generate artificially used oil data. The second step of the validation process was to assess the accuracy of the initial oil contamination data versus the outcome of the predicted values from the fuel, soot and oxidation map. The next step was to verify the overall accuracy of the lubricant condition rating on the basis of the predicted fuel, soot and oxidation values from the modelled maps. The final part of the validation tests the oil drain prediction forecast performance of the algorithm. The outcome of the model validation will provide a clear picture of the performance of the individual components of the oil condition monitoring concept presented in this research.

7.2 Analysis of Modelled Contaminant Maps

The modelling of each of the characteristic maps to predict fuel, soot and oxidation in the lubricant was conducted using Matlab 7.8.0 (R2009a). The map modelling process used was an advanced gridfit function of Matlab which is available from MathWorks and allows the definition of the input and output data range for each map. This enables an optimal utilisation of the map area as the grid size is limited to $[20 \times 20]$ in order to meet the ECU capability. The map area can be matched to achieve an optimal data distribution. A predefined area can be spanned which will only cover the expected data range. The viscosity range spans [6 – 18] [mm²/s] and the mesh resolution is set to 0.5 [mm²/s] in the range from [7 – 14] [mm²/s]. The other steps are set to 1.0 [mm²/s]. This setup allows good modelling of the grid in the most relevant viscosity area. The permittivity input dimension is defined to cover the range [2.0 – 2.8] [1] and the mesh size is adjusted to have a resolution of 0.025 [1] in the range [2.15 – 2.3] [1]. With normal lubricant ageing during engine operation this area provides the most relevant zone. In this area the maps can be modelled with a fine mesh size to be able to detect the beginning of any severe degradation effects. The other mesh steps for permittivity are set to [0.05] [1]. The grid mesh setup allows a sufficient degree of modelling freedom within the limited map size of $[20 \times 20]$. Engineering and expert knowledge can be implemented to manually calibrate the maps in specific regions. This not only allows the map to be modelled around the limited experimental data but also to implement a specific response characteristic for certain parts of the map to achieve better commonality. The map areas can be adapted to follow a predefined shape based on engineering considerations to optimise individual areas. This is useful if the experimental data does not fully cover all areas but a typical map response is expected from a knowledge of the underlying effects. If the experimental data proves to be noisy in some areas of the map, then manual calibration can be used to model the map to fixed values, thus providing a meaningful output. The following data of each contaminant map provides the engineering conditions premise to verify the model. The coefficient of determination, R^2, provides an indication of the predictive accuracy with respect to the experimental data.

7.2.1 Fuel Map

The fuel map model is able to predict the fuel range covering [0 – 25] [wt.-%]. The input dimensions of viscosity and permittivity are the same for all maps as previously explained. The fuel map model is illustrated using a three-dimensional plot as shown in Figure 7.1. where the black dots illustrate the position of the experimental data.

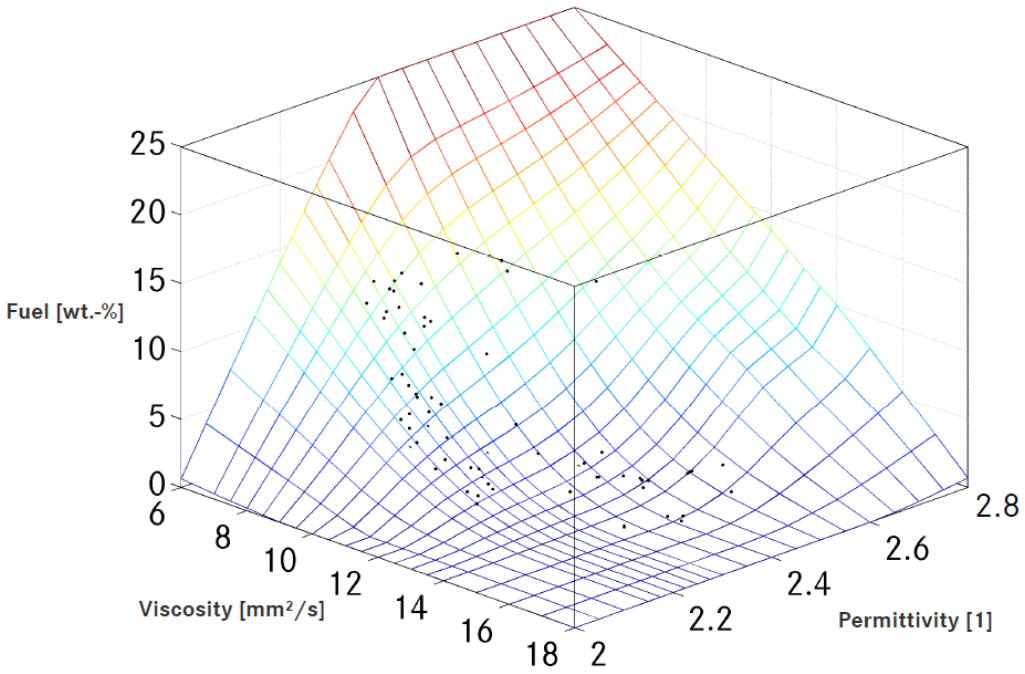

Figure 7.1: Characteristic map - fuel
The fuel map model is able to predict the fuel range covering [0 – 25] [wt.-%] fuel. The black dots illustrate the position of the experimental data. The shape of the map is dominated by the viscosity input. The main gradient changes occur when the viscosity decreases below 11 [wt.-%]. A strong permittivity input influence is observable, especially in the region > 2.4 [1] in combination with low viscosity values < 10 [mm²/s].

The shape of the map is modelled to introduce high viscosity dependence and permittivity sensitivity for higher permittivity values. The following characteristics can therefore be observed:

- It is noticeable that the shape of the map is dominated by the viscosity input. The main gradient changes occur when the viscosity decreases below 11 [wt.-%] which results in an equivalent increase of the predicted fuel content.

- A strong permittivity input influence is observable, especially in the region > 2.4 [1] in combination with low viscosity values < 10 [mm²/s].

As the experimental data did not cover the full map area manual adaption was necessary to improve the accuracy and commonality of the map.

- For viscosity input of 6 [mm²/s] and permittivity > 2.4 [1] the fuel prediction is set to the maximum value of 25 [wt.-%].

- For the region of the map where the viscosity values are 6 – 14 [mm²/s] at a high permittivity of 2.8 [1], a linear fuel decrease from 25 – 10 [wt.-%] is modelled towards lower viscosity.

- In the map area of viscosity > 14 [mm²/s] and low permittivity values the fuel map is set to 0 [wt.-%].

The full fuel map matrix $Z_{CM\ Fuel}$ is shown in the Appendix B and illustrates the regions of manual calibration. Measured viscosity loss as the key input variable mainly dominates the fuel prediction. High permittivity values as an indicator for polar substances from fuel or resulting oxidation products support this prediction. The challenge in the map modelling is that the experimental data only covers a subset of the entire map; however, the requirement is to provide the best compromise between accuracy and commonality for the potential input combinations. Engineering judgement is therefore required to find an appropriate balance between these two aspects. The shape of this fuel map shows high smooth curvature and is expected thus to provide a good commonality. The aim to model commonality with a smoother map results in lower R^2 values. Figure 7.2 shows the correlation plot of the experimental fuel values measured in the laboratory versus the predicted values from the modelled fuel map. The value of the calculated coefficient of determination R^2 indicates that 80.84 % of the data are explained by the model.

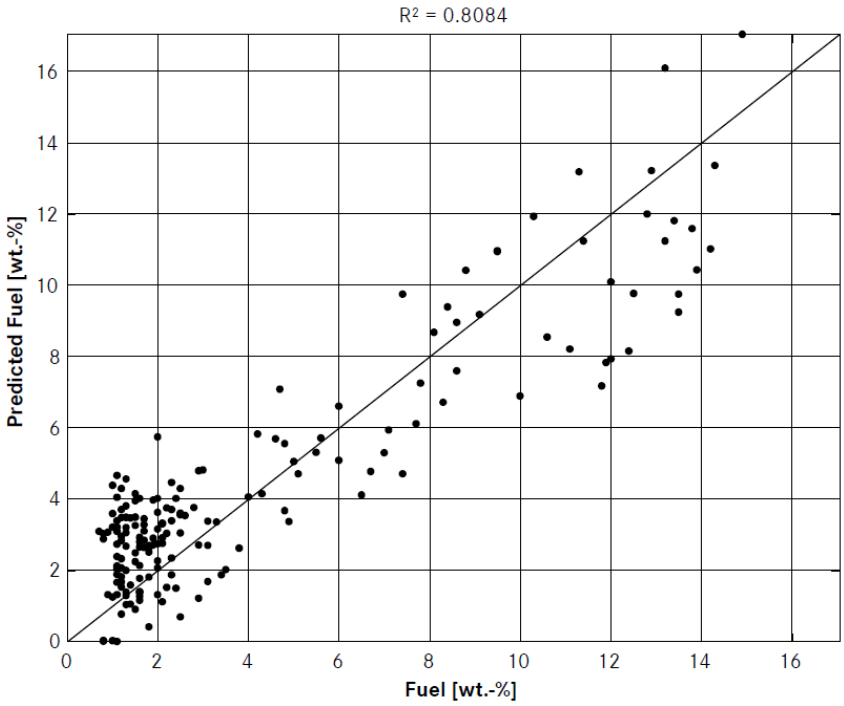

Figure 7.2: Accuracy of the modelled fuel map

Correlation plot of the experimental fuel values measured in the laboratory versus the predicted values from the modelled fuel map. The value of the calculated coefficient of determination R^2 indicates that 80.84 % of the data are explained by the model.

7.2.2 Soot Map

The operational range of the soot map to predict the soot content in the lubricant is defined as 0 – 4 [wt.-%]. The end of oil drain analysis show typically moderate soot levels in the range of 2 – 3.5 [wt.-%]. High soot levels are a typical indicator of combustion problems or hardware problems such as injector nozzle cooking caused by glycerines from the biodiesel. Figure 7.3 shows the final model of the soot map based on the experimental data including additional manual adaption.

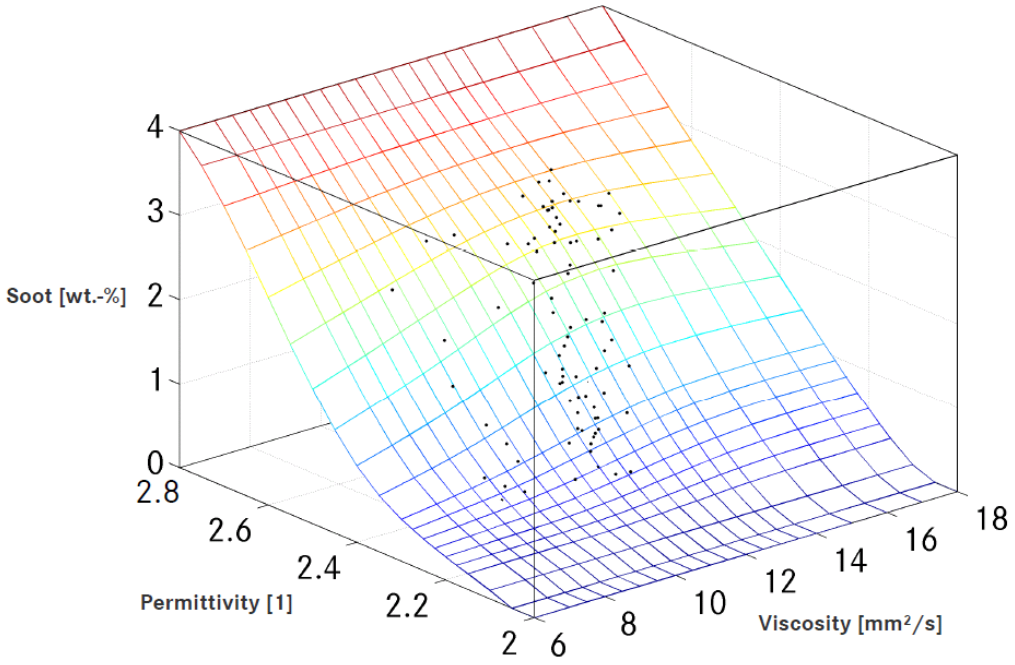

Figure 7.3: Characteristic map - soot
The operational range of the soot map to predict the soot content in the lubricant is defined as 0 – 4 [wt.-%] soot. The black dots represent the position of the experimental data. The soot prediction is dominated by permittivity. Viscosity plays a minor role in the prediction.

Based on the map gradients in viscosity and permittivity shown in Figure 7.3 the following observations can be made:

- The soot prediction is dominated by the permittivity input.
- Viscosity plays an inferior role as the maximum soot level is too low to cause a strong viscosity impact.
- Slight changes in the gradient of the viscosity direction occur at the centre of the map for viscosity values of 8 – 14 [mm²/s] and permittivity values of 2.4 – 2.6 [1].

Since the range of the used oil data does not fully cover equally the entire area of the map then minor manual adjustments are required in the upper and lower map band to ensure a specific response.

- For viscosity values 6 – 18 [mm²/s] and permittivity values of 2.0 and 2.05 [1] the soot prediction is set to 0 [wt.-%].
- For a permittivity of 2.1 [1] it is defined as 0.1 [wt.-%] to achieve a smooth transition to the start of the gradient increase in permittivity.
- The same adjustment is manually modelled at the upper band of the map for all viscosity values 6 – 18 [mm²/s].
- Permittivity values of 2.75 [1] are defined as 3.7 [wt.-%] soot.
- The maximum soot value of 4 [wt.-%] is manually modelled at a permittivity of 2.8 [1].

All other map shaping is based on the experimental data with a map smoothing adjustment which allows the best compromise for a smooth map surface while having a sufficient coefficient of determination R^2. The full characteristic soot map matrix $Z_{CM\ Soot}$ with the manually modelled areas is provided in Appendix B. The accuracy of the map to predict the soot content has a R^2 value of 88.37 % which is very good considering the trade-off between smoothness and accuracy, see Figure 7.4.

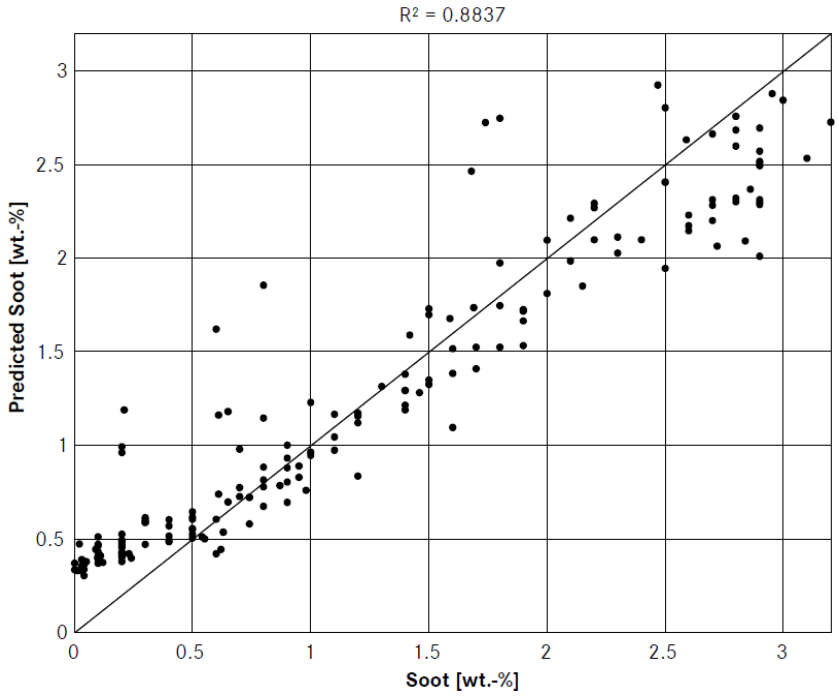

Figure 7.4: Accuracy of the modelled soot map

Correlation plot of the experimental soot values measured in the laboratory versus the predicted values from the modelled soot map. The value of the calculated coefficient of determination R^2 indicates that 88.37 % of the data are explained by the model.

7.2.3 Oxidation Map

The range of prediction for the oxidation is defined as 0 - 45 [A/cm] which covers the most relevant area to monitor the oxidation status during vehicle operation. Figure 7.5 shows the modelled oxidation map based on the experimental data including the additional manual calibration.

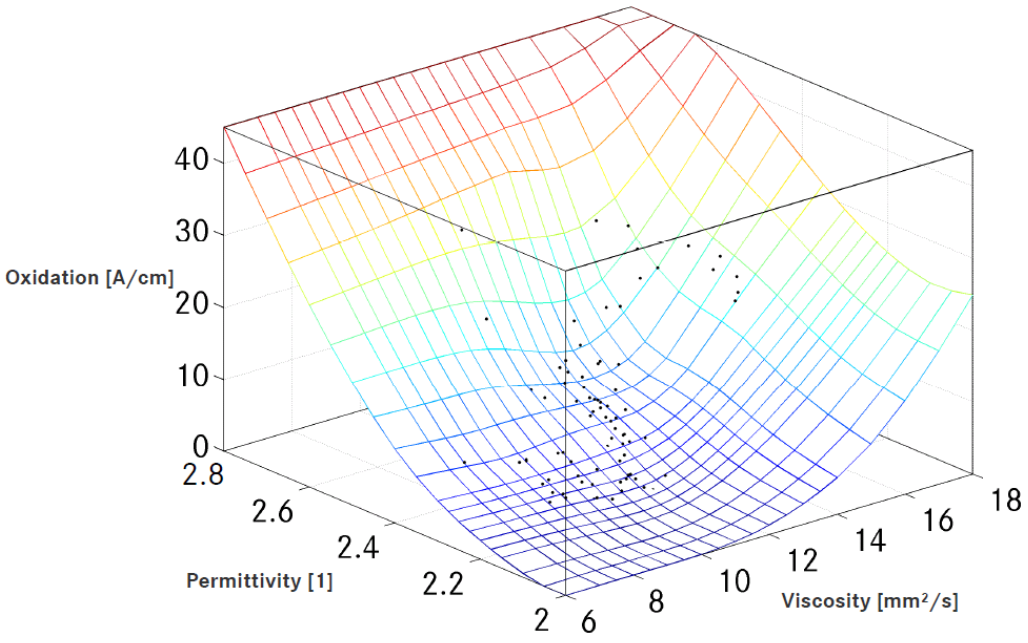

Figure 7.5: Characteristic map - oxidation
The range of prediction for the oxidation is defined as 0 - 45 [A/cm]. The black dots represent the position of the experimental data. The map shows a relatively constant increase in the oxidation prediction with increasing permittivity. The oxidation increase in the viscosity direction starts at viscosity input levels > 13 [mm²/s] and the gradient is much steeper.

The modelling of this map is based on experimental data which increased up to oxidation levels around 25 [A/cm]. This level of oxidation can sometimes occur and is below the defined damage level of 30 [A/cm].

From the modelled map the following observations can be summarised:

- The map shows a relatively constant increase in the oxidation prediction with increasing permittivity values which is expected due to the potential acidification of the oil from the oxidation process.

- The oxidation increase in the viscosity direction starts at viscosity input levels > 13 [mm²/s] and the gradient is seen to be much steeper compared with the oxidation increase in the permittivity direction. From a theoretical standpoint this is correct as the polymerisation is delayed due to the initial acidification of the oil.

- An important aspect with this map is the constant oxidation increase with increasing input variables.

- The slight curvature in the centre of the map results from the experimental data where it seems that the polymerisation process is about to begin but has not really affected the viscosity yet.

To improve the prediction accuracy of the map it is manually adapted at positions where no experimental data were available.

- For viscosity values of 6 – 9.5 [mm²/s] and permittivity values of < 2.1 [1] the oxidation prediction was defined as 0 [A/cm]. With this input combination it was unlikely that oxidation products in the oil would have been formed yet.

- The map is also manually adapted for a viscosity value of 18 [mm²/s] and permittivity value of 2 [1]. The gradient here aims to predict oxidation in the oil which results from a rapid viscosity increase due to polymerisation without having a strong influence on the permittivity value.

- For the complete viscosity range 6 – 18 [mm²/s] and the maximum permittivity value of 2.8 [1] the oxidation prediction is defined as 45 [A/cm].

The full list of coefficients of the oxidation map with the manually modelled areas is provided in the map matrix $Z_{CM\ Oxidation}$ in Appendix B. The map shows a smooth curvature which enables good practical application and accurate prediction results. It must be recognised that taking oxidation measurements in the laboratory is difficult due to the number of potential failures from interference with bonds in the same spectrum. The accuracy achieved for the modelled characteristic map as indicated by the calculated coefficient of determination R^2 gives a value of $R^2 = 70.78$ %, see Figure 7.6.

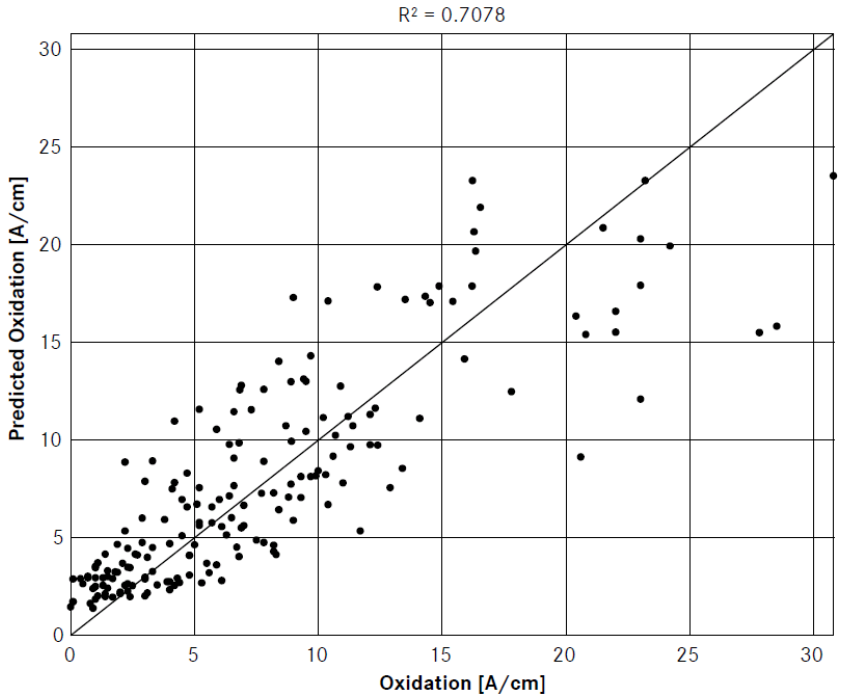

Figure 7.6: Accuracy of the modelled oxidation map
Correlation plot of the experimental oxidation values measured in the laboratory versus the predicted values from the modelled oxidation map. The value of the calculated coefficient of determination R^2 indicates that 70.78 % of the data are explained by the model.

7.3 Oil Condition Model Validation

This section provides details of the steps which were required to validate the performance of the oil condition model in this work. It starts with an insight of the data which was generated for the assessment. The complete oil condition model assessment is subdivided into three individual components. The first part is an assessment of the accuracy for predicting the capability of each of the three contaminant maps. The statement of the accuracy of the maps in Chapter 7.2 was only provided in relation to the data base used to model the maps. The study in this step uses the maps together with a different data set to assess the predicted outcome of each contaminant. The next step of the model validation looks at the overall lubricant condition rating result and compares the rating based on the initial contaminant data with the derived rating from the characteristic maps. Details of the condition rating method were presented in Chapter 6.3. The final step of the model validation tests the algorithm's remaining mileage forecasting capability. This statement will provide the most interesting information from a customer's point of view as based on this information the actual warning or information to the driver will be generated in a real application.

7.3.1 Data Generation – Vehicle Simulation

Testing of the algorithm requires a substantial data basis. A representative number of vehicles need to provide the full data set consisting of the sensor data permittivity and viscosity as well as the oil analysis results of the fuel, soot and oxidation level in the oil. Furthermore the data per vehicle needs to cover the complete oil drain interval range in regular steps in order to assess the contaminant prediction progress and the performance of the remaining mileage forecast. Data covering all these requirements could not be retrieved from the oil data base and could not be generated from vehicle trials in the course of this research due to the cost and time aspects. To be able to validate the algorithm it was decided to use artificially generated data from a vehicle simulation developed in the course of this research work. The data aims to simulate the oil ageing process during the vehicle operation with current diesel engines. Three different types of vehicle usage, i.e. load profiles, were generated having individually designed characteristics which are summarised in Table 7.1. The 'Taxi' profile was designed to meet a typical low load operation profile with idling, stop and go and many short trip driving distances.

Most single driving distances are less than 20 [km] / 12.43 [mi] as is typical for urban taxi operation but also for customers with extremely short driving distances like the school run and shopping trips. The 'Normal' driver profile represents the regular driving characteristics where most of the trips are short to medium distance. The single driving distance is typically between 10 [km] / 6.22 [mi] and 50 [km] / 31.08 [mi]. This is the driving distance for people going to work by car every day, visiting friends or relatives who live not close by or who visit for instance shopping sites or cultural events on the weekends. The 'Long Distance' profile represents the load profile of a commercial sales representative or a business customer using the car mainly for long distances to visit customers or business partners where over 50 % of the single driving distances are further than 25 [km] / 15.54 [mi]. Table 7.1 provides a contaminant mileage dependent slope factor 'Contaminant_slope'. It is defined that the fuel, soot and oxidation slope is decreasing with longer driving distances. With longer driving distances less fuel accumulation occurs as the engine and the lubricant is at the operating temperature. DPF regeneration can be fully completed during longer driving distances and less fuel is diluted into the oil due to aborted regeneration. The formation of soot particles is temperature dependent and less soot gets formed when the engine is operating at its normal temperature as this is the case with longer driving distances. The slope factor for oxidation is chosen to be equal to the fuel factor as the presence of fuel in the oil promotes the oxidation process. The simulated driving profile of Table 7.1 also contains distortion or noise factors for each contaminant 'd_Contaminant' to be able to generate noise on top of the random contaminant values. Due to the volatile character of fuel in the oil and the fact that more fuel enters the oil with short distance driving, the distortion factor for fuel is higher with short distances. The distortion factor for soot and fuel are constant as no mileage dependent effects exist. For all of the profiles, the mileage distribution (%), the slope factors (Contaminant_slope) and the distribution numbers (d_Contaminant) are based on engineering considerations and expert knowledge. The numbers for each profile are summarised in Table 7.1.

Table 7.1: Simulated load profiles

Mileage [km]/[mi]	**0/ 0**	**0.001/ 0.00062**	**5/ 3.11**	**10/ 6.22**	**1 / 9.32**	**20/ 12.43**	**25/ 15.54**	**50/ 31.08**	**75/ 46.61**	**100/ 62.15**
Taxi %	0	6	15	25	20	15	10	5	2	2
Normal %	0	1	2	12	15	20	25	15	5	5
Long Dist. %	0	1	2	5	10	15	17	10	20	20
Fuel_slope	1.5	2	4	2	1.25	1	0.95	0.85	0.6	0.3
Soot_slope	1.5	2.25	3.25	1.75	1	0.975	0.95	0.85	0.8	0.75
Oxidation_slope	1.5	2	4	2	1.25	1	0.95	0.85	0.6	0.3
d_fuel	1	1	1	1	0.75	0.75	0.75	0.5	0.5	0.5
d_soot	0.5	0.5	0.5	0.5	0.5	0.5	0.5	0.5	0.5	0.5
d_Oxidation	1	1	1	1	1	1	1	1	1	1

The number of vehicles n = 1,000 is generated which provides a suitable data basis to test the algorithm. The driving profile distribution is defined as 5 % ‘Taxi’, 65 % ‘Normal’ and 30 % ‘Long Distance’. The accumulated mileage per vehicle is 25,000 [km] / 15,534 [mi]. The first step of the algorithm generates the vehicle type by generating n_vehicle numbers block distributed [0 …1]. The numbers from 0.0 – 0.05 are assigned to the ‘Taxi’ profile, the numbers from 0.05 – 0.7 are assigned to the ‘Normal’ drivers and from 0.7 – 1 are the ‘Long Distance’ drivers. A loop over each of the three vehicle groups is used to generate for each vehicle in the particular group 20 block distributed numbers per loop. Each number is converted into a single driving distance using linear interpolation and the predefined distribution of the distance from Table 7.1. Every new generated driving distance for each vehicle is added to the previous generated overall mileage. This process is repeated until every vehicle from all three load profiles reached an overall mileage of > 25,000 [km] / 15,534 [mi] simulating the oil drain interval. Based on the different driving profiles and the random mileage the number of generated single driving distances to reach the maximum mileage, is different for each simulated vehicle. This approach aimed to simulate a variety of real customer’s driving characteristics for the data generation. As a next step the contaminants need to be defined. For all contaminant values are the parameter minimum value, maximum value and the damage value defined which is assumed to be reached at the maximum mileage M_{Max} 25,000 [km] / 15,534 [mi]. The nominal slope for each contaminant is calculated as:

$$Cont\_slope\_nominal = \frac{Cont\_lim - Cont\_min}{M_{Max}} \tag{7.1}$$

A virtual oil refill probability during the oil drain interval is also introduced. This random factor is used to simulate a temporary oil condition improvement during the interval due to the top up of fresh oil. The next step is the generation of the simulated contaminants for each of the previously generated single driving distances of each of the n_vehicles. A loop over the i = 1 … n vehicles is used while the accumulated mileage is $< M_{Max}$. The random oil top up number is generated using a block distributed [0 … 1] number which is compared with the predefined thresholds for each driving profile. If the random number is lower than the threshold the refill factor is set to 1 which means no oil refill. If the random number is higher than the threshold the refill factor is set to 0.9 which means a 10 % improvement of the latest soot or oxidation value. It is defined that the soot value improves by a refill due to thinning of the soot particles. The oxidation value improves due to the fresh additives and better alkaline reserve which improves the oxidation inhibition. From practical experience the fuel value in a used oil sample is not typically affected by an oil refill and it is therefore defined that the fuel value remains unchanged with an oil refill. The single driving distance of the i-th vehicle is read from the previously random generated driving distances, see Figure 7.7.

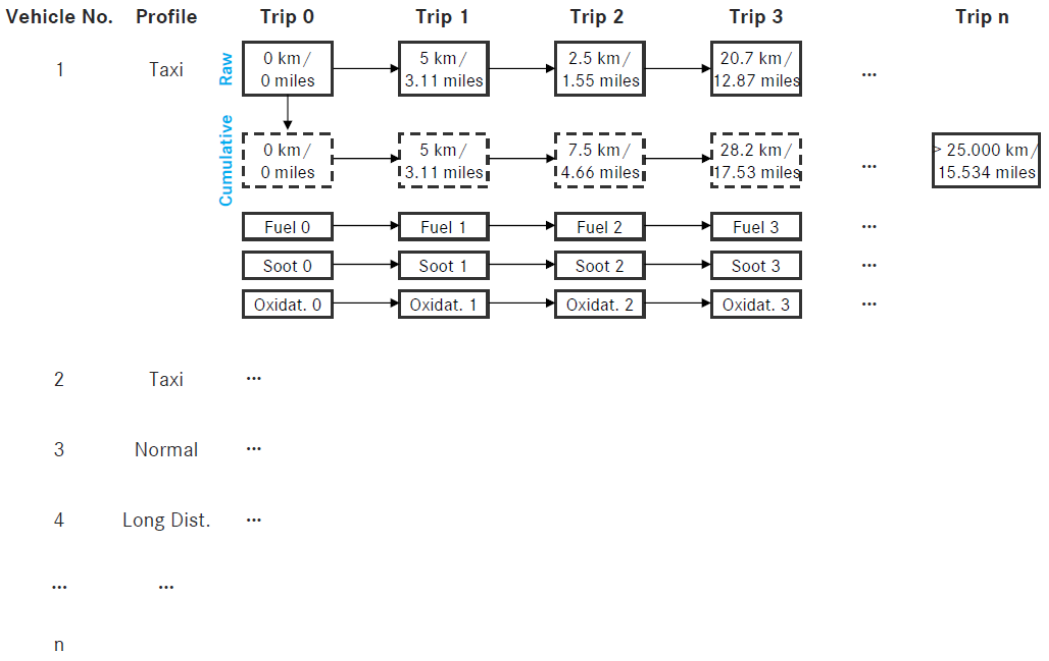

Figure 7.7: Single driving distance and contaminant generation

The algorithm generates the vehicle type by generating n_vehicle numbers block distributed [0 …1]. The numbers from 0.0 – 0.05 are assigned to the 'Taxi' profile, the numbers from 0.05 – 0.7 are assigned to the 'Normal' drivers and from 0.7 – 1 are assigned the 'Long Distance' drivers. A loop over each of the three vehicle groups is used to generate for each vehicle in the particular group 20 block distributed numbers per loop. Each number is converted into a single driving distance using linear interpolation and the predefined distribution of the distance from Table 7.1. Every new generated driving distance for each vehicle is added to the previously generated overall mileage. This process is repeated until every vehicle from all three load profiles reached an overall mileage of > 25,000 [km] / 15,534 [mi] simulating the oil drain interval. Based on the different driving profiles and the random mileage the number of generated single driving distances to reach the maximum mileage is different for each simulated vehicle. The added contaminant for each single driving distance per vehicle uses the nominal slope for each contaminant, which are the driving distance dependent 'contaminant_slope' factor and the driving distance dependent distribution factor defined in Table 7.1.

The added contaminant for each single driving distance per vehicle uses the nominal slope for each contaminant, the driving distance dependent 'Contaminant_slope' factor and the driving distance dependent distribution factor defined in Table 7.1. The term 'Cont' is used here and can be for either fuel, soot or oxidation. As a first step the contaminant increase calculated without the random distribution factor 'd_Contaminant' can be written as:

$$Cont\_add = Cont\_slope\_nominal \cdot driving\ distance \cdot Cont\_slope \tag{7.2}$$

The standard deviation factor 'd_Contaminant' of the normal distribution is taken from Table 7.1. The random process for every driving distance provides an additional random contaminant increase or decrease. This random process mainly represents evaporation losses of the fuel but also measurement tolerances of the soot or oxidation measurement. This effect is aimed to bring the simulated contaminant data closer to real data from the used oil analysis.

The random effect for each contaminant is generated by the multiplication of the nominal contaminant slope, the single driving mileage, the distribution factor and a normal distributed random number and is defined in equation 7.3.

$$\begin{aligned} Cont\_rand = {} & Cont\_slope\_nominal \cdot driving\ distance \cdot \\ & d\_Contaminant \cdot \left(\mathrm{N} \sim \sigma, \mu = 0\right) \end{aligned} \tag{7.3}$$

Figure 7.8 summarises the principle of the three elements contributing to the generation of each random contaminant, which are the nominal slope, the mileage dependent 'Contaminant_slope' factor and the random deviation for each simulated single driving distance m_i using the 'd_Contaminant' random process.

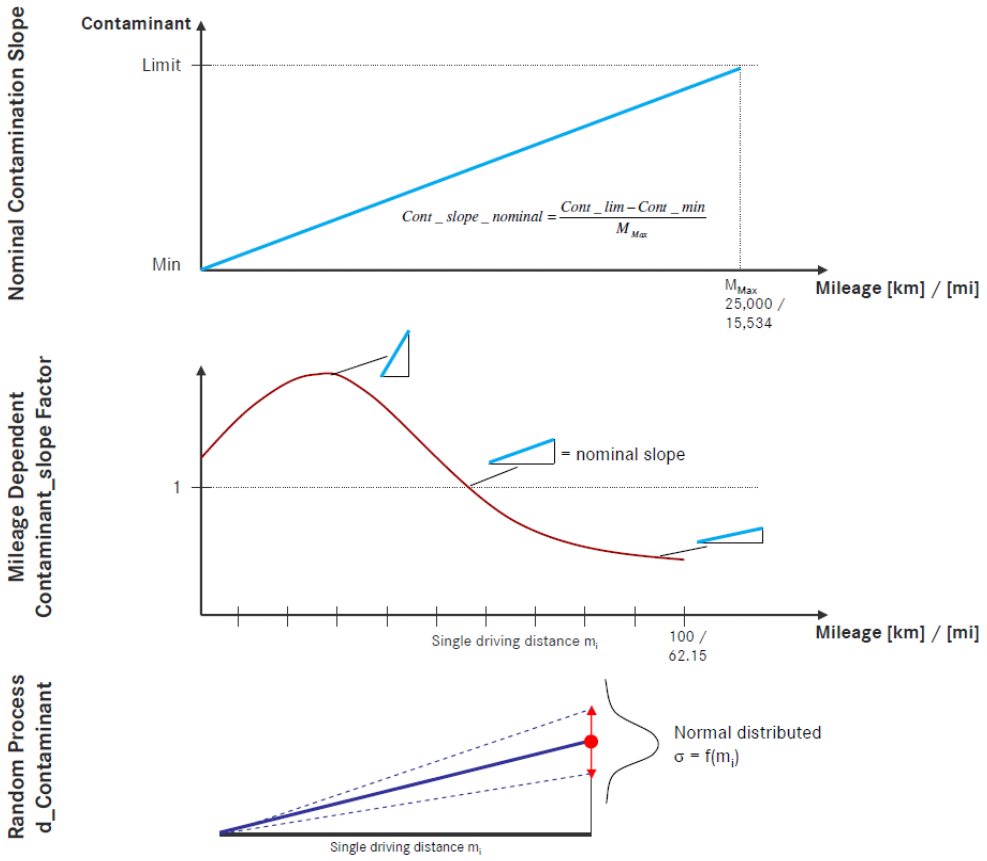

Figure 7.8: Elements of the mileage dependent contaminant simulation
The random effect for each contaminant is generated by the multiplication of the nominal contaminant slope, the mileage dependent 'Contaminant_slope' factor and the random deviation for each simulated single driving distance mi using the 'd_Contaminant' random process.

The final added fuel contaminant value for each individually simulated driving distance can now be defined as:

$$Fuel\_new = Fuel\_old + Fuel\_add + Fuel\_rand \tag{7.4}$$

For soot and oxidation the random oil refill factor can also be implemented and the new contamination value for each single driving distance is defined as:

$$Soot\_new = Refill\_factor \cdot Soot\_old + Soot\_add + Soot\_rand$$

$$Oxidation\_new = Refill\_factor \cdot Oxidation\_old + Oxidation\_add + \\ + Oxidation\_rand \tag{7.5}$$

All random processes in this simulation are designed so that they can never generate values below zero as zero contamination during real engine operation is not possible. After completing the single driving distances the i-th vehicle is tested if the accumulated mileage exceeds the maximum mileage of 25,000 [km] / 15,534 [mi]. All mileage steps greater than the virtual oil drain interval distance are removed. The complete algorithm to simulate the driving profiles and the different oil ageing characteristics is illustrated using a Nassi-Shneiderman diagram (DIN 66261, 1985), see Figures 7.9 and 7.10.

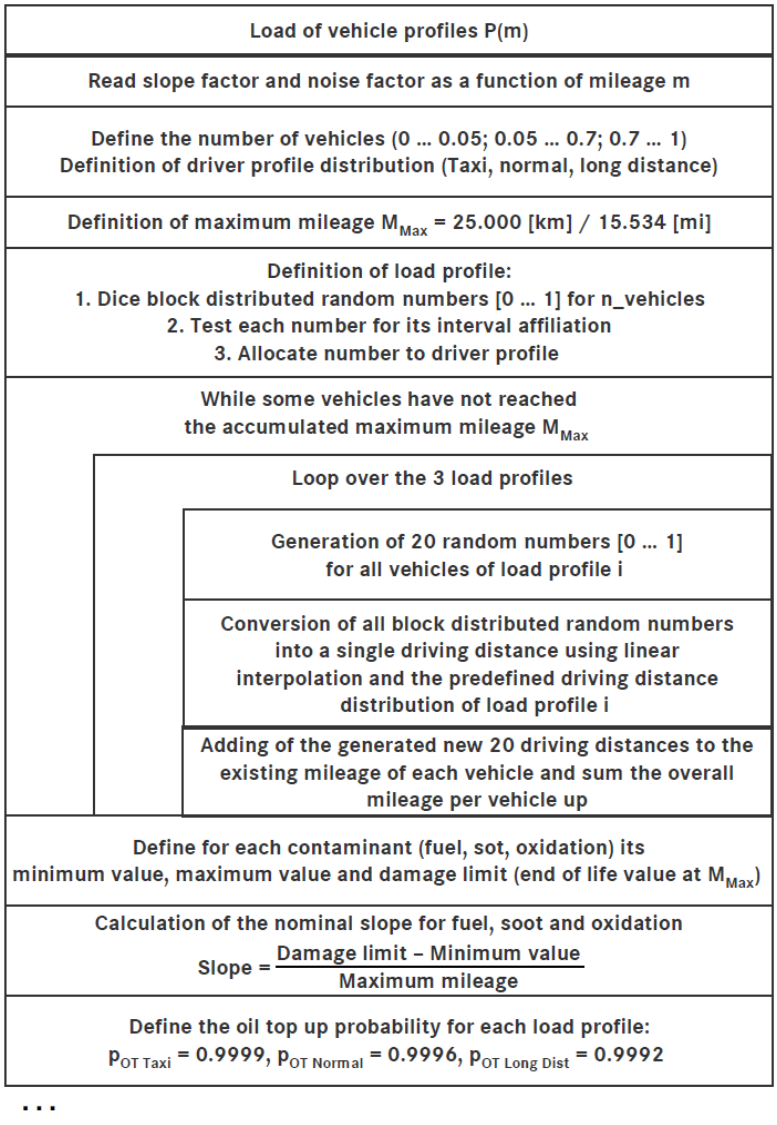

Figure 7.9: Nassi-Shneiderman diagram of the vehicle oil ageing simulation (a)

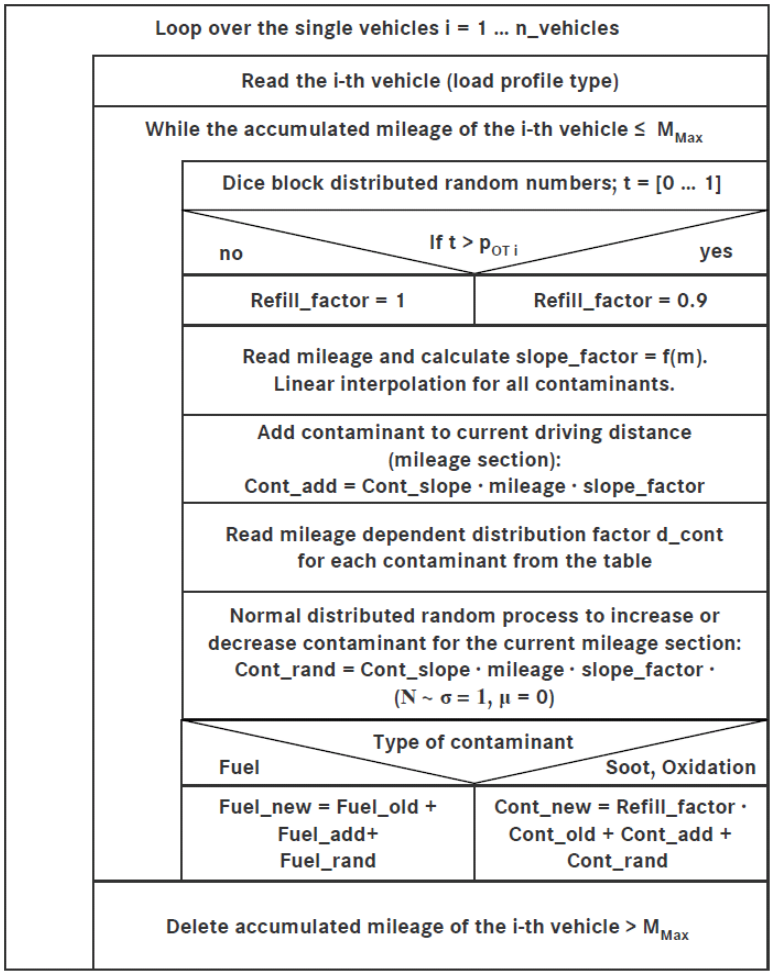

Figure 7.10: Nassi-Shneiderman diagram of the vehicle oil ageing simulation (b)

The following section presents the results of the simulated driving profiles and the corresponding virtual engine oil contamination for each load condition. The bar chart on the left hand side of Figure 7.11 shows the single driving distribution of the 'Taxi' profile. According to the specifications in Table 7.1 the majority of driving distances are short trips below 25 [km] / 15.54 [mi] per trip. The cumulative percentage is plotted on the right hand side of Figure 7.11. The blue solid line represents the accumulated distance profile versus the dashed black line representing the definition from Table 7.1. This shows that 90 % of the accumulated overall mileage is within 25 [km] / 15.54 [mi] per trip. The typical urban Taxi profile is therefore considered to provide an accurate simulation.

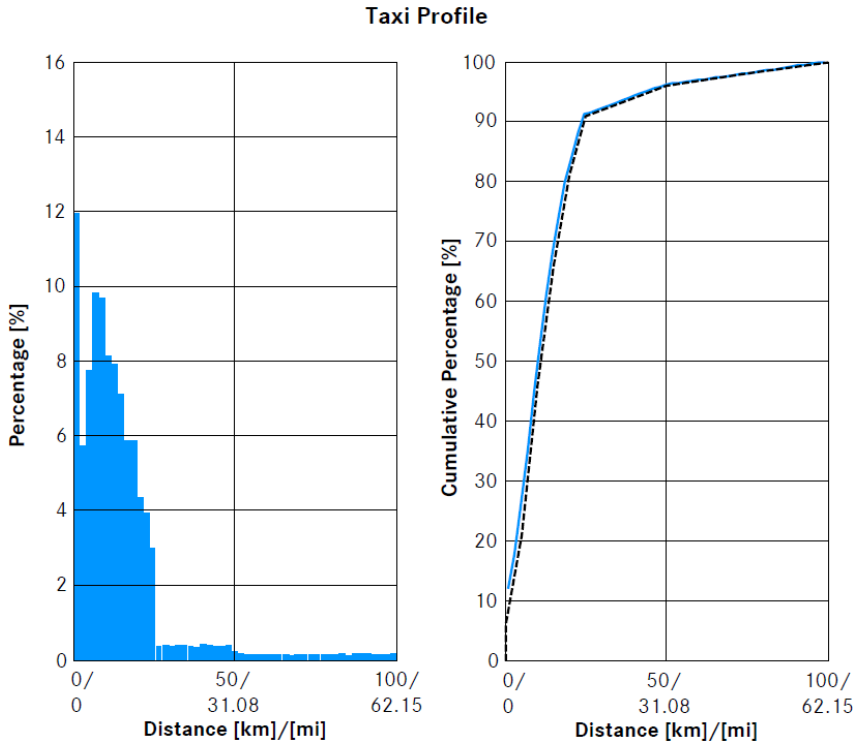

Figure 7.11: Driving distance simulation – 'Taxi' profile

The blue bar chart on the left hand side shows the single driving distribution of the 'Taxi' profile. According to the specifications in Table 7.1 the majority of driving distances are short trips below 25 [km] / 15.54 [mi] per trip. The cumulative percentage is plotted on the right hand side. The blue solid line represents the accumulated distance profile versus the dashed black line representing the definition from Table 7.1.

The green bar chart on the left hand side of Figure 7.12 shows the single driving distribution of the 'Normal' driving profile. According to the specifications in Table 7.1 this profile has more components with individual driving distances higher than 25 [km] / 15.54 [mi] per trip. The cumulative percentage is plotted on the right hand side of Figure 7.12. The green solid line represents the accumulated distance profile versus the dashed black line representing the definition from Table 7.1. The characteristic indicates that 75 % of the trips are within 25 [km] / 15.54 [mi] which can be assumed as a typical one way trip to work. About 15 % of the accumulated overall mileage comes from single trips having a distance of up to 50 [km] / 31.08 [mi]. The other 10 % of the accumulated mileage are up to 100 [km] / 62.15 [mi] which can be assumed as holiday or weekend trips. The generated profile reflects a good driving profile of the normal customer such as the use of a family car within one oil drain interval.

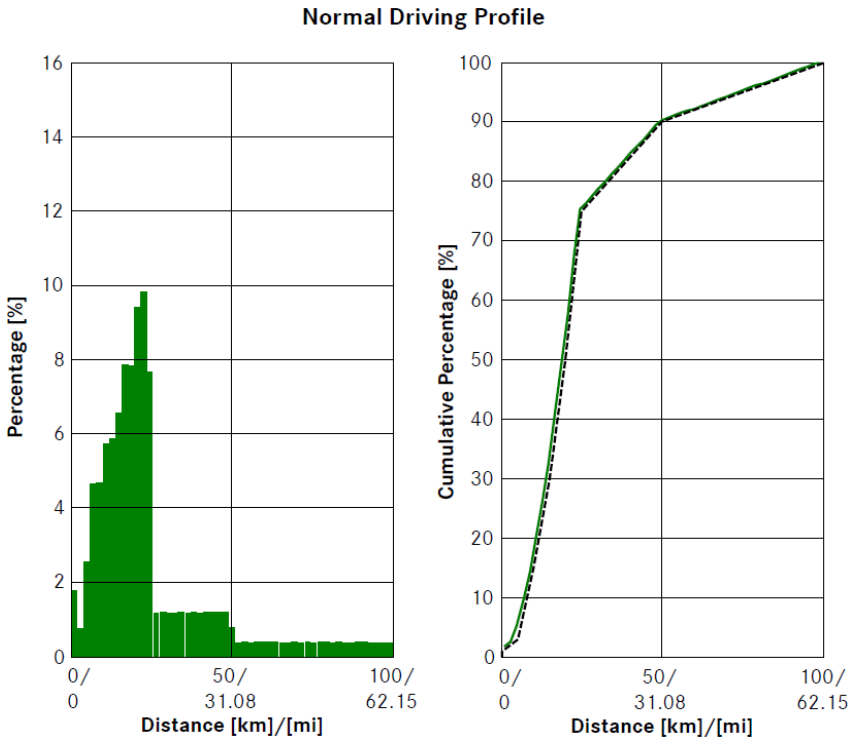

Figure 7.12: Driving distance simulation – 'Normal' driving profile

The green bar chart on the left hand side shows the single driving distribution of the 'Normal' driving profile. According to the specifications in Table 7.1 this profile has more components with individual driving distances higher than 25 [km] / 15.54 [mi] per trip. The cumulative percentage is plotted on the right hand side. The green solid line represents the accumulated distance profile versus the dashed black line representing the definition from Table 7.1.

The red bar chart on the left hand side of Figure 7.13 shows the single driving distribution of the 'Long Distance' driving profile. According to the specifications in Table 7.1 this profile has half of the individual driving distances with mileages higher than 25 [km] / 15.54 [mi] per trip. The cumulative percentage is plotted on the right hand side of Figure 7.13. The red solid line represents the accumulated distance profile versus the dashed black line representing the definition from Table 7.1. The characteristic indicates that 60 % of the trips are within 50 [km] / 31.08 [mi] which can be assumed as the travel to work or to clients residing in a close vicinity. The other 40 % of the accumulated overall mileage comes from single trips having a distance of up to 100 [km] / 62.15 [mi] which can be assumed as longer business trips to customers and business locations. The generated profile fits well with the intention of providing a long distance scenario as a contrast to the other profiles with mainly short to mid distance trips.

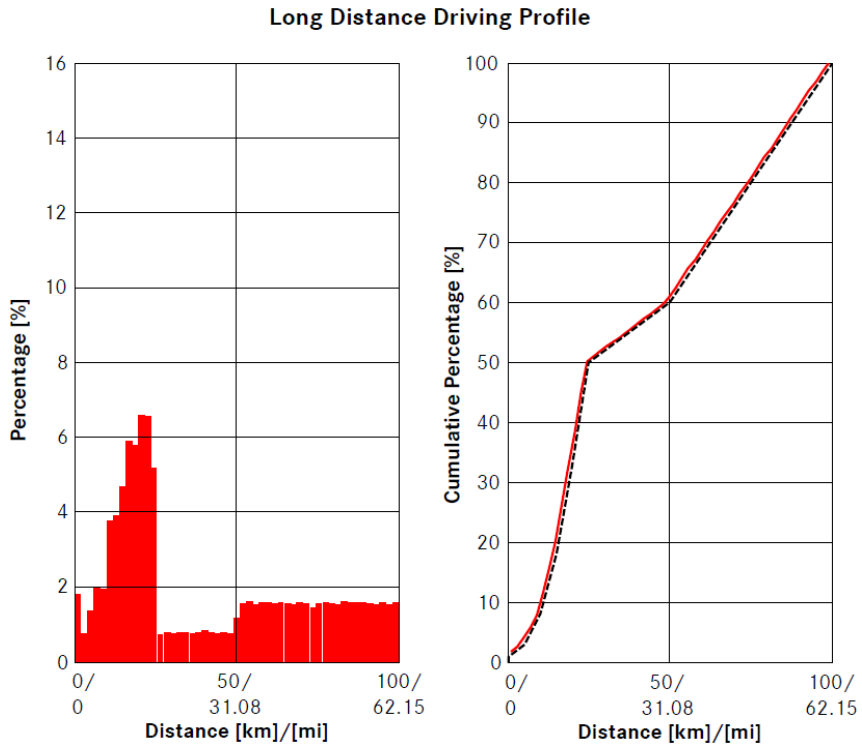

Figure 7.13: Driving distance simulation – 'Long Distance' driving profile

The red bar chart on the left hand side shows the single driving distribution of the 'Long Distance' driving profile. According to the specifications in Table 7.1 this profile has half of the individual driving distances with mileages higher than 25 [km] / 15.54 [mi] per trip. The cumulative percentage is plotted on the right hand side. The red solid line represents the accumulated distance profile versus the dashed black line representing the definition from Table 7.1.

The corresponding simulated fuel contamination of the oil plotted over the drain interval for each profile is shown in Figure 7.14. Each line represents one simulated vehicle over the oil drain interval. The influence of the introduced random process is well recognisable.

- A fuel accumulation of more than 10 [wt.-%] for the worst case condition with the blue 'Taxi' profile is reasonable due to idling and many short trip, stop and go cycles.

- The green accumulation shows the 'Normal' driving profile which shows the defined damage limit for fuel accumulation of 8 [wt.-%] indicated by the horizontal red line.

- The red lines show the accumulation of the 'Long Distance' profile. The aim of having less fuel in the oil with this simulation due to the hotter operation works well. The fuel content is about 5 - 6 [wt.-%] at the maximum mileage which is not a concern.

The fuel accumulation simulation for the three different profiles shows a good comparison with the real fuel accumulation results of used engine oil in these scenarios.

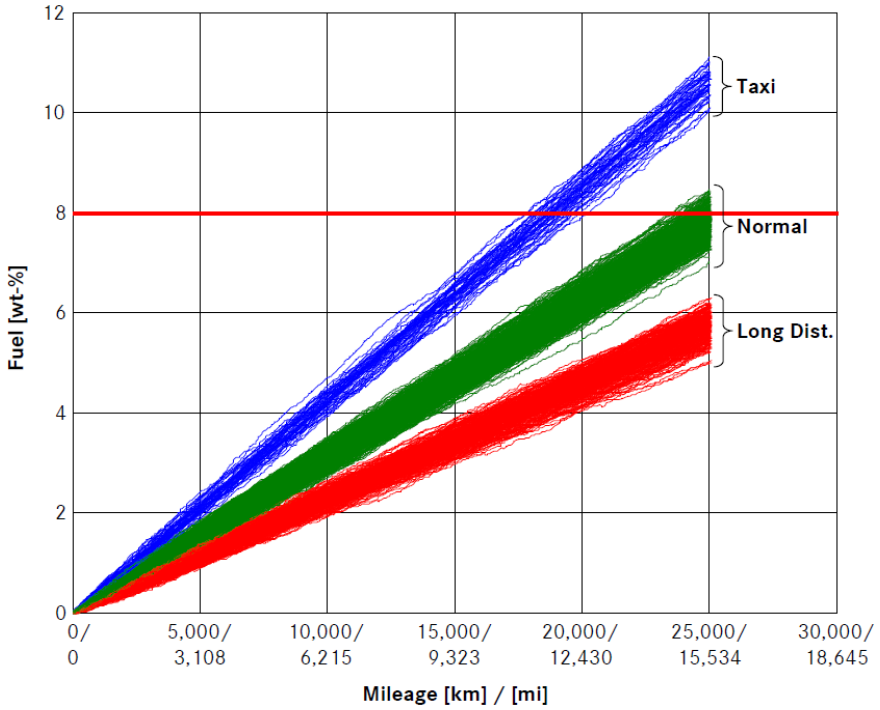

Figure 7.14: Simulated fuel accumulation in the oil for the different driving profiles

The blue lines represent the fuel accumulation of the 'Taxi' profile. The green lines represent the fuel accumulation of the 'Normal' profile. The red lines represent the fuel accumulation of the 'Long Distance' profile. The red bar indicates the defined fuel damage limit of 8 [wt-%]. The fuel accumulation simulation for the three different profiles shows a good comparison with the real fuel accumulation results of used engine oil in these scenarios.

The soot loading of the oil plotted over the drain interval for each profile is shown in Figure 7.15. The influence of the random process and the random oil refill for some vehicles is well recognisable.

- A soot content of more than 3 [wt.-%] for the worst case condition with the blue 'Taxi' profile is realistic due to the cold driving operation.

- The green accumulation shows the 'Normal' driving profile which ends up between 2.2 and 3.1 [wt.-%]. The damage limit defined for soot of 3 [wt.-%] is indicated by the horizontal red line.

- The red lines show the accumulation loading of the 'Long Distance' profile. The soot content is about 2.0 to 2.6 [wt.-%] and is below the defined threshold due mainly to suitable engine operation temperature.

The soot accumulation simulation for the three different profiles shows realistic soot values which are found in real used oil analysis. It is assumed that no extraordinary high soot content values are caused by any hardware defects.

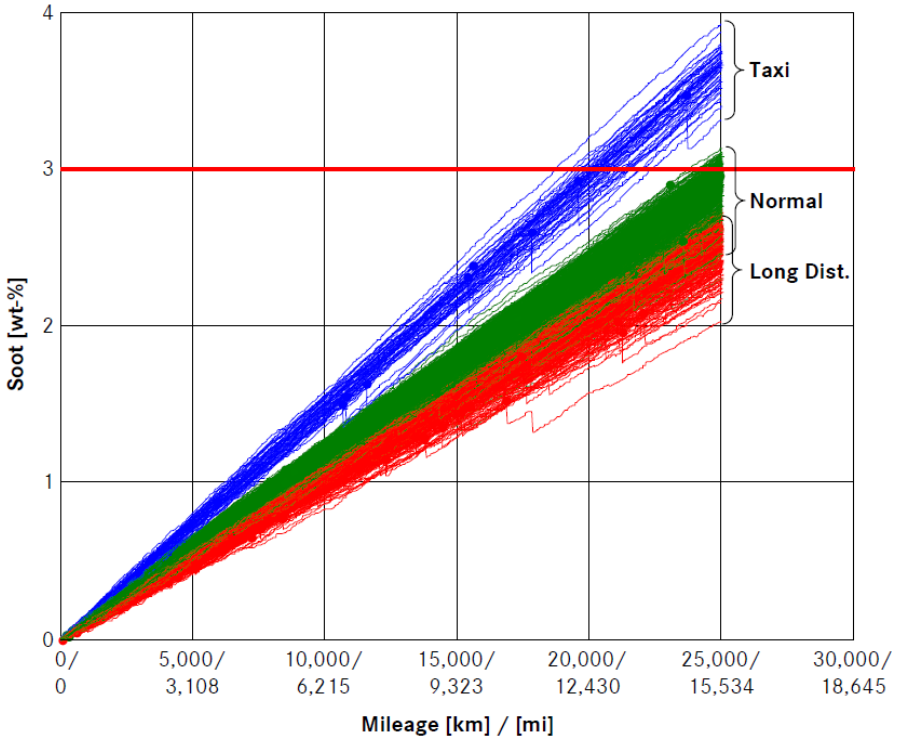

Figure 7.15: Simulated soot accumulation in the oil for the different driving profiles

The blue lines represent the soot loading for the 'Taxi' profile. The green lines represent the soot accumulation of the 'Normal' profile. The red lines represent the soot loading of the 'Long Distance' profile. The red bar indicates the defined soot damage limit of 3 [wt-%]. The soot accumulation simulation for the three different profiles shows realistic soot values which are found in real used oil analysis.

Figure 7.16 shows the oxidation of the oil plotted over the drain interval for each simulated profile. The influence of the random process and the random oil refill is well recognisable.

- Due to the high fuel content for the 'Taxi' profile the oxidation level is considerably higher. The simulated oxidation level is in the range of 35 - 43 [A/cm] and exceeds the defined damage limit of 30 [A/cm] indicated by the horizontal red line.

- The green lines from the 'Normal' driving profile are in the range of 22 - 32 [A/cm] at the maximum mileage. A substantial number of vehicles would therefore have reached the full drain interval with this driving profile.

- Due to the low initial fuel content for the 'Long Distance' profile shown with the red lines, causes moderate oxidation over the drain interval. The levels at the maximum mileage are in the range of 15 - 26 [A/cm].

The oxidation simulation for the three different profiles again correlates well with the real used oil analysis for those special profiles.

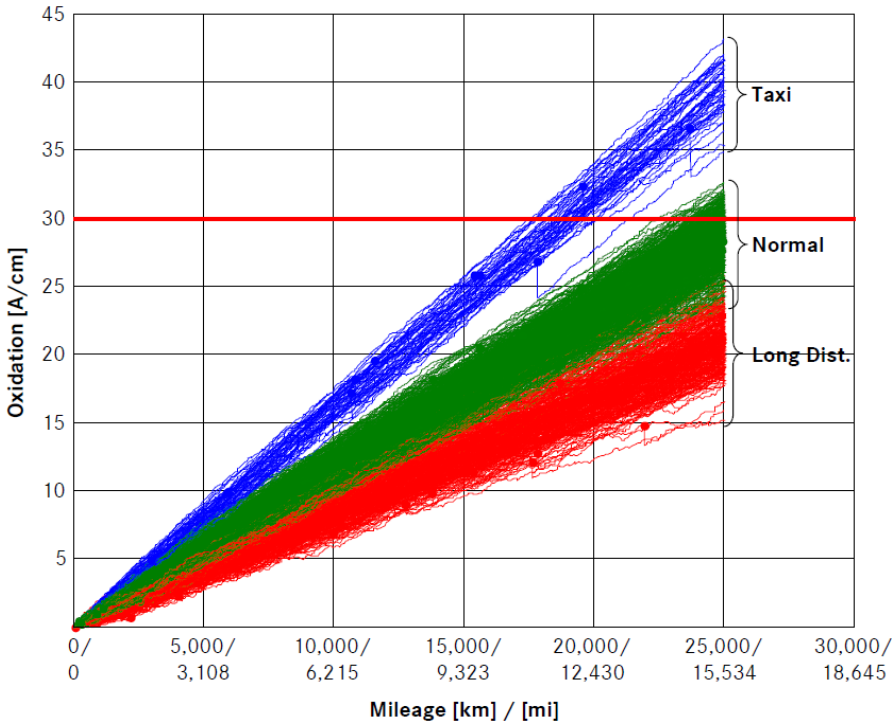

Figure 7.16: Simulated lubricant oxidation progress for the different driving profiles
The blue lines represent the oxidation level for the 'Taxi' profile. The green lines represent the oxidation level of the 'Normal' profile. The red lines represent the oxidation level of the 'Long Distance' profile. The red bar indicates the defined oxidation damage limit of 30 [A/cm]. The oxidation simulation for the three different profiles again correlates well with the real used oil analysis for those special profiles.

The simulated data for the three profiles for fuel contamination, soot loading and oxidation provided realistic figures. The generated data of the 1,000 virtual diesel engine vehicles now provides the basis for further assessment of the different engine oil condition algorithm.

7.3.2 Characteristic Maps Assessment

This assessment verifies the accuracy of each of the characteristic maps which have been developed for fuel, soot and oxidation according to the block diagram shown in Figure 7.17.

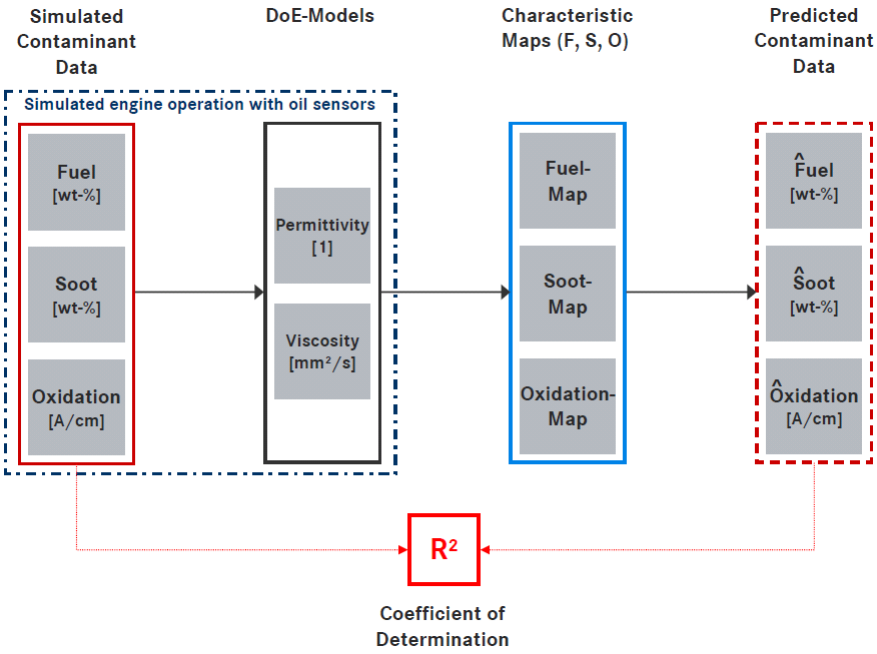

Figure 7.17: Scheme of the characteristic contaminant maps assessment

The simulated artificial oil contaminant data for the different types of vehicle profile forms the data input shown on the left hand side of the block diagram. This contaminant data is the input to simulate the oil condition sensor for data permittivity and viscosity using the developed DoE-models for permittivity and viscosity. The simulated sensor data are indicated by the blue dashed box and are used as the data basis to verify the characteristic maps. The simulated permittivity and viscosity sensor data provide the input for the three characteristic maps to predict the fuel, soot and oxidation level on the right hand side. The outcome of the characteristic map assessment provides a measure of the accuracy of each of the predicted contamination values compared with the initially simulated values using the calculated coefficient of determination R^2.

The simulated artificial oil contaminant data for the different types of vehicle profile forms the data input shown on the left hand side of the block diagram. This contaminant data is used to simulate the oil condition sensor for data permittivity and viscosity. This is achieved by using the DoE-models for permittivity and viscosity from Chapter 5. The analysis in Chapter 5 proved that permittivity and viscosity are a function of fuel, soot and oxidation and can therefore be used to generate simulated sensor data. This is indicated by the blue dashed box and is used as the data basis to verify the characteristic maps. The simulated permittivity and viscosity sensor data provide the input for the three characteristic maps to predict the fuel, soot and oxidation level, see the right hand side of Figure 7.17. The approach using vehicle simulation from this part is no different to an actual vehicle.

The outcome of the characteristic map assessment provides a measure of the accuracy of each of the predicted contamination values compared with the initially simulated values using the calculated coefficient of determination R^2. Based on the previous attempts to introduce random processes and due to the large number of vehicles with three different profiles, a good real world correlation of the simulation can be achieved. The results for the fuel, soot and oxidation prediction are illustrated using a correlation plot which provides information of the data density. Each plot allows an assessment of the accuracy of the individual prediction, also the areas with high and low data point accumulation.

Figure 7.18 shows the correlation plot of the fuel values using the vehicle simulation on the abscissa versus the predicted fuel content in the oil from the characteristic maps on the ordinate.

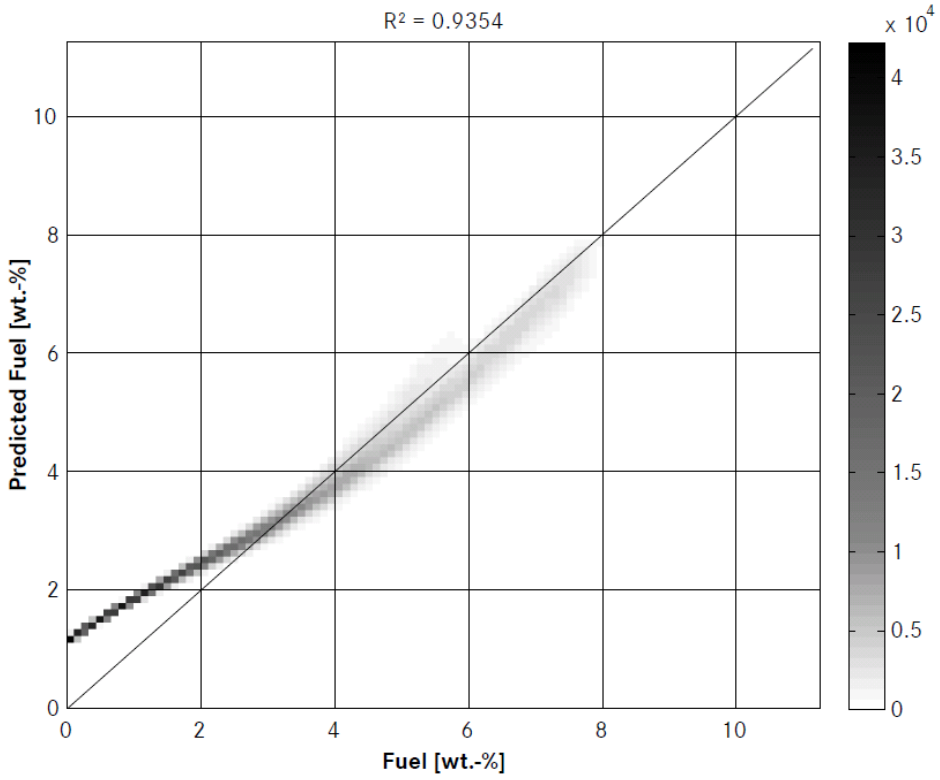

Figure 7.18: Assessment of the fuel prediction quality
Correlation plot of the fuel values using the vehicle simulation on the abscissa versus the predicted fuel content in the oil from the characteristic maps on the ordinate. The coefficient of determination R^2 indicates that the model explains 93.54 % of the data. The plot of density indicates that most of the fuel data points are in the region < 4 [wt.-%].

- The coefficient of determination obtained with R^2 = 93.54 % is an excellent result. This confirms the selected modelling strategy for smooth curvature and therefore more general maps to predict the contaminants in the oil.

- The plot shows conservative results for fuel values < 3 [wt.-%] which means the predicted fuel value is higher than the actual fuel value in the oil.

- For fuel values > 3 [wt.-%] the predicted fuel result is about 0.5 [wt.-%] lower than the actual fuel content.

- For higher fuel values > 7 [wt.-%] the prediction tends towards the actual values.

- The plot of density indicates that most of the fuel data points are in the region < 4 [wt.-%].

- The result proved that the map is able to predict reliably the fuel content for an unknown data set.

The soot correlation plot in Figure 7.19 shows the soot values from the vehicle simulation on the abscissa and the predicted soot content in the oil from the characteristic maps on the ordinate.

- The accuracy of the overall soot prediction is indicated by the R^2 value of 94.71 % which is again an excellent result.

- The soot prediction shows a safe characteristic up to soot values of 2.9 [wt.-%].

- The predicted soot content is about 0.2 – 0.3 [wt.-%] higher than the actual value, especially with very low soot values < 0.25 [wt.-%].

- The soot data points are evenly spread from 0 to 3 [wt.-%] and a higher data point accumulation can be seen for low soot values < 0.5 [wt.-%].

- The results show that the modelled map is able to reliably predict the soot content for an unknown data set. The selected modelling approach for a smooth curvature soot map to provide high commonality is confirmed.

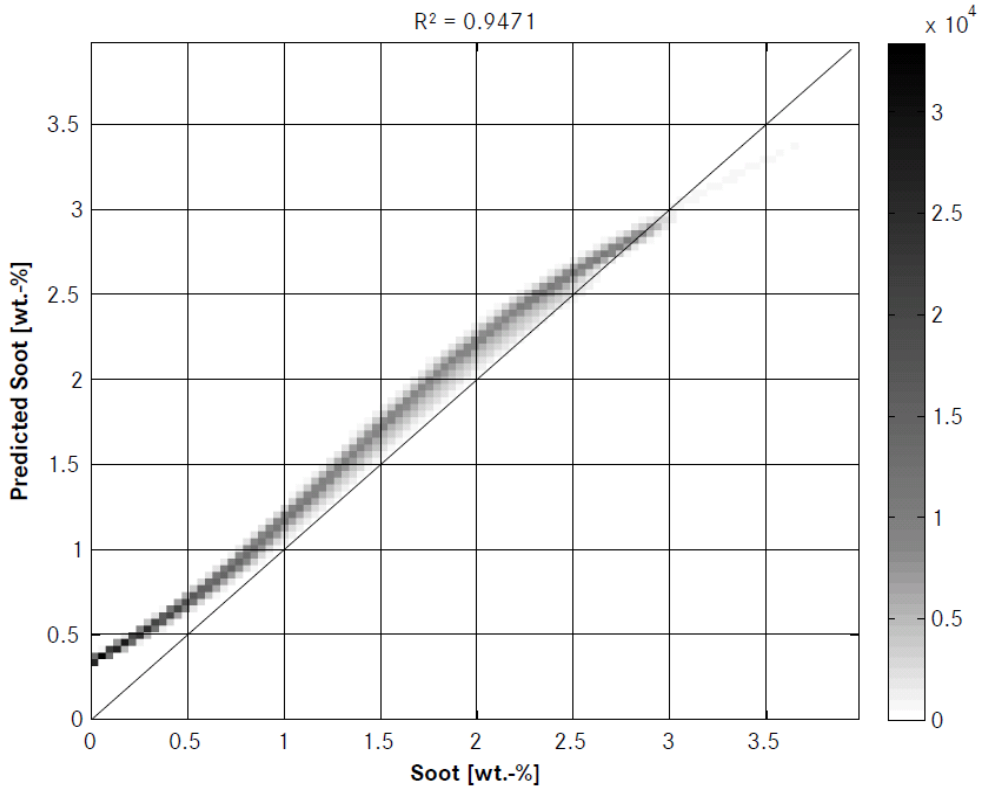

Figure 7.19: Assessment of the soot prediction quality

The soot correlation plot shows the soot values from the vehicle simulation on the abscissa and the predicted soot content in the oil from the characteristic maps on the ordinate. The coefficient of determination R^2 indicates that the model explains 94.71 % of the data. The data density shows that the soot data points are evenly spread from 0 to 3 [wt.-%] and a higher data point accumulation can be seen for low soot values < 0.5 [wt.-%].

Figure 7.20 shows the correlation plot of the oxidation values using the vehicle simulation on the abscissa versus the predicted oxidation content in the oil from the characteristic maps on the ordinate.

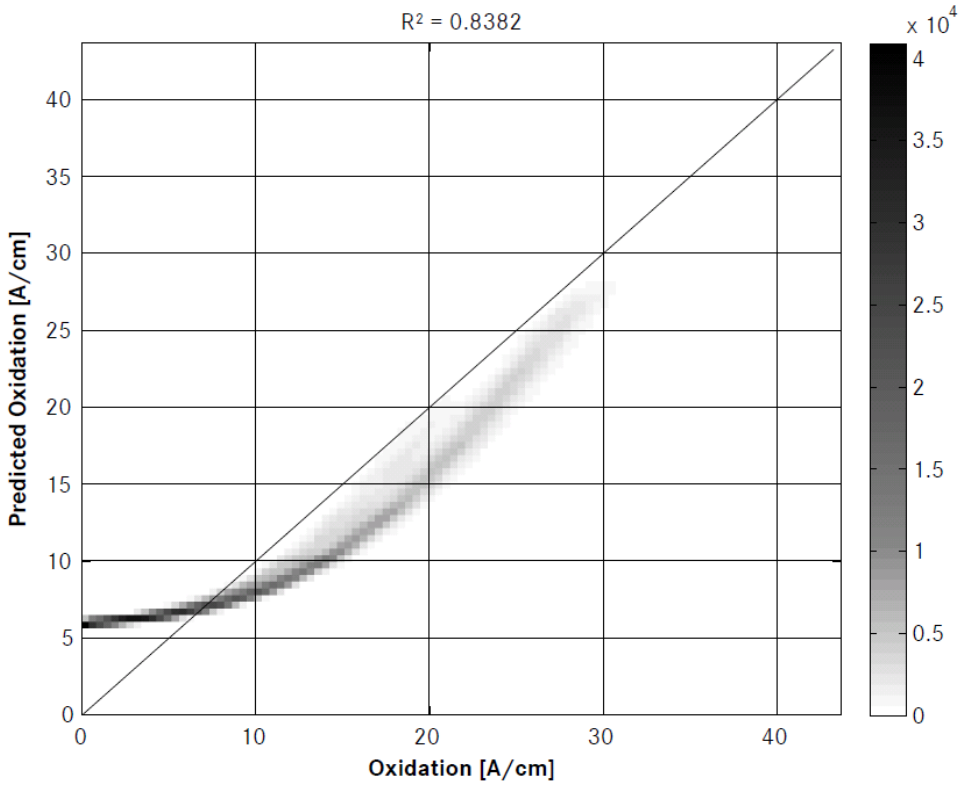

Figure 7.20: Assessment of the oxidation prediction quality

The correlation plot shows the oxidation values using the vehicle simulation on the abscissa versus the predicted oxidation content in the oil from the characteristic maps on the ordinate. The coefficient of determination R^2 indicates that the model explains 83.82 % of the data. The data density plot shows that most of the data are < 20 [A/cm].

- The coefficient of determination is lower compared to the previous results but the value of R^2 = 83.82 % still provides a good result.

- For low oxidation values the predicted oxidation values are about 6 [A/cm] too high.

- For oxidation values > 7.5 [A/cm] the predicted values are about 5 [A/cm] too low. The prediction tends to improve with higher oxidation values.

- The difference at 30 [A/cm] is only 2.5 [A/cm] too low which is an acceptable result.

The defined oxidation damage limit of 30 [A/cm] was chosen on a conservative basis to maximise reliability. There is therefore no reliability concern due to the slight offset in the oxidation prediction. The oxidation data points show a high concentration for oxidation values from 0 – 15 [A/cm] on the abscissa. The rest of the oxidation data points are sufficiently spread over the range up to 30 [A/cm]. The outcome verifies that the modelled oxidation map has good ability to provide a suitable prediction of the oxidation content for an unknown data set. The accuracy of this prediction model is an encouraging outcome as oxidation measurements are difficult in the laboratory and require sophisticated measurement equipment. The approach to model a smooth curvature map with high commonality is successfully confirmed.

7.3.3 Lubricant Condition Rating Performance

Figure 7.21 shows schematically how in the lubricant condition rating is conducted.

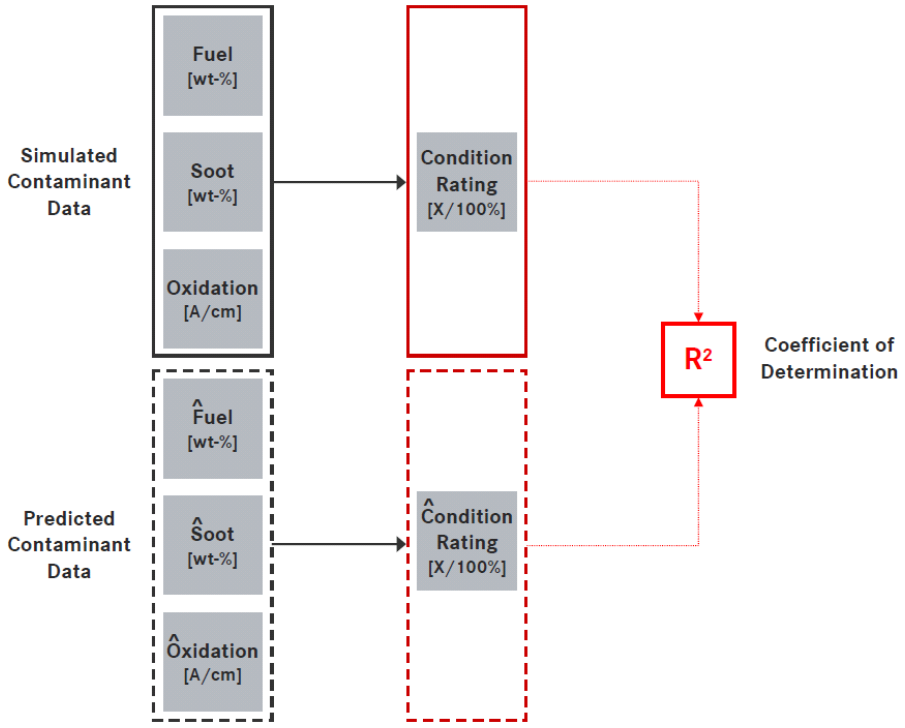

Figure 7.21: Scheme of the condition rating validation
The lubricant rating performance is assessed by generating two condition statements. One is generated with the simulated contaminant data from the vehicle simulation. The oil condition from the predicted fuel, soot and oxidation values from the characteristic maps is generated separately as shown in the lower part. The coefficient of determination R^2 provides a measure of the accuracy of the rating performance of the two independently derived condition statements.

Based on verifying the accuracy of the individual characteristic maps to predict fuel, soot and oxidation this validates the assessment performance of the overall oil condition rating. The accuracy is assessed by deriving the condition of the oil from the original simulated fuel, soot and oxidation data per vehicle which is shown in the upper part of Figure 7.21. The oil condition from the predicted fuel, soot and oxidation values from the characteristic maps is generated separately as shown in the lower part of Figure 7.21. The two independently derived data sets obtained from the oil condition statements are compared using a correlation density plot, see Figure 7.22.

The oil condition status is expressed in percentage where 100 % is defined as the fresh oil condition. The assessment of the resulting condition rating performance of the algorithm uses the coefficient of determination R^2.

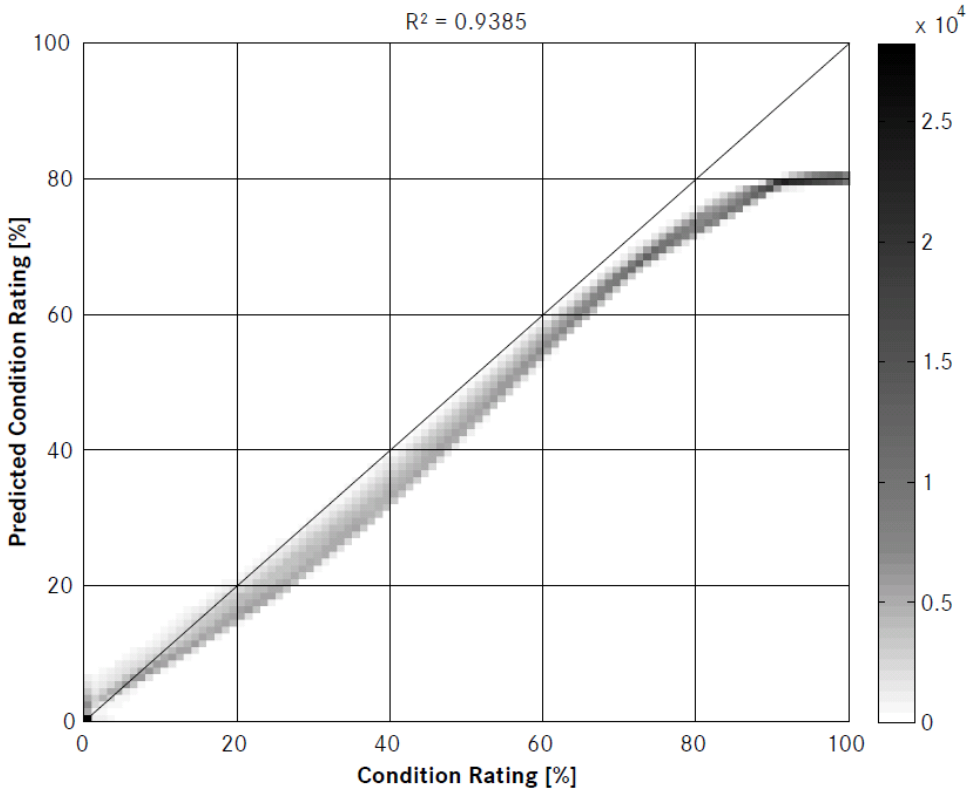

Figure 7.22: Assessment of the oil condition rating performance

The two independently derived data sets obtained from the oil condition statements are compared using a correlation density plot. The oil condition status is expressed in percentage where 100 % is defined as the fresh oil condition. The coefficient of determination R^2 for the condition rating indicates that the model explains 93.85 % of the data. The density shows the high data point concentration for the region from 100 - 60 %.

The following observations and conclusions can be derived from the result in Figure 7.22:

- The coefficient of determination for the condition rating is R^2 = 93.85 % which provides a very good result.
- The plot shows that the condition rating from the characteristic maps is too low which means a reliability orientated rating outcome.
- The rating is significantly too low for fresh oil values but becomes better with condition ratings of about 80 %. The condition rating at that point is 5 - 10 % lower than the rating with the original data.
- The rating for the last 10 % shows the highest accuracy.
- The data density shows the high data point concentration for the region from 100 - 60 %. The rest of the data is evenly distributed over the remaining condition rating range.
- The remaining offset for the condition forecast can be adjusted using a correction function in the next step of the algorithm when the oil condition rating is converted into the remaining mileage forecast.

7.3.4 Remaining Mileage Forecast Capability

The assessment of the remaining mileage forecast performance is illustrated in Figure 7.23 and uses the two independent condition rating statements together with a correction function.

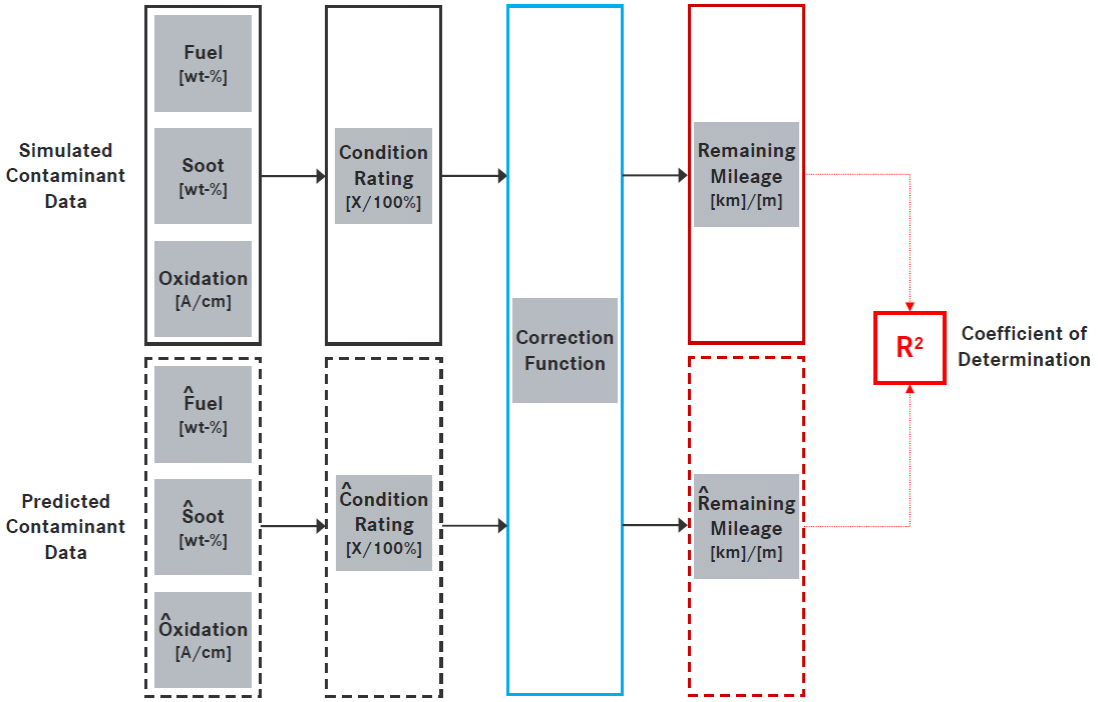

Figure 7.23: Scheme of the remaining mileage forecast performance validation
The previously generated condition rating result is used in combination with a correction function to derive two remaining mileage data. One based on the simulated vehicle data (upper part) and one data set based on the predicted contaminants (lower part). The overall comparison is conducted by assessing the coefficient of determination R^2 derived from the two remaining mileage forecasts.

The remaining mileage calculation was presented in detail in Chapter 6 and provides a linear correlation between the derived condition prediction and the remaining mileage based on a maximum mileage of 25,000 [km] / 15,534 [mi]. In order to improve the remaining mileage forecast performance a correction function is used to minimise the identified offset in Figure 7.22. A 4th order polynomial is used to reduce the offset and is given as:

$$y_{corr}(x) = 1.31E^{-3} \cdot x^4 - 1{,}72E^{-1} \cdot x^3 + 6{,}22E^{0} \cdot x^2 + 2{,}29E^{2} \cdot x - 8{,}47E^{1} \qquad (7.6)$$

With the correction function applied the two independently derived mileage forecasts are compared using a correlation density plot, see Figure 7.24. The remaining mileages from the original data are plotted on the abscissa and the remaining predicted mileage data from the characteristic maps plotted on the ordinate. The performance assessment of the algorithm is conducted using the calculated coefficient of determination R^2.

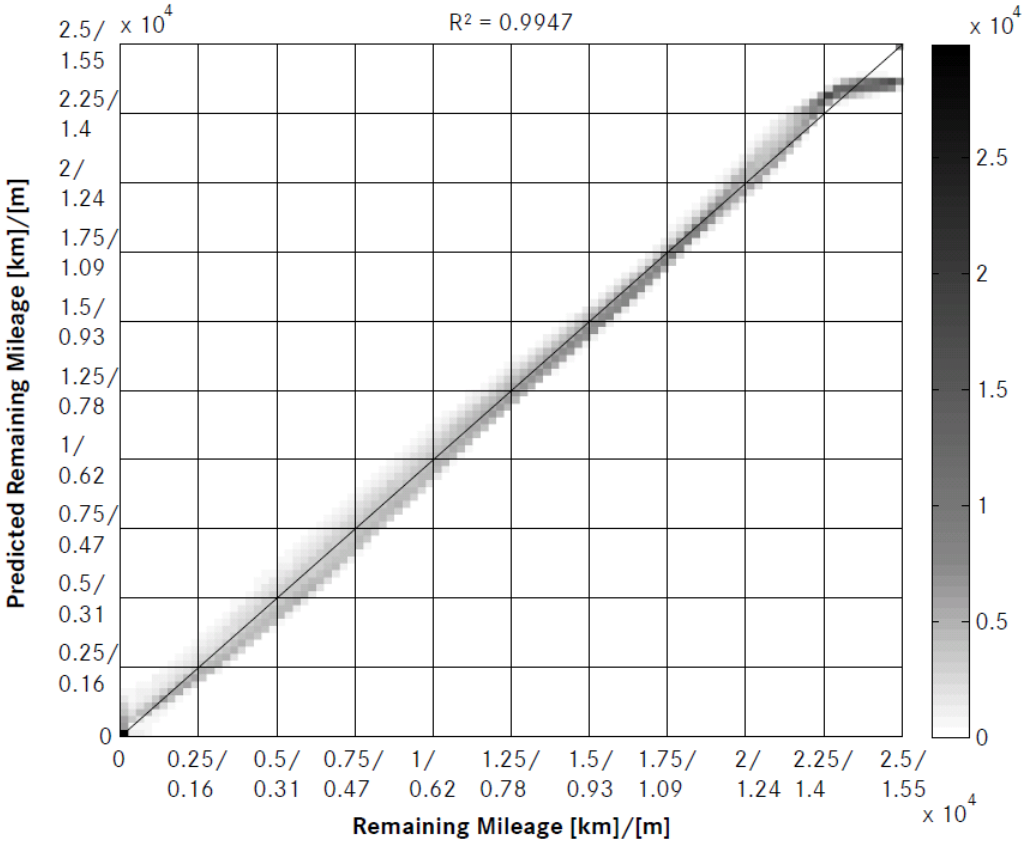

Figure 7.24: Assessment of the remaining mileage forecasting performance
The two independently derived remaining mileage forecast results are assessed using a correlation density plot. The coefficient of determination R^2 for the condition rating indicates that the model explains 99.47 % of the data. The density shows an even data distribution.

- The correction function improved the mileage forecast significantly. The offset is almost completely reduced over the data range with the only remaining deviation occurring at the first 1,250 [km] / 780 [mi] which is acceptable as no significant oil degradation can be expected for this short driving distance.

- The R^2 value of 99.47 % is an exceptionally good result and proves the high performance of the mileage forecast which is based on the high performance of the previous steps for the developed oil condition algorithm.

7.4 Summary

This chapter has investigated the performance of the oil condition monitoring algorithm in the course of this research. The approach using vehicle simulation to generate artificial oil data for three different load profiles was presented and shown realistic simulation basis. The basic items of this novel algorithm were the modelled characteristic maps to predict fuel, soot and oxidation based on viscosity and permittivity input. The modelled results showed that for each map there was a good accuracy achieved based on using real engine oil data. The modelling focus developed smooth curvature maps in order to achieve commonality and to improve the predictive performance for unknown data. The assessment of the maps with the simulated vehicle data fully confirmed this approach and provided very good individual contaminant predictions. The derived oil condition rating based on the predicted fuel, soot and oxidation data showed satisfactory results with some minor offsets. The application of a simple correction function enabled the accuracy of the final step of the algorithm, the mileage forecast, which is the key output data of the oil condition algorithm. The validation of the oil condition algorithm concept accurately and reliably monitored the engine oil condition status over the oil drain interval. The initial research decision to use characteristic maps as the core of this algorithm proved to be a good choice to successfully solve this research problem.

Chapter 8

8 Conclusion and Further Work

8.1 Conclusion

Based on the research objectives of this work the discussion of the achievements and conclusions will summarise all the areas where the research presented in this thesis has provided a significant contribution to knowledge.

The initial theoretical part of this research work summarised all the known potential lubricant degradation effects during engine operation and in particular with regard to the use of the current generation of biofuels. A qualitative risk assessment was conducted which outlined biodiesel as potentially the most critical fuel. The influence of the various degradation effects on the oil condition were investigated based on current sensor measurement principles to provide a comprehensive insight into all the relevant theoretical aspects for the consideration of the research programme. A 'black box' model was used to outline the challenge of oil condition monitoring based on summative measurement methods. From the initial theoretical considerations it was concluded that it is not possible to separate the individual contamination effects using single sensor data or bivariate correlations.

The theoretical considerations were supported by a statistical analysis which investigated how the presence of multiple contaminants in the oil affects the most common sensor data of permittivity, conductivity and viscosity. This analysis was based on used engine oil data which enabled a quantitative assessment of the strength and significance of the key contaminants on the sensor data.

'Design of Experiments' (DoE) models were developed for the permittivity, conductivity and viscosity data and expressing mathematically the relationship between the contaminants having a significant influence on each of the sensor data. The findings of the multivariate analysis identified that the effects on permittivity and viscosity provided reliable information about oil condition changes. The analysis also showed that an increase in permittivity is strongly influenced by soot and oxidation. However the change in the viscosity data is mainly affected by the presence of fuel and oxidation in the oil where the effects have opposite influence on the viscosity change. Conductivity showed no reliable information in detecting changes in the oil condition due to the presence of contaminants.

The concept of an oil condition algorithm in this research was aimed at addressing accuracy and efficiency in predicting the outcome. The novel algorithm model which was developed was subdivided into three functional blocks. The core aspect of the algorithm was the use of characteristic maps based on bi-linear regression to predict the fuel, soot and oxidation levels in the oil using permittivity and viscosity as the input data. The original aspect contributing significant knowledge to this work was the assessment of the three-dimensional characteristic maps based on the input data to predict single contaminant values. The modelling procedure for the map was derived in detail including all relevant theoretical background information. The strategy selected for the modelling process aimed to achieve high commonality and accepting lower R^2 values for the experimental data. Based on the predictions using three contaminant components a method to assess the overall condition status is derived. This overall assessment method included a scheme of identifying damage thresholds for each contaminant and deriving the corresponding condition rating based on experimental data. The condition rating method was intentionally chosen to be conservative as the worst individual contaminant rating defines the overall rating result. The derived condition status provided the input for an oil drain forecast method which monitors the status within the predefined maximum mileage. Also the use of a rolling window approach provided reliable forecasting results with sufficient sensitivity for condition changes. The mileage forecasting method that was developed shifted the condition loss gradient which was defined by the maximum mileage based on the actual condition assessment within the rolling window in order to reliably predict the oil drain interval.

Another achievement from this research was the vehicle simulation for different driving profiles and the corresponding simulation of oil degradations. The selected profiles were for a 'Taxi', 'Normal' driving and 'Long Distance' driving. The resulting simulation of fuel, soot and oxidation levels in the oil showed a high correlation compared with the use of real oil analysis based on engineering judgement.

The quantitative assessment of the simulated contaminant levels compared with the predicted levels obtained from each characteristic map showed excellent prediction performance. The achieved values of R^2 confirmed the modelling strategy towards higher commonality of the maps. This proved to be beneficial in the prediction of unknown contaminant situations which differed from the experimental data set which was initially used to model each map. The derived overall condition rating and mileage forecast prediction also showed very good results.

The results from this research have shown that this new oil condition algorithm concept using bi-linear characteristic maps has enabled the compromise between predictive accuracy and an efficient and transparent algorithm structure. Validation of the results confirms that the algorithm has the potential to minimise and prevent oil condition related engine failures regardless of the actual fuel used. This approach can therefore be used in future real vehicle applications when the oil stress will increase due to higher biofuel usage or vehicle operation in global regions where there are low fuel quality standards.

8.2 Further Work

The development approach could also be applied to other engine or vehicle applications. Potential further research areas would be the use in petrol engines or commercial vehicles such as trucks or vans. The research would need to investigate whether the strength and significance of the contaminants on the sensor data with other vehicle or engine types is the same as found in this work and how the characteristic maps need to be re-modelled.

A further study could look for an oil condition rating using weighting factors which depend on the absolute value and on the speed of the contaminant value changes. This could provide information about how severe the oil condition is affected by contaminants, which would have a direct influence on the rating and the mileage forecast.

The research in this work had two input variables, permittivity and viscosity, but three contaminants to be predicted which were fuel, soot and oxidation. A fundamental sensor study could search for an additional condition value to have the same input data dimension as contaminant dimension to further improve the accuracy. As sensor implementation is always a cost sensitive aspect could a further sensor study search for a less expensive but reliable oil condition measurement system suitable for mass production.

Since the successful demonstration of the algorithm abilities using simulated data, it could be considered to conduct a field trial study to assess the performance of the developed algorithm concept in a real application. The comparison of the results would confirm the algorithm performance and would also provide information on how close the performance results from the simulation in this research are compared with field trial results.

The mileage forecasting model could be refined to predict an oil drain which is only based on the current contaminant prediction without maximum mileage restriction. One research objective would be to develop a driver information system about the actual oil condition and the remaining mileage. It could also be considered to predict the overall vehicle maintenance which would require linking the status of all vehicle parts needing regular maintenance. Information of the vehicle condition could be sent via mobile phone to the garage to automatically book a service date.

An investigation of alternative methods of oil analysis is recommended to improve the basis for future research work. The separation of fossil fuel and biodiesel content in the oil (from various feedstock) should be studied. Better methods of quantifying the lubricant oxidation and nitration level should be considered to enable more precise measurements and results. The analysis should provide more accurate oxidation and nitration measurements regardless of the actual chain reaction process (acidification or polymerisation) and should be robust against interference with other bonds (e.g. esters).

The overall carbon balance should also be investigated to provide a transparent quantification of the potential benefit with the use of biofuels. The CO_2 savings with the use of biofuels should be compared to the amount of energy (and thus CO_2) required by the agricultural industry to produce the biofuels. The lower energy content of biofuels in comparison to fossil fuels must be considered. The use of higher biofuel blends will likely result in shorter oil drain intervals and the increase in engine oil consumption should be taken into account in the carbon balance. Potential technical failures with the use of biofuels and the resulting additional carbon required to produce the spare components should also be estimated.

Chapter 9

9 References

ADM Biodiesel, (2007). 'Französische Autohersteller vorn bei Biokraftstoffen', [Online]. Available at: http://www.biodiesel.de/index.php3?hid=008150. [Accessed 15th July 2009].

Agoston, A., Ötsch, C., Jakoby, B., (2005). 'Viscosity sensors for engine oil condition monitoring – Application and interpretation of results'. *Sensors and Actuators A 121* (2005), p. 327 – 332.

ASTM International, (2001). *ASTM D6751 - 11a Standard Specification for Biodiesel Fuel Blend Stock (B100) for Middle Distillate Fuels*. (http://www.astm.org).

ASTM International, (2008). *ASTM D7467 - 09a Standard Specification for Diesel Fuel Oil, Biodiesel Blend (B6 to B20)*. (http://www.astm.org).

Atkins, PW., (1988). *Physikalische Chemie. (Physical Chemistry).* Weinheim, Basel, Cambridge, New York: VCH.

Atkins, PW., (2001). *The Elements of Physical Chemistry*. Oxford, UK: Oxford University Press.

Awe, RW., (1963). *Silicon antifoams for lubricating oils*. SAE Preprint 774D: p. 1-4. (http://www.sae.org).

Babu, AK., Devaradjane, G., (2003). *Vegetable Oils And Their Derivatives As Fuels For CI Engines: An Overview.* Department of Automobile Engineering, MIT Campus, Anna University. SAE Technical Papers Series 2003-01-0767. (http://www.sae.org).

Bartz, WJ., Möller, UJ., (2000). *Lexikon der Tribologie. (Tribology Lexicon)*. Renningen, GER: Expert Verlag.

Bell, JB., (1972). *Introductory Fourier Transform Spectroscopy*. New York, US: Academic Press.

Bennett, JW., Matsiev, L., Uhrich, M., Kolosov, O., Bryning, Z., Lattin, R., (2006). *New Solid State Oil Condition Sensor for Real Time Engine Oil Condition Monitoring*. 2006 SAE World Congress Detroit, Michigan April 3-6, 2006. SAE Technical Papers Series 2006-01-1324. (http://www.sae.org).

Berry, WW., (1999). 'Developing Biodiesel Fuels for Market - NOPEC Used Oil to Fuel Process', *SAE Clean Diesel Engine Technology TOPTEC*, St. Pete Beach, FL, September 1999.

Binder, KB., (2007). 'Die dieselmotorische Verbrennung. (The diesel engine combustion)'. In: Mollenhauer, K., Tschöke, H., (2007). *Handbuch Dieselmotoren. (Handbook Diesel Engines)*. Berlin, GER: Springer.

Biokraftstoffquotengesetz, (2006). Bundesgesetzblatt Jahrgang 2006 Teil I Nr. 62. *Gesetz zur Einführung einer Biokraftstoffquote durch Änderung des Bundes-Immissionsschutzgesetzes und zur Änderung energie- und stromrechtlicher Vorschriften,* [Online]. Available at: http://www.bgblportal.de/BGBL/bgbl1f/bgbl106s3180.pdf. [Accessed 21st July 2009].

Blume, JD., (1987). *Druck- und Temperatureinfluss auf Viskosität und Kompressibilität von flüssigen Schmierstoffen. (Pressure- and temperature influence on viscosity and compressibility of liquid lubricants).* Dissertation. TH Aachen, GER.

Boeker, E., Grondelle, R., (1999). *Environmental Physics*, Chichester, UK: Wiley.

Bondioli, P., Gasparoli, A., Lanzani, A., Fedeli, E., Veronese, S., Sala, M., (1995). 'Storage Stability of Biodiesel', *Journal of American Oil Chemistry Society 72*, p. 699 – 702.

Boocock, D.G., (2003). 'Single-phase process for production of fatty acid methyl esters from mixtures of triglycerides and fatty acids', US Patent 6,642,399.

Bünger, J., Krahl, J., Munack, A., Ruschel, Y., Schröder, O., Emmert, B., Westphal, G., Müller, M., Hallier, E. and Brüning, T., (2007). 'Strong mutagenic effects of diesel engine emissions using vegetable oil as fuel', *Arch. Toxicol.,* 81(8), p. 599-603.

Buhrdorf, A., Dobrinski, H., Lüdtke, O., Bennett, JW., Matsiev, L., Uhrich, M., Kolosov, O., (2005). 'Multiparameteric Oil Condition Sensor Based on the Tuning Fork Technology for Automotive Applications', In: Valldorf, J., Gessner, W., (2005). *Advanced Microsystems for Automotive Applications 2005*. Berlin, GER: Springer.

Byrnes, J., (2009). *Unexploded Ordnance Detection and Mitigation*. New York, US: Springer.

Canakci, M., Monyem, A., van Gerpen, J. (1999). 'Accelerated Oxidation Process in Biodiesel', *American Society of Agricultural Engineers (ASAE) Power & Machinery Division*, Vol. 42(6), p. 1565 – 1572.

Choi, CY., Bower, GR., Reitz, RD., (1997). *Effects of Biodiesel Blended Fuels and Multiple Injections on DI Diesel Engines.* SAE Technical Papers Series 970218. (http://www.sae.org).

Clarke, LJ., Crawshaw, EH., Lilley, LC., Shell Global Solutions (UK), (2003). 'Fatty Acids Methyl Esters (FAMEs) as diesel blend component', *9th Annual Fuels & Lubes Asia Conference and Exhibition*. Singapore, January 2003.

Department for Transport, (2010). '*UK Reports to the EC on the promotion of Biofuels*'. [Online]. Available at: http://www.dft.gov.uk/pgr/roads/environment/renewablefuels/biofuels/. [Accessed 22nd February 2011].

D'Errico, J., (2005). 'Surface Fitting using gridfit'. [Online]. Available at: http://www.mathworks.com/matlabcentral/fileexchange/8998-surface-fitting-using-gridfit. [Accessed 11th March 2011].

DGMK German Society for Petroleum and Coal Science and Technology, (2005). *DGMK Research Report 611-1. Biofuels- Properties and Experiences with their use – Update.* Hamburg, GER: DGMK.

DIN 40041, (1990). *Dependability; concepts*. Berlin, GER: Beuth.

DIN 51380, (1990). *Testing of lubricants; test for fuel diluent in used automotive engine oils; gas chromatography method*. Berlin, GER: Beuth.

DIN 51452, (1994). *Testing of lubricants; determination of the soot content in used Diesel engine oils; infrared spectrometry*. Berlin, GER: Beuth.

DIN 51453, (2004). *Testing of lubricants - Determination of oxidation and nitration of used motor oils - Infrared spectrometric method*. Berlin, GER: Beuth.

DIN 51562-1, (1999). *Viscometry - Measurement of kinematic viscosity by means of the Ubbelohde viscometer - Part 1: Viscometer specification and measurement.* Berlin, GER: Beuth.

DIN 51626-1, (2009). *Automotive fuels - Requirements and test methods - Part 1: Petrol E10.* Berlin, GER: Beuth.

DIN 66261, (1985). *Information processing; Nassi-Shneiderman flowchart symbols*. Berlin, GER: Beuth.

DIN EN 590, (2010). *Kraftstoffe für Kraftfahrzeuge - Dieselkraftstoff - Anforderungen und Prüfverfahren; Deutsche Fassung EN 590:2009+A1:2010. Automotive fuels - Diesel - Requirements and test methods; German version EN 590:2009+A1:2010*. Berlin, GER: Beuth.

DoD - Department of Defense, (1981). *Military Standard Definitions of Terms for Reliability and Maintainability. MIL-STD-721C.* Washington DC, US: Department of Defense, 1981.

Dobrinski, H., Buhrdorf, A., Lüdtke, O., Knipper, U., (2007). *Multiparameter Oil Condition Sensor Based on the Tuning Fork Principle.* SAE 2007 World Congress Detroit, Michigan, April 16-19, 2007. SAE Technical Papers Series 2007-01-0392. (http://www.sae.org).

Dobrinski, H., Buhrdorf, A., Lindemann, M., Lüdtke, O., (2008). *Combi-sensor for Oil Level and Oil Quality Management.* SAE Technical Papers Series 2008-01-0906. (http://www.sae.org).

EU – European Union, (2003). Official Journal of the European Union. *Directive 2003/30/EC of the European Parliament and of the Council of 8 May 2003 on the promotion of the use of biofuels or other renewable fuels for transport*, [Online]. Available at: http://eur-lex.europa.eu/LexUriServ/LexUriServ.do ?uri=OJ:L:2003:123:0042:0046:EN:PDF. [Accessed 21st July 2009].

FAL – Bundesforschungsanstalt für Landwirtschaft (Federal Research Facility for Agriculture), (2005). *Abschlussbericht zum Forschungsvorhaben: Bestimmung der Emissionen und der Partikelgrößenverteilung (Feinstaub) im Abgas eines modernen Euro-4-Nutzfahrzeugmotors mit SCR-Abgasreinigung im Betrieb mit Biodiesel. (Final research report: Evaluation of exhaust emissions and particulate distribution of a modern Euro-4 commercial vehicle engine equipped with SCR-exhaust aftertreatment system using biodiesel.* Braunschweig, Coburg and Göttingen, GER.

Fang, HL., McCormick, RL., (2006). *Spectroscopic Study of Biodiesel Degradation Pathways.* SAE Technical Papers Series 2006-01-3300. (http://www.sae.org).

Fichtner, W., (2002). *Impedanzmessungen in organischen Flüssigkeiten geringer Leitfähigkeit und ihr Einsatz zur Untersuchung von Schmierölen. (Impedance measurement in organic liquids with low conductivity and their application for the investigation of lubricants).* Dissertation. Technische Universität Dresden, GER.

Fleming, W., (2001). 'Overview of Automotive Sensors'. *IEEE Sensors Journal*, Vol. 1, No. 4, December 2001, p. 296 – 308.

Fox, J., (2008). *Applied Regression Analysis and Generalized Linear Models - 2nd ed*. Los Angeles, US: Sage Publications Inc.

Giroldo, MB., Werninghaus, E., Coelho, E., Makant, W., (2005). *Development of 1.6L Flex Fuel Engine for Brazilian Market*. SAE Technical Papers Series 2005-01-4130 (http://www.sae.org).

Goodlive, SA., Lvovich, VF., Humphrey, BK., Boyle, FP., (2004). *On-Board Sensor Systems to Diagnose Condition of Diesel Engine Lubricants – Focus on Soot*. Powertrain & Fluid Systems, Conference & Exhibition, Tampa, Florida, US. October 25-28, 2004. SAE Technical Papers Series 2004-01-3010. (http://www.sae.org).

Graboski, MS., et al., 2003. 'The Effect of Biodiesel Composition on Engine Emissions from a DDC Series 60 Diesel Engine', U.S. Department of Energy, *NREL Report*, NREL/SR-510-31461, February 2003. (http://www.nrel.gov/docs/fy03osti/31461.pdf).

Gunstone, FD., (1967). *Chemical Properties of Fatty Acids and Their Esters, in An Introduction to the Chemistry and Biochemistry of Fatty Acids and Their Glycerides*, 2nd edn., London, UK: Chapman & Hall Ltd. p. 105–114.

Halalay, IC., Schneider, EW., (2007). *In-Situ Monitoring of Engine Oils through Electrical AC Impedance Measurements.* SAE Powertrain & Fluid Systems Conference & Exhibition, Rosemont, Illinois, October 29 - November 1, 2007.
SAE Technical Papers Series 2007-01-4092. (http://www.sae.org).

Hauptmann, P., (1990). *Sensoren – Prinzipien und Anwendungen. (Sensors – principles and applications).* München, GER: Hanser.

Herrmann, S., (2009). *Einfluss von Biokraftstoffen auf das Motorenöl in modernen Verbrennungsmotoren. (Influence of biofuels on engine oils in modern combustion engines).* Bachelor Thesis. University of Heilbronn, GER.

Irion, E., Land, K., Gürtler, T., Klein, M., (1997). *Oilquality prediction and oil-level detection with the Temic QLT-sensor leads to variable maintenance intervals*.
SAE Technical Papers Series 970847. (http://www.sae.org).

Ishikawa, K., (1990). *Introduction to Quality Control*. London, UK: Productivity Press.

Ivers-Tiffée, E., von Münch, W., (2007). *Werkstoffe der Elektrotechnik. (Electrotechnical materials).* Wiesbaden, GER: Teubner.

Kaltschmitt, M., Hartmann, H., (2001). *Energie aus Biomasse. Grundlagen, Techniken und Verfahren.(Energy from Biomass. Basics, techniques and procedures)*.
Berlin, GER: Springer.

Kanazawa, KK., Gordon, JG., (1985). 'The Oscillation of a Quartz Resonator in Contact with Liquid', *Analytica Chimica Acta*, 175, p. 99 - 105.

Kappus, PE., Fuerhapter, A., Fuchs, H., Fraidl, GK., (2007). *Ethanol Direct Injection on Turbocharged SI Engines – Potential and Challenges.* 2007 World Congress Detroit, Michigan April 16-19, 2007. SAE Technical Papers Series 2007-01-1408.
(http://www.sae.org).

Kaspar, M., Stadler, H., Weiß, T., Ziegler, C., (2000). 'Thickness shear mode resonators ("mass-sensitive devices") in bioanalysis', *Fresenius Journal of Analytic Chemistry* (2000), 366, p. 602 – 610.

Kastner, A., (2001). *Dielektrische Charakterisierung rußgefüllter Elastomere. (Dielectric characterisation soot-filled elastomers).* Dissertation. Technische Universität Darmstadt, GER.

Kauppinen, K., Hollberg, M., (1997). 'Spectrometers, Infrared', *Encyclopedia of Applied Physics*, Vol. 19.

Kawano, D., Ishii, H., Goto, Y., Noda, A., Aoyagi, Y., (2007). *Effect of Exhaust Gas Recirculation on Exhaust Emissions from Diesel Engines Fuelled with Biodiesel*. SAE Technical Papers Series 2007-24-0128. (http://www.sae.org).

Kinast, JA., (2003). 'Production of Biodiesels from Multiple Feedstocks and Properties of Biodiesels and Biodiesel/Diesel Blends', U.S. Department of Energy, *NREL Report*, NREL/SR-510-31460, March 2003, (http://www.nrel.gov/docs/fy03osti/31460.pdf).

Klamann, D., (1982). *Schmierstoffe und verwandte Produkte. (Lubricants and related products).* Weinheim, GER: Verlag Chemie.

Klemens, I., (2008). *Straßentest Opel Corsa - B15. Feldtestdaten Juli 2007 – März 2008 (Streettest Opel Corsa – B15. Field trial data July 2007 – March 2008).* Internal Presentation from Shell Global Solutions to Daimler AG.

Krallmann, J., (2005). *Einsatz eines Multisenors für ein Condition Monitoring von mobilen Arbeitsmaschinen. (Application of a multi-sensor for condition monitoring of mobile agricultural machines).* Dissertation. University Carolo-Wilhelmina Braunschweig, GER.

Krause, H., Scholten, J., (1979) ’Verschleiß – Grundlagen und systematische Behandlung (Wear – Fundamentals and systematic treatment)’ *VDI-Zeitschrift* 21 (15/16): p. 799-805. In: Möller, UJ., Nasser, J., (2002). *Schmierstoffe im Betrieb. (Lubricants in Operation).* Berlin, GER: Springer.

Kremer, F., Fontes, S., (2004). *Alcohol as an Automotive Fuel -Updated Vision of the Brazilian Experience*. SAE Technical Papers Series 2004-05-0398. (http://www.sae.org).

Krüger, M., Breuer, N., (2007). ‘Abgasnachbehandlung. (Exhaust aftertreatment)’. In: Mollenhauer, K., Tschöke, H., (2007). *Handbuch Dieselmotoren (Handbook Diesel Engines)*. Berlin, GER: Springer.

Kunz, K., (1997). *Konstruktion einer neuartigen Kolben/Pleuel-Anbindung im Rahmen des Projekt ‘Ölwechselfreier Motor’. (Construction of a novel piston/con rod-connection in the project ‘Oil drain free engine’).* Diploma thesis. University of Applied Sciences Esslingen, GER.

Leonhardt, H., Reders, K., Froböse, E., Müller, HD., Null, V., Miller, J., Busse, P., (2005). *Motorenöl-Lexikon. (Engine Oil Lexicon)*.
Hamburg, GER: Shell Global Solutions (Deutschland) GmbH.

Liebau, M., (1998). *Resonante Quarzsensoren zum Nachweis von Wechselwirkungen supramolekularer Systeme. (Application of quarz resonators to detect interactions of supra molecular systems).*
Dissertation. Martin Luther Universität Halle-Wittenberg, GER.

Linssen, R., (2010). *Dokumentation Kennfeldrechnung. (Documentation Characteristic Map Calculation).* Internal Documentation. Stuttgart, GER: Daimler AG.

Liu, Y., Künne, B., Jorden, W. (1990). 'Mögliche Ursachen der Differenz zwischen Haft- und Gleitreibwert (Possible reasons for the difference between static and sliding friction coefficients)', *Tribologie und Schmierungstechnik* 37 (6): 362-363. In: Möller, UJ., Nasser, J., (2002). *Schmierstoffe im Betrieb. (Lubricants in Operation)*. Berlin, GER: Springer.

Lorenz, W., (2007). *Verfahren zur Bestimmung des Motorölzustands und Prognostizierung der Ölwechsel in Nutzfahrzeugen. (Method to determine the engine oil condition and prognosticate the oil drain interval in heavy duty vehicles).* Diploma thesis. Technische Universität Kaiserslautern, GER.

Luther, R., (2008). 'Alternative Kraftstoffe aus Sicht der Motorenschmierung (Alternative Fuels from Engine Lubrication Prospective)', *MTZ* 03/2008 (69), p. 230 – 236.

Mackos, N., Baybutt, M., Palmer, CA., Tario, JD., (2008). *Providing Embedded, In-situ Oil Quality Monitoring for Improved Maintenance and On-Board Diagnostics in Trucking and Automotive Applications*. SAE Technical Papers Series 2008-01-2614. (http://www.sae.org).

Magorian, VG., (1980). 'Keeping air out of hydraulic systems'. *Machine Design* 52, Nr. 18: p. 71 – 76. In: Möller, UJ., Nasser, J., (2002). *Schmierstoffe im Betrieb. (Lubricants in Operation)*. Berlin, GER: Springer.

Marsh, S., Corradi, M., (2007). 'The Effect of Biodiesel on Engine Lubricants', *Lubes 'N' Greases Magazine*, June 2007.

Martin, SJ., Cernosek, RW., Spates, JJ., (1994). 'Sensing Liquid Properties with Shear-Mode Resonator Sensors', *Sandia National Laboratories supported by the U.S. Department of Energy*, Contract No. DE-AC04-94AL85000.

Mang, T., Dresel, W., (2001). *Lubricants and Lubrication*. Weinheim, GER: Wiley-VCH.

Maples, R., (2000). *Petroleum Refinery Process Economics*. *2nd*. *Edition*. Tulsa, US: Pennwell Books.

Matsiev, LF., (1999). 'Application of Flexural Resonators to Simultaneous Measurements of Liquid Density and Viscosity', *Proceedings of 1999 IEEE Ultrasonics Symposium*. v.1, p. 457 – 460.

Matsiev, LF., (2000). 'Application of Flexural Mechanical Resonators to High Throughput Liquid Characterization', *Proceedings of 2000 IEEE Ultrasonics Symposium*. v.1, p. 427 – 434.

McTavish, S., Ney, J., (2009-1). *Impact of Biodiesel Fuels on Crankcase Lubricant Performance*. Internal Presentation from Infineum UK Ltd. to Daimler AG.

McTavish, S., Ney, J., (2009-2). *Impact of Bioethanol Fuels on Crankcase Lubricant* Perform*ance*. Internal Presentation from Infineum UK Ltd. to Daimler AG.

Meislish, H., Nechamkin, H., Sharefkin, J., (1977). *Theory and problems of Organic Chemistry*. New York, US: McGraw-Hill Publishing Company.

Mitra, S., Kebbekus BB., (1998). *Environmental Chemical Analysis*. London, UK: Blackie Academic & Professional.

Möller, UJ., Nasser, J., (2002). *Schmierstoffe im Betrieb. (Lubricants in Operation)*. Berlin, GER: Springer.

Mohr, R., (2003). *Statistik für Ingenieure und Naturwissenschaftler. (Statistics for Engineers and Scientists)*. Renningen, GER: Expert Verlag.

Mollenhauer, K., Tschöke, H., (2007). *Handbuch Dieselmotoren. (Handbook Diesel Engines)*. Berlin, GER: Springer.

Moore, R., (1999). 'Tabellen für Verteilungsfunktionen und Quantile.
(Tables for distribution functions and quantiles)'. [Online]. Available at:
http://www.mathematik.uni-ulm.de/ stochastik/lehre/ss03/wirtschaftsstatistik/
skript9/node47.html. [Accessed 16th March 2011].

Murphy, JD., McCarthy, K., (2004). 'Ethanol production from energy crops and wastes for use as a transport fuel in Ireland', In: *Applied Energy* 82 (2005), p. 148 – 166.

O'Donnell, RJ., Zakarian, JA., (1984). 'Survey of two parameter equations for the viscosity-temperature behaviour of lubricating oils', *Industrial Engineering Chemistry Proc*. Des. Dev. 23 (3), p. 491-495.

Ollus, R., K. Juoperi, (2007). 'Alternative fuels experiences for medium-speed diesel engines', *2007 CIMAC Congress*, Vienna, AUT, Paper 234.

Orazem, ME., Tribollet, B., (2008). *Electrochemical Impedance Spectroscopy*.
New York, US: John Wiley & Sons.

Paddon, C., (2008). *Oxidation Part 1*.
Internal Presentation from Shell Global Solutions to Daimler AG.

Press, WH., Teukolsky, SA., Vetterling, WT., Flannery, BP., (2007).
Numerical Recipies: The Art of Scientific Computing. 3rd ed.
New York, US: Cambridge University Press.

Pruckner, E., (2007). *Vorlesungsskript Wärme- und Stoffübertragung.
(Lecture Notes Heat- and Materialtransfer)*. University of Heilbronn, GER.

Römpp Online – Thieme Chemistry Database, Version 3.6 (2009). Thieme Verlag.
(http://www.roempp.com).

SAE Fuels and Lubricants Technical Committee, (2006). *J357 Physical and Chemical Properties of Engine Oils.* (http://www.sae.org).

SAE International Standards, (2009). *J300_200901 Engine Oil Viscosity Classification*. (http://standards.sae.org)

Sappok, A., Wong, V., (2010). *Ash Effects on Diesel Particulate Filter Pressure Drop Sensitivity to Soot and Implications for Regeneration Frequency and DPF Control*. Massachusetts Institute of Technology. SAE Technical Papers Series 2010-01-0811. (http://www.sae.org).

Sato, H., Tokuoka, N., Yamamoto, H., Sasaki, M., (1999). *Study on Wear Mechanism by Soot Contaminated in Engine Oil (First Report: Relation Between Characteristics of Used Oil and Wear).* International Fall Fuels & Lubricants Meeting & Exposition Toronto, Ontario, Canada. October 25-28, 1999.
SAE Technical Papers Series 1999-01-3573. (http://www.sae.org).

Sauerbrey, G., (1959). Z Phys 115, p. 206 – 222.

Schmitigal, J., Moyer, S., (2005). *Evaluation of Sensors for On-Board Diesel Oil Condition Monitoring of U.S. Army Ground Equipment*. 2005 SAE World Congress, Detroit, Michigan, US. April 11-14, 2005. SAE Technical Paper Series 2005-01-1810. (http://www.sae.org).

Schumacher, L., Borgelt, SC., (1996). *Fueling a Diesel Engine with Methyl-Ester Soybean Oil*. SAE Technical Papers Series 1996-962233. (http://www.sae.org).

Schwab, AW., Bagby, MO., Freedman, B., (1987). 'Preparation and Properties of Diesel Fuels from Vegetable Oils', *Fuel* 66, p. 1372–1378.

Schweyer, M., Hilton, J., Munson, J., Andle, J., Hammond, J., Lec, R., (1997). 'A Novel Monolithic Piezoelectric Sensor', *1997 IEEE International Frequency Control Symposium*, p. 32 – 40.

Sem, TR., (2004). *Effect of Various Lubricating Oils on Piston Deposits in Biodiesel Fueled Engines.* SAE Technical Papers Series 2004-01-0098. (http://www.sae.org).

Smiechowski, MF., (2005). *Electrochemical Characterisation of Lubricants for Microfabricated Sensor Applications*.
Dissertation. Case Western Reserve University, US.

Spurk, JH., (1996). *Strömungslehre. (Fluid mechanics).* Berlin, GER: Springer.

Stepina, V., Vesely, V., (1992). *Lubricants and Special Fluids*.
Amsterdam, NL: Elsevier Science Publisher.

Stöckl, M., Winterling, KH., (1973). *Elektrische Messtechnik (Electrical Measeurement Technology).* Stuttgart, GER: Teubner.

Taupp, M., (2001). *Biodiesel. Seminararbeit. (Biodiesel Study)*.
Würzburg, GER: Bayerische Julius-Maximilians-Universität.

Tojo, G., Fernández, M., (2007). *Oxidation of Primary Alcohols to Carboxylic Acids*.
New York, US: Springer.

Ullman, (2007). *Ullmann's Encyclopedia of Industrial Chemistry*. Electronic Release 2007. New York, US: John Wiley & Sons.

UN - United Nations, (1998). *Kyoto Protocol to the United Nations Framework Convention on Climate Change,* [Online].
Available at: http://unfccc.int/resource/docs/convkp/kpeng.pdf .
[Accessed 21st July 2009].

Vaughn, T., Hammill, M., Harris, M., Marchese, AJ., (2006). *Ignition Delay of Bio-Ester Fuel Droplets*. SAE Technical Papers Series 2006-01-3302. (http://www.sae.org).

Van Basshuysen, R., Schäfer, F., (2002). *Handbuch Verbrennungsmotoren (Handbook of Combustion Engines).* Wiesbaden, GER: Vieweg.

Van den Bulk, R., (2008). 'The Impact of Biodiesel Use on the Lubrication of Diesel Engines', Presented at: *Technische Arbeitstagung Hohenheim*, March 11th 2008.

Van Gerpen, JH., B. Shanks, R. Pruszko, D. Clements, G. Knothe, (2004). 'Biodiesel Production Technology August 2002 - January 2004', *National Renewable Energy Laboratory*, Golden, Colorado, NREL/SR-510-36244, (http://www.nrel.gov/docs/fy04osti/36244.pdf).

Von Münch, W., (1987). *Elektrische und magnetische Eigenschaften der Materie. (Electric and magnetic properties of elements).* Stuttgart, GER: Teubner.

Viswanath, DS., Prasad, DHL., Dutt, NK., Rani, KY., (2007). *Viscosity of Liquids - Theory, Estimation, Experiment, and Data*. Dordrecht, NL: Springer.

Vogelpohl, G., (1954). 'Die Stribeck-Kurve als Kennzeichen des allgemeinen Reibungsverhaltens geschmierter Gleitflächen. (The Stribeck-Curve as a charactersitics of the general friction condition of lubricated surfaces)', *VDI-Zeitschrift* 96 (9): 261-268. In: Möller, UJ., Nasser, J., (2002). *Schmierstoffe im Betrieb (Lubricants in Operation)*. Berlin, GER: Springer.

Wang, WG., Lyons, DW., Clark, NN., Gautam, M., Norton, PM., (2000). 'Emissions from Nine Heavy Trucks Fueled by Diesel and Biodiesel Blend without Engine Modification', *Environmental Science & Technology*, Vol. 34, No. 6, p. 933 – 939.

Warnecke, W., Müller, HD., Heinen, J., Kollmann, K., Land, K., Gürtler, T., (1998). 'Belastungsgerechte Ölwartung mit ASSYST. (Load dependent oil drain with ASSYST)', *MTZ Motortechnische Zeitschrift*, Vol. 59, No. 7/8, 1998, p. 414 – 421.

Waynick, JA., (1997). 'Evaluation of the Stability, Lubricity, and Cold Flow Properties of Biodiesel Fuel', *6th International Conference on Stability and Handling Liquid Fuels*, Vancouver, BC October 13-17.

Zabler, E., (2001). 'Bosch Gelbe Reihe - Sensoren im Kraftfahrzeug', *Holland + Josenhans*: 1. Auflage Deutschland 06/2001.

Zhang, C., George, H., Soukup, B., Kornbrekke, R., Boyle, FP., Goodlive, SA., (2004). 'Chemical Sensor Development for Measuring Soot Caused Lubricant Oil Thickening', *2004 IEEE International Ultrasonics, Ferroelectrics, and Frequency Control Joint 50th Anniversary Conference*, p. 200.

Appendix

Appendix Part A: Discussion of Potential Source of Errors in the Empirical Data

Potential error source: People - false reading of values.

Potential effect: Storage of wrong analysis values in the database - potential outliers.

Identifiable: Typically not - only in the case of significant outliers.

Method: Visual data inspection using bivariate correlation plots and box-plot diagrams - plausibility check.

Measure: Deleting of entire analysis result from the complete data set if outliers identified. No correction model exists as the correct value cannot subsequently be reproduced.

Potential impact on data accuracy: High.

Probability estimation: Low, due to qualified laboratory staff.

Potential error source: People - incorrect manual operation of equipment.

Potential effect: Inaccurate analysis results - potential outliers, noise.

Identifiable: Typically not - only in the case of significant outliers.

Method: Visual data inspection using bivariate correlation plots and box-plot diagrams - plausibility check.

Measure: Deleting of data set if outliers identified - no correction model exists as the true value cannot subsequently be reproduced.

Potential impact on data accuracy: Medium.

Probability estimation: Low, due to precise procedures and qualified laboratory staff.

Potential error source: People - false or mixed allocation of measured values to a particular engine/vehicle test run.

Potential effect: Faulty data set for this engine run.

Identifiable: Typically not if the values are in the range with the other data.

Method: None.

Measure: None.

Potential impact on data accuracy: High, as the correlations of contaminants and sensor data might be inaccurate for this data set.

Probability estimation: Medium, due to many manual intermediate steps.

Potential error source: People - wrong allocation of oil sample to a particular engine/vehicle test run.

Potential effect: Complete data is wrong set for this particular engine run.

Identifiable: In general not as the values might be in the typical range as with other test results.

Method: None, as typically not identifiable.

Measure: None.

Potential impact on data accuracy: Low, as only one type of engine was considered and the correlations for contaminants and sensor data will still be provided.

Probability estimation: Typically low due to precise labelling of oil samples.

Potential error source: People - false manual data input into the database.

Potential effect: Wrong data for this oil analysis data set of a particular engine run. Outliers or noise in the data can occur.

Identifiable: Only in the case of significant outliers.

Method: Visual data inspection using bivariate correlation plots and box-plot diagrams, plausibility check.

Measure: Deleting of data set if outliers identified - no correction model exists as the true value cannot be reproduced.

Potential impact on data accuracy: High, as the correlations of contaminants and sensor data might be wrong for this data set.

Probability estimation: Low, due to qualified and experienced laboratory staff.

Potential error source: Process – incorrect oil sample taking from the engine.

Potential effect: Measured contaminants might be biased if an inhomogeneous oil sample is taken. The resulting oil and sensor data does not represent the actual oil condition.

Identifiable: No, as the real values are unknown.

Method: None.

Measure: None.

Potential impact on data accuracy: Low, as the range of contaminants within different potential oil layers does not provide extreme variation.

Probability estimation: Low, as all oil samples were taken according to a defined oil sampling procedure.

Potential error source: Equipment – calibration of laboratory equipment.

Potential effect: Incorrect measurements.

Identifiable: Typically not if the measurements are still within the range of all data for this particular parameter.

Method: None.

Measure: None.

Potential impact on data accuracy: Low, as the measurements will likely still in an acceptable range with regard of the entire range of a particular parameter.

Probability estimation: Low, as all laboratory equipment is regularly calibrated.

Potential error source: Measurement – false measurement.

Potential effect: Faulty or wrong measured parameter in the case of a systematic failure due to violation of defined analysis procedure. Outliers or noise in the data can occur.

Identifiable: Typically not if the measurements are still within the range of all data for this particular parameter.

Method: Visual data inspection using bivariate correlation plots and box-plot diagrams - plausibility check.

Measure: Deleting of data set if outliers identified - no correction model exists as the true value cannot be reproduced.

Potential impact on data accuracy: Medium, as the correlations of contaminants and sensor data might be inaccurate for this particular data set.

Probability estimation: Low, due to well defined analysis procedures and qualified laboratory staff.

Potential error source: Environment – interference of contaminants.

Potential effect: Faulty or wrongly measured parameter - resulting correlation results might be wrong. Noise in the data is very likely.

Identifiable: Typically not - only in the case of significant outliers.

Method: Visual data inspection using bivariate correlation plots and box-plot diagrams - plausibility check.

Measure: Deleting of data set if implausible outliers identified – correction not possible as the true value cannot be determined.

Potential impact on data accuracy: Medium, as the correlation of contaminants and sensor data would be wrong for this particular parameter.

Probability estimation: Low, as the initially defined data range of the individual contaminants was selected with regard to the measurement range of each analysis method to prevent the interference of effects.

Potential error source: Machine – data from failed engines.

Potential effect: High levels of contaminants, distortion of standard analysis methods. Storage of wrong analysis values in the database, potential outliers.

Identifiable: If contaminant and abrasion metal content is at an abnormal level.

Method: Visual data inspection using bivariate correlation plots and box-plot diagrams - plausibility check.

Measure: Deleting of entire analysis result from the complete data set if outliers identified. No correction model exists as the correct value cannot subsequently be reproduced.

Potential impact on data accuracy: High.

Probability estimation: Low - as identified problems during test runs are typically documented.

Appendix Part B: Data Matrix - Characteristic Maps

Table B.1: Data matrix – characteristic fuel map

Fuel [wt.-%]

Permittivity [1] \ Viscosity [mm²/s]	6	7	7,5	8	8,5	9	9,5	10	10,5	11	11,5	12	12,5	13	13,5	14	15	16	17	18
2	0,64	0,40	0,29	0,18	0,10	0,04	0,01	0,00	0,00	0,00	0,00	0,00	0,00	0,00	0,00	0,00	0,00	0,00	0,00	0,00
2,05	4,05	3,23	2,83	2,42	2,01	1,58	1,15	0,71	0,30	0,00	0,00	0,00	0,00	0,00	0,00	0,00	0,00	0,00	0,00	0,00
2,1	7,41	6,04	5,34	4,65	3,94	3,24	2,56	1,92	1,36	0,91	0,59	0,37	0,23	0,13	0,06	0,02	0,00	0,00	0,00	0,00
2,15	10,70	8,79	7,83	6,88	5,93	5,00	4,11	3,29	2,54	1,89	1,35	0,92	0,59	0,34	0,17	0,06	0,00	0,00	0,00	0,00
2,175	12,32	10,14	9,06	7,98	6,91	5,86	4,86	3,92	3,07	2,31	1,68	1,16	0,75	0,45	0,23	0,08	0,00	0,00	0,00	0,00
2,2	13,93	11,48	10,26	9,06	7,87	6,70	5,58	4,52	3,55	2,69	1,96	1,37	0,90	0,54	0,28	0,10	0,00	0,00	0,00	0,00
2,225	15,54	12,79	11,44	10,11	8,79	7,50	6,25	5,06	3,98	3,02	2,21	1,55	1,02	0,62	0,33	0,12	0,00	0,00	0,00	0,00
2,25	17,13	14,08	12,58	11,11	9,66	8,24	6,86	5,56	4,36	3,30	2,42	1,69	1,12	0,69	0,37	0,14	0,00	0,00	0,00	0,00
2,275	18,70	15,32	13,67	12,05	10,46	8,92	7,42	6,01	4,70	3,56	2,60	1,82	1,21	0,75	0,40	0,16	0,00	0,00	0,00	0,00
2,3	20,25	16,51	14,70	12,93	11,20	9,53	7,93	6,42	5,03	3,80	2,77	1,95	1,30	0,81	0,44	0,18	0,00	0,00	0,00	0,00
2,35	23,10	18,60	16,48	14,43	12,46	10,59	8,82	7,17	5,65	4,30	3,16	2,23	1,50	0,95	0,53	0,22	0,00	0,00	0,00	0,00
2,4	25,00	20,02	17,75	15,58	13,52	11,56	9,70	7,97	6,38	4,96	3,72	2,70	1,88	1,24	0,75	0,38	0,04	0,00	0,00	0,00
2,45	25,00	20,67	18,54	16,45	14,43	12,49	10,64	8,90	7,29	5,82	4,52	3,41	2,50	1,78	1,22	0,78	0,29	0,12	0,05	0,00
2,5	25,00	21,02	19,05	17,10	15,20	13,37	11,61	9,95	8,40	6,97	5,67	4,52	3,54	2,72	2,06	1,53	0,85	0,46	0,21	0,00
2,55	25,00	21,29	19,47	17,68	15,92	14,23	12,61	11,08	9,65	8,33	7,12	6,01	5,02	4,14	3,37	2,72	1,75	1,03	0,47	0,00
2,6	25,00	21,59	19,91	18,27	16,66	15,10	13,62	12,22	10,93	9,74	8,66	7,67	6,76	5,91	5,11	4,33	2,91	1,76	0,82	0,00
2,65	25,00	21,93	20,42	18,92	17,45	16,02	14,65	13,34	12,14	11,04	10,06	9,19	8,36	7,58	6,81	5,92	4,09	2,57	1,28	0,07
2,7	25,00	22,31	20,98	19,66	18,35	17,05	15,77	14,53	13,33	12,21	11,20	10,29	9,40	8,52	7,66	6,81	5,07	3,43	1,83	0,24
2,75	25,00	22,72	21,58	20,45	19,32	18,20	17,06	15,91	14,73	13,53	12,37	11,40	10,43	9,47	8,52	7,57	6,11	4,37	2,45	0,47
2,8	25,00	23,13	22,19	21,25	20,31	19,38	18,44	17,50	16,56	15,63	14,69	13,75	12,81	11,88	10,94	10,00	7,72	5,38	3,04	0,70

manual application

Table B.2: Data matrix – characteristic soot map

Soot [wt.-%]

Permittivity [1] \ Viscosity [mm²/s]	6	7	7,5	8	8,5	9	9,5	10	10,5	11	11,5	12	12,5	13	13,5	14	15	16	17	18
2	0,00	0,00	0,00	0,00	0,00	0,00	0,00	0,00	0,00	0,00	0,00	0,00	0,00	0,00	0,00	0,00	0,00	0,00	0,00	0,00
2,05	0,00	0,00	0,00	0,00	0,00	0,00	0,00	0,00	0,00	0,00	0,00	0,00	0,00	0,00	0,00	0,00	0,00	0,00	0,00	0,00
2,1	0,10	0,10	0,10	0,10	0,10	0,10	0,10	0,10	0,10	0,10	0,10	0,10	0,10	0,10	0,10	0,10	0,10	0,10	0,10	0,10
2,15	0,18	0,19	0,19	0,19	0,19	0,19	0,19	0,19	0,20	0,21	0,22	0,23	0,24	0,25	0,27	0,28	0,29	0,30	0,30	0,30
2,175	0,23	0,23	0,23	0,24	0,24	0,24	0,25	0,25	0,27	0,28	0,30	0,32	0,34	0,36	0,37	0,39	0,41	0,42	0,42	0,42
2,2	0,27	0,28	0,29	0,29	0,30	0,31	0,32	0,33	0,35	0,37	0,39	0,42	0,44	0,47	0,49	0,51	0,54	0,55	0,55	0,55
2,225	0,32	0,34	0,35	0,36	0,37	0,38	0,40	0,42	0,44	0,47	0,50	0,54	0,57	0,60	0,62	0,64	0,67	0,68	0,68	0,68
2,25	0,37	0,40	0,42	0,43	0,45	0,47	0,50	0,53	0,56	0,60	0,63	0,67	0,71	0,74	0,76	0,79	0,81	0,82	0,82	0,82
2,275	0,43	0,47	0,50	0,52	0,55	0,58	0,61	0,65	0,69	0,74	0,78	0,82	0,86	0,89	0,92	0,94	0,96	0,97	0,97	0,96
2,3	0,50	0,55	0,58	0,62	0,65	0,69	0,74	0,79	0,84	0,89	0,94	0,98	1,02	1,06	1,08	1,10	1,12	1,12	1,11	1,10
2,35	0,66	0,75	0,80	0,85	0,91	0,97	1,04	1,11	1,18	1,24	1,30	1,35	1,39	1,42	1,45	1,46	1,46	1,45	1,42	1,39
2,4	0,91	1,03	1,09	1,16	1,23	1,30	1,38	1,47	1,55	1,63	1,69	1,75	1,79	1,82	1,84	1,84	1,82	1,78	1,73	1,68
2,45	1,22	1,37	1,44	1,51	1,59	1,67	1,75	1,84	1,92	2,00	2,07	2,13	2,17	2,20	2,21	2,21	2,17	2,11	2,04	1,98
2,5	1,60	1,75	1,82	1,90	1,97	2,05	2,12	2,20	2,27	2,34	2,40	2,45	2,49	2,51	2,51	2,51	2,47	2,41	2,34	2,27
2,55	2,03	2,16	2,22	2,28	2,35	2,41	2,47	2,53	2,59	2,63	2,68	2,71	2,73	2,75	2,76	2,76	2,74	2,69	2,63	2,56
2,6	2,47	2,57	2,62	2,66	2,71	2,75	2,80	2,84	2,87	2,90	2,93	2,95	2,96	2,97	2,98	2,98	2,97	2,94	2,90	2,85
2,65	2,92	2,97	3,00	3,03	3,05	3,08	3,10	3,13	3,15	3,16	3,18	3,19	3,19	3,20	3,20	3,21	3,20	3,18	3,16	3,13
2,7	3,33	3,35	3,36	3,38	3,39	3,39	3,40	3,41	3,42	3,42	3,43	3,43	3,44	3,44	3,44	3,44	3,44	3,43	3,42	3,41
2,75	3,70	3,70	3,70	3,70	3,70	3,70	3,70	3,70	3,70	3,70	3,70	3,70	3,70	3,70	3,70	3,70	3,70	3,70	3,70	3,70
2,8	4,00	4,00	4,00	4,00	4,00	4,00	4,00	4,00	4,00	4,00	4,00	4,00	4,00	4,00	4,00	4,00	4,00	4,00	4,00	4,00

manual application

Table B.3: Data matrix – characteristic oxidation map

Oxidation [A/cm]

Permittivity [-] \ Viscosity [mm²/s]	6	7	7,5	8	8,5	9	9,5	10	10,5	11	11,5	12	12,5	13	13,5	14	15	16	17	18
2	0,00	0,00	0,00	0,00	0,00	0,00	0,00	0,06	0,19	0,43	0,80	1,32	2,00	2,85	3,89	5,11	8,37	12,96	18,64	25,00
2,05	0,00	0,00	0,00	0,00	0,00	0,00	0,00	0,04	0,17	0,43	0,86	1,46	2,25	3,22	4,37	5,70	9,11	13,57	18,76	24,31
2,1	0,54	0,48	0,41	0,32	0,22	0,13	0,07	0,08	0,21	0,50	0,97	1,66	2,55	3,65	4,93	6,39	9,95	14,31	19,15	24,16
2,15	1,43	1,31	1,21	1,09	0,94	0,78	0,64	0,56	0,60	0,83	1,30	2,03	3,04	4,28	5,73	7,32	11,04	15,38	20,04	24,78
2,175	1,97	1,84	1,74	1,63	1,50	1,33	1,17	1,04	1,03	1,19	1,62	2,35	3,40	4,72	6,24	7,89	11,70	16,06	20,66	25,32
2,2	2,55	2,41	2,33	2,24	2,14	1,99	1,81	1,65	1,58	1,67	2,05	2,77	3,86	5,24	6,80	8,51	12,42	16,81	21,36	25,96
2,225	3,19	3,03	2,96	2,90	2,83	2,73	2,57	2,40	2,30	2,34	2,67	3,37	4,45	5,81	7,40	9,15	13,19	17,62	22,15	26,69
2,25	3,90	3,71	3,64	3,59	3,55	3,49	3,39	3,24	3,14	3,17	3,47	4,12	5,11	6,42	8,00	9,79	14,03	18,49	22,99	27,51
2,275	4,68	4,45	4,37	4,30	4,27	4,24	4,21	4,14	4,12	4,20	4,45	4,95	5,80	7,01	8,57	10,41	14,92	19,38	23,88	28,41
2,3	5,54	5,26	5,15	5,06	5,02	4,99	5,02	5,08	5,18	5,33	5,48	5,80	6,46	7,55	9,07	10,95	15,79	20,28	24,81	29,38
2,35	7,63	7,21	6,98	6,77	6,65	6,72	6,93	7,15	7,29	7,37	7,36	7,37	7,61	8,37	9,73	11,57	16,82	21,93	26,77	31,58
2,4	10,26	9,85	9,65	9,49	9,39	9,42	9,43	9,37	9,23	9,05	8,87	8,74	8,81	9,18	10,15	11,81	17,44	23,28	28,69	34,02
2,45	13,41	13,22	13,15	13,10	13,05	12,94	12,69	12,26	11,70	11,09	10,51	10,07	9,93	10,21	11,14	12,84	18,44	24,52	30,56	36,54
2,5	17,06	17,12	17,12	17,11	17,07	16,95	16,67	16,17	15,46	14,60	13,67	12,88	12,46	12,77	13,89	15,64	20,50	26,31	32,60	39,01
2,55	21,06	21,34	21,46	21,58	21,67	21,69	21,61	21,36	20,86	20,16	19,33	18,50	17,83	17,57	17,93	19,01	23,30	28,82	34,97	41,39
2,6	25,37	25,78	25,99	26,20	26,42	26,62	26,80	26,91	26,88	26,71	26,44	26,06	25,59	25,13	24,87	25,07	27,62	32,12	37,59	43,52
2,65	29,96	30,41	30,64	30,88	31,13	31,41	31,72	32,07	32,44	32,73	33,01	33,34	33,52	32,95	32,36	32,03	33,00	36,08	40,27	45,00
2,7	34,81	35,19	35,39	35,59	35,81	36,02	36,23	36,43	36,63	36,82	37,01	37,22	37,34	37,61	37,66	37,68	38,17	40,12	42,81	45,00
2,75	39,86	40,08	40,19	40,30	40,42	40,52	40,62	40,72	40,81	40,91	41,00	41,11	41,17	41,30	41,48	41,66	42,09	43,27	45,00	45,00
2,8	45,00	45,00	45,00	45,00	45,00	45,00	45,00	45,00	45,00	45,00	45,00	45,00	45,00	45,00	45,00	45,00	45,00	45,00	45,00	45,00

manual application